Defining How the 26S Proteasome Recognizes Ubiquitinated Substrates

A DISSERTATION
SUBMITTED TO THE FACULTY OF THE GRADUATE SCHOOL
OF THE UNIVERSITY OF MINNESOTA
BY

Leah Ann Randles

IN PARTIAL FULFILLMENT OF THE REQUIREMENTS
FOR THE DEGREE OF
DOCTOR OF PHILOSOPHY

Advisor: Kylie J. Walters

December 2012

Acknowledgements

I would like to acknowledge some of the important groups of people that made this thesis possible. I would like to first thank my advisor, Dr. Kylie J. Walters, for guiding me through my graduate school career. I would also like to thank both past and present members of the Walters lab for training me in new techniques and for making the lab such a great place to be. In addition I have to give a huge thank you to my family and friends because without them this thesis would not have been possible.

Dedication

I would like to dedicate this thesis to my family and friends.

Thesis Abstract

Regulated protein degradation in eukaryotes is performed predominantly by the ubiquitin-proteasome pathway. Prior to their degradation by the 26S proteasome, protein substrates become covalently modified with ubiquitin chains. Such ubiquitination enables the 19S regulatory particle of the proteasome to recognize the doomed protein substrate. My thesis research focuses on defining how the 19S regulatory particle of the proteasome recognizes ubiquitinated substrates. When I began my thesis research, S5a/Rpn10 was the only known proteasomal ubiquitin receptor; yet, it is not essential for degradation of ubiquitinated substrates by the proteasome. My thesis research helped establish Adrm1/ARM1/Rpn13 as the missing proteasomal ubiquitin receptor. I used NMR spectroscopy to provide mechanistic insights into how human Rpn13 binds ubiquitinated substrates. I adapted a protocol developed by the late Cecile Pickart to fine tune polyubiquitin synthesis for use in NMR structural studies. By using this approach, I selectively labeled individual subunits within polyubiquitin to determine Rpn13's selective binding to the proximal subunit of K48-linked diubiquitin (diUb). These results, along with additional results from my lab and our collaborators' labs, are described in Chapters 2 and 3.

I continued to explore Rpn13's role as a ubiquitin receptor by testing whether it is able to work in cooperation with S5a/Rpn10. Along with other members of my lab, we solved the structure the S5a/K48-linked diUb complex by utilizing the method I optimized for synthesizing selectively labeled polyubiquitin. I then helped expand this work to reveal that Rpn13 and S5a are able to bind a common ubiquitin chain and thereby

work cooperatively to capture ubiquitinated substrates. These results are described in Chapter 4.

In Chapter 5, I describe a novel interaction of Rpn13's Pru domain to a ubiquitin processing enzyme, namely E2 ubiquitin conjugating enzyme Cdc34. NMR experiments reveal that an Rpn13 surface that neighbors its ubiquitin-binding loops binds to Cdc34's unique C-terminal tail and that this interaction does not restrict Rpn13 binding to ubiquitin. Immunoprecipitation experiments performed on HeLa cells with endogenous protein levels demonstrate Rpn13 and Cdc34 to be in complex in the cellular environment. The Rpn13:Cdc34 interaction suggests that Rpn13 may play a role in SCF-mediated ubiquitination.

Proteasome dysfunction is implicated in many diseases, such as cancer, cystic fibrosis, heart disease, and neurodegenerative diseases and the ubiquitin-proteasome pathway has therefore become a major pharmaceutical target. My thesis research in trying to understand how the proteasome recognizes ubiquitinated substrates provides structural and mechanistic information that could be used to help develop new drugs and possible treatments for these diseases.

Table of Contents

List of Tables

List of Figures

Chapter 1 - Introduction

Ubiquitin and its binding domains

Leah Randles *and Kylie J Walters*
Department of Biochemistry, Molecular Biology and Biophysics, University of Minnesota, Minneapolis, MN, 55455, USA

Reprinted with permission from Frontiers in Bioscience, Vol 17, pp 2140-57[a]

Leah Randles contributions: Produced all figures/tables and contributed equally to the writing of the published manuscript.

[a] We gratefully acknowledge Dr. Xiang Chen for useful discussions. Research in the K.J.W. laboratory is supported by the National Institutes of Health (CA097004, CA117888, and CA136472) and the American Cancer Society (RSG-07-186-01-GMC). L.R. was funded by a University of Minnesota Doctoral Dissertation Fellowship.
[a] We thank members of our laboratories, as well as D. Hoeller, G. Dittmar, J. Lipscomb and M. Schmidt, for discussions, comments and reading of the manuscript. We also thank the University of Minnesota's NMR facility, Minnesota Supercomputing Institutes's

1.1 Synopsis

Post-translational modification by ubiquitin (ubiquitination, ubiquitylation, ubiquitinylation) is used as a robust signaling mechanism in a variety of processes that are essential for cell homeostasis. Its signaling specificity is conferred by the inherent dynamics of ubiquitin, the multivalency of ubiquitin chains, and its subcellular context, often defined by ubiquitin receptors and the substrate. Greater than 150 ubiquitin receptors have been found and their ubiquitin-binding domains (UBDs) are structurally diverse and include alpha-helical motifs, zinc fingers (ZnF), pleckstrin-homology (PH) domains, ubiquitin conjugating (Ubc)-related structures and src homology 3 (SH3) domains. New UBD structural motifs continue to be identified. In this manuscript, we highlight several ubiquitin receptors from the multiple UBD folds with a focus on the structural characteristics of their interaction with ubiquitin.

1.2 Introduction: ubiquitin and protein ubiquitination

The 76-amino acid protein ubiquitin is attached covalently to other proteins to in turn, modify or expand their cellular activities. The most common sites of ubiquitin attachment are Lys epsilon-amino groups and the substrate's amino terminus, as reviewed in (*1*). In rare cases, ubiquitin can also be attached to Ser hydroxyl and Cys thiol groups (*2, 3*). Ubiquitination is tightly regulated and generally requires a 3-step catalytic cycle that includes E1 activating, E2 conjugating, and E3 ligating enzymes (Figure 1.1A). The human genome has been demonstrated to encode two E1 (Uba1 and Uba6), ~40 E2, and greater than 600 E3 enzymes, as reviewed in (*4*). E1 enzymes activate ubiquitin with a

two-step ATP-dependent reaction to form an E1-thiolester~ubiquitin intermediate (*5*), from which ubiquitin is transferred to an E2 catalytic Cys by a thioester transfer reaction, as reviewed in (*6, 7*). The transfer of activated ubiquitin to a substrate generally requires an E3 ligase. Depending on the E2-E3 pair, ubiquitin is either transferred to the target substrate directly from the E2 or after passage to an E3 catalytic Cys. The former mechanism is performed by RING (Really Interesting New Gene) domain E3s, which are the most populated class of E3. These act as scaffolds by orienting E2s for ubiquitin transfer to a substrate, as reviewed in (*4*). HECT (Homologous to E6AP C-Terminus) domain E3s, by contrast, form a thioester bond with ubiquitin *en route* to its substrate transfer, as reviewed in (*8*). Recently, the mechanistic distinction between RING and HECT E3s has become blurred as two E3s that belong to the RING-in-between-RING (RBR) family were proposed to act as RING/HECT hybrids by forming a thiolester~ubiquitin intermediate via a conserved RING domain cysteine prior to ubiquitin transfer to substrate (*9*).

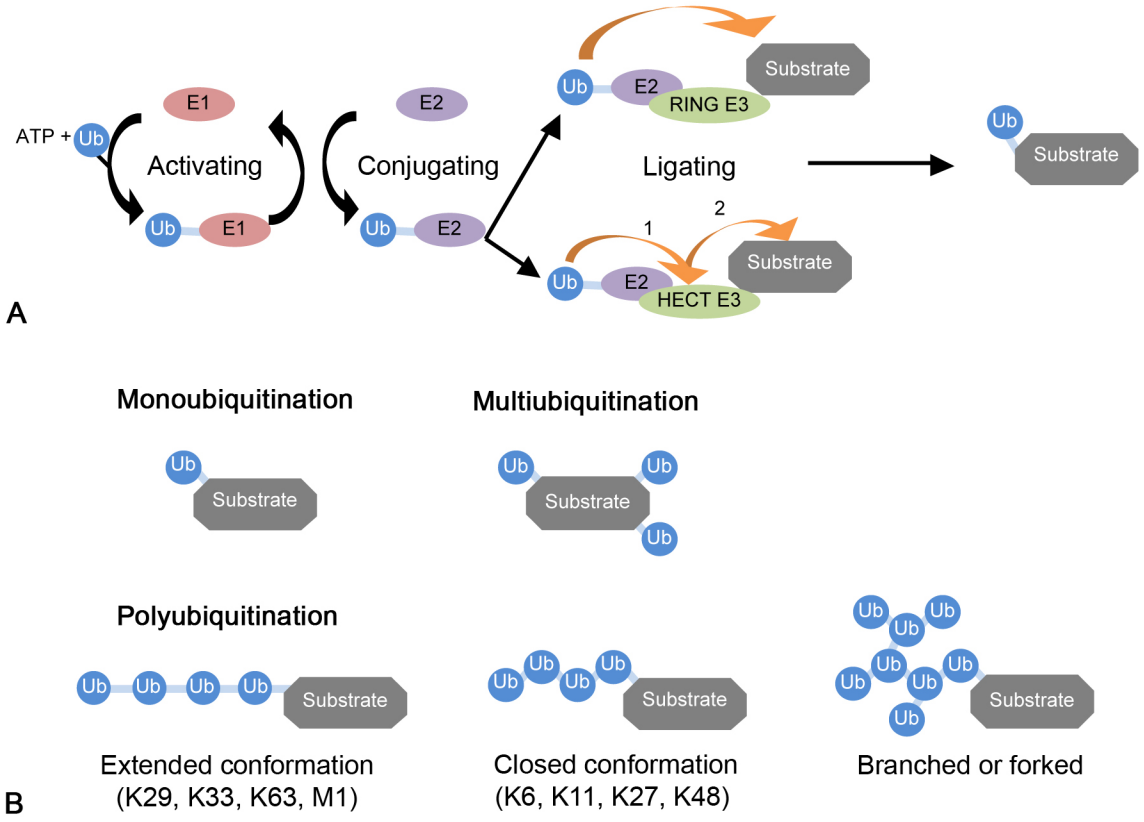

Figure 1.1 Ubiquitination (A) E1-E2-E3 enzymatic cascade leading to substrate ubiquitination, (B) Diversity of ubiquitin modification.

A single passage through an E1-E2-E3 enzymatic cascade results in a monoubiquitinated substrate. Additional passages yield multiubiquitinated substrates, with ubiquitin moieties at multiple sites, and/or polyubiquitinated substrates, with additional ubiquitins ligated to previously attached ones (Figure 1.1B). Ubiquitin moieties are linked by an isopeptide bond between a Gly76 carboxyl group and either a Lys sidechain primary amino group (Lys6, Lys11, Lys27, Lys29, Lys33, Lys48, or Lys63) or the ubiquitin amino terminus (Met1) (*10-12*). Quantitative mass spectrometry (MS) experiments in *Saccharomyces cerevisiae* (*13*) and mammalian cells (HEK293) (*14*) revealed differences in polyubiquitin linkage abundance. Although Lys48 and Lys63

linked chains are abundant in both cell types, their population is greater in HEK293 cells, as *S. cerevisiae* contained more Lys6 and Lys11 linkages (Table 1.1). It is possible that these differences are of physiological origin, but they may also be due to the use of different experimental procedures. The *S. cerevisiae* study captured His-tagged ubiquitin conjugates for MS analyses, whereas isotope enriched media was used to grow the HEK293 cells with total cell lysate used for subsequent MS experiments (*13, 14*).

Table 1.1. Ubiquitin linkage abundance determined by quantitative mass spectrometry

HEK293 Mammalian Cells (*14*)	
Lys6	≤ 0.5%
Lys11	2%
Lys27	≤ 0.5%
Lys29	8%
Lys33	≤ 0.5%
Lys48	52%
Lys63	38%
***Saccharomyces cerevisiae* (*13*)**	
Lys6	10.9% ± 1.9%
Lys11	28.0% ± 1.4%
Lys27	9.0% ± 0.1%
Lys29	3.2% ± 0.1%
Lys33	3.5% ± 0.1%
Lys48	29.1% ± 1.9%
Lys63	16.3% ± 0.2%

Ubiquitin's seven lysines can be used to synthesize homotypic chains of one linkage type or heterotypic chains with multiple linkage types, as reviewed in (*15*). Certain E2-E3 enzyme pairs have been shown *in vitro* to synthesize exclusively homotypic chains, as in the case of UbcH5-Nedd4, or heterotypic chains, as in the case of UbcH5-Mdm2 (*16*). UbcH5-Mdm2 has an added capacity of forming branched

heterotypic chains (Figure 1.1B) *in vitro*. The physiological role and abundance of branched heterotypic chains is speculative, but they have been proposed to act as dominant negative inhibitors of the proteasome (*16*). Distinct functional roles have been associated with certain ubiquitin chain linkage types. Lys48-linked chains target their substrates for degradation by the 26S proteasome, as reviewed in (*17*), or lysosome, as reviewed in (*18*). Lys63 linked chains function in NF-kappaB signaling, DNA repair, and receptor endocytosis, as reviewed in (*19, 20*). Linear ubiquitin chains have also been implicated in the regulation of NF-kappaB activity, as reviewed in (*21*). Function specific to the other linkages has not yet been assigned, although some associations exist. Lys29-linked chains can target proteins for degradation by lysosome and are synthesized *in vitro* by the E3's AIP4 (atrophin-1-interacting protein 4) and UBE3C/KIAA10, although both of these enzymes also synthesize Lys48-linked chains (*22, 23*). Heterotypic Lys29/Lys33-linked chains are found on ARK5/NUAK1 (AMPK Related Kinase 5) and MARK4 (Microtubule-Affinity-Regulating Kinase 4). These two substrates belong to the AMPK-related kinase family, which is involved in cell polarity and proliferation and blocking kinase activation by interfering with phosphorylation sites (*24*). Homotypic Lys11-linked chains are associated with many cellular processes, including ERAD (Endoplasmic Reticulum Associated Degradation), endocytosis, TNF (Tumor Necrosis Factor) signaling, WNT signaling, and cell cycle control, as reviewed in (*25*). Lys6- and Lys27-linkages are the least well characterized; however, Lys6 may regulate DNA repair (*26*) and Lys27 may function in stress response pathways (*27*).

1.3 Ubiquitin: a protein modifier

1.3.1. Monoubiquitin: placidity for multifaceted recognition

Ubiquitin adopts a compact globular fold that is formed by a 5-stranded beta-sheet, a short 3_{10} helix, and a 3.5-turn alpha-helix (Figure 1.2A). This fold is also the foundation of a larger family of ubiquitin-like (UBL) domains, which will not be discussed in this manuscript, but are reviewed in (*28, 29*). The majority of UBDs interact with a hydrophobic patch formed on the surface of ubiquitin's beta-sheet by Leu8, Ile44 and Val70 (Figure 1.2A). The amino acids surrounding this hydrophobic triad are disparate in terms of charge and size enabling diverse UBD binding modes to this common surface (Figure 1.2B) (*30*). For example, TSG101's UEV (Ubiquitin-conjugating enzyme E2 Variant) domain directly contacts ubiquitin's Gln62 (*31*), whereas this amino acid is not contacted by the Hrs DUIM (Double-sided Ubiquitin-Interacting Motif) (*32*). Comparison of multiple UBD:ubiquitin complexed structures demonstrates differences in ubiquitin with its various binding partners. This variability is not generated by UBD binding, but rather present in free ubiquitin due to its intrinsic motions, according to NMR experiments (*33*). UBDs thus appear to select for their optimal conformer from ubiquitin molecules that have variable amino acid sidechain exposure for the canonical UBD recognition surface, including Leu8 and the beta1-beta2 loop (Figure 1.1A) (*33*). Despite its conformational placidity, ubiquitin is a very stable protein that retains its fold at pH 4 up to ~75°C (*34*); for comparison, ubiquitin-like protein SUMO (Small Ubiquitin-like MOdifier) of similar fold and size denatures at ~52°C (pH 5.6) (*35*). Ubiquitin's placidity, coupled with its multifaceted recognition

surface, enables a broad spectrum of structural folds to be used as UBDs, 24 of which are listed in Table 1.2.

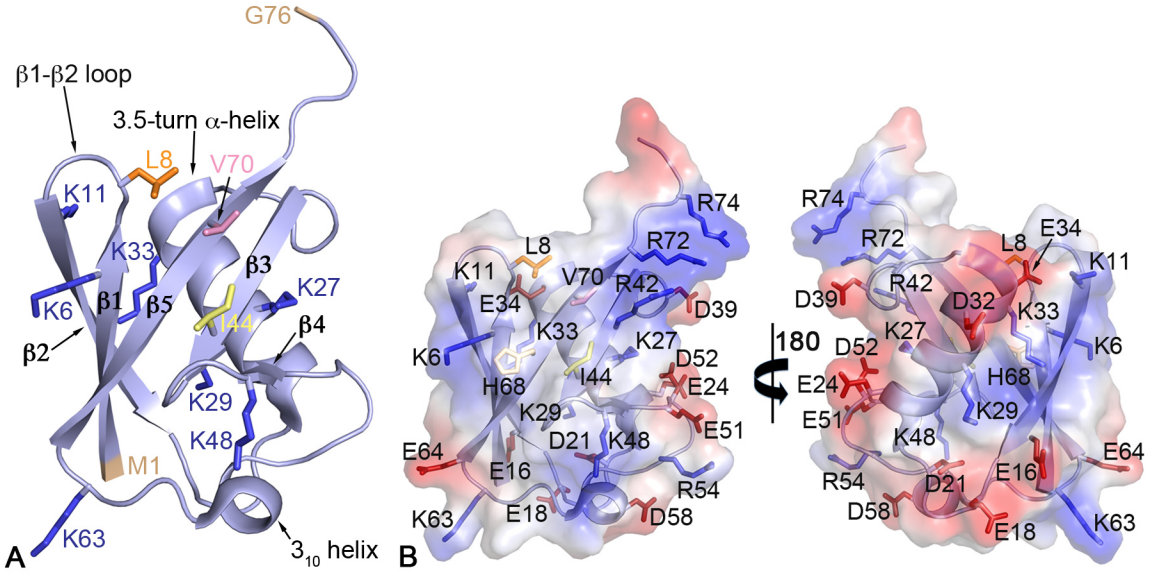

Figure 1.2. Features of monoubiquitin (A) Ribbon diagram of monoubiquitin (PDB 1D3Z) highlighting its seven lysines (blue), hydrophobic triad (Leu8, orange; Ile44, yellow; Val70, pink), and termini (Met1 and Gly76, beige). Secondary structural elements are labeled. (B) Electrostatic surface diagram of monoubiquitin rendered over its ribbon diagram with positive and negative charges displayed on the surface in blue and red, respectively, and hydrophobic regions in white. Heavy atoms of several charged amino acids, as well as those mentioned in the text are rendered as sticks and labeled.

1.3.2 Polyubiquitin: diversity in chains

Ubiquitin chains contribute an additional layer of diversity to the ubiquitin modifier, as these vary in both length and linkage type, as discussed in Section 1.2. They also expand the placidity present in monoubiquitin, as the linker region connecting ubiquitin moieties is flexible and allows diverse configurations for UBD-bound complexes (Figure 1.3). For example, Lys63-linked diubiquitin adopts a more compact conformation when bound to a Lys63-linkage specific antibody (*36*) than when bound to AMSH (Associated Molecule with the Src Homology 3 domain of signal-transducing

adapter molecule), an endosome-associated ubiquitin isopeptidase (*37*). When not bound to a UBD, Lys48-linked tetraubiquitin exchanges (*38*) between a compact configuration with its ubiquitin moieties packed tightly against each other (*39*) and a more extended one (*40*) . The canonical UBD-binding surface is not accessible in the compact form of Lys48-linked diubiquitin (*41*) (Figure 1.3B) or tetraubiquitin (*39*) and UBDs are therefore expected to bind moieties in the extended form. For example, hHR23a's C-terminal UBA (UBiquitin-Associated) domain interacts with the hydrophobic patches of both ubiquitin moieties from Lys48-linked diubiquitin (Figure 1.4C), which are inaccessible in its compact form (*42*).

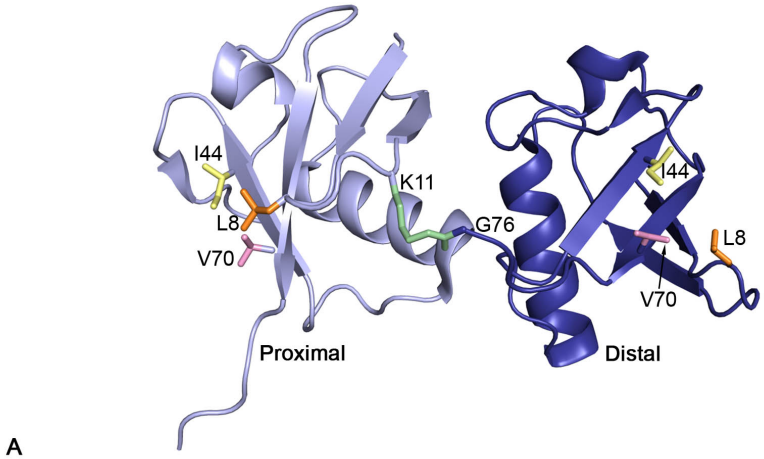
I44
K11
L8
G76
V70
I44
L8
V70
Proximal
Distal

A

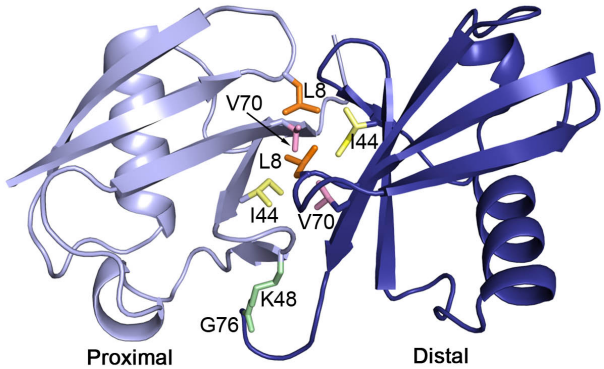
V70
L8
I44
L8
I44
V70
K48
G76
Proximal
Distal

B

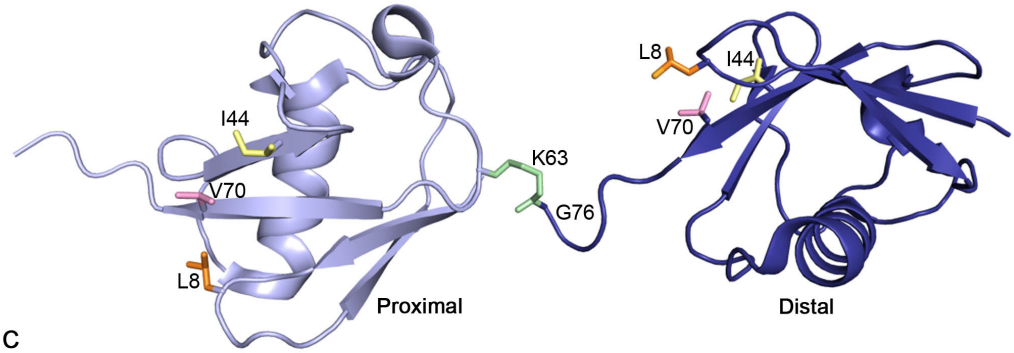
L8
I44
V70
I44
K63
V70
G76
L8
Proximal
Distal

C

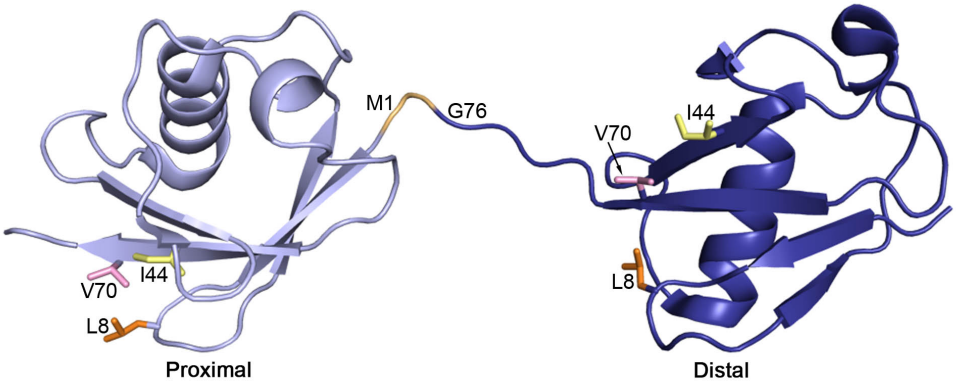
M1
G76
V70
I44
V70
I44
L8
L8
Proximal
Distal

D

Figure 1.3. Diversity of ubiquitin polymers. Ribbon representation of diubiquitin with the ubiquitin moieties linked via Gly76 and (A) Lys11 (PDB 2XEW), (B) Lys48 (PDB 1AAR), (C) Lys63 (PDB 2JF5), and (D) Met1, so-called linear (PDB 2W9N). In all cases, the ubiquitin moiety with its Gly76 available for conjugation to a substrate is displayed in light blue whereas the more distal moiety is dark blue. The hydrophobic triad is colored as in Figure 1.2A and the lysine ligated to Gly76 is displayed in green for Lys11, Lys48, and Lys63 linkages or beige for Met1.

Steric clashes prevent the ubiquitin moieties of Lys63-linked and linear polyubiquitin from packing against each other (*43*) (Figure 1.3C and D), whereas this configuration is possible for Lys11-linked chains as demonstrated by X-ray crystallography (*44, 45*) (Figure 1.2A) and predicted by molecular modeling (*46*). Lys6 and Lys27 linkages are predicted to enable a compact conformation, whereas Lys29 and Lys33 linkages are not (*46*). It is possible that the isolation of ubiquitin hydrophobic patches that occurs in compactly configured ubiquitin chains prevents them from engaging in non-specific interactions.

1.4 Ubiquitin-binding domains (UBDs)

1.4.1 Structural diversity of UBDs

No general ubiquitin binding consensus element has been identified, requiring all UBDs to be discovered experimentally. As a group, UBDs use all structural elements to bind ubiquitin, and new UBDs continue to be identified. UBDs can be alpha-helical, ZnF, PH, Ubc-related, SH3, or WD40 beta-propellers. The following sections describe binding modes and functions of various UBD structural folds (summarized in Table 1.2).

Table 1.2. UBD structures

Structural Fold	Subclass	Example Proteins	Ubiquitin Signaling Role	References
Alpha-helical	UIM	Rap80	DNA repair	(*47, 48*)
		Vps27	Endocytosis	(*49*)
		S5a/Rpn10	Proteasomal degradation	(*50-52*)
		STAM	Endocytosis	(*53*)
		Epsins		(*54*)
		Ataxin 3	Deubiquitination	(*55*)
	IUIM/MIU	Rabex-5	Endocytosis	(*56-58*)
		RNF168	DNA repair	(*59*)
	DUIM	Hrs	Endocytosis	(*32*)
	UBM	Polymerase iota	DNA repair	(*60, 61*)
		Reversionless 1		(*60*)
	UBAN	NEMO	NF-kappaB signalling	(*62, 63*)
		ABIN1/2/3		(*64*)
	UBA	hPLIC/Dsk2	Proteasomal degradation	(*65, 66*)
		hHR23/Rad23		(*66-68*)
		NBR1	Autophagy	(*69*)
		p62		(*70*)
	CUE	Vps9	Endocytosis	(*71*)
	GAT	TOM1		(*72, 73*)
		GGA3		(*74, 75*)
	VHS	STAM		(*76, 77*)
		GGA3		(*78*)
	UMI	RNF168	DNA repair	(*79*)
Zinc-finger (ZnF)	UBZ	Polymerase eta		(*80*)
		Polymerase iota		(*81*)
		TAX1BP1	NF-kappaB signaling	(*82*)
	NZF	TAB2/3		(*83-85*)
		Vps36	Endocytosis	(*86*)
		Npl4	ERAD	(*87*)
	ZnF A20	Rabex-5	Endocytosis	(*56-58*)
		A20	NF-kappaB signalling	(*88*)
	ZnF UBP	IsoT/USP5	Deubiquitination	(*89*)
		HDAC6	Autophagy	(*90, 91*)

Pleckstrin-homology (PH)	PRU	Rpn13	Proteasomal degradation	(*92, 93*)
	GLUE	Eap45	Endocytosis	(*94-96*)
Ubiquitin conjugating (UBC)-related	UEV	TSG101	Viral budding and VPS	(*31, 97*)
		Mms2	DNA repair	(*98*)
	UBC	UbcH5c	Ubiquitin conjugation/chain assembly	(*99*)
Src homology (SH)	SH3	Sla1	Endocytosis	(*100, 101*)
		CIN85		(*102*)
WD40	WD40 beta-propeller	PLAA/Doa1	ERAD	(*103*)
		Cdc4	Ubiquitin chain assembly	
Additional UBDs	PFU	PLAA/Doa1	ERAD	(*104, 105*)
	JAB1/MPN	Prp8	Pre-mRNA processing	(*106*)
	DC-UbP_N	DC-UbP	Ubiquitinated substrate delivery	(*104*)
	MDA-9/ syntenin UBD	MDA-9/syntenin	Endocytosis	(*107*)

Abbreviations: UIM (Ubiquitin-Interacting Motif), IUIM/MIU (Inverted UIM/Motif Interacting with Ubiquitin), DUIM (Double-sided UIM), UBM (Ubiquitin Binding Motif), UBAN (Ubiquitin Binding in ABIN and NEMO), UBA (UBiquitin Associated), GAT (GGA And TOM), CUE (Coupling of Ubiquitin conjugation to Endoplasmic reticulum degradation), VHS (Vps27/Hrs/STAM), ubiquitin-like binding domain of Ufd2, UMI (UIM- and MIU-related), UBZ (Ubiquitin-Binding ZnF), NZF (Npl4 (Nuclear protein localization 4) Zinc Finger), ZnF A20 (Zinc Finger A20), ZnF UBP/PAZ (Zinc Finger UBiquitin-specific Protease/Polyubiquitin Associated Zinc finger), PRU (Pleckstrin-like Receptor for Ubiquitin), GLUE (Gram-Like Ubiquitin-binding in Eap45), UEV (Ubiquitin-conjugating enzyme E2 Variant), UBC (UBiquitin-Conjugating), SH3 (Src Homology 3), PFU (PLAA Family Ubiquitin binding), Jab1/MPN (Jun Activation-domain Binding protein 1/Mpr-Pad1-N-terminal), DC-UbP_N (Dendritic Cell-derived UBiquitin-like Protein N-terminal domain), WD40 beta-propellers (WD40 beta-Prps), MDA-9/syntenin (Melanoma Differentiation Associated gene 9), ERAD (Endoplasmic Reticulum Associated Degradation), VPS (Vacuolar Protein Sorting)

1.4.1.1 Alpha-helical motifs

Ubiquitin binding surfaces are most commonly formed by alpha-helices (Table 1.2). A single alpha helix can define a UBD, as in the case of the UIM (Ubiquitin Interacting Motif), IUIM/MIU (Inverted UIM/Motif Interacting with Ubiquitin), UMI (UIM- and MIU-related) and DUIM (Double-sided UIM) domains. Ubiquitin binding is localized to a single surface of UIMs, MIUs, and the UMI. Experimentally derived structures of UIMs and an MIU have been solved complexed with ubiquitin; however, no experimental structure is available for the UMI, which is expected to be alpha-helical based on its sequence composition and so-named because of its sequence similarity to UIMs and MIUs (*79*). UIMs use a conserved LeuXXAlaLeu motif to bind the hydrophobic patch of ubiquitin, reviewed in (*108, 109*), whereas MIUs bind in an opposite orientation (LeuAlaXXLeu). The RING-finger ubiquitin ligase RNF168 contains two MIUs and a UMI (*59, 79*), which uses a dileucine motif and not the conserved Ala residue of UIMs and MIUs to interact with ubiquitin (*79*). DUIMs harbor two ubiquitin-binding surfaces at opposite sides of a helix, as displayed in the X-ray crystallographic structure of Hrs (Hepatocyte growth factor-Regulated tyrosine kinase Substrate) complexed with two monoubiquitin molecules (*32*); Hrs functions in protein sorting during endocytosis, as reviewed in (*110, 111*).

Alpha-helical ubiquitin-binding elements are invariably just one functional module within a multi-domain ubiquitin receptor, which can have multiple UBDs that are used together in novel ways to increase affinity for ubiquitin chains and in some cases, to define ubiquitin chain linkage specificity. Proteasome component S5a (*51, 52*),

endosomal sorting protein Vps27 (*49*), deubiquitinating enzyme Ataxin-3 (*55*), and DNA repair protein Rap80 (*47, 48*) are examples of ubiquitin receptors with multiple UIMs. In all cases, the UIMs are separated by flexible linker regions that are exploited to fit the signaling needs of the ubiquitin receptor. S5a's two UIMs are poorly defined relative to each other when unbound or complexed with monoubiquitin (*51*). In binding to Lys48-linked diubiquitin, however, S5a's flexible linker region adapts to enable each UIM to contact a ubiquitin moiety simultaneously and thereby confer a significant increase in affinity compared to that for monoubiquitin (8.9 microM versus 350 microM to UIM1 and 73 microM to UIM2) (*52*) (Figure 1.4A). The pliability of the region linking S5a's UIMs likely contributes to its ability to also bind Lys63-linked chains with similar binding affinity (*51, 112*) and Lys29-, Lys6-, and Lys11-linked chains, albeit with lower affinity (*112-114*). The adaptability of S5a's UIM region may contribute to the proteasome's capacity to degrade substrates of all ubiquitin chain linkages, an ability indicated by mass spectrometry-based experiments in *S. cerevisiae* (*13*). By contrast, the region linking Rap80's UIMs undergoes a conformational switch to generate a continuous helix that spans its two UIMs and orients them optimally to bind Lys63-linked chains (*47, 48*). The resulting specificity for Lys63-linked chains is consistent with Rap80's role in DNA damage response (DDR) pathways, as reviewed in (*115*).

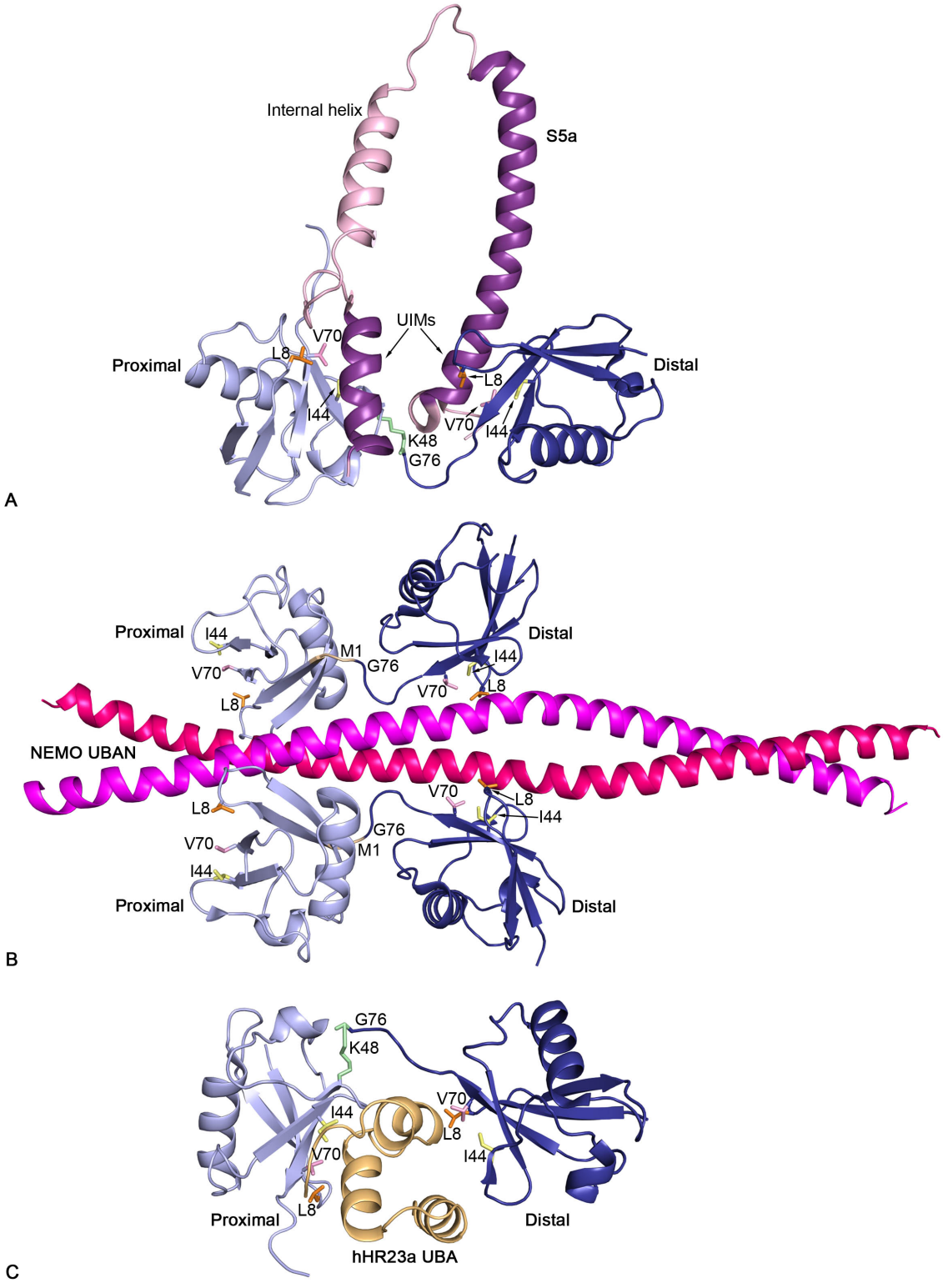

Figure 1.4. Alpha-helical ubiquitin-binding motifs. Ribbon representation of (A) S5a's

UIM region (purple and pink) bound to Lys48-linked diubiquitin (PDB 2KDE), (B) NEMO's UBAN domains (pink and magenta) bound to two linear diubiquitins (PDB 2ZVO), and (C) hHR23a's UBA domain (gold) sandwiched between the two ubiquitin moieties of Lys48-linked diubiquitin (PDB 1ZO6). The coloring scheme for diubiquitin follows that of Figure 1.3.

UBDs can also gain ubiquitin linkage specificity by oligomerization. The UBAN (Ubiquitin Binding in ABIN and NEMO) domain of NEMO (NF-kappaB Essential MOdifier) (*62, 63, 116*) forms a coiled-coil homodimer that binds preferentially to Lys63-linked (*63, 116-118*) and linear ubiquitin chains (*43, 62, 116*). Its affinity for linear ubiquitin chains however is 100-fold higher than Lys63-linked chains (*116*), as the UBAN monomers bind in a bipartite manner to neighboring ubiquitin moieties of linear chains. Hydrophobic amino acids of one monomer interact with the Leu8-Ile44-Val70 triad of the distal ubiquitin while polar amino acids of the other monomer interact with a surface adjacent to the proximal ubiquitin's hydrophobic patch (*62*) (Figure 1.4B). When binding to Lys63-linked chains, NEMO recapitulates the interactions of the hydrophobic residues only, resulting in a single site-binding mode (*63*). The bipartite binding mode of UBAN to linear ubiquitin chains appears to be important for NEMO's function as an NF-kappaB activator, as mutation of either ubiquitin-binding site leads to the loss of IkappaBalpha degradation following TNF-alpha induction (*62*).

Multiple alpha-helices can also define a UBD, as in the case of the UBM (Ubiquitin Binding Motif), CUE (Coupling of Ubiquitin conjugation to Endoplasmic reticulum), GAT (GGA and TOM), UBA (UBiquitin Associated), and VHS (Vps27/Hrs/STAM) domains. The UBM domains of the Upsilon DNA polymerase iota (Pol iota) and Reversionless 1 (Rev1) are the smallest multiple helical UBDs with two

amphipathic helices that bind a ubiquitin surface centered on Leu8 (*119, 120*). CUE, GAT, and UBA domains make up the bulk of the multiple alpha-helical domains and are comprised of a three-helix bundle. CUE and UBA domains are structurally similar, despite low sequence identity (17% between Vps9p CUE and Rad23 internal UBA (UBA1)) (*71*). Both use their alpha1 and alpha3 helices to bind ubiquitin's hydrophobic patch, but UBA domains use a conserved Met/Leu-Gly-Phe/Tyr motif (*121*), whereas CUE domains use a Met-Phe-Pro motif (*71*). UBA domains are diverse in their preferences for ubiquitin chains of certain length and linkage type (*112*). Whereas the UBA from hPLIC1 (ubiquilin1) shows little preference between Lys29-, Lys48-, and Lys63-linked polyubiquitin (*112, 122*), hHR23a's C-terminal UBA domain (UBA2) prefers Lys48 linkages over Lys63 linkages, as it sandwiches between neighboring ubiquitin moieties of Lys48-linked chains (Figure 1.4C) (*42, 112, 123*). Full length hHR23a has two UBA domains that can bind concomitantly to ubiquitin (*124*), and its UBA1 also exhibits stronger affinity for Lys48-linked chains (*67*). Whereas dimeric UBA domains become monomeric to bind ubiquitin (*125*), CUE domains can bind to monoubiquitin as homodimers, as in the case of the Vps21p GTPase exchange factor Vps9p (*71*). CUE domains are published to prefer monoubiquitin, based on *S. cerevisiae* two-hybrid screens with ubiquitin mutants that lack primary sites for ubiquitin chain formation (*126*). They have however been found to bind to Lys48-linked chains *in vitro* (*127*). In contrast to CUE and UBA domains, GAT domains have been reported to bind two ubiquitin molecules through two distinct binding sites, or one ubiquitin molecule and an additional binding partner, as in the case of ESCRT (Endosomal Sorting Complex

Required for Transport) pathway proteins Tom1 (Target of Myb1) and GGA3 (Golgi-localized, Gamma-ear-containing, ARF-binding protein 3) (*72, 74*).

VHS domains contain the most alpha helices of a UBD known to date with eight alpha-helices, and this UBD has recently been found to have Lys63-linkage specificity (*53, 77*). A surface that is primarily composed of amino acids from alpha2 and alpha4 is used by the VHS domains of ESCRT proteins Stam1 (*76, 128*) and Stam2 (*77*) to bind ubiquitin.

1.4.1.2 Zinc finger (ZnF)

The second most abundant UBD structural fold is the ZnF domain, which is relatively small and stabilized by its coordination of one or more Zn ions. These have been shown to bind to three different regions of ubiquitin. Some bind to the Leu8-Ile44-Val70 hydrophobic patch, such as UBZ (Ubiquitin-Binding ZnF) and NZF (Npl4 (Nuclear protein localization 4) Zinc Finger) domains. NF-kappa B activator proteins TAB2 (TAK1-Binding protein 2) and TAB3 (TAK1-Binding protein 3) contain NZF domains that contact the Ile44-centered surface of neighboring ubiquitin moieties of Lys63-linked chains simultaneously (*83, 85*) (Figure 1.5) to preferentially bind this chain type (*21, 83-86*). The distal ubiquitin moiety binds a Thr-Phe dipeptide motif that is highly conserved among NZF domains and also used by Npl4's NZF domain to bind monoubiquitin (*83, 85-87*). Direct contact to the Lys63 isopeptide linkage is not made by these NZF domains; however, the placement of the ubiquitin's other lysines and Met1 demonstrates that concurrent contact to the two distinct binding surfaces is likely to be

prohibited for chains formed by linkages other than Lys63 (Figure 1.5).

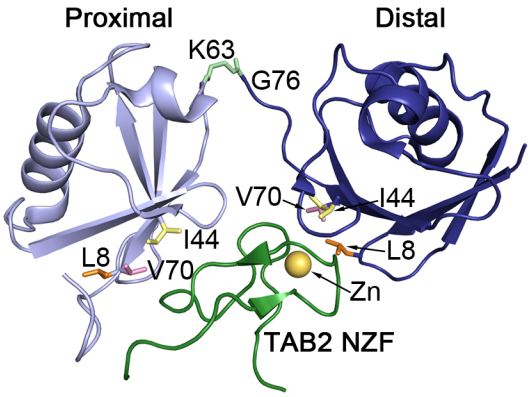

Figure 1.5. Zinc-finger domain of TAB2. Ribbon diagram of TAB2's NZF domain (green) complexed with K63-linked diubiquitin (PDB 3A9J). TAB2's single zinc ion is rendered as a gold sphere and the coloring for diubiquitin follows that of Figure 1.3.

The ZnF UBD of the E3 ligase Rabex-5 (Rab5 guanine Exchange factor) binds to a ubiquitin surface centered on Asp58 (Figure 1.2B) to which its Ser36 forms two hydrogen bonds (*56, 57*). Key contacts are also formed by two aromatic amino acids (Tyr25 and Tyr26) of Rabex-5 to ubiquitin's Arg54, Thr55, Ser57, Asp58, Tyr59 and Asn60 (*56, 57*). This dityrosine motif plays an integral role in Rabex-5's ability to bind to a ubiquitin-loaded E2 (UbcH5c), as binding is lost by its mutation to Ala (*56*).

Deubiquitinating enzymes disassemble ubiquitin chains by catalyzing the hydrolysis of the isopeptide bonds that link the individual moieties together. These linkage sites use ubiquitin's C-terminal Gly76, which was demonstrated to be required for interaction between ubiquitin and the ZnF UBP/PAZ of deubiquitinating enzyme isopeptidase T (IsoT/USP5) (*89*). This UBD has a deep pocket into which Gly75 and Gly76 insert and IsoT amino acids that interact with these glycines are required for its catalytic activation (*89*). A newly deposited crystal structure of HDAC6's UBP/PAZ

domain bound to ubiquitin (PDB 3PHD) demonstrates ubiquitin's C-terminal amino acids to be similarly sequestered into a deep pocket. IsoT/USP5 and HDAC6 use analogous contacts to ubiquitin's C-terminal tail, as all but two of the seven interacting amino acids are conserved or functionally equivalent (*89*).

1.4.1.3 Pleckstrin-homology (PH)

Pleckstrin-homology (PH) domains are comprised of a 7-stranded beta-sheet with a C-terminal alpha-helix and many bind phosphoinositides (PIs) within membranes to function in intracellular signaling. Two PH domains have been reported to bind to ubiquitin, including that within ESCRT-II Eap45, termed GLUE (Gram-Like Ubiquitin-binding in Eap45) (*96*), and the proteasome component Rpn13, termed PRU (Pleckstrin-like Receptor for Ubiquitin) (*92, 93*). A region of Eap45's GLUE domain that contains the C-terminal end of its alpha-helix, beta5, beta6, and the beta6-beta7 loop binds to the Ile44 centered surface of ubiquitin, as demonstrated by X-ray crystallography (*94, 95*) (Figure 1.6A). This ubiquitin-binding surface is at an opposite location relative to the proposed site that binds PIs, thereby suggesting that these two surfaces are used together to bring ubiquitinated cargo to the endosomal membrane (*94, 95, 129, 130*).

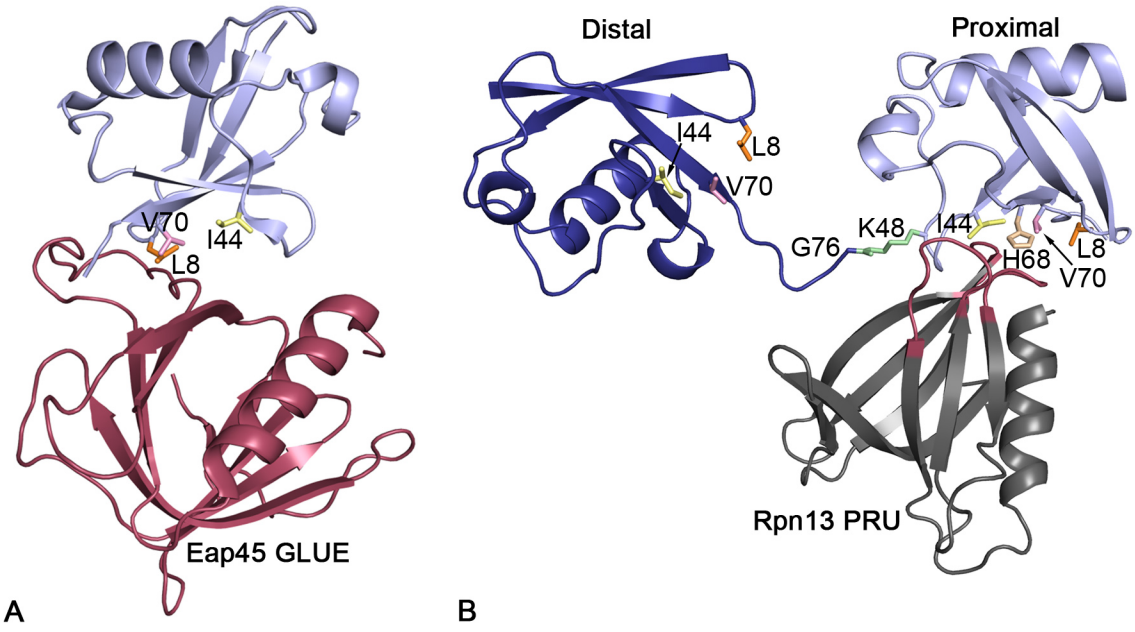

Figure 1.6. Pleckstrin-homology domains. Ribbon representation of (A) Eap45's GLUE domain (red) bound to monoubiquitin (PDB 2DX5) and (B) Rpn13's PRU domain (grey with ubiquitin-binding loops in red) bound to Lys48-linked diubiquitin (generated from PDB 2Z59 and 1D3Z). The ubiquitin coloring is as described in Figure 1.3, but with His68 included in beige.

Rpn13's PRU domain by contrast does not appear to bind to PIs, but rather uses a surface opposite to its ubiquitin-binding one to dock into the proteasome (*93*) (Figure 1.6B). It uses three loops to contact ubiquitin (Figure 1.6B), including its beta4-beta5 loop, which contains two Asp's (Asp78 and Asp79) that form hydrogen bonds with ubiquitin's His68. Phe76 from this loop interacts with ubiquitin's Ile44, Gln49, and Val70 and its mutation to Arg abrogates Rpn13's ability to bind to ubiquitin (*93*). Rpn13's PRU has a high affinity for ubiquitin (300 nanoM for monoubiquitin, 90 nanoM for Lys48-linked diubiquitin) (*92*) compared to S5a (*52*), the proteasome's other ubiquitin receptor. This affinity however is reduced in the full length protein due to interactions between its PRU domain and its C-terminal Uch37-binding domain (*131*), as discussed

further in Section 1.4.2. When binding to a Lys48-linked chain, Rpn13 prefers the proximal subunit (Figure 1.6B), most likely due to the loss of charge on its Lys48 (*93*). The use of loops to bind ubiquitin highlights the difficulty in predicting UBDs based on sequence information alone and the discovery that Rpn13 is a ubiquitin receptor in the proteasome (*92*) was 14 years after S5a was reported to be one (*132*).

1.4.1.4 Ubiquitin-conjugating (Ubc)-related

Ubc (UBiquitin-Conjugating) domains are found in E2 enzymes and are comprised of ~150 amino acids that fold into four standard helices and a 4-stranded antiparallel beta-sheet, as reviewed in (*133*). Generally, Ubc domains contain a conserved catalytic cysteine that forms a thiolester bond with ubiquitin, as discussed in Section 1.2. All E2's interact with ubiquitin covalently, but noncovalent interaction surfaces have also been identified, as in UbcH5c (*99*). UbcH5c's non-covalent ubiquitin-binding surface is opposite to the E2 catalytic Cys (Figure 1.7A) and is essential for the processive nature of BRCA1 (BReast CAncer type 1)-mediated polyubiquitination, allowing multiple ubiquitination cycles to a bound substrate (*99*). UbcH5a and UbcH5b also use this non-covalent ubiquitin-binding surface (*134*), and UbcH5a has an additional ubiquitin-binding surface that is proposed to govern Lys11-linked chain formation, as a surface adjacent to its catalytic Cys interacts with a ubiquitin surface that flanks its Lys11 (*135*).

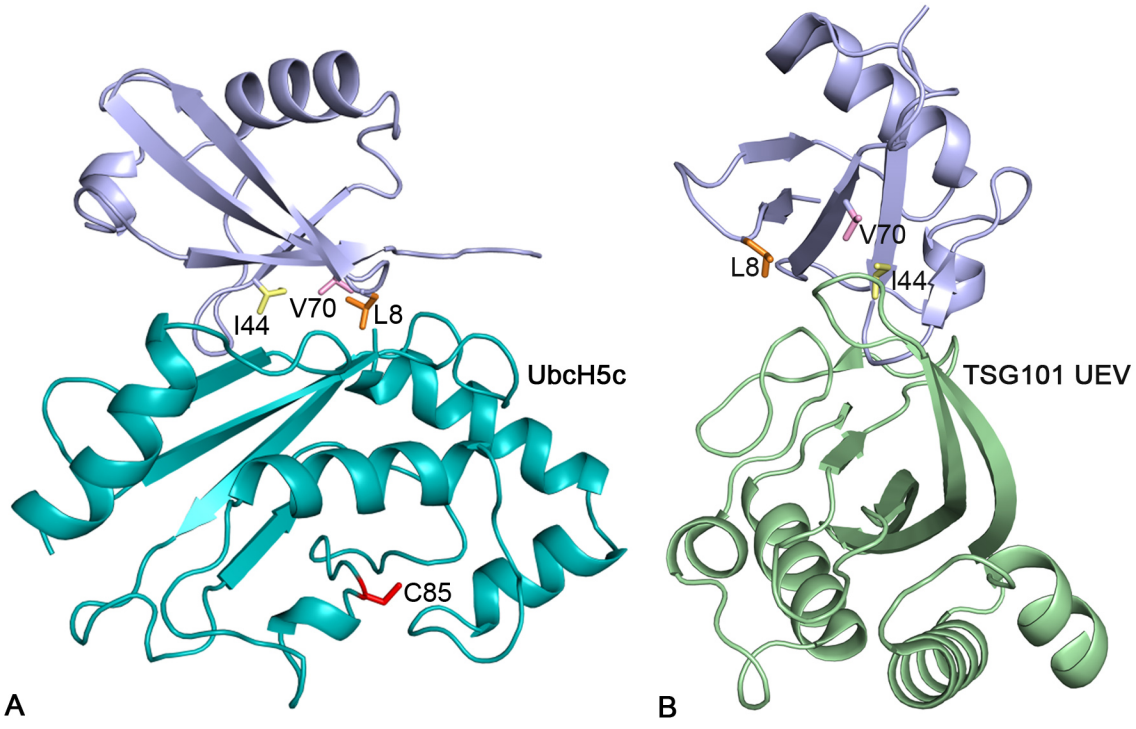

Figure 1.7. Ubc-like domains complexed with ubiquitin. Ribbon representation of (A) UbcH5c (cyan, PDB 2FUH) and (B) TSG101 UEV (green, PDB 1S1Q) bound to monoubiquitin colored as in Figure 1.3. UbcH5c's catalytic cysteine (Cys85) is displayed in red.

The UEV (Ubiquitin-conjugating enzyme E2 Variant) domain has an alpha/beta fold similar to Ubc domains, but has an additional N-terminal helix, an extended beta-hairpin linking beta1 and beta2 and lacks Ubc's two C-terminal helices (*31*). UEV domains are not E2's as they lack the catalytic Cys residue, but they can bind ubiquitin non-covalently, as in the case of TSG101, which functions in Human Immunodeficiency Virus-1 (HIV-1) budding and MVB (MultiVesicular Body) sorting (*31*). TSG101's UEV domain and UbcH5c bind ubiquitin differently (Figure 1.7), as the extended beta-hairpin is used by this UEV as well as the loop that follows beta4 (Figure 1.7B) (*31, 99*).

1.4.1.5 Src homology 3 (SH3)

Approximately 300 SH3 domains are encoded in the human genome (*136*). They are formed by ~60 amino acids, which assume a beta-barrel fold and tend to promote protein-protein interactions, most often by binding to proline-rich regions (ProXXPro) (*137*). SH3 domains of *S. cerevisiae* Sla1 (*101*), its mammalian orthologue CIN85 (*102*), and amphiphysin (*100*) are reported to bind to ubiquitin. Sla1's third SH3 (SH3-3) domain uses complementary hydrophobic residues from a shallow groove present in all SH3 domains to bind the hydrophobic patch of monoubiquitin, as revealed by solution NMR (*101*) (Figure 1.8). This shallow groove is typically used to bind ProXXPro or ProXXProArg motifs (*100-102*), suggesting a competition between ubiquitin and ProXXPro/Arg binding partners. Like its yeast orthologue, CIN85 contains three SH3 domains, but in contrast to Sla1, all three bind ubiquitin (*100, 102*).

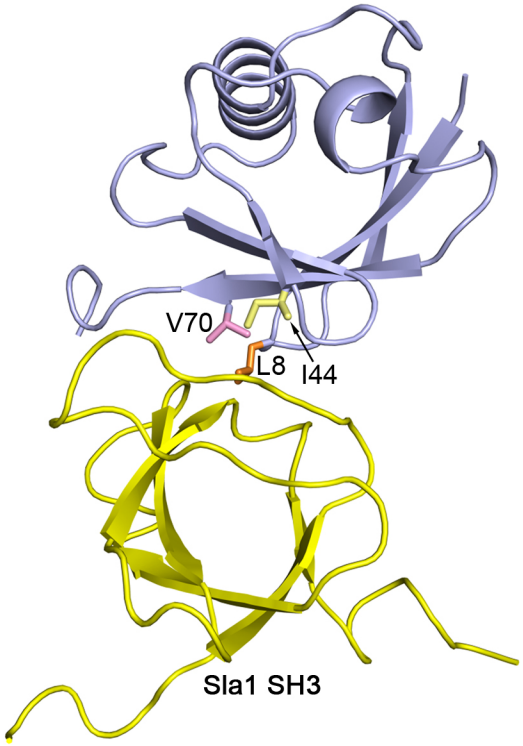

Figure 1.8. SH3 domain of Sla1. Ribbon representation of the SH3 domain of Sla1 (yellow) bound to monoubiquitin colored as in Figure 1.3 (PDB 2JT4).

1.4.1.6 Additional UBDs

Many other structural folds have evolved ubiquitin-binding surfaces. In the past year, novel UBD structural folds have been described in the N-terminal domain of DC-UbP (*104*), WD40 beta-propellers (*103*), and MDA-9/syntenin (*107*). DC-UbP's N-terminal ubiquitin-binding domain forms an alpha-alpha-alpha-beta-beta pattern with a short C-terminal alpha-helix (*104*). It binds to ubiquitin's hydrophobic patch and C-terminal residues (Leu71, Arg72, and Leu72) by using amino acids from the alpha1-alpha2 loop, alpha2, alpha3, and the beta1-beta2 loop (*104*). The C-terminal region of DC-UbP contains a UBL domain (*138*), thereby linking it to the UBL-UBA family of proteins, which include hHR23 and hPLIC, discussed in Section 1.4.1.1.

WD40 beta-propellers from functionally diverse proteins bind to ubiquitin's hydrophobic patch through a conserved surface made up of loops; these include components of SCF ubiquitin E3 ligases and AAA ATPase Cdc48/p97 adaptor Doa1/Ufd3 (*103*). Doa1/Ufd3 also contains a PFU domain (PLAA family Ub-binding domain), which binds to ubiquitin (*105*). It is not yet known whether Doa1's UBDs are used synergistically to confer specificity for ubiquitin chain linkage type, however it appears to bind preferentially to longer ubiquitin chains (*139*).

1.4.2 UBD Regulation

There are many mechanisms to keep UBDs in check, which have perhaps arisen due to their widespread use and abundance. UBD regulation can occur through intramolecular activities involving the ubiquitin receptor or alternatively, by modification of the substrate. Intramolecular interactions between UBDs and other domains within a ubiquitin receptor or that involve a ubiquitin conjugated to the receptor itself can reduce a receptor's affinity for ubiquitinated substrates. Ubiquitin receptors Rpn13 and hHR23a, which function in proteasome-mediated protein degradation, have additional domains that interact with their UBDs. Rpn13's PRU binds its C-terminal Uch37-binding domain, which reduces the exposure of its ubiquitin binding surface and in turn, its affinity for ubiquitin (*131*). Rpn13 docking into the proteasome appears to abrogate this intramolecular interaction, thereby functionally coupling its activity as a ubiquitin receptor to its localization to proteasome (*131*). hHR23a's UBA and UBL domains similarly interact to reduce ubiquitin accessibility (*140*). Moreover, monoubiquitination

of UBD-containing proteins causes the UBD to interact with its own conjugated ubiquitin rather than a substrate-attached one. This process, termed coupled monoubiquitination (*141, 142*), regulates Eps15 (UIM), Sts1 (UBA), Sts2 (UBA), Hrs (DUIM) and the MDA-9/syntenin UBD (*141, 143, 144*). Intermolecular interactions involving UBDs can also regulate ubiquitin receptor binding to ubiquitinated substrates, as in the case of p47, which is unable to bind monoubiquitin via its UBA domain unless it is complexed with p97 (*145, 146*). Post-translational modifications of substrates can also regulate UBD activity, including selective methylation of Lys residues, phosphorylation (as reviewed in (*147*)), and conjugation with ubiquitin-like proteins (such as SUMO, as reviewed in (*29, 148*)). Methylation of Lys side-chains prevents ubiquitination, causing loss of UBD interaction and prolonged protein half-life (*149*). A recent MS study done on the *S. cerevisiae* 26S proteasome suggests that 43% of Lys methylation sites in over 40 proteins are also sites for ubiquitination (*150*).

1.5 Perspective: summary and future

Ubiquitin's signaling prowess was first discovered for its ability to target substrates for degradation by proteasome (*151, 152*), but has now expanded to encompass a myriad of processes including regulatory roles in DNA repair, transcription, pre-mRNA splicing, endocytosis and autophagy, as reviewed in (*18*). Its function as a signaling molecule in such a broad spectrum of activities is tightly coupled to its multilingualism for a plethora of diverse receptors, which is contributed by monoubiquitin's dynamic sampling of slightly different confomers, the diversity of the region connecting moieties

within a ubiquitin chain, and the variations available in ubiquitin chain length and linkage. Structures of UBDs complexed with ubiquitin polymers have provided valuable insights into how ubiquitin signals for such a large repertoire of events with specificity. Some questions remain however. With the notable exception of ZnF domains, which can bind to three different ubiquitin surfaces, the vast majority of UBDs seek a common surface on ubiquitin, thus suggesting a packing problem as ubiquitin is shuttled from one receptor to another, or as multiple receptors are present and available for binding. It is tantalizing to speculate that these potential hurdles have been evolutionarily exploited, such as by preventing two receptors from distinct pathways from battling over where to shuttle their commonly bound substrate. New UBDs and mechanisms for their regulation continue to be discovered and it is interesting that so many structural domains can form surfaces that bind ubiquitin. Yet, it is not always clear how one domain type assumed ubiquitin-binding capacity for some of its members. Finally, it is often challenging to extrapolate the intricacies of a ubiquitin signaling cascade from the snapshots provided by UBD:ubiquitin complexes. It is hopeful that the future will offer atomic resolution images of ubiquitinated substrates complexed with their ubiquitin receptors as they are shuttled through a ubiquitin signaling pathway. Such information would provide a greater appreciation of how individual UBDs are integrated into the ubiquitin signaling highway.

Chapter 2

Proteasome subunit Rpn13 is a novel ubiquitin receptor

Koraljka Husnjak[1,2,], Suzanne Elsasser[3,*], Naixia Zhang[4,*], Xiang Chen[4], **Leah Randles[4]**, Kay Hofmann[5], Kylie Walters[4], Daniel Finley[3] and Ivan Dikic[1,2]*

[1]Institute of Biochemistry II, Goethe University Medical School, Theodor-Stern-Kai 7, D-60590 Frankfurt (Main), Germany
[2]Tumor Biology Program, Mediterranean Institute for Life Sciences, Mestrovicevo setaliste, 21000 Split, Croatia
[3]Department of Cell Biology, Harvard Medical School, 200 Longwood Avenue, Boston, MA 02115, USA
[4]Department of Biochemistry, Molecular Biology and Biophysics, University of Minnesota, Minneapolis, MN 55455, USA
[5]Miltenyi Biotec GmbH, Stoeckheimer Weg 1, D-50829, Koeln, Germany
[*]These authors contributed equally to this work.

Reprinted with permission from Nature Publishing Group Vol 453, Issue 7194, pp 481-8[a]

Leah Randles Contributions: Performed experiments and produced figures for 2.4A, 2.4B, 2.4G, and 2.S5. Contributed to all NMR experiments and sample preparation associated with NMR and tryptophan quenching experiments. Contributed to writing of published manuscript.

---

[a] We thank members of our laboratories, as well as D. Hoeller, G. Dittmar, J. Lipscomb and M. Schmidt, for discussions, comments and reading of the manuscript. We also thank the University of Minnesota's NMR facility, Minnesota Supercomputing Institutes's Basic Sciences Computing Laboratory and E. Arriaga for allowing us to use his spectrofluorometer. We thank G. Zapart for the initial Y2H ubiquitin screening, and M. Groll and P. Schneider for allowing us to use the mRpn13–ubiquitin coordinates to generate Figure 2.5C. This work was supported by grants from Deutsche Forschungsgemeinschaft (DI 931/3-1), the Cluster of Excellence 'Macromolecular Complexes' of the Goethe University Frankfurt (EXC115) (I.D.) and the National Institutes of Health (CA097004 to K.J.W.; GM043601 to D.F.; GM008700-CBITG to L.R.).

2.1 Synopsis

Proteasomal receptors that recognize ubiquitin chains attached to substrates are key mediators of selective protein degradation in eukaryotes. In this chapter we report the identification of a new ubiquitin receptor, Rpn13/ARM1, a known component of the proteasome. Rpn13 binds ubiquitin through a conserved amino-terminal region termed the pleckstrin-like receptor for ubiquitin (Pru) domain, which binds K48-linked diubiquitin with an affinity of approximately 90 nM. Like proteasomal ubiquitin receptor Rpn10/S5a, Rpn13 also binds ubiquitin-like (UBL) domains of UBL-ubiquitin-associated (UBA) proteins. In yeast, a synthetic phenotype results when specific mutations of the ubiquitin binding sites of Rpn10 and Rpn13 are combined, indicating functional linkage between these ubiquitin receptors. Because Rpn13 is also the proteasomal receptor for Uch37, a deubiquitinating enzyme, our findings suggest a coupling of chain recognition and disassembly at the proteasome.

2.2 Introduction

In eukaryotes, selective protein degradation is performed primarily by the ubiquitin–proteasome pathway. The 26S proteasome is a huge macromolecular machine that contains a proteolytically active 20S core particle capped at one or both ends by a 19S regulatory particle (*153*). The regulatory particle recognizes ubiquitinated substrates, deconjugates ubiquitin chains and unfolds substrates before their translocation into the core particle. Proteasome subunit Rpn10/S5a was shown to bind ubiquitin chains through ubiquitin-interacting motifs (UIMs) (*132*). Receptors were subsequently identified that

are not integral proteasome subunits, but deliver ubiquitinated targets to the proteasome (for reviews, see refs (*154*) and (*155*)). Canonical members of this UBL/UBA family of receptors are Rad23 (hHR23a/b in humans), Dsk2 (hPLIC-1/2 in humans) and Ddi1 (refs (*156-160*)). UBA domains of this protein family bind ubiquitin(*124, 161, 162*), whereas (*163*) their UBL domains interact reversibly with the proteasome, principally through Rpn1, but potentially also through Rpn10 (refs (*164-166*)).

Another interesting component of the proteasome is Rpn13/ADRM1/ARM1 (refs (*163, 167-171*)), which docks at the regulatory particle through an N-terminal region that binds Rpn2 (refs (*169*), (*163, 172, 173*)). Its carboxy-terminal region binds deubiquitinating enzyme Uch37/UCHL5 and enhances its isopeptidase activity(*169, 171*). Uch37 may function as an editing isopeptidase that rescues poorly ubiquitinated substrates from being degraded (*174*).

2.3 Results

2.3.1 A ubiquitin-interactor screen identifies Rpn13

Using a yeast two-hybrid screen, with a bait of ubiquitin lacking the last two glycines to prevent its conjugation (*119*), we identified the N-terminal segment of human Rpn13 (hRpn13) as a ubiquitin-binding partner. The interaction was confirmed using murine Rpn13 (mRpn13) as bait against monoubiquitin and Rpn2 as prey (Figure 2.1A). Rpn13 from *Saccharomyces cerevisiae* (scRpn13) aligns with the ubiquitin-binding N-terminal region of hRpn13 (Figure 2.1B). Comprehensive sequence analysis using profiles and hidden Markov models failed to reveal similarity to known ubiquitin- or

proteasome-binding motifs (Figure 2.1C and data not shown). Deletion mutants encompassing residues 1–150 were tested for tetraubiquitin binding, thus mapping the minimal binding domain to residues 1–130 (Figure 2.1D). Although smaller fragments of mRpn13 also showed detectable binding to ubiquitin, they were unstable and expressed poorly as glutathione *S*-transferase (GST) fusions.

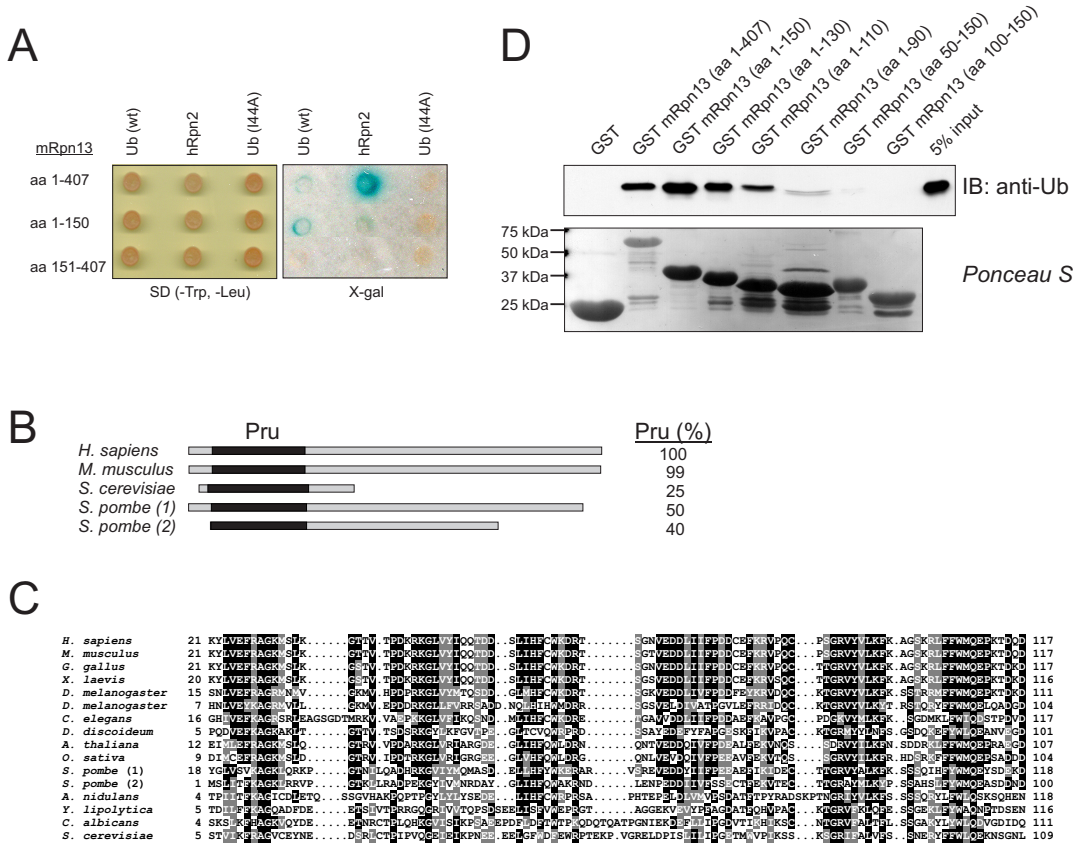

Figure 2.1. Murine Rpn13 binds ubiquitin chains. (A) mRpn13 cDNA fragments were cloned into pYTH9 vector in frame with the Gal4 DNA-binding domain. The resulting bait vectors were transformed into yeast strain Y190 with prey pACT2 vectors containing wild-type ubiquitin, I44A ubiquitin or hRpn2 (positive binding control) cDNA in frame with Gal4 DNA-activating domain. (B) Architecture of Rpn13 from various species. The N-terminal domain is generally conserved (black box) whereas the C-terminal region (grey box) is absent in *S. cerevisiae* and has diverged beyond recognition in one of the

two *Saccharomyces pombe* proteins (*S. pombe* (1)). *S. pombe* (1) = SPCC16A11.16; *S. pombe* (2) = SPBC342.04. The percentage identity to the conserved hRpn13 Pru domain is provided at right. (C) Alignment of Rpn13 N-terminal sequences. Residues that are invariant or conserved in at least 50% of sequences are shaded in black or grey, respectively. (D) To identify the minimal region required for ubiquitin binding, mRpn13 deletion mutants were expressed as GST-fused proteins, purified and tested for their binding to linear tetraubiquitin by immunoblotting with anti-ubiquitin antibodies. Tetraubiquitin was obtained by thrombin cleavage of GST-fused tetraubiquitin (GST 4×Ub) and equivalent amounts of GST-fused deletion mutants were used in GST pull-down assay.

The significance of the ubiquitin–Rpn13 interaction would be supported if it were conserved from yeast to mammals, particularly as budding yeast Rpn13 is truncated and the conserved N-terminal region (Figure 2.1C) is only 25% identical to mammalian forms (Figure 2.1B). The existence of an unidentified ubiquitin receptor in yeast had been evident to us from the viability of an *rpn10-uim rad23*Δ *dsk2*Δ *ddi1*Δ mutant (data not shown). *rpn13*Δ mutants, which are viable but show defects in protein degradation (*167, 175*), were used to test whether Rpn13 binds ubiquitin chains in the context of intact, purified proteasomes.

2.3.2 Rpn13 docks ubiquitin conjugates at the proteasome

Ubiquitin chain binding by purified proteasomes can be assayed by native gel electrophoresis(*156, 165*). Proteasomes are visualized in this system by an activity stain, using a fluorogenic peptide substrate. For wild type, the predominant proteasome species contains one regulatory particle on either end of the core particle cylinder (RP_2CP). Ubiquitin chains, produced by the E2 enzyme Cdc34, bind to the proteasomes and confer reduced mobility (Figure 2.2A). This shift is not dependent on UBL/UBA proteins, because the proteasomes were prepared from *rad23*Δ *dsk2*Δ *ddi1*Δ mutants. A block

substitution within the UIM in Rpn10 results in attenuation of the shift, reflecting Rpn10's known ubiquitin receptor function (Figure 2.2A; refs (*156*) and (*157*)). However, the existence of marked residual electrophoretic retardation by added chains (lane 4) indicates the presence of at least one additional ubiquitin receptor in purified proteasomes.

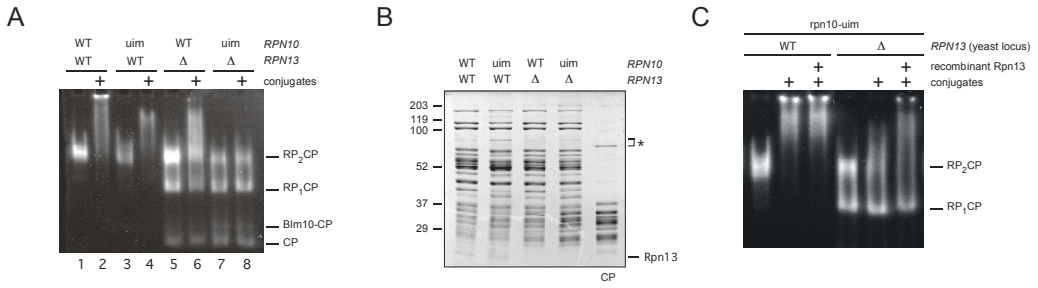

Figure 2.2. Rpn13 contributes to recognition of ubiquitin conjugates by the proteasome. (A) *rpn13*Δ proteasomes show defects in ubiquitin conjugate binding. Proteasomes were purified from strains (SY733, SY729, SY725 and SY722) bearing the indicated mutations. Proteasomes (4 pmol) were mixed with autoubiquitinated Cdc34 (16 pmol), resolved by native PAGE, and visualized using *N*-succinyl-Leu-Leu-Val-Tyr-(7-amino-4-methylcoumarin) (LLVY–AMC). Note that UBL/UBA proteins cannot contribute to ubiquitin chain binding in these experiments, because all proteasomes used in this figure are from a *rad23*Δ *dsk2*Δ *ddi1*Δ genetic background. *ubp6*Δ is also in the genetic background, to prevent chain disassembly during the assay. (B) Proteasome composition is maintained in the absence of Rpn13. Proteasomes from (A) (25 μg) were resolved by SDS–PAGE and stained with Coomassie blue. An asterisk marks contaminating protein. (C) Reconstitution of ubiquitin conjugate binding. A subset of proteasomes from (A) (4 pmol each) was incubated with scRpn13 (20 pmol) cleaved from the GST moiety (+ lanes) or GST alone (remaining lanes) to allow reassembly, then mixed with autoubiquitinated Cdc34 (16 pmol). Complexes were resolved by native PAGE and visualized as in (A).

Addition of conjugates to proteasomes lacking Rpn13 resulted in an electrophoretic shift comparable to that of *rpn10-uim* samples (Figure 2.2A). Thus the yeast orthologue of mRpn13 is active in ubiquitin chain binding and can bind ubiquitin in

the context of intact proteasomes. Indeed, its capacity for chain binding in this assay compares well with that of Rpn10. Remarkably, we observed an ostensibly complete abrogation of chain-dependent electrophoretic retardation when *rpn10-uim rpn13*Δ proteasomes were used (Figure 2.2A), suggesting that Rpn10 and Rpn13 are the two major ubiquitin receptors in the yeast proteasome. However, by varying the conditions of this assay, we could, as shown below, detect residual ubiquitin chain binding with *rpn10-uim rpn13*Δ proteasomes, consistent with the existence of a still-unidentified proteasomal ubiquitin receptor. The greater abundance of the RP_1CP and core particle bands in *rpn13*Δ samples suggests that Rpn13 contributes to the stability of the regulatory particle–core particle interaction *in vitro* (*175*).

To determine whether *rpn13*Δ proteasomes were properly assembled, they were analyzed by SDS–polyacrylamide gel electrophoresis (SDS–PAGE) (Figure 2.2B). Apart from the absence of Rpn13 itself, the mutant proteasomes appeared to be wild type in composition. When recombinant Rpn13 was reconstituted onto mutant proteasomes after purification, their chain-binding defect was corrected (Figure 2.2C). Thus, the chain-binding assay appears to report on a specific Rpn13–ubiquitin chain interaction, and not a gross structural defect of *rpn13*Δ proteasomes. GST pull-down assays also indicated direct interaction of scRpn13 with ubiquitin (data not shown). In summary, these data indicate that Rpn13 is a novel proteasomal ubiquitin receptor.

2.3.3 Loops of yeast Rpn13 bind ubiquitin

To create mutants of scRpn13 deficient in ubiquitin binding and to study the

functional significance of the interaction *in vivo* subsequently, we initially used NMR to solve the structure of full-length scRpn13. These studies revealed that Thr6–Leu101 forms two contiguous, antiparallel β-sheets with a configuration similar to the pleckstrin-homology structural domain (Figure 2.3A). In particular, a β-sheet comprising four antiparallel β-strands formed by I8–R11, E32–P37, W46–W50, and I64–L66 packs against a three-stranded sheet formed by M74–V76, I86–V90, and R96–W100. Juxtaposed to the three-stranded sheet are two β-strands formed by C15–N18 and L23–P26. The configuration of the β-strands centers around interactions between conserved aromatics within the protein core, including F10, F48, W50, W75, F87, F91, F98, F99 and W100. These findings are consistent with the crystal structure, described in Chapter 3, of mRpn13. We thus named this domain pleckstrin-like receptor for ubiquitin (Pru). In a canonical pleckstrin-homology domain, K117–N130 of scRpn13 would be α-helical, consistent with secondary structure predictions for K119–G127. Residues S106–G127 are absent, however, from all acquired spectra, suggesting that this region undergoes conformational exchange and does not form a rigid helix. In contrast, the cognate residues in mRpn13 and hRpn13 do form helices (*93*). K117–N130 of scRpn13 shares 35.7% sequence identity with mRpn13, but the presence of a glycine at position 127 likely destabilizes the helix, as might substitution of the sequence QDE at the beginning of the helix with the more basic sequence KDK in scRpn13. Also, a salt bridge, described in Chapter 3, between E119 and R122 of mammalian Rpn13 is lost, as R122 is substituted with N123 in scRpn13.

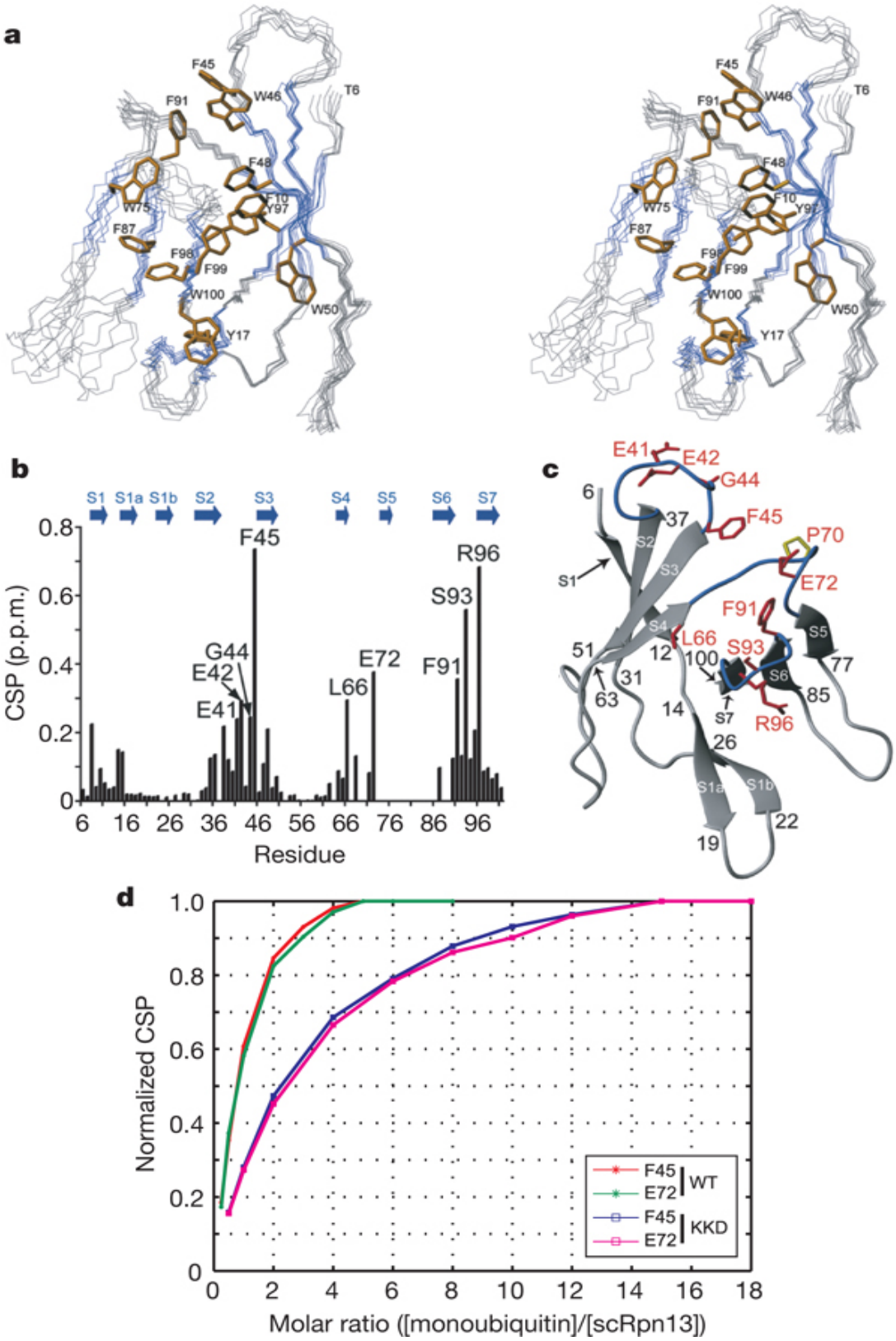
a
F45
W46
T6
F91
F48
F10
Y97
W75
F87
F98
F99
W100
W50
Y17
b
S1 S1a S1b S2 S3 S4 S5 S6 S7
CSP (p.p.m.)
0.8
0.6
0.4
0.2
0
F45
R96
S93
G44
E42
E41
E72
L66
F91
6 16 26 36 46 56 66 76 86 96
Residue
c
E41
E42
G44
6
37
F45
P70
S1
S2
S3
E72
F91
S4
L66
S93
S5
51
12
100
77
31
S6
63
85
14
S7
R96
26
S1a
S1b
22
19
d
Normalized CSP
1.0
0.8
0.6
0.4
0.2
0
0 2 4 6 8 10 12 14 16 18
Molar ratio ([monoubiquitin]/[scRpn13])
F45
E72
WT
F45
E72
KKD

Figure 2.3. Rpn13 uses loops to bind ubiquitin. (A) Stereo view of scRpn13, spanning residues T6–L101, in which β-strands are indicated in blue and hydrophobic side chains in yellow. (B) NMR titration experiments reveal scRpn13 residues that contact ubiquitin. The data were prepared as described in Methods and plotted. (C) ScRpn13 residues that bind ubiquitin are within the S2–S3, S4–S5 and S6–S7 loops. Residues significantly affected by ubiquitin addition are displayed and labeled in red with their secondary structures in blue. (D) scRpn13-KKD affinity for monoubiquitin is significantly reduced compared with wild type. Normalized chemical-shift perturbation values are plotted against molar ratios of monoubiquitin to wild-type scRpn13 (WT, red, green) or monoubiquitin to scRpn13-KKD (KKD, blue, purple). Each data line represents a specific amino acid, namely F45 (red and blue) and E72 (green and purple). Using Matlab version 7.2, the data were fitted to determine a binding constant of 65 μM for wild-type scRpn13 and an eightfold reduction in the affinity of scRpn13-KKD for monoubiquitin.

To determine how scRpn13 binds ubiquitin, we performed an NMR titration series (Figure 2.S1), which implicated E41, E42, G44, F45, L66, E72, F91, S93 and R96 as being at the ubiquitin contact surface (Figure 2.3B). Interestingly, these residues are in the S2–S3, S4–S5 and S6–S7 loops (Figure 2.3C). The S4–S5 loop is strongly conserved in higher eukaryotes, as is F91, which is in the S6–S7 loop (Figures 2.1C and 2.3A). scRpn13 binding to monoubiquitin is in 'fast exchange' by NMR, which is ideal for determining binding affinity by this method, and the affinity of scRpn13 for monoubiquitin was determined to be 65 μM (Figure 2.3D).

2.3.4 Rpn13 binds K48-linked diubiquitin with high affinity

We used NMR titration experiments to determine the stoichiometry of hRpn13 for monoubiquitin, K48-linked diubiquitin and tetraubiquitin (see Section 2.7.1). Monoubiquitin and diubiquitin bound to Rpn13 with 1:1 stoichiometry, whereas two Rpn13 molecules bound one tetraubiquitin (Figure 2.4A,B). Therefore, although three

potential diubiquitin elements exist within tetraubiquitin, no more than two Rpn13 molecules can be accommodated simultaneously. The exclusion of a third Rpn13 molecule is consistent with model structures of Rpn13–tetraubiquitin, in which steric clashes arise when three hRpn13 molecules bind neighboring K48-linked ubiquitin subunits (Figure 2.S2). That Rpn13 binds diubiquitin elements of K48-linked chains is further validated in Chapter 3.

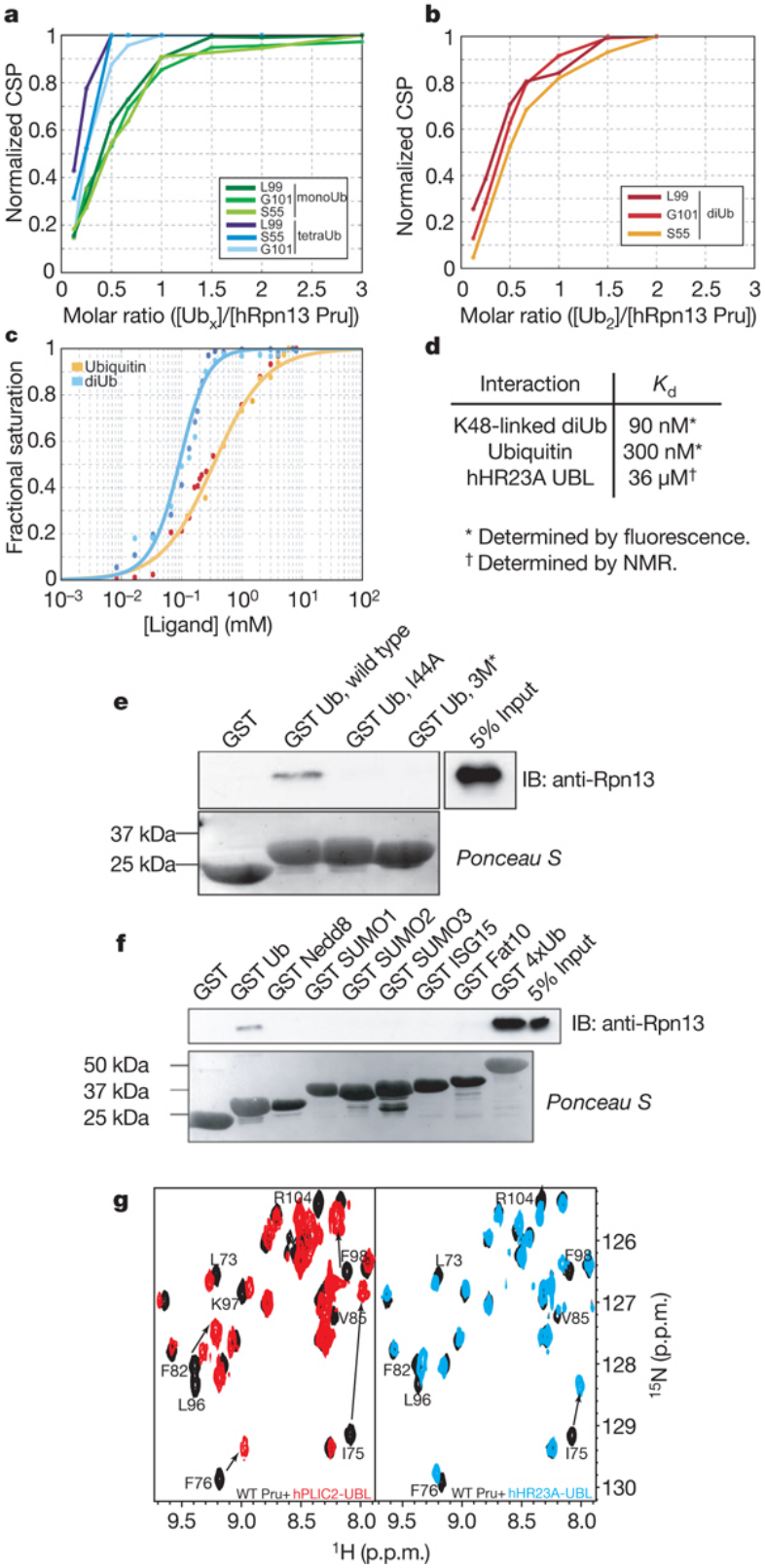
a
Normalized CSP
Molar ratio ([Ub$_x$]/[hRpn13 Pru])
L99
G101
S55
monoUb
L99
S55
G101
tetraUb
b
Normalized CSP
Molar ratio ([Ub$_2$]/[hRpn13 Pru])
L99
G101
S55
diUb
c
Fractional saturation
[Ligand] (mM)
Ubiquitin
diUb
d
Interaction | K_d
K48-linked diUb | 90 nM*
Ubiquitin | 300 nM*
hHR23A UBL | 36 μM†
* Determined by fluorescence.
† Determined by NMR.
e
GST
GST Ub, wild type
GST Ub, I44A
GST Ub, 3M*
5% Input
IB: anti-Rpn13
37 kDa
25 kDa
Ponceau S
f
GST
GST Ub
GST Nedd8
GST SUMO1
GST SUMO2
GST SUMO3
GST ISG15
GST Fat10
GST 4xUb
5% Input
IB: anti-Rpn13
50 kDa
37 kDa
25 kDa
Ponceau S
g
R104
L73
F98
K97
V85
F82
L96
I75
F76
WT Pru+ hPLIC2-UBL
WT Pru+ hHR23A-UBL
^{15}N (p.p.m.)
^{1}H (p.p.m.)

Figure 2.4. Rpn13 binds to ubiquitin and UBLs of proteasomal receptors. (A),(B) hRpn13 Pru binds K48-linked diubiquitin and monoubiquitin with 1:1 stoichiometry, whereas two hRpn13 Pru molecules bind one K48-linked tetraubiquitin. Normalized chemical shift perturbation values are plotted against varying molar ratios of Rpn13 to tetraubiquitin ((A), shades of blue), diubiquitin ((B), shades of red), or monoubiquitin ((A), shades of green) to reveal respective Rpn13–ubiquitin binding stoichiometries of 2:1, 1:1 or 1:1. Each data line represents a specific amino acid as indicated in the figure, with values determined as described in Section 2.6.1 (C) Binding curves for hRpn13 Pru binding to monoubiquitin or K48-linked diubiquitin as determined by intrinsic tryptophan fluorescence. Normalized fluorescence intensity values are plotted for two data sets against varying concentrations of monoubiquitin (red and orange) or diubiquitin (blue and light blue). The data were fitted by assuming 1:1 binding for hRpn13 Pru and monoubiquitin (orange) or diubiquitin (light blue). (D) Table of hRpn13 Pru binding affinities for K48-linked diubiquitin, monoubiquitin and the UBL domain of hHR23a. Values for ubiquitin binding were determined by using the fluorescence data of (C). NMR titration curves were used to determine the value for the UBL domain of hHR23a. (E) mRpn13 Pru binds to the hydrophobic patch of ubiquitin containing I44. mRpn13 Pru domain was used in GST pull-down assays to assess binding to GST-tagged monoubiquitin and its mutant derivatives (I44A and triple mutant (3M*) L8–I44–V70). **f**, mRpn13 Pru domain was used in GST pull-down assays (as in (E)) to assess its binding to GST-fused ubiquitin-like protein modifiers. (G) Rpn13 binds to the hPLIC2 and hHR23A UBL domains. ^{1}H, ^{15}N heteronuclear single-quantum coherence spectra of ^{15}N-labelled hRpn13 Pru alone (black) and with twofold molar excess hPLIC2 (red) or hHR23A (blue) UBL domain indicates their direct interaction. Although the effect is greater for hPLIC2, these two UBL domains affect common residues in hRpn13 Pru, suggesting that they bind the same surface.

In contrast to scRpn13, resonances broaden and shift as hRpn13 Pru binds monoubiquitin (Figure 2.S3). This behavior is associated with stronger K_d values, but prohibits their accurate calculation by the method used to determine the scRpn13–ubiquitin affinity. Fluorescence spectrophotometry was therefore used to determine hRpn13's affinity for monoubiquitin and diubiquitin, as hRpn13 (residues 1–150) contains two tryptophan residues and ubiquitin none. hRpn13 showed a surprisingly high affinity, with a K_d value for monoubiquitin of about 300 nM (Figure 2.4C,D) and for diubiquitin of about 90 nM (Figure 2.4C,D). The value for diubiquitin binding is about 15-fold lower than that of hHR23a for tetraubiquitin (*67*). The higher affinity of hRpn13

for ubiquitin, compared with scRpn13, reflects amino-acid substitutions at the contact surface. For example, residues F76 and D78 of hRpn13 were implicated in hRpn13 binding to monoubiquitin, as discussed in Chapter 3. In scRpn13, however, these residues are substituted with isoleucine and glycine, respectively.

2.3.5 Rpn13 recognizes a subset of ubiquitin-like proteins

We next analyzed whether Rpn13 exhibits specificity for ubiquitin or broadly recognizes ubiquitin family members. Using GST pull-down assays, we confirmed that ubiquitin binds to full-length mRpn13 and that this interaction requires ubiquitin's hydrophobic patch, consisting of L8, I44 and V70 (Figure 2.4E). mRpn13 bound more potently to linear tetraubiquitin expressed as a GST fusion (GST 4×Ub) or to purified K48-linked chains than to monoubiquitin (Figure 2.4E and data not shown). Under the same experimental conditions, no binding was observed between the mRpn13 Pru domain and SUMO, Nedd8, ISG15 or FAT10 (Figure 2.4F). By contrast, mRpn13 appeared to bind to the UBL domains of multiple UBL/UBA proteins (Figures 2.S4 and 2.S5). We verified that hRpn13 Pru binds directly to the hHR23a and hPLIC2 UBL domains by NMR (Figure 2.4G), and determined a K_d value of 36 μM for the hRpn13 Pru–hHR23a UBL domain complex (Figures 2.4G and 2.S5). Overlapping residues in hRpn13 were affected by the addition of these UBL domains (Figure 2.4G) or ubiquitin (*93*), suggesting that these interactions may be mutually exclusive.

2.3.6 Rpn13 mutant defective in ubiquitin recognition

Experiments described above implicated residues in Rpn13's S2–S3, S4–S5 and S6–S7 loops in binding ubiquitin (Figure 2.3). After introducing non-conservative substitutions for these residues individually or in combination, the resulting proteins were expressed in *Escherichia coli*, purified and characterized. We sought mutants that were defective in ubiquitin chain binding while being properly folded and proficient in proteasome binding. Separation of these functions is critical, as exemplified by previous studies of proteasomal ubiquitin receptor Rpn10. The *rpn10*Δ phenotype does not accurately reflect its function in ubiquitin recognition, because Rpn10 plays additional roles in the proteasome (*157, 176*). The proteasome is destabilized in the absence of Rpn10 (ref. (*176*)), as is also observed in *rpn13*Δ mutants, at least under certain *in vitro* conditions (Figure 2.2; ref. (*175*)). For Rpn13, unlike Rpn10, proteasome and ubiquitin binding are conferred by the same structural domain, and thus can be effectively separated only by precisely targeted mutations. Moreover, ubiquitin contact residues in Rpn13 are distributed over three distinct loops, and thus differ from those of Rpn10 by being non-contiguous and so not subject to simple block mutagenesis.

We assayed Rpn13–proteasome binding by adding GST–Rpn13 to purified proteasomes. Because of the GST moiety, the fusion protein results in strong electrophoretic retardation in native gels; this effect is seen with *rpn13*Δ but not wild-type proteasomes (Figure 2.5A). Thus Rpn13 assembled into the proteasome was not exchangeable with added GST–Rpn13, indicating that scRpn13 is a true proteasome subunit. Two putative ubiquitin contact-site mutants of Rpn13 were shown to be

proficient in proteasome assembly (Figure 2.5B). Several other mutants failed to pass this and other preliminary assays, typically because of global folding defects (data not shown). E41 and E42 are in the S2–S3 loop, and S93 in the S6–S7 loop (Figure 2.5C). These sites, though greater than 22 Å apart, are both situated proximally to bound ubiquitin in a model based on the mRpn13–monoubiquitin structure described in Chapter 3 (Figure 2.5C).

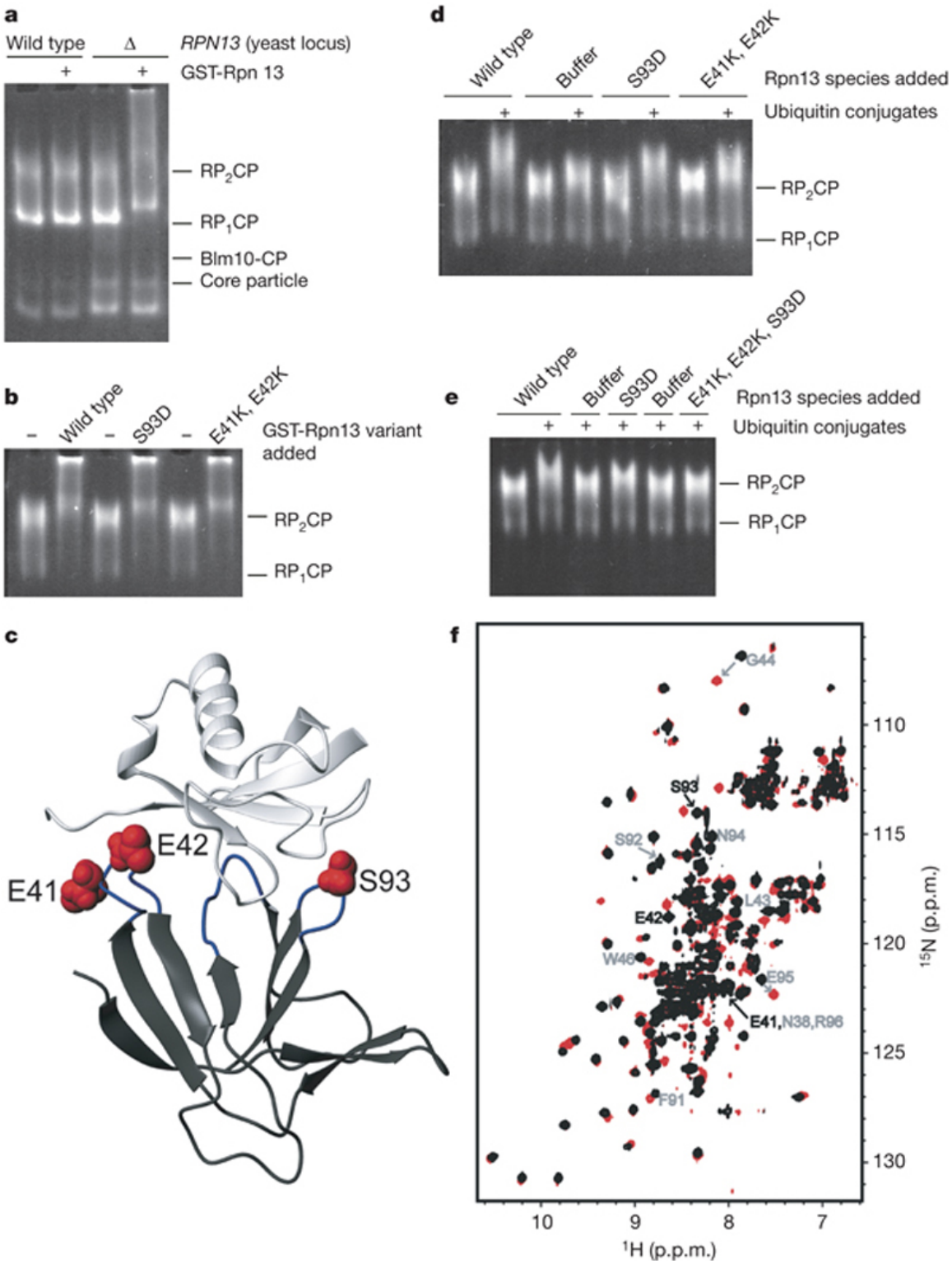

Figure 2.5. An Rpn13 mutant specifically defective in ubiquitin chain binding. (A) Reconstitution of proteasomes with recombinant GST–Rpn13. Proteasomes were purified

from strains containing or lacking Rpn13 (SY775 and SY723). GST–Rpn13 (40 pmol) or buffer was mixed with proteasomes (5 pmol), which were resolved on native PAGE and visualized using suc–LLVY–AMC. The mobility shift caused by GST–Rpn13 is an indicator of its assembly into proteasomes. The presence of GST on Rpn13 is required to cause a mobility shift. All proteasomes used in this figure are from an *rpn10-uim ubp6*Δ genetic background. (B) Mutations in Rpn13 do not attenuate assembly of Rpn13 into the proteasome. Reconstitution assays were performed as in (A), but using a fourfold molar excess of GST–Rpn13. (C) Structural model with mutations. Mutated residues (see (D)-(F)) were mapped onto a model structure of scRpn13 (dark grey) complexed with monoubiquitin (light grey). E41, E42 and S93 are displayed in red, ubiquitin-binding loops in blue. These residues map to the S2–S3 (E41K, E42K) and S6–S7 (S93D) loops. (D) Mutations in single loops of Rpn13 attenuate its proteasomal ubiquitin receptor function. Rpn13 variants (12 pmol) cleaved from GST were incubated with proteasomes (3 pmol) to allow reassembly. Autoubiquitinated Cdc34 (18 pmol) was then added. After 15 min at 30 °C, complexes were resolved by native PAGE and visualized using suc–LLVY–AMC. (E) Rpn13 mutant E41K, E42K, S93D (Rpn13-KKD) abrogates the ubiquitin receptor activity of Rpn13. Experiment performed as in (D). (F) Superposition of ^{1}H, ^{15}N heteronuclear single-quantum coherence spectra of wild-type Rpn13 (black) and Rpn13-KKD (red). Shifted resonances are labeled in grey, and those corresponding to E41, E42 and S93 in black. Chemical shift assignments are only available for the wild-type protein.

To assay mutational effects on ubiquitin chain binding, we used the native gel-based assay introduced in Figure 2.2A. Note that the mobility shift resulting from addition of GST–Rpn13 to the proteasome (Figure 2.5A,B) is irrelevant to the chain-binding assay, because Rpn13 itself does not affect proteasome migration in gels. Only the larger GST-tagged form of Rpn13 can do so, and, in the ubiquitin chain-binding assay, untagged Rpn13 was used. Neither the S93D mutant nor the E41K, E42K mutant conferred a strong defect in the proteasome–ubiquitin interaction, although both conferred reduced mobility shifts compared with wild-type Rpn13 (Figure 2.5D). To impair ubiquitin binding further, we combined the S2–S3 and S6–S7 mutations. The resulting protein, a E41K, E42K, S93D triple mutant, referred to as scRpn13-KKD, was comparable to a buffer control in its influence on the proteasome's electrophoretic

mobility in the presence of ubiquitin conjugates (Figure 2.5E). NMR titrations revealed that scRpn13-KKD binds monoubiquitin approximately eightfold more weakly than wild type (Figure 2.3D; see also Section 2.7). To ensure that these mutations did not affect Rpn13 structural integrity, we compared a ^{1}H, ^{15}N heteronuclear single-quantum coherence spectrum recorded on ^{15}N-labelled scRpn13-KKD with that of wild type (Figure 2.5F). Only resonances corresponding to the mutated residues or their immediate neighbors were shifted, indicating that these surface mutations did not affect Rpn13's structure. In addition, we identified the hRpn13 surface that binds Rpn2, which is remote from the substituted residues (*93*). The corresponding surface in scRpn13 is preserved in Rpn13-KKD as none of the residues within it were affected. Thus, Rpn13-KKD appeared to be suitable for *in vivo* analysis of the physiological function of ubiquitin recognition by Rpn13.

2.3.7 Phenotype of the Rpn13-ubiquitin binding-site mutant

To test the biological significance of the Rpn13–ubiquitin interaction, we integrated the triple mutant allele into yeast in place of the wild-type chromosomal sequence. Functional defects in proteasomes can be revealed by plate assays such as sensitivity to the arginine analogue canavanine, whose incorporation into proteins causes misfolding and accelerated degradation. The enhanced substrate load is lethal to mutants lacking proper proteasome function (see, for example, ref. (*156*)). *rpn13-KKD* mutants proved sensitive to 8 μg ml^{-1} of canavanine when in the genetic background of an *rpn10-uim* mutation (Figure 2.6A). Thus, the *rpn13-KKD* mutation leads to a defect in

proteasome function, and interacts synthetically with another specifically targeted proteasomal ubiquitin receptor mutation. Because Rpn13 can bind UBL/UBA proteins (Figure 2.4G), we also investigated its genetic relationship with Dsk2 and Rad23. *rpn13-KKD* also showed a strong synthetic interaction with a null allele of proteasomal ubiquitin receptor Dsk2 (Figure 2.6A). In the case of Rad23, the genetic interaction was comparatively modest. These data support the view that the docking of ubiquitin conjugates at the proteasome by UBL/UBA proteins is not mediated obligatorily by Rpn13. In addition, binding assays performed with purified proteasomes and the UBL domains of Rad23 and Dsk2 indicate that Rpn13 is not the sole receptor for UBL/UBA proteins on the proteasome (Figure 2.S7). The results of the binding assays are consistent with our previous report that proteasome subunit Rpn1 binds UBL/UBA proteins (*165*). Further work is required to define more precisely the extent to which Rpn13-dependent docking of ubiquitin conjugates at the proteasome is mediated or regulated by UBL/UBA proteins.

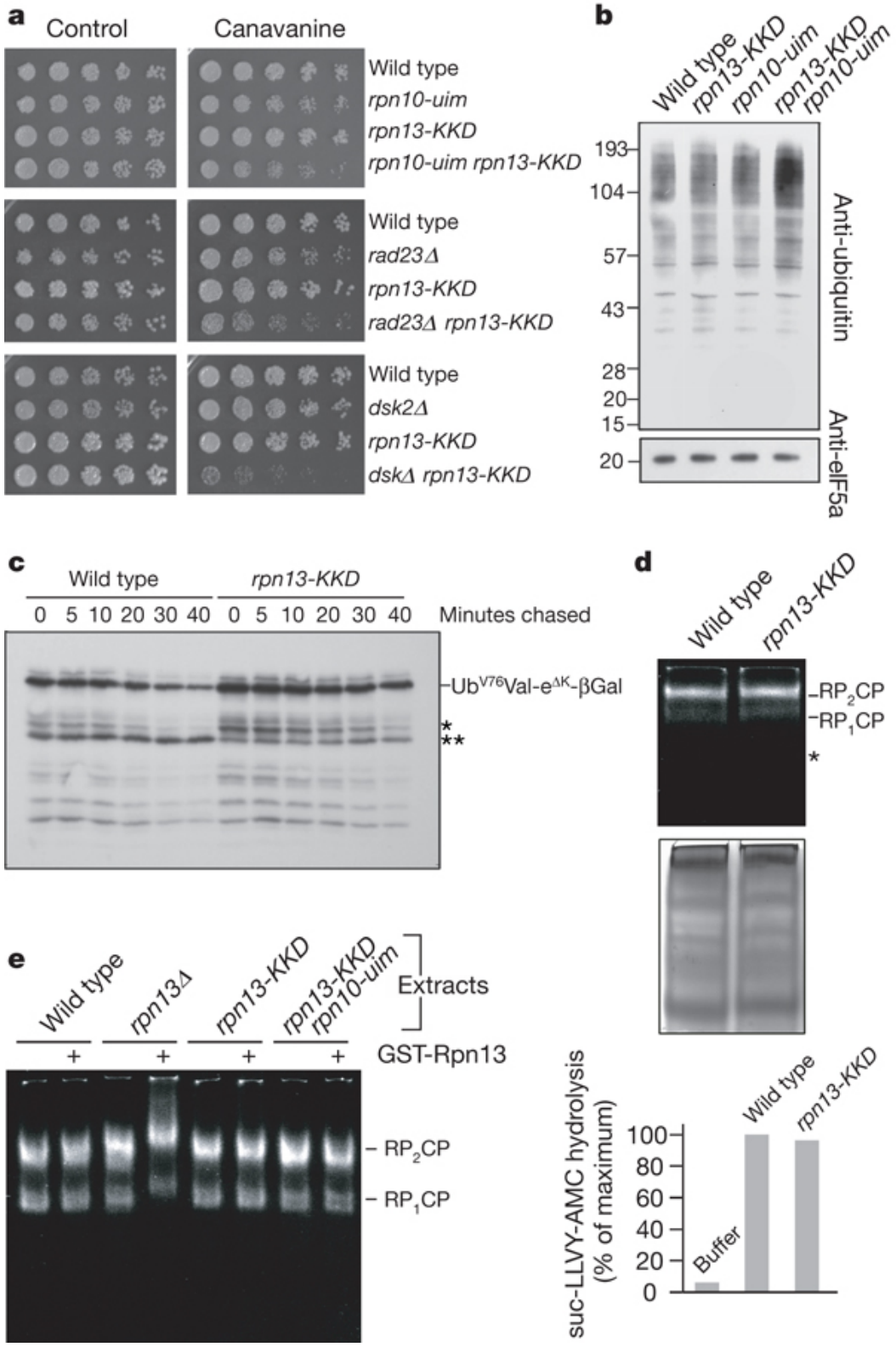

Figure 2.6. Phenotypic effects of the loss of ubiquitin receptor function by Rpn13. (A)

Canavanine sensitivity of single and double mutants in ubiquitin receptor genes. Cells in late log phase (top: SY998b, SY980f, SY1004c and SY920b; middle: SY1076, SY1073a, SY1012a and SY1080a; bottom: SY1076, SY1074a, SY1012a and SY1082a) were serially diluted and stamped on plates using a pin array. Plates were incubated at 30 °C for either 2 (left) or 3 (right) days. (B) Endogenous ubiquitin conjugate levels in proteasomal ubiquitin receptor mutants. Cells (SY998a, SY980a, SY1004a and SY920a) were grown to log phase, and whole-cell extracts prepared. Proteins were resolved by 4–12% gradient SDS–PAGE, transferred to polyvinylidene fluoride, and probed with antibody against ubiquitin. The membrane was stripped and probed with antibody against eIF5a. (C) Substrate stabilization in *rpn13-KKD* mutants. Cells (SY992b, SY1004b) expressing Ub^{V76}–Val-eΔ^{K}–β-gal from a *GAL* promoter were grown to mid-log phase under inducing conditions. Protein synthesis was quenched at time zero by adding cycloheximide. Aliquots were withdrawn at the time points indicated, and lysates prepared. Proteins were visualized by SDS–PAGE/immunoblot analysis, using an antibody to β-galactosidase, and quantified with imaging software (KodakEDAS 290). The rate of degradation of Ub^{V76}–Val-eΔ^{K}–β-gal was reduced approximately twofold in the *rpn13-KKD* mutant compared with wild type. Asterisks indicate distinct β-galactosidase-derived partial breakdown products, whose relative intensities differ between wild type and mutant. (D) *rpn13-KKD* mutants are not deficient in proteasome levels. Cells (SY992a, SY1004a) were grown and lysed as in **e**. Extract (150 μg) was resolved by native PAGE, and proteasome complexes visualized using suc–LLVY–AMC (top) and Coomassie blue as a loading control (middle). The asterisk indicates the expected position of the proteasome core particle, which is not visualized owing to low levels. Extracts were also subject to a quantitative proteasome assay, using suc–LLVY–AMC (bottom). (E) Proteasomes from *rpn13-KKD* mutants are loaded with Rpn13-KKD protein. Cells (SY933, SY936, SY950 and SY952) were grown to late log phase at 30 °C in yeast extract (10 g l^{-1}), peptone (20 g l^{-1}) and dextrose (20 g l^{-1}) (YPD), harvested and lysed as described (see Section 2.6.1). Extract (100 μg) was incubated with 1 μg of either GST–Rpn13 (+ lanes) or GST only (samples where GST–Rpn13 is absent) on ice. Proteasome complexes were resolved by native PAGE and visualized by suc–LLVY–AMC overlay assay.

To test whether amino-acid substitutions in the ubiquitin-binding loops of Rpn13 can lead to global defects in ubiquitin metabolism, whole-cell extracts from our mutants were examined by immunoblotting. High molecular mass ubiquitin conjugates, which are enriched in proteasome substrates, accumulated in the *rpn13-KKD rpn10-uim* double mutant (Figure 2.6B). The defect is synthetic, as with the canavanine sensitivity of the double mutant (Figure 2.6A). We also observed an *in vivo* proteolytic defect in the *rpn13-*

KKD mutant (Figure 2.6C), using the model proteasome substrate Ub^{V76}–Val-$e^{\Delta K}$–β-gal (ref. (*177*)), which was previously found to be stabilized in an *rpn13*Δ mutant (*167*).

Defects in proteasome assembly have been observed in *rpn13*Δ proteasomes (Figure 2.2; ref. (*175*)), and could potentially account for the phenotypes observed in Figure 2.6A–C. We therefore analyzed the assembly state of *rpn13-KKD* proteasomes by running native gels on freshly prepared, unfractionated cell extracts (*178*). We observed no significant change in level, assembly or peptidase activity in *rpn13-KKD* proteasomes (Figure 2.6D). Surprisingly, no assembly defect was observed for *rpn13*Δ proteasomes (Figure 2.6E). Thus, assembly defects previously observed for *rpn13*Δ proteasomes are apparently a result of *in vitro* handling.

Although the recombinant Rpn13-KKD protein is properly folded and assembled onto purified proteasomes *in vitro*, it remained possible that the mutant protein would be absent from proteasomes *in vivo* as a result of its being rapidly degraded. To assess the extent of Rpn13-KKD loading of endogenous proteasomes, we used the GST–Rpn13 add-back assay of Figure 2.5a, where purified proteasomes were used. In unfractionated cell extracts, GST–Rpn13 similarly shifted *rpn13*Δ proteasomes (Figure 2.6E). *rpn13-KKD* proteasomes behaved as wild type in this assay, indicating that they were fully loaded with Rpn13-KKD. We conclude that the phenotypes of the *rpn13-KKD* mutant do not reflect deficient proteasome assembly or deficient loading of Rpn13 onto proteasomes, but are specifically related to its impaired ubiquitin-binding site.

2.4 Discussion

We report here the identification of a new ubiquitin receptor for the proteasome, Rpn13, which is unrelated to Rpn10 and the three UBL/UBA proteins. Moreover, Rpn13 defines a new class of ubiquitin recognition surfaces, differing dramatically from other proteasomal ubiquitin receptors. First, whereas the UBL/UBA proteins (and perhaps Rpn10) have distinct ubiquitin- and proteasome-binding domains that are separated by flexible linkers, Rpn13 is docked into the proteasome through a surface that is in close spatial proximity to its ubiquitin-binding region. Thus Rpn13 may provide for a ubiquitin chain with precise positioning and polarity. Second, the UBL/UBA proteins, having a large population free of the proteasome and often multiple ubiquitin-binding domains, are better equipped than Rpn13 to capture ubiquitinated substrates and then deliver them to the proteasome. Third, UBL/UBA proteins are also capable of protecting the chain during transit to the proteasome, as they inhibit deubiquitination (*157, 179, 180*). In striking contrast, Rpn13 promotes chain deubiquitination (*163, 169, 171*). Binding to Rpn13 both facilitates the deubiquitinating activity of Uch37 (refs (*171*) and (*163*)) and links Uch37 to the proteasome, suggesting that Rpn13 plays a major role in ubiquitin chain disassembly at the proteasome. Third, Rpn13 is exceptionally proficient at binding monoubiquitin and diubiquitin compared with other ubiquitin receptors associated with proteasome-mediated degradation. Although it is widely supposed that extended ubiquitin chains are required for degradation, contrary observations have been reported, in which monoubiquitin targets proteins to the proteasome (*174, 181, 182*). Such substrates, although possibly rare, may be more strongly dependent on Rpn13 than those marked by

chains.

Rpn13 resembles Rpn10 in its ability to bind ubiquitin-like domains of the UBL/UBA ubiquitin receptors (Figure 2.4D,G and Figures 2.S4 and 2.S5), implying that Rpn13 may recruit substrates to the proteasome directly or indirectly through UBL/UBA proteins. These observations support a hypothetical model whereby conjugates bind UBL/UBA family members, which dock them to the proteasome and pass them to the intrinsic receptors Rpn10 and Rpn13. In addition, compound complexes may be formed, in which a single conjugate is simultaneously bound by an intrinsic ubiquitin receptor and a UBL/UBA protein. Compound complexes may be favored when longer chains are delivered, leading to more stable chain–proteasome interactions, and thus more rapid substrate degradation.

Ubiquitin and the proteasome are both essential, but remarkably the inactivation of all five known proteasomal ubiquitin receptors in the same yeast strain does not appear to be lethal (data not shown). In our assays, the residual chain-binding capacity of *rpn10-uim rpn13-KKD rad23*Δ *dsk2*Δ *ddi1*Δ proteasomes is modest (Figure 2.5E), suggesting that the highest-affinity intrinsic receptors are now known. The unidentified receptor may be of lower affinity but comparable functionality, or it may be a receptor of typical affinity that is not intrinsic to the proteasome, such as Rad23/hHR23.

The phenotypic properties of multiply receptor-deficient strains suggest functional redundancy (Figure 2.6; refs (*156*) and (*179*)). This may reflect robustness in their principal function of delivering substrate to the proteasome. Given the number of known receptors, it is likely that docking of the chain at any of multiple locations in the

proteasome will support breakdown of the target protein. However, there is apparently a deeper and more interesting functional relationship among ubiquitin receptors as well, in which they play distinct roles. For example, they have various phenotypes in isolation, albeit not lethal ones. Furthermore, proteasome function appears substantially compromised in multiple receptor-deficient strains (refs (*156*) and (*179*), and S.E. and D.F., unpublished observations). When different receptor mutants are compared, the relative strengths of the degradation defects vary from substrate to substrate (*157*). Thus, the receptors show *in vivo* specificity, although it remains unclear how specific they are and what the mechanistic basis of this specificity is. Finally, functionally redundant behavior as inferred from mutant phenotypes may not reflect the functioning of the wild-type system in a straightforward manner, because compensation can mask differentiated activities. With more detailed characterization, the individuality of proteasomal ubiquitin receptors and its mechanistic basis should become clearer.

2.5 Methods summary

2.5.1 Yeast genetics and two-hybrid screen

Standard methods were used for yeast genetics, growth assays and protein turnover assays (see Section 2.7.1). A complete list of yeast strains is given in Section 2.7.1.12 (Table 2.1). Sequences corresponding to mouse ubiquitin lacking two terminal glycines (UbΔGG) were subcloned into pYTH9 vector (*183*), creating fusion proteins with the Gal4 DNA-binding domain (bait). Yeast strain Y190 was transformed with bait vector, and human fetal brain complementary DNA (cDNA) library (Clontech) was

screened as previously described (*183*).

2.5.2 Antibodies and plasmids

Antibodies used were: anti-myc (9E10) and anti-Ub (P4D1) from Santa Cruz Biotechnology; anti-ADRM1 (anti-Rpn13) from Biomol; and anti-β-galactosidase (Promega). All constructs used in this study are described in Section 2.7.1.

2.5.3 Protein purification and biochemical assays

Recombinant proteins were expressed in and purified from Rosetta cells (Novagen). Proteasome was affinity-purified essentially as described (*184*). Immunoprecipitation, immunoblotting and GST pull-down assays were performed as previously described (*119*). Native gel analysis was performed as in ref. (*156*). More detailed descriptions are available in Section 2.7.1.

2.5.4 NMR spectroscopy

We determined the structure of full-length scRpn13 as described in Section 2.7.1, with the data summarized in Table 2.S1. The resulting structures are available through Protein Data Bank accession number 2Z4D. Binding surfaces and affinities were determined as described in Section 2.7.1.

2.6 Supplementary information

2.6.1 Material and methods

2.6.1.1 Plasmids for expression of mammalian proteins

The expression construct encoding full-length wild-type mRpn13 was kindly provided by Dr. N. Lamerant and described previously(*185*). Full-length mRpn13 cDNA was subcloned into pcDNA3-myc (*EcoRI/XhoI*) and pGEX-4T1 (*BamHI/XhoI*, Amersham) vectors and used for subsequent subcloning of different deletion mutants. UBL domains of hHR23A, hHR23B, hPLIC2 and Ddi1 were subcloned into pGEX-4T1 (*BamHI*, Amersham). Fat10-pGEX-4T3 was a generous gift of M. Groettrup. GST-Ub, GST-4xUb, GST-SUMO1, GST-SUMO2 and Nedd8-pGEX-2TK were kindly provided by Drs. L. Hicke, E. Friedberg, J. Palvimo, F. Melchior and K. Tanaka, respectively. ISG15 was subcloned into pGEX-4T1.

2.6.1.2 GST pull-down assays

For assaying binding of ubiquitin to immobilized ligands, GST-fused tetraubiquitin was absorbed to resin, then cleaved with thrombin (Novagen) for 4 h at 4°C in a cleavage buffer containing 20 mM Tris-HCl (pH 8.4), 150 mM NaCl, 2.5 mM $CaCl_2$ and 1 mM DTT. Thrombin was inactivated with addition of PMSF, and GST bound to resin was removed by centrifugation. Supernatant was incubated with immobilized GST-fusion proteins in incubation buffer (cleavage buffer with 10% glycerol and 1% Triton X-100). After 5 hours of incubation at 4°C, beads were washed three times with incubation buffer. Bound proteins were boiled for 5 minutes in SDS sample buffer and analyzed by

SDS-PAGE and immunoblotting. The same approach was used for assaying binding of GST-fused mRpn13 cleaved with thrombin to different ubiquitin mutants and UBLs, which were expressed as GST-fused proteins.

2.6.1.3 Plasmids for expression of yeast proteins

An expression construct for GST-scRpn13 was generated by cloning the scRpn13 ORF into a derivative of pGEX-6P1 (GE Healthcare), which includes an HMK site (TRRASV). The PreScission protease site (LEVLFQGP) in this variant is followed by LTRRASVGS, where GS coincides with an in-frame BamHI site used for cloning. The *scRPN13* ORF follows the GS directly. Mutations giving rise to *scRPN13* variants were made by using a matched pair of oligos and amplifying with iProof (BioRad). They were verified by sequencing. *RPN13* integrating constructs were prepared by assembling a series of modules: the *RPN13* ORF, the 3' UTR from *CYC1*, the natMX cassette (*186*) and the *RPN13* 3'UTR. For the *rpn13- E41K, E42K, S93D* mutation, a diagnostic restriction site was engineered upstream of the mutations. Further details are available upon request.

2.6.1.4 Strain construction

Disruptions of *RAD23, DSK2, DDI1,* and *UBP6* are precise ORF replacements using the markers indicated. (For marker descriptions, see (*186-188*)) The Protein A sequence fused to RPN11 has been described previously (*184*). The reporter construct *Pcup-Ub-K-TRP1::hphMX* is as described previously (*189*), except that the original

natMX marker has been replaced by hphMX through recombination via the regions of homology within the MX cassettes. Modifications in the *RPN10* gene are as described previously (*156*), except that the kanMX cassette was used in place of the previously reported natMX cassette. Modifications at the *RPN13* locus were made using the integrative constructs described above.

2.6.1.5 Proteasome purification

Proteasomes were purified essentially as described (*156*). Cells were grown to late log phase (OD_{600} of roughly 6.0) and harvested by centrifugation. Cells were resuspended in lysis buffer (50 mM Tris-HCl [pH 8.0], 1 mM EDTA, 5 mM $MgCl_2$, and 1 mM ATP), and lysed by French press. Extract was cleared by centrifugation at 20,000 g and 4°C for 30 minutes, then filtered through coarse filter paper (porosity excluding 25 μm particles [VWR]). Cleared extract was incubated with IgG Sepharose (MP Biomedicals) for 90 min at 4°C with tumbling. Resin was washed with 25 bed volumes of column buffer (50 mM Tris-HCl [pH 7.4], 1 mM EDTA, 5 mM $MgCl_2$, 1 mM ATP, and 100 mM NaCl), then with 10 bed volumes of elution buffer (50 mM Tris-HCl [pH 7.4], 1 mM EDTA, 5 mM $MgCl_2$, 1 mM ATP). Protein was released from the column by incubation with TEV protease (Invitrogen), which acts on the cleavage site between Protein A and Rpn11. For visualization of proteasome in extract, extract was prepared as described above through the filtration step, and in the presence of protease inhibitors (250 ug/ml AEBSF, 160 ug/ml benzamidine, and 1 ug/ml leupeptin [Sigma]). Core particle was purified conventionally (*190*).

2.6.1.6 Recombinant Rpn13

GST-Rpn13 and mutant variants were expressed in pGEX-based vectors. Cells were grown at 24°C to an OD_{600} of roughly 0.8, and expression was induced by the addition of IPTG to 250 µM. Induction was allowed to continue overnight. Cells were harvested by centrifugation, then resuspended and lysed in lysis buffer (50 mM Tris-HCl [pH 7.4], 100 mM NaCl, 1 mM DTT, 1 mM ATP, 1 mM EDTA, 1 mM EGTA, 125 µg/ml AEBSF, 160 µg/ml benzamidine, 2.5 µg/ml leupeptin), then cleared by centrifugation at 20,000 g and 4°C for 30 minutes. Fusion proteins were adsorbed to Glutathione Sepharose (GE Healthcare) for 90 min, and unbound material was removed by a series of batch washes with wash buffer (50 mM Tris- HCl [pH 7.4], 100 mM NaCl, 1 mM DTT). Resin was equilibrated in elution buffer (50 mM Tris-HCl [pH 7.4], 100 mM NaCl, 1 mM DTT, 10% glycerol), and bound protein was eluted with 20 mM glutathione in elution buffer. When required, GST was cleaved from the fusion proteins by incubating with PreScission protease (GE Healthcare) overnight at 4°C.

2.6.1.7 Preparation of ubiquitin conjugates

HIS-Cdc34 and HIS-Uba1 were purified as previously described (*165*). Ubiquitin, purified from bovine red blood cells, was purchased from Sigma. Conjugates were prepared by incubating 1.5 µM HIS-Uba1, 2 µM HIS-Cdc34, and 50 µM ubiquitin in buffer (20 mM Tris-HCl [pH 7.5], 10 mM $MgCl_2$, 0.1 mM DTT, and 2 mM ATP) for 15 to 20 hours at 30°C.

2.6.1.8 Native gel assays

Native gels were prepared, run, and developed essentially as previously described (*191*). Briefly, native PAGE gels containing 3.6% acrylamide (acrylamide:bisacrylamide::40:1) were prepared and run in buffer containing 90 mM Tris base, 90 mM boric acid, 6 mM $MgCl_2$, 0.5 mM EDTA, 1 mM ATP. Gels were run at 4°C, 100 V, and for 2.5 to 3.5 hours. Bands containing catalytically active proteasomes were identified by incubating with 100 μM suc- LLVY-AMC in 50 mM Tris-HCl (pH 7.4), 6 mM $MgCl_2$, and 1 mM ATP for 15 minutes at 30°C. Cleavage products were visualized by UV-induced fluorescence. For suc-LLVY-AMC hydrolysis in extract, 20 μl (600 μg of extract) was mixed with 80 μl of assay buffer, incubated at 30°C for 10 minutes, quenched with 1% SDS, and conversion measured with fluorimetry, using an excitation and emission wavelengths of 365 nm and 440 nm, respectively.

Protein complexes were formed by mixing components in the amounts indicated (see Figure Legends) and incubated under various conditions. For experiments involving ubiquitin conjugates, proteins were incubated for 20 min at 30°C (Figures 2.2A, 2.2C, 2.5D, and 2.5E). For experiments with GST-Rpn13, incubations were carried out for 10 min at 30°C when using purified proteasomes (Figures 2.5A,B), and for 10 min at 4°C when using extract (Figure 2.6C).

2.6.1.9 Plating assays

Strains were inoculated from YPD plates into synthetic medium (2% dextrose, 0.67% yeast nitrogen base without amino acids, 50 mg/L adenine hemisulfate, 500 mg/L

uridine, 200 mg/L phenylalanine, 200 mg/L isoleucine, 300 mg/L valine, 40 mg/L tyrosine, 600 mg/L proline, 100 ml/L glycine, 300 mg/L alanine, 300 mg/L serine, 200 mg/L threonine, 400 mg/L glutamate, 200 mg/L aspartate, 800 mg/L glutamine, 200 mg/L asparagine, 150 mg/L histidine, 450 mg/L lysine, 150 mg/L methionine, 400 mg/L leucine and 400 mg/L tryptophan), grown overnight in a roller drum at 30°C to an OD of roughly 4. Cells were diluted to an OD_{600} of 0.1, and three-fold serial dilutions were prepared in microtiter plates using the same synthetic medium. Cells were plated using a pin array onto solid synthetic medium with and without 8 µg/ml canavanine.

2.6.1.10 Protein turnover

Strains were transformed with a plasmid expressing pGAL-Ub^{V76}-Val-$e^{\Delta K}$-ßgal and selected for uracil prototrophy in synthetic plates (2% dextrose, 0.67% yeast nitrogen base without amino acids, 20 mg/L arginine, 30 mg/L histidine, 60 mg/L isoleucine, 30 mg/L leucine, 40 mg/L lysine, 20 mg/L methionine, 60 mg/L phenylalanine, 50 mg/L threonine, 40 mg/L tryptophan, and 10 mg/L adenine). Transformants were inoculated into synthetic medium while continuing to maintain the selection for uracil prototrophy (2% dextrose, 0.67% yeast nitrogen base without amino acids, 0.5% casamino acids, 40 mg/L tryptophan and 10 mg/L adenine), grown to saturation, then subcultured twice in medium inducing the expression of Ub^{V76}-Val-$e^{\Delta K}$-ßgal (2% raffinose, 2% galactose, 0.67% yeast nitrogen base without amino acids, 0.5% casamino acids, 40 mg/tryptophan, and 10 mg/L adenine**)**. Cells were harvested at an OD_{600} of roughly 3.0, and resuspended at a density of 50 OD_{600} per ml. Maintaining cells at 30°C using a dry bath, protein

synthesis was inhibited by the addition of cycloheximide from a fresh stock of 10 mg/ml to a final concentration of 100 µg/ml. 50 µl samples were withdrawn at various time points, mixed with an equal volume of ice cold quench mix (300 mM NaCl, 100 mM NaF, 2 mM NaN_3, 20 mM EDTA), and placed in an ice bath. After the time course, cells were harvested in a microcentrifuge for 10 seconds, resuspended in 75 µl lysis solution (50 mM NaOH, 2% SDS, 5% β-mercaptoethanol, 10% glycerol, and phenol red [sufficient to yield a colored but transparent solution]), and lysed by heating to 98°C for 5 minutes. pH was titrated to neutrality using 2.5 µl of 1N HCl. Titration was followed by the phenol red indicator, which shifts from magenta to red-orange when the pH drops below 8.0. Cell debris was removed by spinning in a microfuge for 5 minutes and at maximum speed. 12 µl of the supernatant was resolved by SDS-PAGE.

2.6.1.11 Immunoblot analysis of endogenous ubiquitin conjugates

Cells were grown overnight in YPD at 30ºC, diluted five-fold in YPD, and grown to an OD_{600} of roughly 0.9. Cells were processed as for the protein turnover experiment, except that 40 mM 2-deoxyglusocose was used in the quench mix, and cells were not concentrated prior to sampling.

2.6.1.12 Yeast strains

All strains were prepared in the SUB62 background (*lys2-801 leu2-3, 2-112 ura3-52 his3- Δ200 trp1-1 (192)*)

Table 2.1. Yeast strains produced in study

Strain	Genotype	Figure
SY722	*MATa rpn11-TEV-ProA::HIS ubp6::HIS rad23::hphMX dsk2::KlTRP1 ddi1::kanMX rpn13::CaURA3MX rpn10-*	2.2

	uim::natMX	
SY725	*MATa rpn11-TEV-ProA::HIS ubp6::HIS rad23:: hphMX dsk2::KlTRP1 ddi1::kanMX rpn13::CaURA3MX*	2.2
SY729	*MATa rpn11-TEV-ProA::HIS ubp6::HIS rad23::hphMX dsk2::KlTRP1 ddi1::kanMX rpn10-uim::natMX*	2.2
SY733	*MATa rpn11-TEV-ProA::HIS ubp6::HIS rad23::hphMX dsk2::KlTRP1 ddi1::kanMX*	2.2
SY775	*MATa rpn11-TEV-ProA::HIS ubp6::HIS RPN13(wt)::natMX rpn10-uim::kanMX*	2.5
SY723	*MATa rpn11-TEV-ProA::HIS ubp6::HIS rpn13::CaURA3MX rpn10-uim::natMX*	2.5
SY998 b	*MATa RPN13(WT)::natMX RPN10(WT)::kanMX*	2.6A, top
SY980 f	*MATa RPN13(WT)::natMX rpn10-uim::kanMX*	2.6A, top
SY1004 c	*MATa rpn13(41K-42K-93D)::natMX RPN10(WT)::kanMX*	2.6A, top
SY920 b	*MATa rpn13(41K-42K-93D)::natMX rpn10-uim::kanMX*	2.6A, top
SY1076	*MATa RPN13(WT)::natMX*	2.6A, middle and bottom
SY1012 a	*MATa rpn13(41K-42K-93D)::natMX*	2.6A, middle and bottom
SY1073 a	*MATa RPN13(WT)::NAT rad23::kanMX*	2.6A, middle
SY1080 a	*MATa rpn13(41K-42K-93D)::natMX rad23::kanMX*	2.6A, middle
SY1074 a	*MATa RPN13(WT)::natMX dsk2::TRP*	2.6A, bottom
SY1082 a	*MATa rpn13(41K-42K-93D)::natMX dsk2::TRP*	2.6A, bottom
SY998 a	*MATa RPN13(WT)::natMX RPN10(WT)::kanMX*	2.6B
SY980 a	*MATa RPN13(WT)::natMX rpn10-uim::kanMX*	2.6B
SY1004 a	*MATa rpn13(41K-42K-93D)::natMX RPN10(WT)::kanMX*	2.6B
SY920 a	*MATa rpn13(41K-42K-93D)::natMX rpn10-uim::kanMX*	2.6B
SY992 b	*MATa RPN10(wt)::kanMX*	2.6C
SY1004 b	*MATa rpn13(41K-42K-93D)::natMX RPN10(wt)::kanMX*	2.6C
SY933	*MATa Pcup-Ub-K-TRP1::hphMX rpn13-E41K/E42K/S93D::natMX rpn10-uim::kanMX*	2.6D

SY936	*MATa Pcup-Ub-K-TRP1::hphMX rpn13-E41K/E42K/S93D::natMX*	2.6D
SY950	*MATa Pcup-Ub-K-TRP1::hphMX RPN13(wt)::natMX*	2.6D
SY952	*MATa Pcup-Ub-K-TRP1::hphMX rpn13(KO)::natMX*	2.6D
SY992 a	*MATa RPN10(wt)::kanMX*	2.6E
SY1004 a	*MATa rpn13(41K-42K-93D)::natMX RPN10(wt)::kanMX*	2.6E

2.6.1.13 Preparation of NMR samples

scRpn13, mRpn13, and hRpn13 were prepared as described above for scRpn13, but in M9 minimal media with ^{13}C, ^{15}N, or ^{2}H incorporated by using ^{13}C labeled glucose, ^{15}N labeled ammonium chloride or D_2O, respectively. hHR23a UBL and hPLIC2 UBL were prepared by following the protocols as described in (*140, 193*).Unlabeled monoubiquitin was purchased (Boston Biochem Inc.), and K48-linked diubiquitin and tetraubiquitin synthesized by using a previously described method (*194*).

2.6.1.14 Chemical shift assignments and structure determination

Chemical shift assignments for scRpn13 were obtained by using modern NMR techniques. Briefly, two pairs of triple resonances experiments were acquired, namely HNCA/HNCOCA and HNCO/HNCACO, as well as an HNCACB experiment. Each of these was acquired on ^{15}N, ^{13}C, and 70% ^{2}H labeled Rpn13 and on Varian 600 or 800 MHz spectrometers equipped with cryogenically cooled probes. Samples ranged from 0.4 – 0.7 mM protein concentration and all spectra were acquired in Buffer 1 (20 mM $NaPO_4$, 50 mM NaCl, 4 mM DTT at pH 6.5) and at 25°C. All crosspeaks present in the ^{1}H, ^{15}N HSQC spectrum were assigned. The backbone amide groups of residues T73 – I86 and S106 – G127 are absent from all spectra, including the ^{1}H, ^{15}N HSQC spectrum;

however, ^{13}C based NOE crosspeaks were available and used to define the structure of T73 – P77. Importantly, the secondary structural elements present in the solution structure of scRpn13 are supported by chemical shift index values for C' and Cα atoms as well as the NOEs present in the ^{13}C dispersed NOESY spectrum.

Distance constraints for structure calculations were obtained by using a 3D ^{15}N-dispersed NOESY spectrum on a ^{15}N, 50% ^{2}H labeled sample (200 ms mixing time) and a ^{13}C-dispersed NOESY on a ^{13}C labeled sample dissolved in D_2O (80 ms mixing times). Each was acquired at 800 MHz and with a cryogenically cooled probe. Backbone φ and ϕ torsion angle constraints were derived by using the program TALOS (*195*). Spectra were processed by NMRPipe (*196*) and visualized in XEASY (*197*).

The NOE-derived distance constraints, hydrogen bonds and dihedral angle constraints (Table 2.S1) were used in XPLOR version 3.851 to determine the structure of scRpn13. Eight structure from 35 starting ones had no NOE or dihedral angle violation greater than 0.3 Å or 5°, respectively.

2.6.1.15 NMR titration experiments

We used chemical shift perturbation analysis to determine protein contact surfaces. In all cases ^{1}H, ^{15}N HSQC experiments were recorded on ^{15}N labeled protein with increasing molar ratios of unlabeled binding partner. For all but hRpn13 binding to hRpn2 (797-953), the binding was in the fast exchange regime, such that affected resonances could be readily followed from their free to their bound states as increasing amounts of the binding partner was added. The concentration of hRpn13 was kept

constant and between 0.20-0.40 mM; the spectra were recorded at 25°C and on either 600 MHz or 800 MHz NMR spectrometers. Experiments involving scRpn13 were in Buffer 1 (20 mM $NaPO_4$, 50 mM NaCl, 4 mM DTT at pH 6.5) whereas those involving hRpn13 were in Buffer 2 (20 mM $NaPO_4$, 30 mM NaCl, 2 mM DTT at pH 6.5). Resulting chemical shift perturbation values ($\Delta\delta_{avg}$) for ^{15}N and ^{1}H nuclei were derived from Equation 2.1:

$$\Delta\delta_{avg} = (0.2 \times \Delta\delta_N^2 + \Delta\delta_H^2)^{1/2}$$

where $\Delta\delta_N$ and $\Delta\delta_H$ represent the chemical shift perturbation value of the amide nitrogen and proton, respectively.

To determine the binding constants for wild-type scRpn13 binding to monoubiquitin, we acquired data at the following molar ratios, 4:1, 2:1, 1:1, 1:2, 1:3, 1:4, 1:5, 1:6, 1:8. The chemical shift perturbation values for two residues (F45 and E72) were normalized and then plotted to obtain a K_d by using Matlab v. 7.2 and the method described in (*198*). Normalized chemical shift perturbation data for scRpn13-KKD binding to monoubiquitin was acquired at the following molar ratios, 2:1, 1:1, 1:2, 1:4, 1:6, 1:8, 1:10, 1:12, 1:15, 1:18. Two residues (F45 and E72) were chosen to determine K_d values for scRpn13-KKD binding to monoubiquitin, by using the method described for wild-type scRpn13. In this case, saturation was achieved at a molar ratio of 1:15 scRpn13-KKD:monoubiquitin. The concentration of scRpn13-KKD in these experiments

was 0.3 mM, and at the titration points with the higher ubiquitin concentrations, ubiquitin aggregation appeared to have compromised the accuracy of our determined K_d value. The data could be fit to the standard equation for 1:1 binding only by the exclusion of data from the 1:6, 1:8, 1:10, 1:12, 1:15 and 1:18 titration points.

The K_d value for hHR23a UBL domain binding to hRpn13 Pru was determined by acquiring a series of $^{1}H,^{15}N$ HSQC experiments detecting the amide resonances of hHR23a UBL domain at molar ratios 8:1, 4:1, 2:1, 1.5:1, 1:1, 1:1.5, 1:2, 1:3 hHR23a UBL:hRpn13. The chemical shift perturbation for three residues (T14, G52, and E68) were normalized and then plotted to obtain the K_d value, as described for scRpn13 binding to monoubiquitin (Figure 2.S3).

To determine the stoichiometry for hRpn13 Pru binding to mono-, di- and tetraubiquitin, we acquired data at varying molar ratios, and plotted the normalized chemical shift perturbation values. The plots yielded steep curves and K_d values too small to be accurately determined by NMR, which requires high protein concentrations.

2.6.1.16 Affinity measurements by fluorescence spectroscopy

The K_d values for the hRpn13 Pru binding to mono- or diubiquitin were determined by monitoring the change in fluorescence emission spectra of the hRpn13 Pru upon their addition at 298K. Intrinsic fluorescence of the two Trp residues in 1 μM hRpn13 Pru was measured on a JASCO FP-6200 spectrofluorometer without and with increasing molar quantities of ubiquitin or diubiquitin (0.0083 μM ~ 8 μM), as shown in Figure 2.S6. Emission spectra were recorded between 300 and 500 nm, with an excitation

wavelength of 280 nm and spectral bandwidths for excitation and emission of 5 nm. The change in fluorescence intensity at 348 nm upon addition of monoubiquitin or diubiquitin was used to generate the binding curves of Figure 2.4C by using Microsoft Excel and curve fitting was achieved with Matlab v. 7.2.

2.6.1.17 Modeling the scRpn13:ubiquitin complex

Chemical shift perturbation analysis implicated the S2-S3, S4-S5, and S6-S7 loops within scRpn13 as binding monoubiquitin. In the accompanying manuscript, we determined the mRpn13:ubiquitin structure using NOE-derived distance constraints to similarly reveal these loops as being at the ubiquitin-contact surface. Therefore, we modeled the scRpn13:ubiquitin complex by superimposing the backbone atoms of the three ubiquitin binding loops within scRpn13 onto those of mRpn13 in the mRpn13:ubiquitin complex structure. 1000 steps of Powell energy minimization (SYBYL, Tripos Inc.) were then used to optimize the model structure of scRpn13:ubiquitin.

2.6.2 Supplementary table

Table 2.S1. Structural statistics for NMR structure of scRpn13

NOE distance restraints (total)	949
Inter-residue	492
Medium-range ($\|i-j\| \leq 4$)	51
Long-range ($\|i-j\| > 4$)	276
Hydrogen bonds	56
Dihedral angle restraints (deg.)	79
φ ($C'_{(i-1)}$ - N_i - C_i^{α} - C_i')	47
ψ (N_i - C_i^{α} - C_i' - $N_{(i+1)}$)	32
Ramachandran plot	
Most-favorable region (%)	66.2

Additionally allowed region (%)	30.0
Generously allowed region (%)	2.8
Disallowed region (%)	0.9
r.m.s.d of backbone atoms from average structure within well defined regions (Å) (T6-N38, F45-L68, I86-V90, R96-L101)	0.61
r.m.s.d of all heavy atoms from average structure within well defined regions (Å) (T6-N38, F45-L68, I86-V90, R96-L101)	1.38

2.6.3 Supplementary Figures

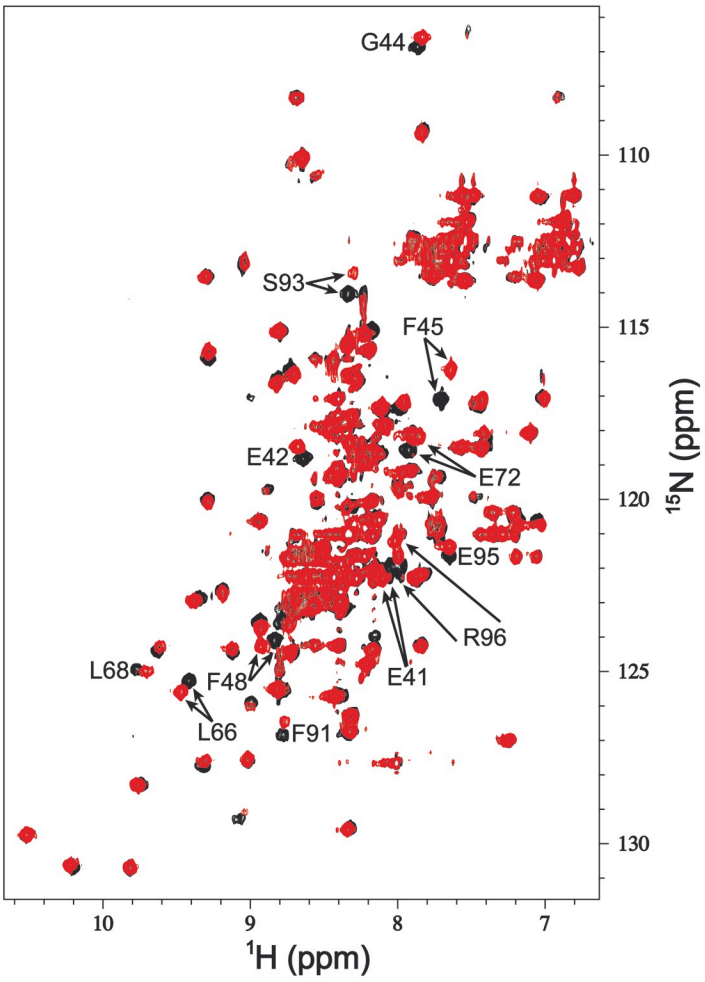

Figure 2.S1. Superposition of ^{1}H, ^{15}N HSQC spectra of ^{15}N labeled Rpn13 alone (black) and with equimolar ubiquitin (red) reveals residues at the ubiquitin contact surface.

Figure 2.S2. Example of steric problems in structures generated with three hRp13 Pru molecules (red, yellow, or green) bound to neighboring subunits of K48- linked tetraubiquitin (grey). In this example, two neighboring Rpn13 Pru molecules interact and exhibit steric clashes between N130 and Q51 (displayed in cyan) of the structure displayed in and K34, G35, T36 and T37 (displayed in black) of the structure displayed in red. The interaction of these residues is not supported by additional chemical shift perturbations when Rpn13 binds tetraubiquitin versus monoubiquitin. Other geometries are also yielded from the calculations, which are performed in XPLOR using the intermolecular NOE interactions between hRpn13 Pru and monoubiquitin; however, in all cases unsupported interactions and steric clashes occur, either between hRpn13 Pru molecules or the ubiquitin subunits. It is worth noting that the steric problems will be increased when full length hRpn13 interacts with polyubiquitin in this manner. It is formally possible that a structure exists with no steric clashes, which is not found due to the computational limitations of having so many atoms in this system; however, the clear entropic disadvantages of forming what would be a very restricted configuration most likely contribute to the experimental results indicating that this binding arrangement is not detectable.

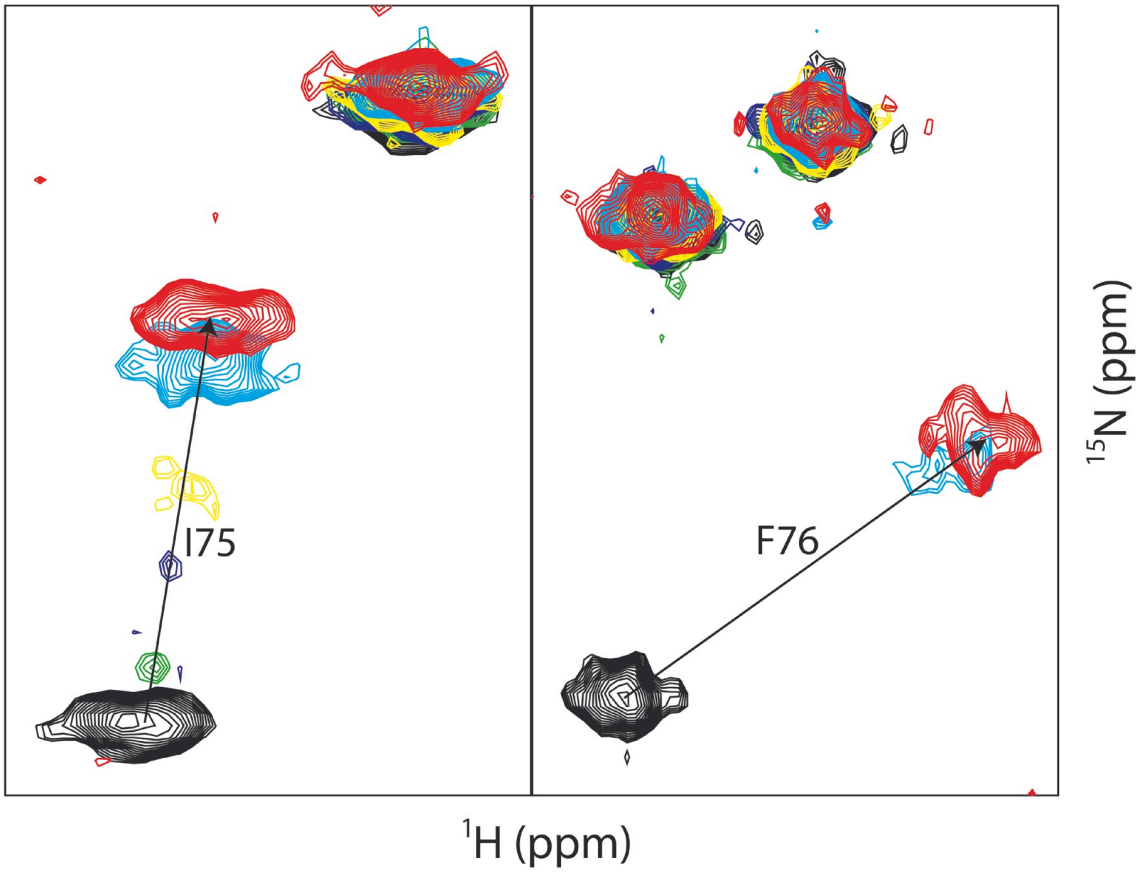

Figure 2.S3. Monoubiquitin binding to hRpn13 causes resonance attenuation as well as shifting. Superposition of ^{1}H,^{15}N HSQC spectra of ^{15}N-labeled hRpn13 Pru without (black) or with monoubiquitin acquired at molar ratios of 8:1 (green), 4:1 (dark blue), 2:1 (yellow), 1:1 (light blue), and 1:2 (red) hRpn13:monoubiquitin.

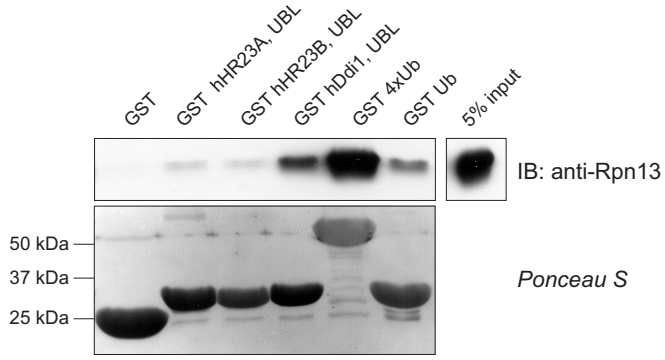

Figure 2.S4. Rpn13 binds UBLs of polyubiquitin receptors. Pru domain of mRpn13 was expressed as GST-fused protein, cut with thrombin and used in GST pull-down assays to access its binding to UBLs of polyubiquitin receptors hHR23A, hHR23B, and hDdi1, which were expressed as GST-fused proteins.

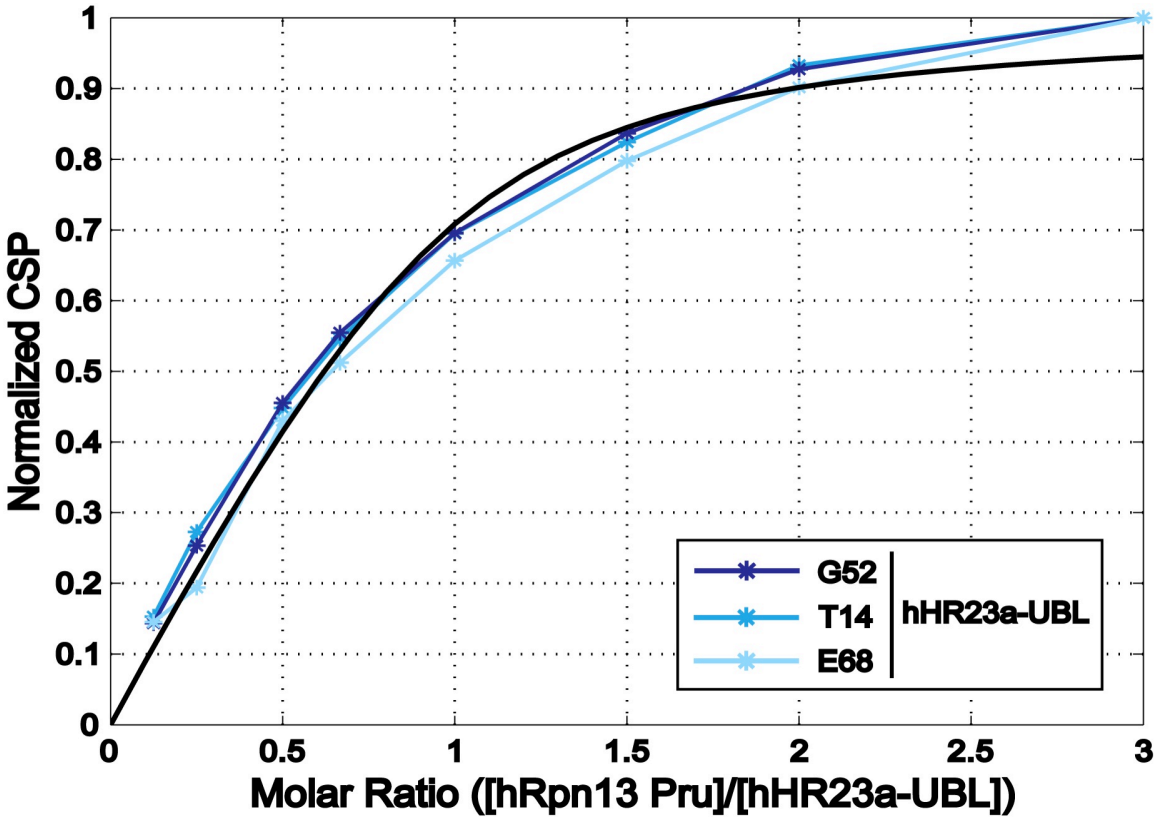

Figure 2.S5. hRpn13 Pru binds hHR23a UBL domain. Normalized chemical shift perturbation values are plotted against varying molar ratios of hRpn13 Pru to hHR23a UBL domain. Each data line represents a specific amino acid as indicated in the figure. The data were fit (solid black line) to determine a binding constant of 36μM by using Matlab v. 7.2.

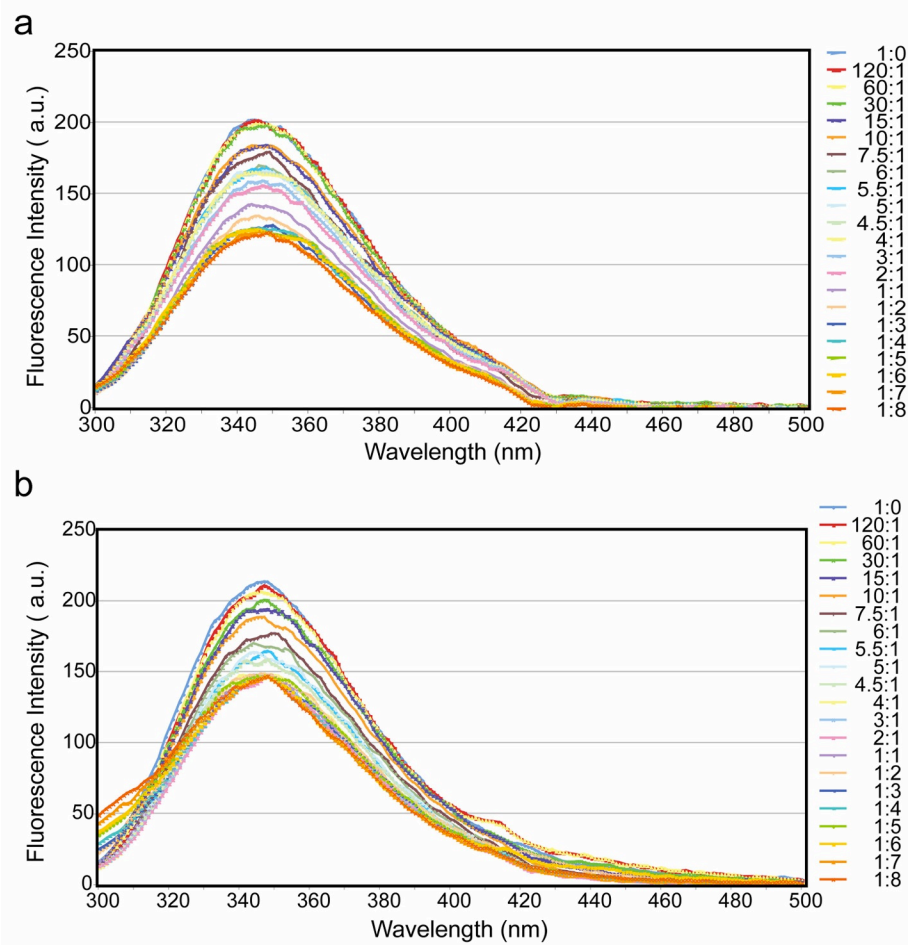

Figure 2.S6. Fluorescence emission spectra of hRpn13 Pru in the absence and presence of different concentrations of monoubiquitin (A) or diubiquitin (B). The hRpn13 Pru concentration is kept at 1 μM in 20 mM $NaPO_4$, 30 mM NaCl (pH 6.5) buffer. The molar ratio of hRpn13 Pru to ubiquitin (A) or diubiquitin (B) is indicated.

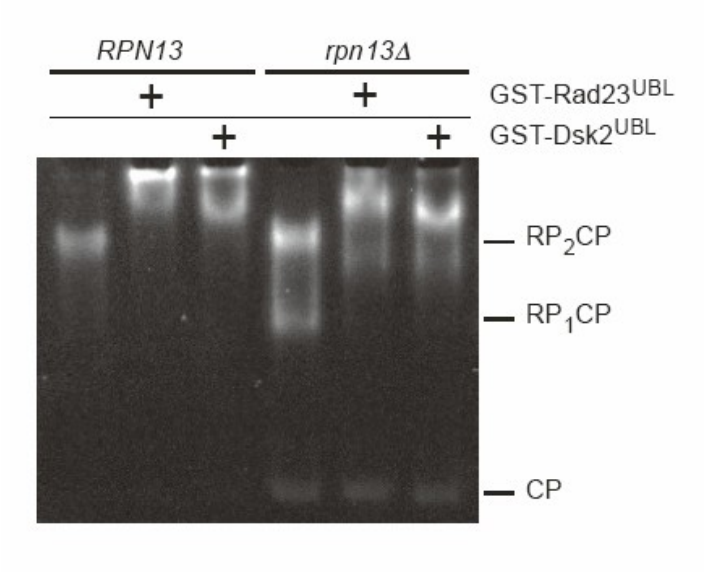

Figure 2.S7. Binding of UBL domains to proteasomes does not require Rpn13. Four pmol of proteasomes (see Figure 2.2A, lanes 1 and 5) were incubated with 400 pmol of Rad23 and Dsk2 UBL domains fused to GST for 10 minutes at 30°C. Proteasome complexes were resolved by native PAGE and visualized by suc-LLVY-AMC overlay assay.

Chapter 3

Ubiquitin docking at the proteasome through a novel pleckstrin-homology domain interaction

Patrick Schreiner[1], Xiang Chen[2*], Koraljka Husnjak[3,4*], **Leah Randles[2]**, Naixia Zhang[2], Suzanne Elsasser[5], Daniel Finley[5], Ivan Dikic[3,4], Kylie Walters[2] and Michael Groll[1,6]*

[1] Institut für Organische Chemie und Biochemie, Department Chemie, Technische Universität München, Lichtenbergstrasse 4, D-85747 Garching, Germany.
[2] Department of Biochemistry, Molecular Biology and Biophysics, University of Minnesota, Minneapolis, MN 55455, US
[3] Institute of Biochemistry II, Goethe University Hospital, Theodor-Stern-Kai 7, D-60590 Frankfurt (Main), Germany
[4] Tumor Biology Program, Mediterranean Institute for Life Sciences, Mestrovicevo setaliste, 21 000 Split, Croatia
[5] Department of Cell Biology, Harvard Medical School, 200 Longwood Avenue, Boston, MA 02115, USA
[6] Institute of Biochemistry, Charité-Universitatsmedizin Berlin CCM, Monbijoustraße 2, D-10117 Berlin, Germany
[*] These authors contributed equally to this work.

Reprinted with permission from Nature Publishing Group Vol 453, Issue 7194, pp 548-52[a]

Leah Randles Contributions: Devised methodology and produced samples used to produce Figure 3.3A, 3.3C and 3.S7. Contributed to all NMR experiments and sample preparation for NMR experiments. Contributed to the writing of the published manuscript.

---

[a] The help of G. Bourenkov (DESY, BW6, Hamburg, Germany) during synchrotron data collection is gratefully acknowledged. We also thank J. Lary, J. Cole and the National Analytical Ultracentrifugation Facility of the University of Connecticut for performing the sedimentation experiments. NMR data were acquired at the University of Minnesota and the data processed in the Minnesota Supercomputing Institute's Basic Sciences Computing Laboratory. This work was supported by National Institutes of Health CA097004 (K.W.), GM43601 (D.F.) and GM008700-Chemistry Biology Interface Training Grant (L.R.), Deutsche Forschungsgemeinschaft (DI 931/3-1) and the Cluster of Excellence 'Macromolecular Complexes' of the Goethe University Frankfurt (EXC115) to I.D., and Deutsche Forschungsgemeinschaft SFB740/TP B4 (M.G.).

3.1 Synopsis

Targeted protein degradation is largely performed by the ubiquitin–proteasome pathway, in which substrate proteins are marked by covalently attached ubiquitin chains that mediate recognition by the proteasome. It is currently unclear how the proteasome recognizes its substrates, as the only established ubiquitin receptor intrinsic to the proteasome is Rpn10/S5a (ref. (*132*)), which is not essential for ubiquitin-mediated protein degradation in budding yeast (*199*). In this chapter we report that Rpn13 (refs (*163, 167, 169-171*)), a component of the nine-subunit proteasome base, functions as a ubiquitin receptor (*92*), complementing its known role in docking de-ubiquitinating enzyme Uch37/UCHL5 (refs (*163, 169, 171*)) to the proteasome. Here we merge crystallography and NMR data to describe the ubiquitin-binding mechanism of Rpn13. We determine the structure of Rpn13 alone and complexed with ubiquitin. The co-complex reveals a novel ubiquitin-binding mode in which loops rather than secondary structural elements are used to capture ubiquitin. Further support for the role of Rpn13 as a proteasomal ubiquitin receptor is demonstrated by its ability to bind ubiquitin and proteasome subunit Rpn2/S1 simultaneously. Finally, we provide a model structure of Rpn13 complexed to diubiquitin, which provides insights into how Rpn13 as a ubiquitin receptor is coupled to substrate deubiquitination by Uch37.

3.2 Results

The structure of murine Rpn13 (mRpn13) (amino acids 1–150) was determined at 1.7-Å resolution by X-ray crystallography, and found to contain a pleckstrin-homology

domain (PHD) fold (Figure 3.1A, B) (structure determination and refinement statistics are provided in Section 3.6). In particular, whereas the first 21 amino- and last 20 carboxy-terminal amino acids are unstructured, residues 22–130 form a PHD fold. This result was surprising, as primary sequence alignment did not identify Rpn13 as being homologous to previously characterized proteins. This finding, coupled with its ubiquitin receptor properties (*92*), prompted us to name the N-terminal domain of Rpn13 pleckstrin-like receptor for ubiquitin (Pru).

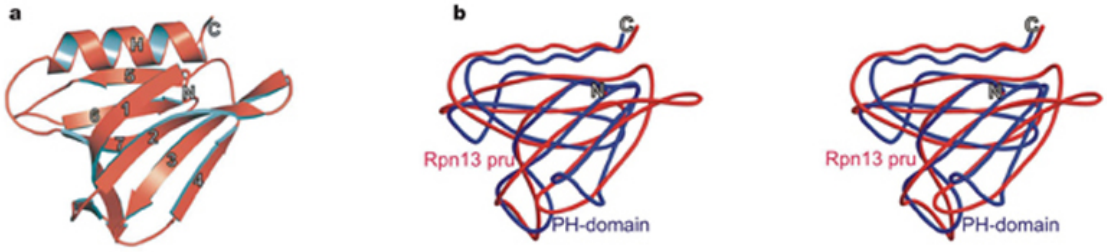

Figure 3.1. Crystal structure of mRpn13 Pru reveals typical pleckstrin-homology fold. (A) Ribbon representation of Rpn13 pleckstrin-like receptor for ubiquitin (Rpn13 Pru). The pleckstrin-homology fold consisting of a seven-stranded β-sandwich structure (1–7) capped by the C-terminal α-helix. (B) Stereo representation of the structural alignment of Rpn13 Pru (red) and the PHD (blue) from Pleckstrin (PDB accession code 1PLS).

Though very divergent at their sequence level, all PHDs have a common β-sandwich fold. The PHD of Rpn13 is composed of a four-stranded twisted antiparallel β-sheet (β_{1-4}: residues 22–34, 45–52, 56–62, 71–74) that packs almost orthogonally against a second triple-stranded β-sheet (β_{5-7}: residues 80–85, 92–98, 103–110) (Figure 5.S1). Like other PHDs, Rpn13 Pru forms a hydrophobic core containing conserved hydrophobic residues (F26, V47, I49, F59, F82, Y94, L96, F107 and M109), which are located within β-sheets. One end of the β-sandwich is capped by a long C-terminal

amphipathic α-helix (residues 117–128), which is stabilized by interactions between V124 and L128, whereas the other corner of the hydrophobic core is closed by three loops formed by residues located between strands S1/S2, S3/S4 and S6/S7 (Figure 3.1A and 3.S1).

Despite much effort, we were unable to crystallize the Rpn13 Pru–ubiquitin complex; however, we determined the structure of this complex by molecular docking, based on the crystal structure of mRpn13 Pru and intermolecular nuclear Overhauser enhancements (NOEs) as well as data from chemical shift perturbation derived by NMR titration experiments. The topology of the complexed structure was readily defined by 12 unambiguous intermolecular NOE interactions between human Rpn13 (hRpn13) Pru and ubiquitin (Figure 3.2A). We were able to use the hRpn13:ubiquitin NOEs with the mRpn13 crystal structure because all of the amino acids exhibiting intermolecular NOEs are strictly conserved between murine and human Rpn13. Importantly, the mRpn13 Pru–ubiquitin structure reveals a novel ubiquitin-binding mode in which residues of the S2–S3, S4–S5 and S6–S7 loops capture ubiquitin (Figure 3.2B). At the core of the contact surface, hydrogen bonds are formed between side-chain oxygens of D78 and D79 in hRpn13, and Nϵ2 and Nδ1 of H68 in ubiquitin, respectively. Moreover, F76 engages in hydrophobic interactions with I44, Q49 and V70 of ubiquitin (Figure 3.S2). These contacts are enabled by the strictly conserved P77, which causes the S4–S5 loop to turn. The intermolecular NOE data for this complex were fully satisfied without Rpn13 Pru or ubiquitin structural rearrangements, and the root mean squared deviations between the free and complexed state of Rpn13 Pru and ubiquitin were 0.91 and 0.75 Å for backbone

atoms, and 1.20 and 1.15 Å for all non-hydrogen atoms, respectively.

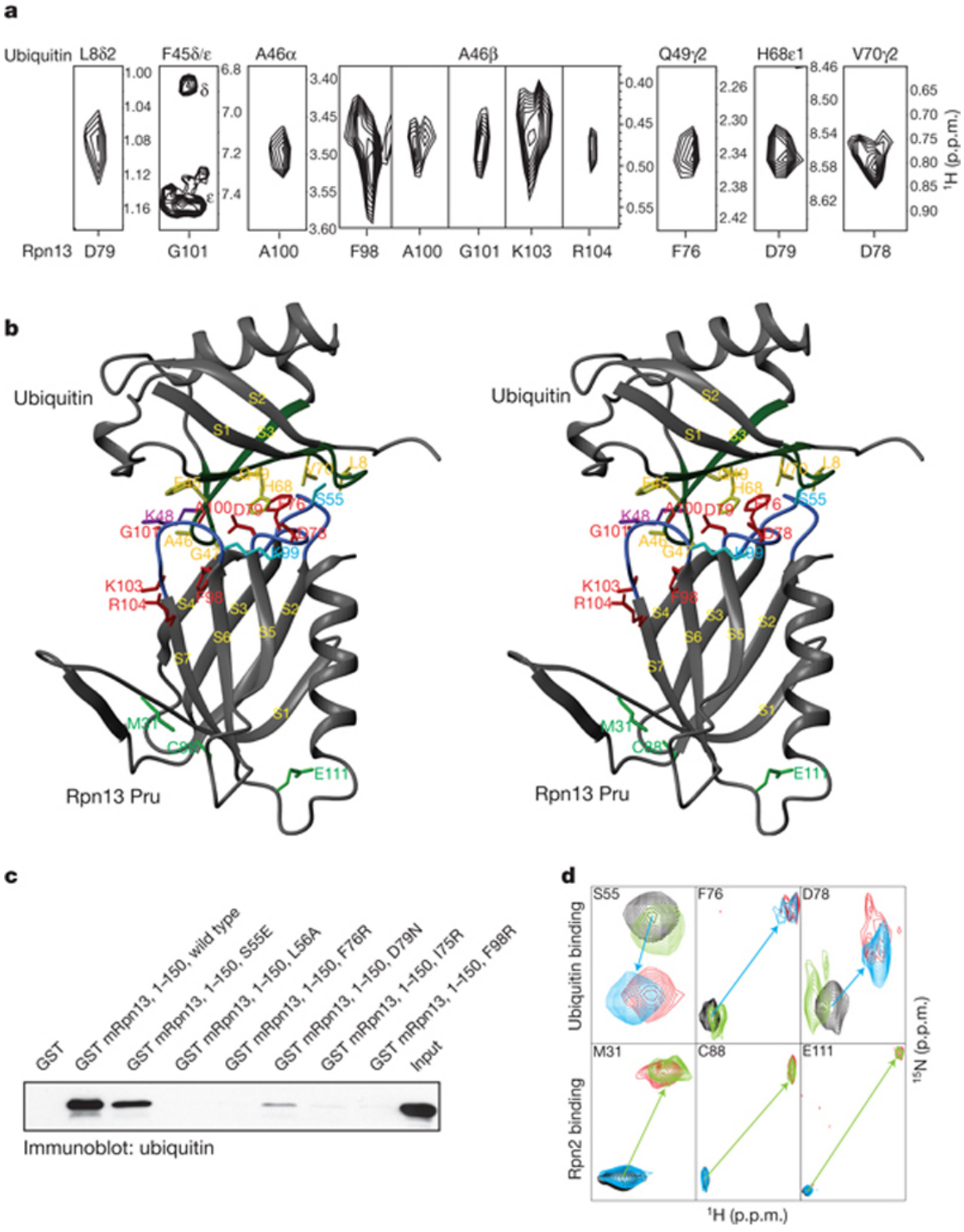

Figure 3.2. Structure of Rpn13 Pru-ubiquitin complex defines a novel ubiquitin-binding

motif. (A) Representative NOE interactions identified between Rpn13 Pru and ubiquitin. Each panel contains a selected region of a ^{15}N-dispersed nuclear Overhauser enhancement spectroscopy experiment recorded on ^{15}N-, ^{13}C- and 70% ^{2}H-labelled hRpn13 Pru mixed with equimolar quantities of unlabeled ubiquitin. All of the resonances displayed in this panel were unambiguously assigned as intermolecular NOE interactions with ubiquitin. Ubiquitin and Rpn13 Pru assignments are provided at the top and bottom of the expanded regions, respectively. (B) Stereo representation of the mRpn13 Pru–ubiquitin complex oriented with ubiquitin at the top. At the interaction surface, secondary structural elements of ubiquitin and Rpn13 Pru are displayed in green and blue, respectively. Residues at the contact surface with intermolecular NOEs are in yellow (ubiquitin) or red (Rpn13 Pru), whereas those suggested to be at the contact surface only by the NMR titration experiments are displayed in purple (ubiquitin) or cyan (Rpn13 Pru). M31, C88 and E111, which shift upon hRpn2 (amino acids 797–953) addition, are displayed in dark green. (C) Specific amino-acid substitutions were made within the S2–S3, S4–S5 and S6–S7 loops of mRpn13 Pru by *in vitro* mutagenesis. The protein products were expressed as GST fusions and used in GST pull-down assays to highlight the importance of these loops for tetraubiquitin binding. (D) Ubiquitin (blue), hRpn2 (amino acids 797–953) (green) or ubiquitin and hRpn2 (amino acids 797–953) (red) were added to the hRpn13 Pru domain, which was monitored by ^{1}H, ^{15}N heteronuclear single-quantum coherence experiments. Comparison with the spectrum acquired on the protein alone (black) indicates that S55, F76 and D78 bind ubiquitin in a manner that is independent of hRpn2 (amino acids 797–953), whereas M31, C88 and E111 bind hRpn2 in a ubiquitin-independent manner.

Additional hydrophobic contacts exist, as Rpn13's side-chain methyl group of A100 and the Cα group of G101 partly bury ubiquitin's F45, which is solvent-exposed in the free protein. Similarly, Rpn13's strictly conserved F98 located on S6 also becomes less solvent-accessible through interactions with A46 and G47 of ubiquitin. Calculation of the electrostatic potential of mRpn13 illustrates that a hydrophobic region within its ubiquitin-binding surface that contains L56 and F76 is available to interact with ubiquitin's L8, I44 and V70 (Figure 3.S3). Complementary electrostatic interactions between Rpn13 Pru and ubiquitin also stabilize the complex, including interactions of D78 and D79 of Rpn13 Pru with ubiquitin's H68, as well as D53 and D54 with ubiquitin's R42 and R72.

In total, the contact surface of Rpn13 Pru and ubiquitin comprises 1256 $Å^2$, which is large for ubiquitin receptors. Thus, the relatively high affinity of hRpn13 binding to monoubiquitin, described in Chapter 2, is partly explained by the enlarged contact surface compared with that of EAP45 GLUE (1000 $Å^2$ in total) (*95*). Published values for the total buried surface of Cue2-1^{cue} and $Dsk2^{UBA}$ upon ubiquitin binding are even smaller: 960 and 800 $Å^2$, respectively (*65, 198*).

To analyze the significance of specific interactions identified in the mRpn13–ubiquitin complex, we made several amino-acid substitutions including L56A, I75R, F76R, D79N and F98R. The ubiquitin-binding competency of the resulting amino-acid-substituted proteins was tested by using GST-4xUb (created by the in-frame expression of glutathione *S*-transferase (GST) and four ubiquitin sequences) in pull-down assays (Figure 3.2C). These experiments validated our mRpn13–ubiquitin structure and provided strong evidence for the importance of the S2–S3, S4–S5 and S6–S7 loops in ubiquitin binding by mRpn13. In particular, the single amino-acid substitutions L56A, I75R, F76R and F98R abrogate ubiquitin binding, and a strong reduction is observed for the D79N mutation. We tested how three of these mutations affect mRpn13 structural integrity. In particular, NMR experiments were performed on mRpn13 Pru with the L56A, F76R or D79N mutations incorporated and compared with the wild-type mRpn13 Pru domain. These comparisons demonstrated that the loss of ubiquitin binding was not caused by loss of structural integrity (Supplementary Figure 3.S4). Altogether, our results demonstrate that ubiquitin binding is defined by key interactions with residues within the S2–S3, S4–S5 and S6–S7 loops.

To function as a proteasomal ubiquitin receptor, Rpn13 must bind ubiquitin and proteasome components simultaneously. In yeast and mammals, Rpn13 binds to Rpn2 through its Pru domain (*169, 172, 173*). Although the Pru domain also binds ubiquitin, we found that Rpn2 binding does not disturb the Rpn13 loops that bind ubiquitin. By using a nested set of N-terminal deletions in human Rpn2 (hRpn2), we determined a fragment spanning amino acids 797–953 to bind mRpn13 (Figure 3.S5). The addition of this fragment (hRpn2 (797–953)) to hRpn13 did not affect residues at the ubiquitin contact surface, which shift only upon ubiquitin addition, as demonstrated for S55, F76 and D78 (Figure 3.2D). By contrast, M31, C88 and E111, which are unaffected by ubiquitin, shift after hRpn2 (797–953) addition. Furthermore, when both Rpn2 and ubiquitin were added, S55, F76 and D78 contact ubiquitin whereas M31, C88 and E111 contact Rpn2 (Figure 3.2D), indicating that the two binding surfaces are largely independent. M31, C88 and E111 are conserved in mRpn13 and map to S1, the S5–S6 loop, and the region linking S7 to H1, respectively. These elements are clustered in a region that is opposite to the ubiquitin-binding loops of Rpn13.

26S proteasomes exhibit high affinity for ubiquitinated substrates. Ubiquitin chains linked by isopeptide bonds between K48 and the C-terminal glycine of neighboring ubiquitin molecules are known to trigger proteasomal degradation of the labeled protein (*200, 201*). We found that Rpn13 Pru binds K48-linked tetraubiquitin in a manner comparable to that of monoubiquitin. More specifically, tetraubiquitin and monoubiquitin caused chemical-shift changes to the same hRpn13 residues (Figure 3.S6A), including L56, F76 and F98, and shifted them almost identically (Figure 3.3A).

Only two residues in hRpn13 exhibit changes that are specific to K48-linked tetraubiquitin, namely L73 and R104 (Figure 3.3A and Figure 3.S6A, red). These residues and the side-chain atoms of neighboring K103 are proximal to each other; in the mRpn13–monoubiquitin structure they are directed towards the side-chain atoms of K48. This arrangement is congruent with Rpn13 binding the proximal subunit of diubiquitin, namely that which forms an isopeptide using K48 (Figure 3.3B). We tested this model further by monitoring the side-chain atoms of the proximal or distal subunit of diubiquitin upon addition of hRpn13 Pru. More specifically, unlabeled hRpn13 Pru was added to diubiquitin with either its proximal or distal subunit ^{13}C labeled, and the effect recorded by ^{1}H, ^{13}C heteronuclear multiple-quantum coherence experiments. Significant resonance shifting characteristic of hRpn13 binding was observed for the I44 γ_1, I44 δ_1 and A46 methyl groups of the proximal subunit (Figure 3.3C, left panel, and Figure 3.S7A). By contrast, resonances of the distal subunits exhibited only minor perturbations, most likely because of loss of intramolecular interactions with the proximal subunit. These data provide strong evidence that the major contacts formed between hRpn13 Pru and diubiquitin involve residues of the proximal subunit, at least when these two proteins are at equimolar concentration. Further evidence of this binding mode is provided by analytical ultracentrifugation data, which revealed 1:1 binding stoichiometry between hRpn13 Pru and diubiquitin (Figure 3.S7B).

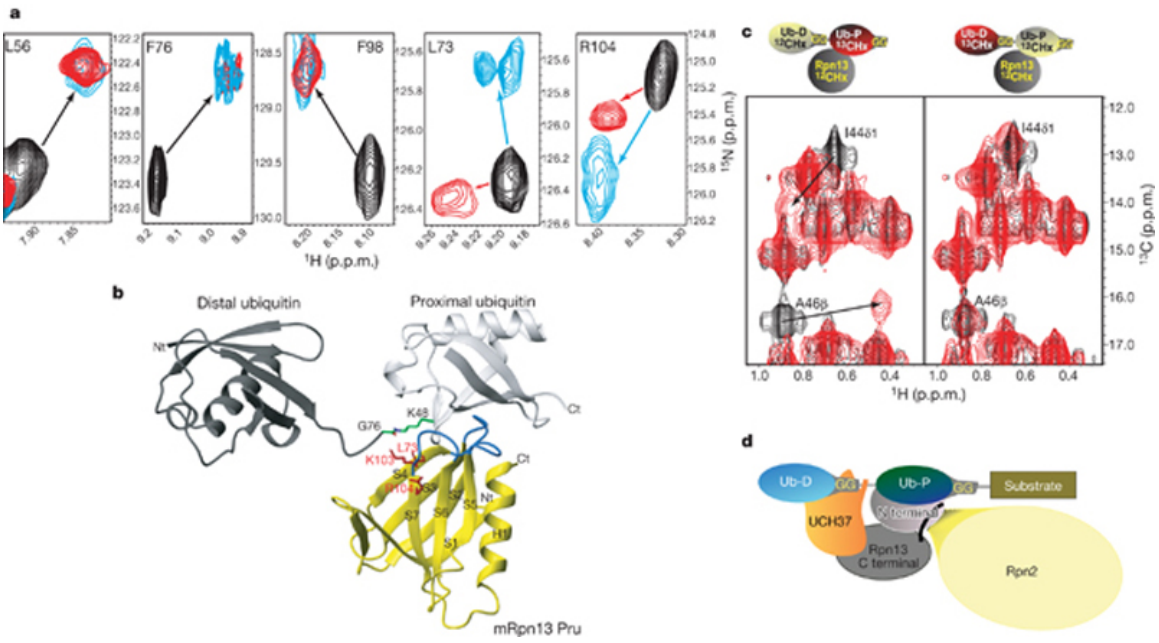

Figure 3.3. Preferential binding to the proximal subunit of K48-linked diubiquitin by Rpn13 Pru allows Uch37 access to the distal subunit. (A) Comparison of spectra acquired with monoubiquitin versus K48-linked tetraubiquitin reveals identical effects for Rpn13's L56, F76 and F98 but differences for L73 and R104. Monoubiquitin (red) or tetraubiquitin (cyan) was added to hRpn13, which was monitored by ^{1}H, ^{15}N heteronuclear single-quantum coherence experiments. The spectrum of free hRpn13 is indicated in black, and the molar ratio of monoubiquitin (red) or tetraubiquitin (cyan) to hRpn13 was 1:1 in the represented spectra. (B) Computer-generated model of the mRpn13 Pru–diubiquitin complex. White and grey ribbon diagrams display the proximal and distal ubiquitin, respectively, whereas a balls-and-sticks representation is used for the K48-G76 isopeptide bond linkage. Rpn13 Pru is cultured in yellow and loops recognizing ubiquitin in blue, whereas L73, K103 and R104 are displayed in red. Diubiquitin was created by Insight II software based on atomic coordinates for the mRpn13 Pru–ubiquitin complex and monoubiquitin (PDB entry 1D3Z). In this model, the distal subunit of diubiquitin is positioned arbitrarily, as its only constraints prohibit steric clashes with other atoms. (C) hRpn13 Pru interacts with the I44 δ_1 and A46 methyl groups of the proximal subunit. ^{1}H, ^{13}C heteronuclear multiple-quantum coherence spectra were acquired on samples containing either no (black) or equimolar unlabeled hRpn13 (amino acids 1–150) (red) mixed with diubiquitin in which its proximal (left) or distal (right) subunit is labeled with ^{13}C. The shifted resonances are labeled. (D) Model for how Rpn13 participates in Uch37 deconjugation of ubiquitinated substrates. Rpn13's C-terminal domain (grey) binds Uch37 (orange) as its N-terminal domain binds the polyubiquitin chain and Rpn2/S1 (yellow). In this model, Uch37 binds to the distal subunit (light blue) of the chain while Rpn13 binds the proximal subunit (dark blue).

3.3 Conclusion

In conclusion, we reveal that the ubiquitin-binding region of proteasome subunit Rpn13 adopts a PHD fold, and we solve its structure complexed with ubiquitin to unveil a new ubiquitin-binding mode. PHDs are present in a remarkably large number of proteins (*202*), but Rpn13 Pru is the first example of a PHD structure within the 26S proteasome. Rpn13, like many other ubiquitin receptors, binds to the L8, I44 and V70 hydrophobic pocket of ubiquitin (Figure 3.2B). However, it is the first to bind this region using exclusively loops (Figure 3.4A). Most of the ubiquitin receptors characterized so far use α-helices to bind this surface of ubiquitin, including the ubiquitin-associated (UBA)-domain, coupling ubiquitin to endoplasmic reticulum degradation (CUE)-domain, ubiquitin-interacting motif (UIM), double-sided UIM (DUIM), inverted UIM (MIU), as well as GAT (GGA and TOM)-binding motifs (GGA, golgi-localized, γ-ear-containing, Arf (ADP-ribosylation factor)-binding protein; TOM, target of Myb). Among them, the UBA and CUE domains are structurally homologous, with a common three-helical bundle architecture. Cue2-1^{cue} binds ubiquitin through the α1 and α3 helices (Figure 3.4B) (*198*), whereas the Dsk2^{UBA} uses the loop between α1 and α2, as well as the C-terminal part of α3 (Figure 3.4C) (*65*). Structural characterization of the UIMs demonstrated that a single α-helix is sufficient for binding this region of ubiquitin (*49, 51, 203*). The UIM helix includes a conserved alanine neighbored by a bulky hydrophobic residue, each of which packs against ubiquitin's I44 as demonstrated in the S5a UIM1–ubiquitin complex (Figure 3.4D) (*51*). Rabex-5 MIU/IUIM (*56, 57*) and the polymerase η ubiquitin-binding zinc finger domain (*204*) similarly bind this region in

ubiquitin through a single α-helix, but in the reverse orientation (Figure 3.4E). The GLUE domain of ESCRT-II EAP45, which exhibits a split pleckstrin-homology topology, is the only previously known ubiquitin-binding PHD (*94*). However, it binds ubiquitin in a different manner: the I44-containing surface of ubiquitin is contacted by residues within secondary structural elements including the EAP45 C-terminal helix corresponding to H1 in Rpn13 (*94*) (Figure 3.4F). Moreover, although the longer S6–S7 loop of EAP45 is involved in binding ubiquitin, the S2–S3 and S4–S5 loops are not; instead, contacts are formed by residues from S5 and S6.

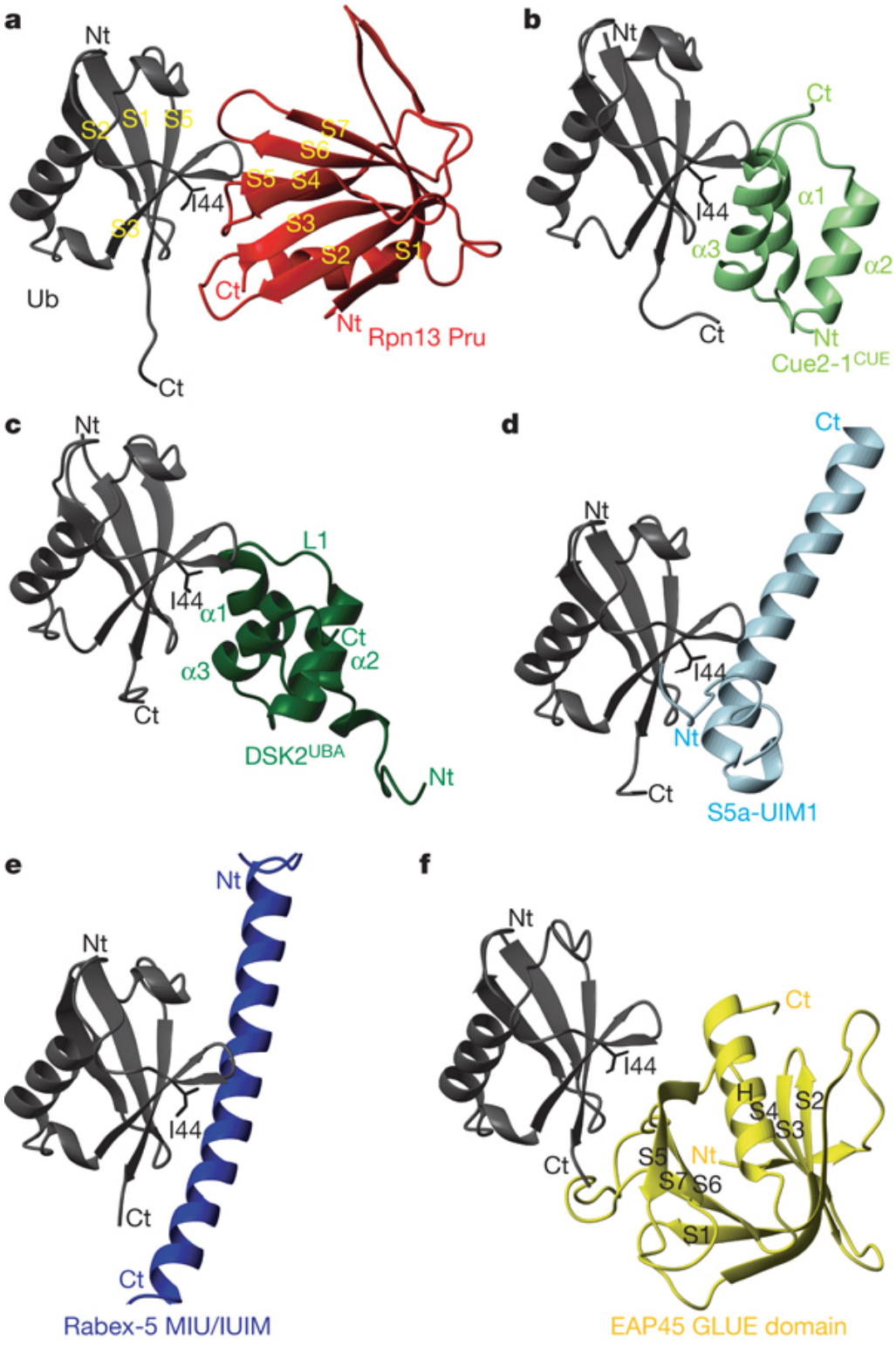

Figure 3.4. Structural comparison of ubiquitin receptors complexed with ubiquitin. Complex structures of ubiquitin and specific receptors displayed with ubiquitin in the

same orientation (grey) and ubiquitin's I44 shown in black sticks. Each receptor has a unique color coding: (A) Rpn13 Pru (red); (B) Cue2-1^{CUE} (PDB code 1OTR; light green); (C) Dsk2^{UBA} (PDB code 1WR1; dark green); (D) S5a-UIM1 (PDB code 1YX5; light blue); (E) Rabex-5 MIU/IUIM (PDB code 2FIF; dark blue); (F) EAP45 GLUE domain (PDB code 2HTH; yellow). All structures are compared by a best-fit superposition of bound ubiquitin (grey). In (C) L1 denotes the loop connecting α1 and α2.

In addition to its unique monoubiquitin-binding mode, we have demonstrated that Rpn13 has a novel preference for diubiquitin elements within K48-linked chains, as described in Chapter 2, and that it most likely interacts directly with the isopeptide bond within a ubiquitin chain. This ubiquitin-binding mode is consistent with Rpn13's functional relationship with Uch37, which it adds to the collection of chain-processing enzymes in the proteasome's regulatory particle (*163, 169, 171*). For diubiquitin, hRpn13 binding to the proximal subunit would leave the distal one available to interact with Uch37 (Figure 3.3D). Evidence exists for Uch37 binding to the distal subunit of polyubiquitin; it is reported to be incapable of disassembling ubiquitin chains in which the distal ubiquitin contains the L8A and I44A mutations (*205*) and dismantles chains by removing one ubiquitin moiety at a time from the distal end (*174*). Uch37's distal-end deconjugation of ubiquitin chains (*174*) complements that of Ubp6 and Rpn11, as Ubp6 can deconjugate multiple ubiquitins in a single cleavage event (*189*) and Rpn11 performs 'en bloc' deubiquitination from the proximal end (*206, 207*). Deubiquitinating activities, particularly that of Ubp6, are antagonized by another regulatory particle component, the chain elongation factor Hul5 (*208*). With so many receptors and chain-processing enzymes within the regulatory particle, the detailed pathway by which a substrate is degraded may be subject to many stochastic variations. Whether this unanticipated design promotes high substrate flux through the proteasome is unclear, but it seems well suited

to allow the cell to fine-tune proteasome activity.

3.4 Methods Summary

3.4.1 Expression, purification, crystallization and structure determination of mRpn13 Pru

mRpn13 Pru was overexpressed in *Escherichia coli* strain BL21(DE3) RIL (Stratagene) and purified by GST-affinity chromatography using a PreScission Protease (GE Healthcare) cleavage site followed by size-exclusion chromatography. Rpn13 Pru was crystallized by the hanging-drop vapor-diffusion method and frozen in a stream of liquid nitrogen during X-ray exposure. Single anomalous dispersion methods were performed using synchrotron radiation at the BW6 beamline at the DESY-centre in Hamburg, Germany. Native data were collected to 1.7-Å resolution (Table 3.S1). Details about recombinant DNA modifications, expression and purification of mutant forms of Rpn13 Pru, data processing, phase determination, model building and structural refinement are described in Section 3.6.1.

3.4.2 NMR Spectroscopy

Chemical shift assignments and spectra were acquired as described in Section 3.6.1. mRpn13 Pru–ubiquitin and mRpn13 Pru–diubiquitin complexes were generated as described in Section 3.6.1.

3.5 Supplementary information

3.5.1 Material and methods

3.5.1.1 Cloning of murine Rpn13 Pru

The mammalian expression vector pcDNA3.1/myc-his containing the full-length cDNA of mRpn13 (murine Adrm1/Rpn13, Swiss-Prot: Q9JKV1; was kindly provided by Dr. Lamerant, Centre de Biophysique Moléculaire, France, (*185*) and used for subcloning into pcDNA3-myc (EcoRI/XhoI). The N-terminal part (1-150) of the mRpn13 cDNA was amplified by PCR using primers 5`-GCGGATCCATGACGACTTCAGGCGCTCTG-3` and 5`- GCGGATCCTCACAGTGCTGAAAGCTC-3`, thereby introducing flanking *BamHI* (underlined) restriction sites. The *BamHI*-cleaved PCR product was subcloned into *E. coli* expression vector pRSET-GST-PP. The pRSET-GST-PP vector was derived from the pRSET vector (Invitrogen) by cutting out the MCS with restriction enzymes *NdeI* and *BamHI* and insertion of the DNA encoding GST-tag followed by a PreScission Protease cleavage site. Mutants of mRpn13 (S55E, L56A, I75R, F76R, D79N, and F98R) were created b site-directed mutagenesis (Stratagene). Deletion mutants of hRpn2 (695-953, 797-953, 881-953, and 902-953) were amplified by PCR, subcloned into pEGFP-C1 (Clontech) and pGEX-4T1 (Amersham).

3.5.1.2 Expression and Purification of Rpn13 Pru

Rpn13 Pru was overexpressed in *E. coli* strain BL21(DE3) RIL (Stratagene). Expression was induced by addition of 0.5 mM IPTG at an OD_{600}nm of ~0.6 and cells were grown at 24 °C overnight. Cell pellets were resuspended in 1/100 of culture volume

in buffer A (20 mM Tris-Cl, pH 8.0; 100 mM NaCl; 1 mM DTT). Cells were lysed by sonication at 0°C and the suspension was clarified by centrifugation at 4°C and 20000 g for 20 min. GST-fused protein was purified from bacterial lysate by affinity chromatography using Glutathione Sepharose 4B (Amersham Biosciences). Recombinant protein was eluted from glutathione beads by cleavage with PreScission Protease at 30°C for 1 h in buffer A. The eluted protein was further purified in buffer B (20 mM Tris-Cl, pH 8.0; 40 mM NaCl; 1 mM DTT) on a Superdex 200 gel filtration column (Amersham Biosciences). The typical yield of purified soluble Rpn13 Pru from 3 L of culture was ~4 mg. For selenomethionine labeling, Rpn13 Pru was overexpressed in the methionine auxotroph *E. coli* strain B834(DE3) (Novagen). Cells were grown in New Minimal Medium (*209*) at 37°C to an OD_{600}nm of ~0.6, expression was induced with 0.5 mM IPTG. Incubation was continued at 24°C overnight. Purification of selenomethionine-labeled protein was performed according to the same procedure as for native protein.

3.5.1.3 Biochemical pull-down assays

For GST pull-down of purified proteins, GST-fused tetraubiquitin coupled to beads was cleaved with thrombin (Novagen) 4 h at 4°C in a cleavage buffer containing 20 mM Tris-HCl (pH 8.4), 150 mM NaCl, 2.5 mM CaCl2 and 1 mM DTT. Thrombin was inactivated with addition of PMSF and GST bound to beads was removed by centrifugation. Supernatant was further used for GST pull-down with GST and various GST-fused proteins in incubation buffer containing cleavage buffer, 10% glycerol and 1% Triton X-100. After 5 hours of incubation at 4°C, beads were washed three times with

incubation buffer. Bound proteins were boiled for 5 minutes in SDS sample buffer and analyzed by SDS-PAGE and immunoblotting.

3.5.1.4 Crystal growth

Crystals grew at 20°C within two days to the size of 500 x 200 x 200 μm^3. Crystallization drops contained equal volumes of protein (5 mg/ml) and reservoir solution (15 % (w/v) PEG 4000, 200 mM NaOAc, 1 mM DTT, 100 mM Tris-HCl, pH 8.5). Before exposure to X-rays, crystals were soaked in a solution of mother liquor including 15% PEG 400 for 5 min and subsequently frozen in a stream of cold nitrogen gas at 100 K (Oxford Cryosystems).

3.5.1.5 Data processing and structure determination

Data were processed with DENZO and SCALEPACK (*210*). The space group of Rpn13 Pru was $P2_12_12_1$ with unit cell dimensions of a=42.4 Å, b=56.2 Å, c=63.2 Å. Phase determination was performed by crystal structure analysis of an Rpn13 Pru-SeMet-derivative. SAD data were collected at 2.7 Å resolution using absorption peak wavelengths (0.9793 Å, see Table 3.S1). Two Se-sites were localized using SHELXD (*211*). Subsequent phasing with MLPHARE (*212, 213*) and solvent flattening with DM (*214*) resulted in an interpretable electron density map, which was traced and phase extended to the native data set at 1.7 Å resolution using ARP-WARP (*215*). The model was completed using the interactive three-dimensional graphic programs MAIN (*216*) and refined with REFMAC5 (*217*). Temperature factors were refined with restraints

between bonded atoms and between non-crystallographic symmetry related atoms. R_{crys} and R_{free} have been refined to 0.202 and 0.227, respectively (*218*).

3.5.1.6 NMR spectroscopy and the assignment of hRpn13

NMR spectra were acquired at 25°C on a Varian NMR spectrometer operating at 800 MHz with a cryogenically cooled probe. Processing was performed in NMRPipe (*196*) and the resulting spectra visualized with XEASY (*219*). Protein concentrations were calculated by using extinction coefficients based on amino acid composition and absorbance at 280 nm for protein dissolved in 6M guanidine-HCl. All NMR samples were dissolved in buffer C (20 mM $NaPO_4$ (pH 6.5), 30 mM NaCl, 2mM DTT, 0.1% NaN_3, and 10% D_2O).

We performed optimized triple resonance experiments to assign chemical shift values to hRpn13 Pru domain's backbone ($N,H^N,C\alpha,C'$) and $C\beta$ atoms. Chemical shift assignments were made by using 3D HNCA/HNCOCA and HNCACB experiments on 0.6 mM ^{15}N-, ^{13}C- and 70% ^{2}H-labeled hRpn13 Pru in buffer C. An ^{15}N dispersed NOESY spectrum (200 ms mixing time) acquired on ^{15}N-, 50% ^{2}H-labeled human Rpn13 Pru was used to confirm the assignments and that the secondary structural elements match those of the crystal structure (example provided in Figure 3.S8). Due to its favorable chemical shift dispersion, we were able to assign all of the backbone atoms of hRpn13 (1-150), except for V38 and S90.

3.5.1.7 Chemical shift perturbation data

We performed three sets of chemical shift perturbation analyses on hRpn13 Pru complexes with monoubiquitin and tetraubiquitin. In particular, unlabeled monoubiquitin or tetraubiquitin was added to ^{15}N labeled hRpn13 Pru (Figure 3.S6A) or alternatively unlabeled hRpn13 Pru was added to ^{15}N labeled monoubiquitin (Figure 3.S6B). In each case, the ^{15}N labeled protein was observed by ^{1}H, ^{15}N HSQC experiments as it bound its unlabeled binding partner. We mapped the amide nitrogen and hydrogen chemical shift changes for each residue according to Equation 3.S1.

$$\mathrm{CSP} = \sqrt{0.2\Delta\delta_N^{\,2} + \Delta\delta_H^{\,2}} \qquad (3.S1)$$

In this equation $\Delta\delta_N$ and $\Delta\delta_H$ represent the changes in the amide nitrogen and proton chemical shifts (in parts per million), respectively. S55, L56, I75, F76, D79, F82, L96, F98 and G101 all exhibited significant amide resonance shifting as hRpn13 Pru bound ubiquitin (Figure 3.S6A, black). Only two residues in Rpn13, L73 and R104, exhibited effects that were specific to K48-linked tetraubiquitin (Figure 3.S6A, red).

3.5.1.8 Rpn13:ubiquitin structure calculations

We solved the structure of the Rpn13:ubiquitin complex by using NOE-derived distance constraints between hRpn13 and monoubiquitin. These were derived by using an ^{15}N dispersed NOESY experiment acquired on ^{15}N-, ^{13}C- and 70% ^{2}H-labeled hRpn13 Pru mixed with equimolar ratio of unlabeled ubiquitin. For this experiment, no ^{13}C or ^{2}H decoupling was implemented to enable the ready identification of intermolecular NOE interactions. Further validation that the assigned NOEs were intermolecular was achieved

by their absence in an ^{15}N dispersed NOESY experiment acquired under identical conditions on ^{15}N-labeled hRpn13 Pru alone. Chemical shift assignment of the sidechain ubiquitin atoms was obtained by following the assigned resonances of the free protein upon addition of increasing molar rations of unlabeled hRpn13 Pru. In total, we identified twelve explicit intermolecular NOE interactions between L8, F45, A46, Q49, H68, and V70 of ubiquitin and F76, D78, D79, F98, A100, G101, K103, and R104 of hRpn13, Figure 3.2A.

Only five amino acid residues differ between the N-terminal ubiquitin-binding domain of human and murine Rpn13 Pru, and none of these are implicated by the NMR data as binding ubiquitin. Moreover, an ^{15}N dispersed NOESY experiment confirmed that hRpn13 Pru in solution is similar to the crystal structure of mRpn13 in terms of topology and architecture, as well as in the disordered state of the N-terminal 21 and C-terminal 20 amino acids. Therefore, the mRpn13 Pru crystal structure (Figure 3.1A) was used as a starting structure along with the NMR data on hRpn13 to determine the structure of the mRpn13 Pru:ubiquitin complex.

The mRpn13 Pru:ubiquitin complexes were generated by using HADDOCK1.3 (*H*igh *A*mbiguity *D*riven protein-protein *DOCK*ing) (*220*) in combination with CNS (*221*). The atomic coordinates for ubiquitin were obtained from PDB entry 1D3Z (*222*). All atom pairs exhibiting an intermolecular NOE interaction were constrained to be within 1.8 – 6.0 Å of each other. In addition, the constraints from the hydrogen bonds published for ubiquitin (PDB code 1DZ3) were used to maintain its fold, as the protein does not undergo any gross structural change upon binding. Data afforded by NMR

titration experiments that record amide chemical shift changes that result from complex formation have been successfully used to determine the structure of protein complexes (*42, 223, 224*). We therefore generated so-called Ambiguous Interaction Restraints (AIRs) to complement our unambiguous NOE-based distance constraints. Briefly, residues with chemical shift perturbation values greater than one standard deviation value above the average were defined as "active" (Table 3.S2) and their neighbors as "passive" provided they have >50% accessibility. AIRs restrict active residues to be within 2.0 Å of any atom of the binding partner's active or passive residues, as described (*220*). Our mRpn13:ubiquitin complex is well defined and the omission of any one NOE interaction yields identical results.

For the first step of rigid-body energy minimization, 1000 structures were generated. 200 structures having the lowest energy from the rigid-body docking were subjected to semi-flexible simulated annealing in torsion angle space followed by refinement in explicit water. During semi-flexible simulated annealing, atoms at the interface were allowed to move but constrained by the AIRs and unambiguous NOE-derived distance constraints. After water refinement, the resulting structures were sorted according to intermolecular energy and clustered using 1.5 Å cut-off criterions. This treatment resulted in an ensemble of 200 structures with the average RMSD of 0.94 ± 0.31 Å for all backbone atoms and 0.75 ± 0.23 Å for the backbone atoms at the interface. The ten lowest energy structures in the lowest energy cluster were evaluated according to the following criteria: all intermolecular hydrophobic contacts between heavy atoms being less than 3.9 Å, intermolecular hydrogen bond distances between proton-acceptor

and donor-acceptor pair being within 2.7 Å and 3.35 Å, respectively, and minimum angles of 90° for donor-hydrogen-acceptor, hydrogen-acceptor-acceptor antecedent, donor-acceptor-acceptor antecedent atoms of hydrogen bonds (*225*). The ten lowest energy structures are provided as Figure 3.S9. It is worth noting that the NOE-derived distance constraints define the mRpn13 Pru:ubiquitin structure, which does not change upon omission of the AIRs.

3.5.1.9 Modeling the mRpn13 Pru:diubiquitin complex

The model structure of mRpn13 Pru:diubiquitin was built from the structures of the mRpn13 Pru:ubiquitin complex and ubiquitin (PDB entry 1D3Z) by using Insight II (Accelrys, Inc). For diUb, the two monoubiquitin molecules were conjugated by forming the G76-K48 isopeptide bond and allowing rotations in the K48 sidechain of proximal ubiquitin to avoid steric clashes between the distal ubiquitin subunit and Rpn13. The structure was subsequently energy-minimized by using SYBYL (Tripos, Inc.).

3.5.2 Supplementary tables

Table 3.S1: Data collection and refinement statistics

	mRpn13 Pru	mRpn13 Pru SeMet
Crystal parameters		
Space group	$P2_12_12_1$	$P2_12_12$
Cell constants	a=42.4 Å; b=56.2 Å; c=63.2 Å	a=42.7 Å; b=56.4 Å; c=64.2 Å
Heavy metal	-	2
Data collection		
Beamline	BW6, DESY	BW6, DESY
Wavelength (Å)	1.05	0.9793

Resolution range (Å)[a]	99-1.7 (1.70-1.67)	99-2.62 (2.7-2.66)
No. observations	1007679	227878
No. unique reflections[c]	25165	8927
Completeness (%)[b]	99.5 (99.9)	98.9 (100)
R_{merge} (%)[b, c]	5.1 (27.2)	10.0 (35.3)
I/σ (I)[b]	19.1 (2.9)	32.6 (11.4)

Refinement (REFMAC5)

Resolution range (Å)	15-1.7
No. reflections working set	16267
No. reflections test set	813
No. non hydrogen	973
Solvent water	106
R_{work}/R_{free} (%)[d]	19.9 / 22.4
R_{work}/R_{free} (2.74-1.70 Å) (%)[d]	24.5 / 27.7
rmsd bond lengths (Å) / (°)[e]	0.012 / 1.75
Average B-factor (Å^2)	30.67
Ramachandran Plot (%)[f]	92.7 / 7.3 / 0.0

[a] The values in parentheses of resolution range, completeness, R_{merge} and I/σ (I) correspond to the last resolution shell.

[b] Friedel pairs were treated as different reflections.

[c] $R_{merge}(I) = \Sigma_{hkl}\Sigma_j |[I(hkl)_j - I(hkl)]| / [\Sigma_{hkl} I_{hkl}$, where $I(hkl)_j$ is the jth measurement of the intensity of reflection hkl and <I(hkl)> is the average intensity.

[d] $R = \Sigma_{hkl} | |F_{obs}| - |F_{calc}| | / \Sigma_{hkl} |F_{obs}|$, where R_{free} is calculated without a sigma cutoff for a randomly chosen 5% of reflections, which were not used for structure refinement, and R_{work} is calculated for the remaining reflections.

[e] Deviations from ideal bond lengths/angles.

[f] Number of residues in favored region / allowed region / outlier region.

Table 3.S2. List of active and passive residues defined in hRpn13 Pru and Ubiquitin as defined by chemical shift perturbation plots for HADDOCK

Protein	Active residues	Passive residues	Flexible segments
hRpn13 Pru	55,76,78,99,101,104	53,54,74,77,81,83,100,102,103	51-57,72-85,97-106
Ubiquitin	47,48,49,68	6,8,9,10,11,12,16,42,46,51,72	4-18,40-53,66-74

3.5.3 Supplementary Figures

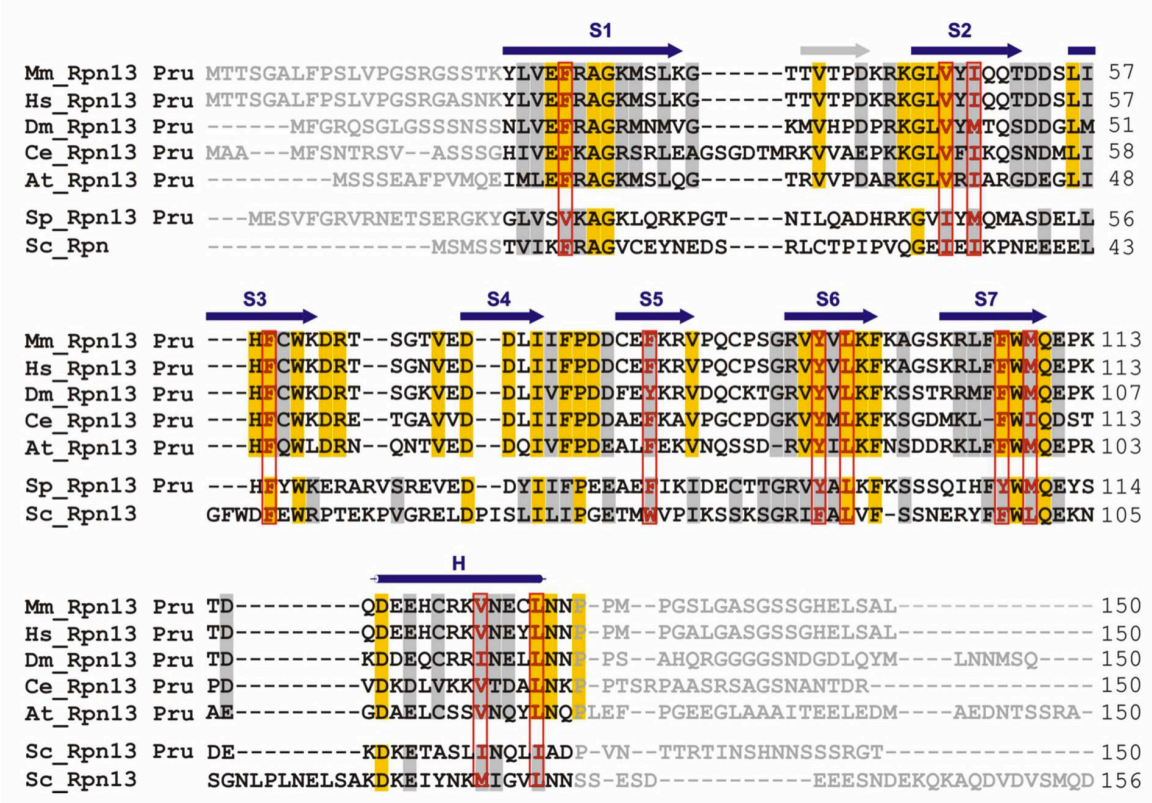

Figure 3.S1. Sequence alignment of Rpn13 Pru homologues from *Mus musculus* (Mm), *Homo sapiens* (Hs), *Drosophila melanogaster* (DM), *Caenorhabditis elegans* (Ce), *Arabidopsis thaliana* (At), *Schizosaccharomyces pombe* (Sp), *Saccharomyces cerevisiae* (Sc). Identical residues of Rpn13 Pru are highlighted against a yellow background, conserved residues against a grey background. Sequence stretches given in grey are disordered in the crystal structure. Residues involved in formation of the hydrophobic core of the PH domain are conserved among all eukaryotes and indicated by red boxes. Secondary structure elements of Rpn13 Pru contributing to the topology of the PH domain are indicated in blue and additional secondary structure elements in grey.

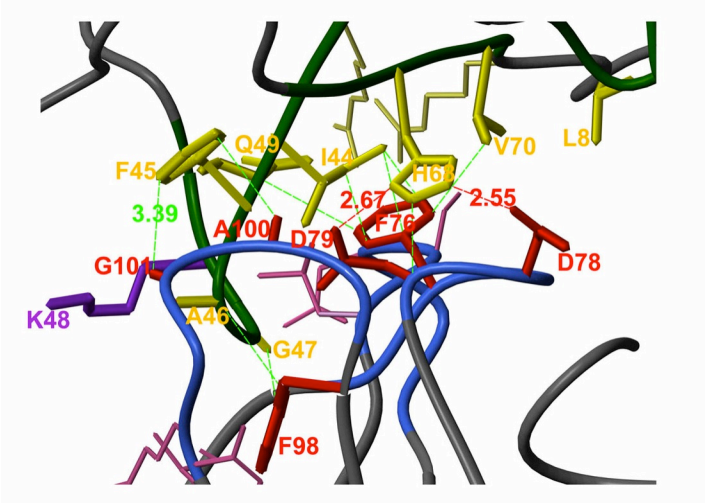

Figure 3.S2. Zoomed view of Figure 3.2B to highlight several key hydrophobic (green dashed lines) or hydrogen bond (red dashed lines) interactions. Several contact residues from ubiquitin (yellow) or Rpn13 (red) are displayed.

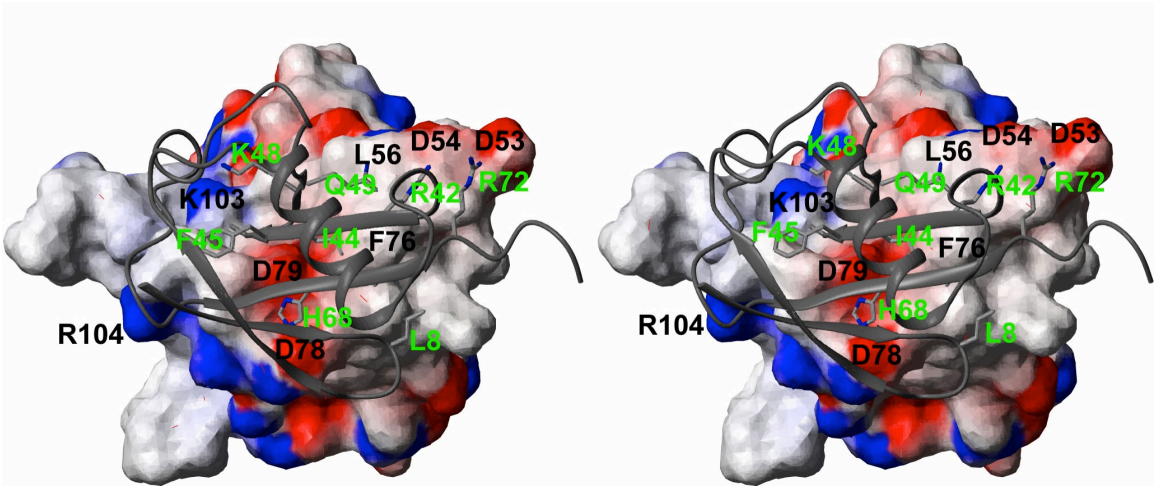

Figure 3.S3. Stereo representation of the electrostatic surface potential of mRpn13 Pru's ubiquitin-binding surface with several of its key ubiquitin-binding residues labeled in black. The surface is color coded according to electrostatic potential, contoured from -25kT/e (intense red, negative charges) to +25kT/e (intense blue, positive charges). A ribbon representation of ubiquitin is displayed with certain contact residues in balls-and-sticks representation and labeled in green.

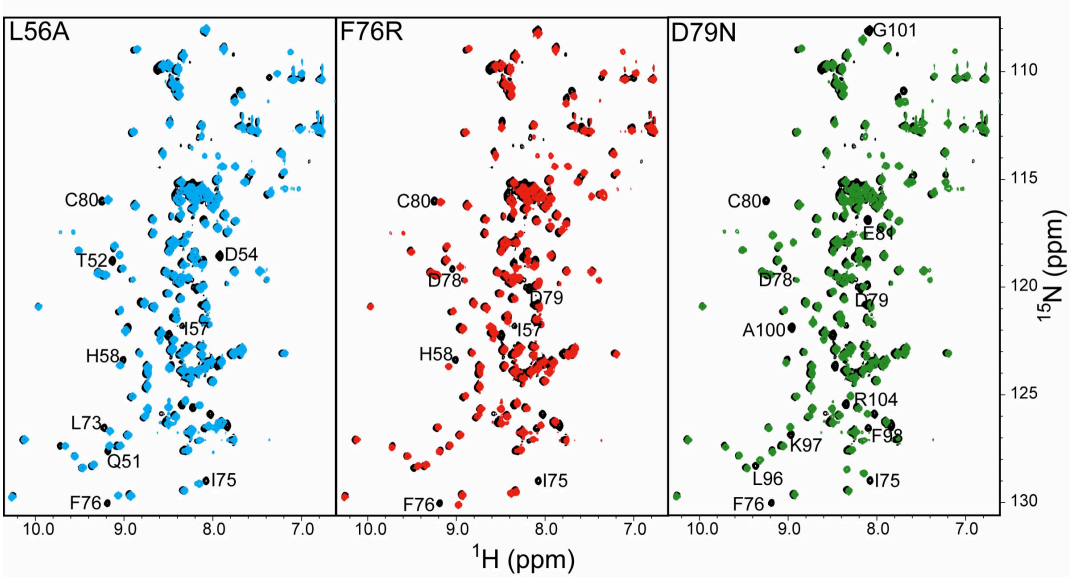

Figure 3.S4. The L56A, F76R and D79N point mutations do not compromise the structural integrity of the mRpn13 Pru domain. Only local effects are observed in superimposed ^{1}H, ^{15}N HSQC spectra of ^{15}N labeled mRpn13 Pru wild-type (black) and L56A (cyan), F76R (red), or D79N (green) protein. Shifted resonances are labeled.

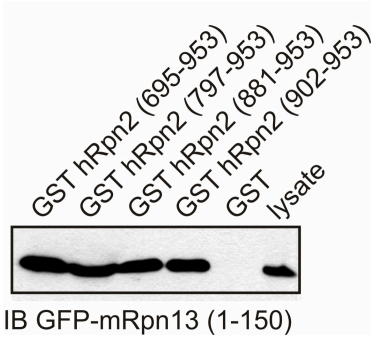

Figure 3.S5. Different deletion mutants of hRpn2 (695-953, 797-953, 881-953 and 902-953) were expressed as GST-fused proteins and tested for their ability to bind mRpn13 (1-150) transiently expressed as myc-tagged protein in HEK293T cells. All deletion mutants of hRpn2 could bind mRpn13, showing that the last 52 amino acids of hRpn2 are sufficient for mRpn13 binding.

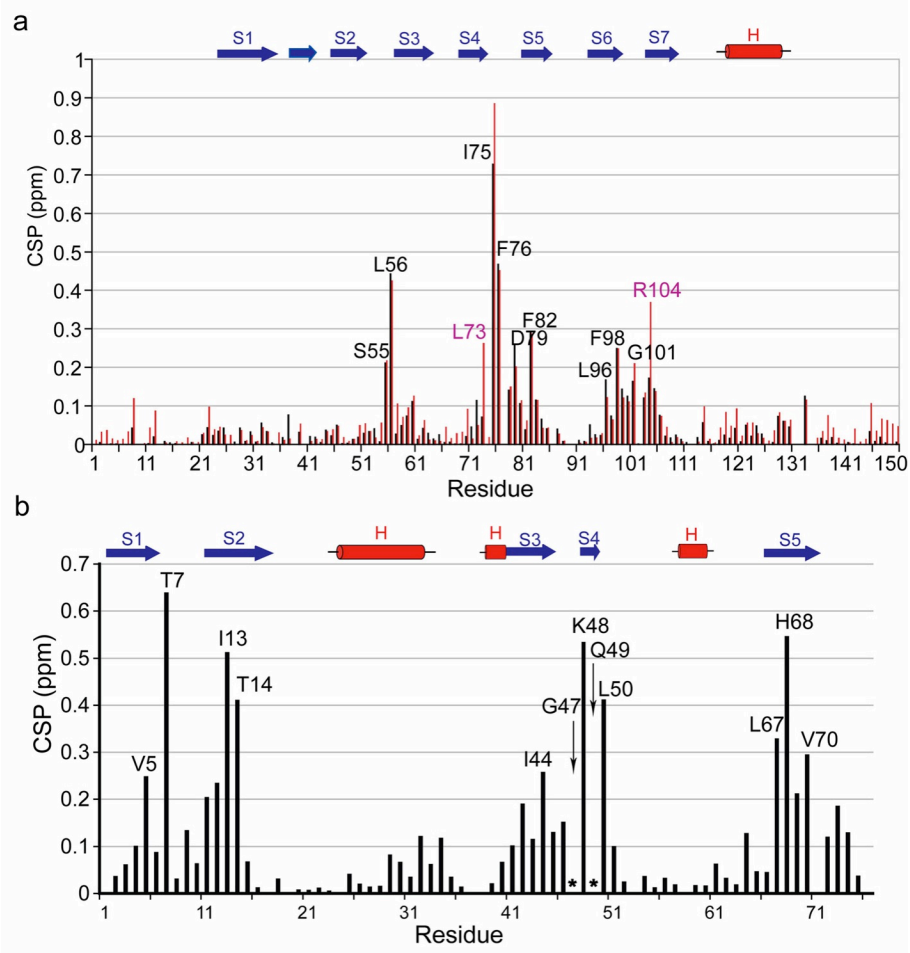

Figure 3.S6. (A) Chemical shift perturbation analysis reveals residues within Rpn13 Pru that bind monoubiquitin (black) and K48-linked tetraubiquitin (red). Amide chemical shift values of hRpn13 Pru alone were compared to values with equimolar quantities of unlabeled ubiquitin (black) or K48-linked tetraubiquitin (red). Data were recorded and quantified by ^{1}H, ^{15}N HSQC experiments as described in Supplementary Information. Residues that were significantly affected by monoubiquitin or tetraubiquitin are labeled. L73 and R104 (labeled in purple) of hRpn13 Pru exhibit effects specific to K48-linked tetraubiquitin. (B) Comparison of amide chemical shift values of free and Rpn13 Pru-bound ubiquitin at equimolar concentration, as described in (A). For this experiment, ubiquitin is ^{15}N labeled and its significantly shifted resonances are labeled; residues that undergo severe broadening are marked with asterisks and emphasized with a black arrow.

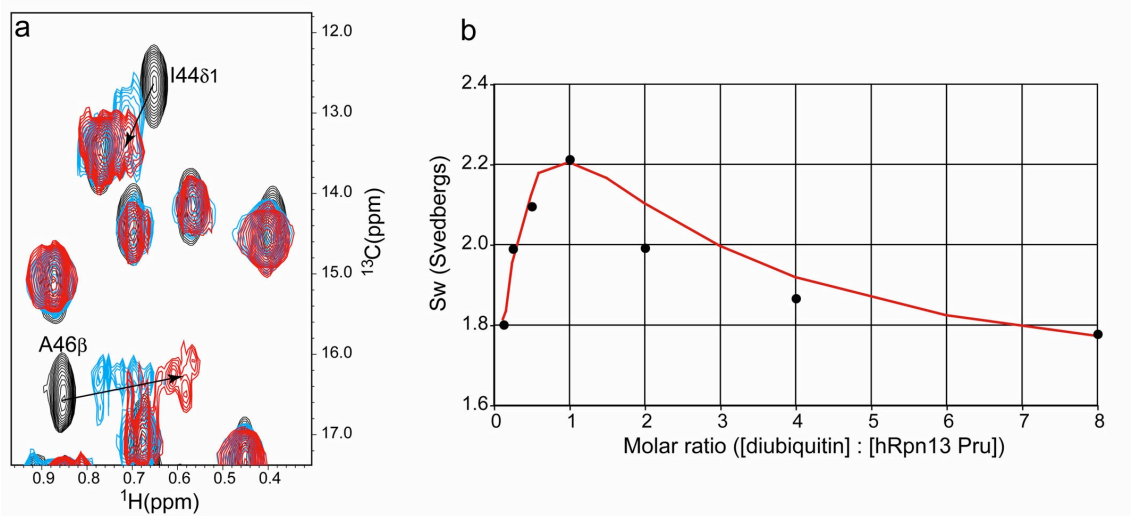

Figure 3.S7. (A) As observed for the proximal subunit of diubiquitin, the I44 δ_1 and A46 methyl groups of monoubiquitin undergo significant resonance shifting upon hRpn13 (1-150) addition. $^{1}H,^{15}N$ HMQC spectra are displayed for 13C-labeled monoubiquitin:hRpn13 (1-150). (B) The weight average sedimentation coefficient as a function of diubiquitin to hRpn13 molar ratios reveals 1:1 binding stoichiometry Experimentally determined values obtained by using sedimentation velocity analysis (black) and theoretical plot for 1:1 binding stoichiometry (red) are included.

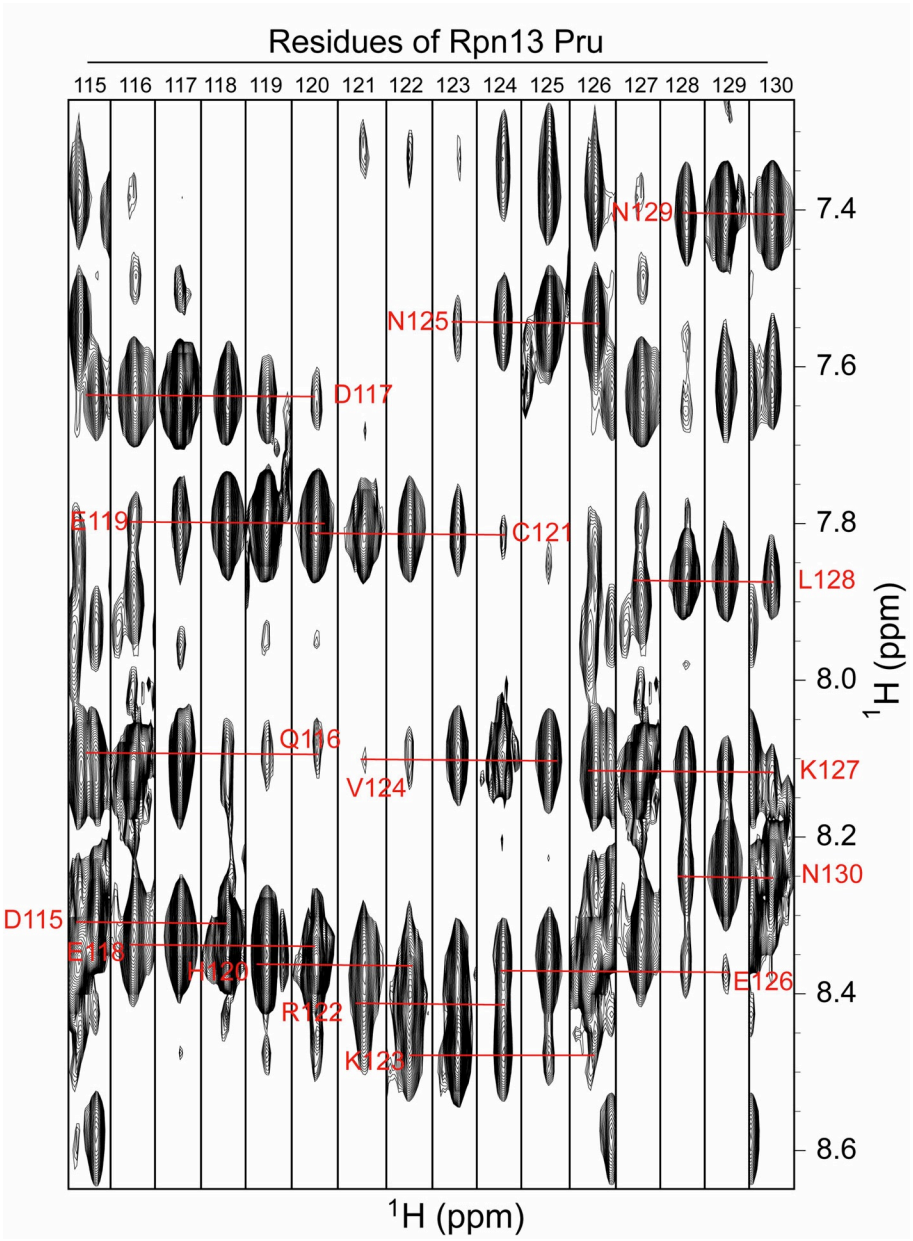

Figure 3.S8. The NOE patterns observed in an ^{15}N dispersed NOESY spectrum confirm that the solution structure of hRpn13 Pru matches the solved crystal structure of mRpn13 Pru. An example is provided for a helical region spanning D115-N130, in which amide-to-amide NOE interactions confirm its helical structure. Consistency with the crystal structure is also evident from chemical shift index analysis for Cα and C' atoms (data not shown).

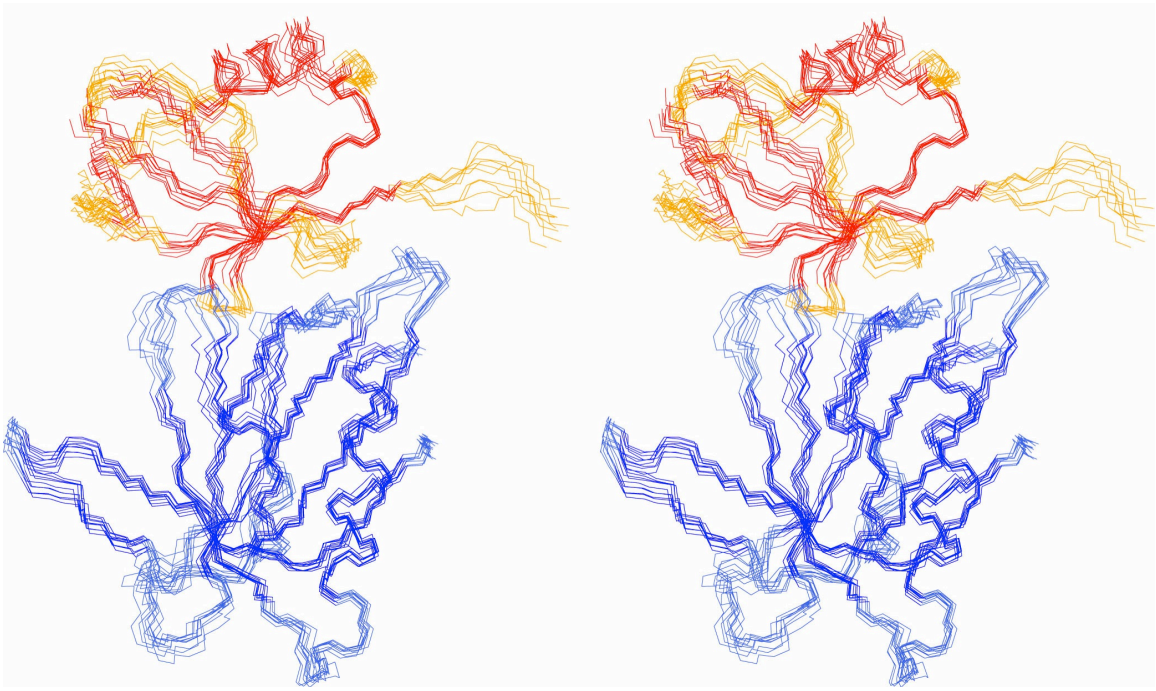

Figure 3.S9. Stereoview of the ten lowest energy structures of the Rpn13 Pru:ubiquitin complex. The lowest energy structure was selected to represent the model. Backbone atoms of Rpn13 Pru and ubiquitin secondary structural elements are displayed in dark blue and red, respectively. Atoms in loops of Rpn13 Pru and ubiquitin are sky blue and orange, respectively.

Chapter 4

Structure of the S5a:K48-linked diubiquitin complex and its interactions with Rpn13

Naixia Zhang[1,], Qinghua Wang[1,4,*], Aaron Ehlinger[1,*], **Leah Randles[1,*]**, Jeffrey W. Lary[2], Yang Kang[1], Aydin Haririnia[3], Andrew J. Storaska[3], James L. Cole[2], David Fushman[3], and Kylie J. Walters[1]*

[1]Department of Biochemistry, Molecular Biology and Biophysics, University of Minnesota, Minneapolis, MN 55455
[2]Analytical Ultracentrifugation Facility, Biotechnology-Bioservices Center, University of Connecticut, Storrs, CT 06269-3149, USA
[3]Department of Chemistry and Biochemistry, Center for Biomolecular Structure and Organization, University of Maryland, College Park, MD 20742
[4]Current address: Department of Biochemistry and Molecular Biology, University of Massachusetts, Amherst, MA 01003
[*]These authors contributed equally to this paper.

Reprinted with permission from Elsevier Inc Vol 35, Issue 3, pp 280-90[a]

Leah Randles Contributions: Devised methodology and synthesized samples used to generate Figures 4.2 & 4.3 as well as synthesized the samples and contributed to the experiments in Figure 4.5. Contributed to the writing of the published manuscript.

---

[a] NMR data were acquired in the NMR facility of the University of Minnesota as well as that at the University of Wisconsin at Madison (NMRFAM) and Biomolecular NMR facility at the University of Maryland (UMD). We are grateful to Drs. Klaas Hallenga (NMRFAM) and Dr. Marco Tonelli (NMRFAM) for their technical assistance as well as Dr. Daoning Zhang (UMD) for preparing some diubiquitin samples. Data processing and visualization occurred in the Minnesota Supercomputing Institute Basic Sciences Computing Lab. Analytical ultracentrifugation data was collected at the National Analytical Ultracentrifugation Facility at the University of Connecticut in Storrs. This work was funded by grants from the National Institutes of Health CA097004 (KJW) and GM065334 (DF), the UMN Grant-in-Aid of Research, Artistry, and Scholarship (KJW), and the Minnesota Medical Foundation (KJW, NMR facility).

4.1 Synopsis

Degradation by the proteasome typically requires substrate ubiquitination. Two ubiquitin receptors exist in the proteasome, S5a/Rpn10 and Rpn13. Whereas Rpn13 has only one ubiquitin-binding surface, S5a binds ubiquitin with two independent ubiquitin interacting motifs (UIMs). In this Chapter, we use NMR and analytical ultracentrifugation to define at atomic level resolution how S5a binds K48-linked diubiquitin, in which K48 of one ubiquitin subunit (the "proximal" one) is covalently bonded to G76 of the other (the "distal" subunit). We demonstrate that S5a's UIMs bind the two subunits simultaneously with a preference for UIM2 binding to the proximal subunit while UIM1 binds to the distal one. In addition, NMR experiments reveal that Rpn13 and S5a bind K48-linked diubiquitin simultaneously with subunit specificity, and a model structure of S5a and Rpn13 bound to K48-linked polyubiquitin is provided. Altogether, our data demonstrate that S5a is highly adaptive and cooperative towards binding ubiquitin chains.

4.2 Introduction

Ubiquitin conjugation plays a key regulatory role in a wide array of biological processes. In its most established role, ubiquitination targets proteins for degradation by the 26S proteasome (*226*), a process important for controlling the lifespan of regulatory proteins, removing misfolded proteins, producing immunocompetent peptides (*227*), and regulating cell cycle progression (*228, 229*).

The 26S proteasome contains a 20S catalytic core particle (CP) capped at either or both ends by 19S regulatory particles (RPs), which prepare substrates for hydrolysis in the CP. RP ubiquitin receptors S5a/Rpn10 (*230*) and Rpn13 (*231*) capture substrates by recognizing their covalently attached ubiquitin chains, which are removed and disassembled by three deubiquitinating enzymes Rpn11 (*206*), Ubp6/Usp14 (*184*) and Uch37/UCHL5 (*174*). These actions of the RP's ubiquitin processing enzymes are complemented with that of six ATPases that unfold protein substrates to allow their passage into the CP for degradation.

Ubiquitin receptors play an integral role in substrate capture and apparently contribute to ubiquitin chain deconjugation, as Rpn13 binds and activates deubiquitinating enzyme Uch37 (*163, 169, 171*). S5a and Rpn13 may receive ubiquitinated proteins from extra-proteasomal receptors, including the hHR23 and hPLIC proteins, which bind to them with ubiquitin-like (UBL) domains (*164, 166, 231*) and to ubiquitin with ubiquitin-associated (UBA) domains (*124, 161, 162*). UBL-UBA proteins can also dock substrates into the proteasome by binding to Rpn1/S2 (*232*), a scaffolding protein that may also bind S5a (*233*). S5a is also abundant free of the proteasome, where it has been demonstrated in budding yeast to prevent the hPLIC homolog Dsk2 from binding to proteasome and inhibiting substrate degradation (*234*). Although not essential in budding yeast (*235*), S5a is essential in mice (*236*) and *Drosophila melanogaster* (*237*).

Unique roles for the ubiquitin receptors associated with proteasome degradation are suggested by their diverse ubiquitin binding properties. hHR23a is sandwiched

between the ubiquitin subunits of K48-linked diubiquitin (*42*), effectively sequesters subunits of polyubiquitin up through octaubiquitin (*238*), and protects ubiquitin chains from deubiquitination (*157, 239*). By contrast, Rpn13 binds preferentially to the proximal subunit of K48-linked diubiquitin leaving the distal one available for other interactions (*240*), presumably including that of Uch37, which may facilitate its distal end (*174*) deubiquitinating activity (*163, 169, 171*).

Although S5a was the first proteasome ubiquitin receptor discovered (*230*), its structure complexed with polyubiquitin has not yet been solved. Like Rpn13, the yeast Rpn10 protein is significantly truncated compared to its human S5a homologue (Figure 4.1A). Whereas mammalian Rpn13 gains a deubiquitinating enzyme binding domain (that of Uch37), the extension in mammalian S5a affords a second UIM that binds ubiquitin more strongly than the conserved one (*241*). In previous work, we solved the structure of S5a (196-306) alone and complexed with monoubiquitin to reveal that its two UIMs act independently in each of these structures (*241*).

In this chapter, we use NMR spectroscopy and analytical ultracentrifugation to solve the S5a (196-306):K48-linked diubiquitin structure. In contrast to S5a's binding of monoubiquitin, its two UIMs bind a common diubiquitin molecule rather than recruit two diubiquitins simultaneously. Moreover, it exhibits subunit specificity and binding determinants that make its interaction with ubiquitin chains unique from that of Rpn13 or hHR23a. In addition, we demonstrate that S5a and Rpn13 bind K48-linked diubiquitin simultaneously with subunit specificity. This research provides fundamental information on how the proteasome recognizes polyubiquitinated substrates.

4.3 Results

4.3.1 S5a's UIMs bind to ubiquitin subunits of K48-linked diubiquitin simultaneously and with different affinities

We used NMR spectroscopy to determine whether S5a's two UIMs bind independently to K48-linked diubiquitin. We added unlabeled K48-linked diubiquitin to ^{15}N labeled human S5a (196-306), which contains its two UIMs (Figure 4.1A), and used ^{1}H,^{15}N HSQC experiments to detect binding. NMR signals belonging to UIM1 and UIM2 residues were affected by diubiquitin addition, thus demonstrating diubiquitin's interaction with both UIMs. Different binding behavior was observed for each of the UIMs however. Upon diubiquitin addition, UIM1 signals shift and broaden progressively to their fully saturated state (Figure 4.1B), indicating that these residues exchange rapidly on the NMR timescale (100 milliseconds) between their free and bound states. UIM2 signals by contrast exhibit two peaks prior to saturation, which are not broadened by exchange (Figure 4.1C, blue spectrum) and are representative of their free and diubiquitin-bound states, according to comparisons of spectra recorded on free (Figure 4.1C, blue spectrum) and fully saturated S5a (Figure 4.1C, red spectrum). Hence, UIM2 with its readily observed diubiquitin-bound state is the stronger binding partner.

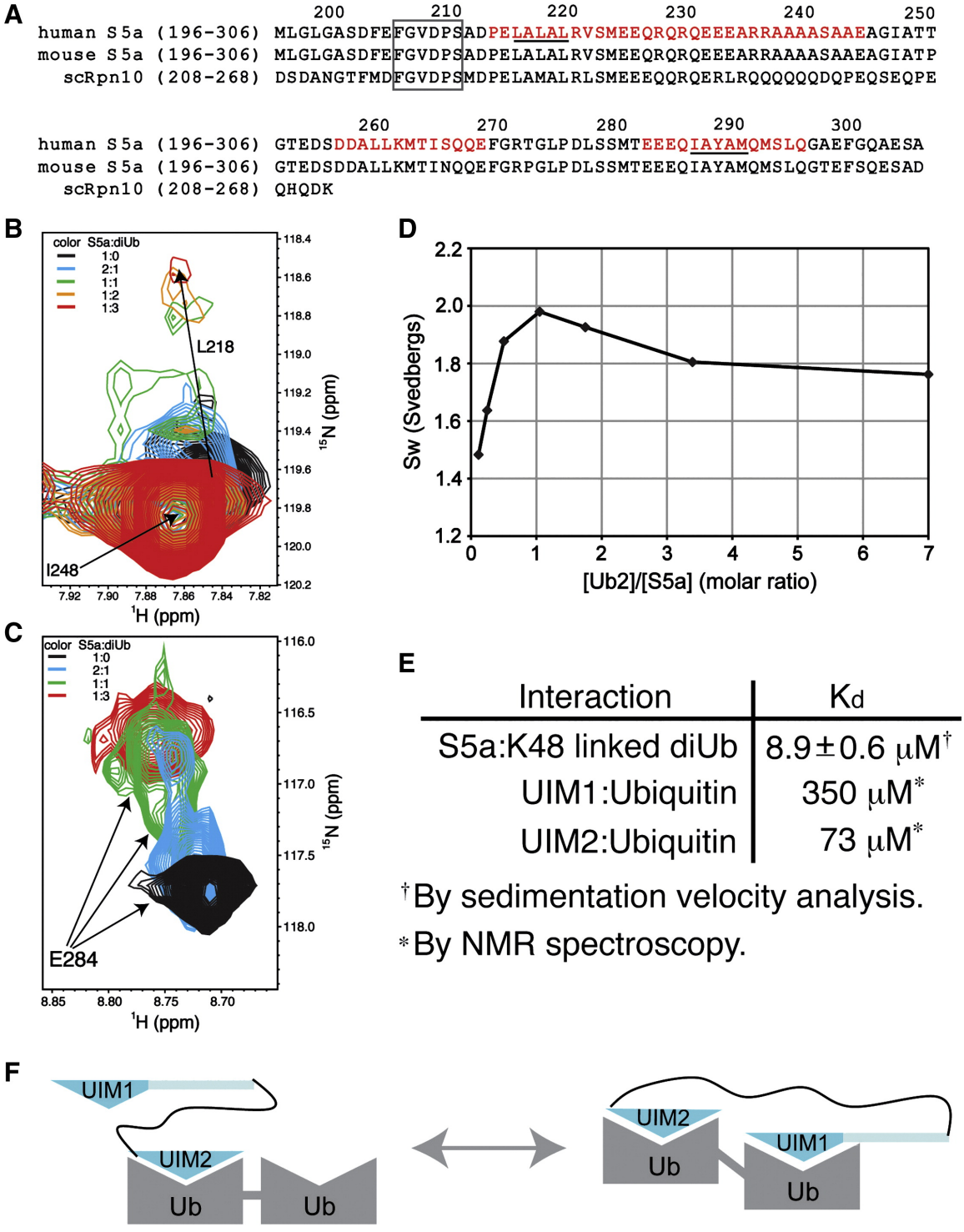

Figure 4.1. S5a's affinity for diubiquitin is enhanced by its two UIMs binding to ubiquitin subunits simultaneously. (A) Sequence alignment of the ubiquitin-binding region of human and mouse S5a with their *Saccharomyces cerevisiae* homologue Rpn10. The helices of S5a are highlighted in red and a strictly conserved region N-terminal to

UIM1 is boxed. The UIM's hallmark LALAL/IAYAM motif is underlined. (B) UIM1 resonances shift and broaden upon binding to K48-linked diubiquitin. $^{1}H,^{15}N$ HSQC spectra expanded to view L218 are displayed for ^{15}N labeled S5a (196-306) alone (black) and at 2:1 (blue), 1:1 (green), 1:2 (orange), and 1:3 (red) S5a:K48-linked diubiquitin molar ratio. The amide resonance of I248, which is not involved in diubiquitin-binding and does not shift with increasing quantities of diubiquitin, overlaps with the L218's unbound resonance. (C) UIM2 resonances exhibit slow exchange dynamics upon binding to K48-linked diubiquitin. $^{1}H,^{15}N$ HSQC spectra expanded to view E284 are displayed for S5a alone (black) and at 2:1 (blue), 1:1 (green), and 1:3 (red) S5a:K48-linked diubiquitin molar ratio. (D) Sedimentation velocity results reveal S5a (196-306) to bind K48-linked diubiquitin with 1:1 stoichiometry and with an affinity of 8.9$\pm$0.6 mM. Experimentally determined averaged sedimentation coefficients (diamonds) are plotted. (E) Binding affinities are displayed for S5a (196-306) binding to diubiquitin, as determined with the data of (D), and for each UIM binding to monoubiquitin (*241, 242*). (F) Model depicting the two S5a:diubiquitin states present at 1:1 molar ratio. The weaker binding UIM1 exchanges between an unbound and bound state. Ub, ubiquitin; UIM1, S5a's ubiquitin interacting motif 1; UIM2, S5a's ubiquitin interacting motif 2.

Unexpectedly, diubiquitin causes signals from the internal helix of S5a (196-306), which spans residues D257-E269, to shift (Figure 4.S1A). Such perturbations were not observed in S5a with monoubiquitin (Figure 4.S1B). This region does not contain a known ubiquitin-binding element and shows no direct contact with monoubiquitin. We tested whether it contacts diubiquitin by using a ^{13}C half-filtered NOESY spectrum in which S5a (196-306) was ^{13}C labeled and diubiquitin was unlabeled. This experiment records intermolecular NOE interactions between S5a and diubiquitin hydrogen atoms that are within 5 Å while selecting against intramolecular NOEs. Whereas such interactions were observed between S5a's UIMs and diubiquitin (as described below), no residues within the intervening helix exhibited such intermolecular NOE interactions (data not shown). Therefore, the spectral perturbation of residues in this region upon diubiquitin addition is not due to its direct contact with diubiquitin. Moreover, the helical

structure of this region is preserved according to ^{15}N and ^{13}C dispersed NOESY spectra (Figure 4.S2). We therefore hypothesized that the spectral changes to this region are caused by physical constraints imposed by the simultaneous binding of both UIMs to diubiquitin.

To test directly whether the two UIMs of S5a bind to the same diubiquitin molecule, we performed sedimentation velocity experiments. Data were recorded at molar ratios of diubiquitin to S5a (196-306) spanning 1:7 to 8:1 and the weight average sedimentation coefficients (s_w) were plotted against molar ratio (Figure 4.1D). This analysis revealed a maximum at a 1:1 mixing ratio, indicating 1:1 binding stoichiometry. The decrease in s_w at lower and higher mixing ratios is due to the presence of free diubiquitin and S5a, respectively. Global analysis of the sedimentation velocity data using this 1:1 binding model gives a best-fit K_d of 8.9$\pm$0.6 μM. This value is substantially lower than that determined for UIM1 and UIM2 binding to monoubiquitin (*241*) (listed in Figure 4.1E). Altogether, these data indicate that the two UIMs bind ubiquitin subunits of diubiquitin simultaneously and that this coordinated binding affords a greater affinity.

The estimated K_d for S5a (196-306) binding to diubiquitin predicts that 86% of S5a is bound to diubiquitin when these two proteins are at equimolar ratio and 0.4 mM protein concentration. As mentioned above, however, S5a's UIM2 exhibits stronger affinity compared to UIM1. The NMR titration experiments revealed that the binding between S5a's UIM1 and diubiquitin is not saturated until diubiquitin is at 3-fold molar excess (Figure 4.1B). Two shifted peaks are observed for L278, S279, E284, A288 and S294 of S5a's UIM2 at equimolar ratio (as demonstrated for E284 in Figure 4.1C), one of

which remains when diubiquitin is at 3-fold molar excess. We propose that the peak present with 3-fold molar excess diubiquitin corresponds to a state in which UIM2 and UIM1 fully occupy diubiquitin whereas the other stems from diubiquitin-bound UIM2 when UIM1 is not bound (Figure 4.1F).

4.3.2 UIM2 binds the proximal subunit while UIM1 binds the distal one

To determine whether distinct binding preferences exist between K48-linked diubiquitin's subunits and S5a's UIMs, we acquired 3D ^{13}C half-filtered NOESY experiments on two different samples (Figure 4.2A, top panel). In these, S5a (196-306) is unlabeled and mixed with diubiquitin with either its proximal (Figure 4.2B, black and Figure 4.S3A) or distal (Figure 4.2B, red) ubiquitin subunit ^{13}C labeled. A hydrophobic patch formed by L8, I44, and V70 is used by ubiquitin to bind many of its receptors. These residues in the proximal, but not distal ubiquitin subunit, exhibit multiple intermolecular NOEs with S5a (196-306). Similarly, NOEs unique to the distal subunit were observed for the C-terminal b-strand of ubiquitin, especially L71 and L73. Importantly, intermolecular NOEs were observed to the residues in the diubiquitin linker region, namely K48 and Q49 of the proximal subunit and G75 or G76 of the distal subunit. Altogether, our data indicate that the two ubiquitin subunits form unique interactions with S5a and that contacts are made to the diubiquitin linker region of K48-linked chains.

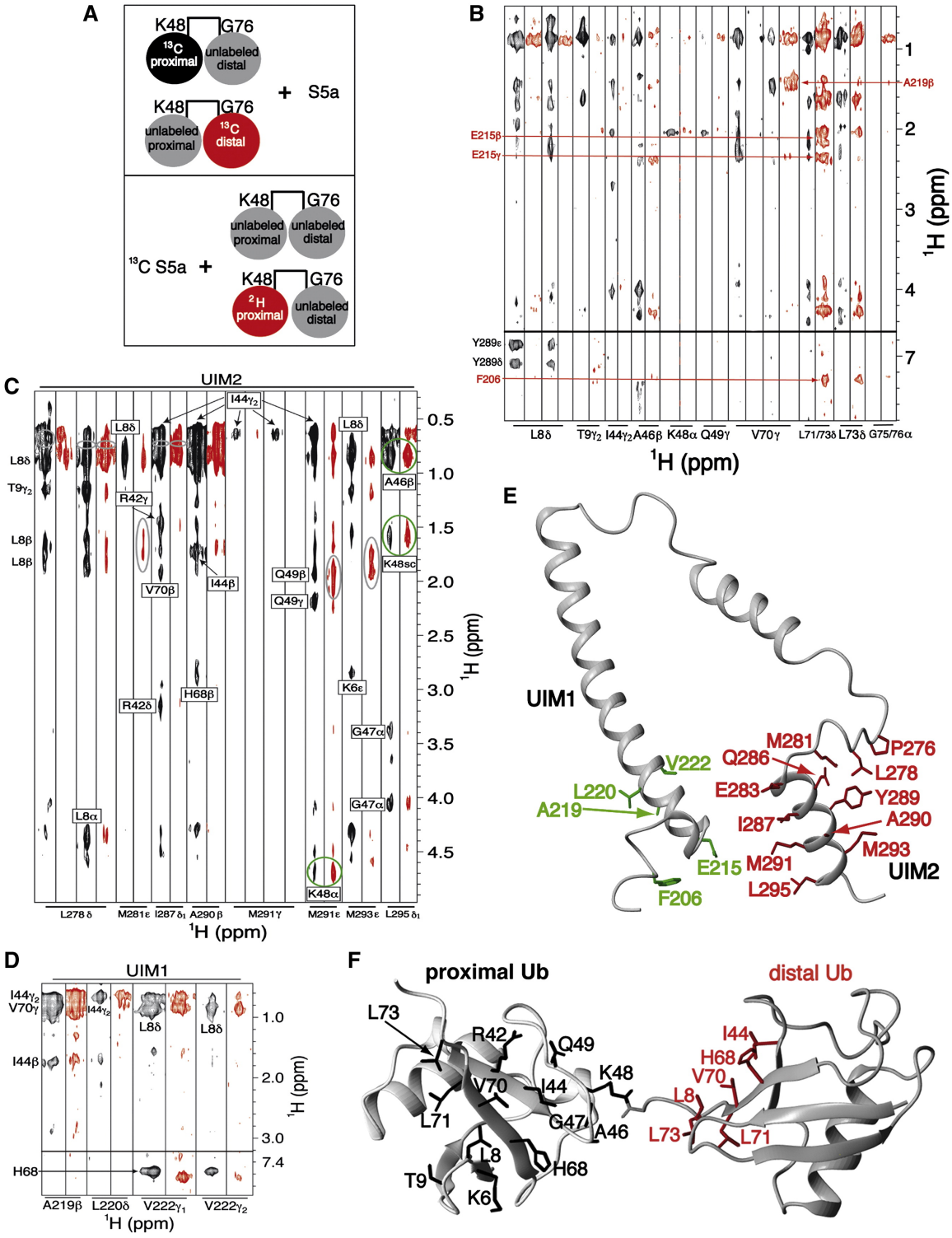

Figure 4.2. S5a prefers to bind K48-linked diubiquitin with its UIM1 bound to the distal subunit while its UIM2 binds the proximal one. (A) Schematic illustrating the NMR samples used for the ^{13}C half-filtered NOESY spectra displayed in (B; top panel) and (C

and D; bottom panel). Coloring matches the associated spectrum, such that the labeled black and red subunits produced the spectra displayed in black and red, respectively. (B) ^{13}C half-filtered NOESY experiments recorded on K48-linked diubiquitin with either its proximal (black) or distal (red) subunit ^{13}C labeled and mixed with unlabeled S5a (196-306). Abundant NOE interactions are observed between UIM2 and the proximal subunit as well as between UIM1 and the distal subunit. Selected interactions are labeled and greater detail is provided in Figure 4.S3A. (C, D) ^{13}C half-filtered NOESY spectra recorded with ^{13}C-labeled S5a (196-306) and 3-fold molar excess unlabeled K48-linked diubiquitin (black) or K48-linked diubiquitin with its proximal subunit deuterated (red). Most interactions with UIM2 residues are mitigated by ^{2}H labeling the proximal subunit (C), whereas those involving UIM1 resonances are not (D). Breakthrough diagonal peaks, which should be treated as noise, are circled in grey. NOE crosspeaks involving UIM2 that are only slightly affected by deuterating the proximal subunit are circled in green; these indicate the presence of a minor species in which UIM2 binds the distal subunit. The sidechain atoms of (E) S5a and (F) diubiquitin residues that form intermolecular NOE contacts in the major binding species are highlighted with UIM1 and UIM2 in green and red, respectively, and diubiquitin's proximal and distal subunits in black and red, respectively.

We next sought to establish whether UIM1/2 binds to the proximal versus distal subunit of diubiquitin. We were able to assign all of the intermolecular NOEs involving diubiquitin's proximal subunit to residues within UIM2 (Figure 4.2B and Figure 4.S3A). To confirm these assignments and to facilitate assigning the intermolecular NOEs involving the distal subunit, we acquired 3D ^{13}C half-filtered NOESY experiments on samples containing ^{13}C labeled S5a (196-306) and unlabeled diubiquitin (Figure 4.2C and 4.2D, black) or diubiquitin in which the proximal subunit is 100% ^{2}H labeled (Figure 4.2C and 4.2D, red), illustrated in the bottom panel of Figure 4.2A. The latter spectrum contains NOE interactions between S5a and the distal ubiquitin subunit only as the ^{2}H labeling silences the proximal subunit in this experiment.

Consistent with our analysis of the ^{13}C half-filtered NOESY experiments described above (Figure 4.S3A), residues of UIM2 displayed abundant intermolecular

NOEs with the L8-I44-V70 hydrophobic patch of diubiquitin (Figure 4.2C, black). Most of these were either eliminated or greatly reduced when the proximal subunit was silenced with ^{2}H labeling (Figure 4.2C, red). A few intermolecular NOEs were only slightly affected by ^{2}H labeling of the proximal ubiquitin subunit; these are between M291 and L295 in the UIM2 motif and A46 and K48 of diubiquitin (Figure 4.2C, circled in green). The comparable intensities of these intermolecular NOEs in the two spectra indicate that a population of S5a:diubiquitin is formed with UIM2 binding to the distal subunit. Moreover, the unique NOE pattern between UIM2 and diubiquitin's distal versus proximal subunit suggests slightly different UIM2:ubiquitin binding motifs, as necessitated by the involvement of K48, which is chemically different in the two subunits.

M291's and L295's side chain methyl groups have slightly different chemical shift values when bound to diubiquitin's proximal versus distal subunit (Figure 4.S4). By obtaining the volume of M291's methyl group NOE to K48 Ha in the proximal versus distal subunit, we estimated that UIM2 binding to diubiquitin's proximal subunit is at 3-fold molar excess compared to distal binding. Consistent with this analysis, NOE interactions between UIM1 and diubiquitin were only slightly affected by ^{2}H labeling of the proximal subunit (Figure 4.2D, black versus red). Altogether, these data provide strong evidence that UIM2 is predominately bound to the proximal subunit of diubiquitin while UIM1 binds the distal subunit, and that a minor population exists with UIM2 bound to the distal subunit. In the next section, we present these two structures; however, it is worth noting here that the difference in the volume of the NOEs from M291's methyl

group and diubiquitin's proximal versus distal K48 Ha is not due to differences in their distances from each other in the two structures as only a 0.2 Å difference is observed. We used standard thermodynamics equations relating population to binding constants and Gibbs free energy (see Section 4.8) to estimate that an energy difference of 2.7 kJ/mol is sufficient for a 3:1 binding preference.

4.3.3 Structure of S5a (196-306):K48-linked diubiquitin

We assigned 59 and 31 NOE interactions between UIM2 and diubiquitin's proximal and distal subunits, respectively. Unambiguous NOEs were also identified between F206, E215, A219, L220 and V222 and diubiquitin's distal subunit (Figure 4.2B and 4.2D and Figure 4.S3B). We were surprised to find intermolecular NOEs between L73's methyl groups of ubiquitin and F206, a conserved S5a residue that is nine amino acids N-terminal to the well-known LALAL ubiquitin-binding motif (Figure 4.1A). The S5a and diubiquitin residues that exhibited intermolecular NOEs are highlighted in Figures 4.2E and 4.2F.

By using our intermolecular NOEs, we calculated a well defined structure for the major S5a (196-306):K48-linked diubiquitin species with no NOE violation above 0.3 Å (Figure 4.3, Table 4.1). For the minor species, we were able to use intermolecular NOEs between UIM2 and distal ubiquitin (Table 4.1). However, there were no NOE interactions between UIM1 and the proximal subunit, most likely because the protein concentration of this species is low (estimated at 0.125 mM) and, in contrast to UIM2, UIM1's binding to diubiquitin causes resonance broadening (Figure 4.1B). Therefore, we

modeled the UIM1:proximal ubiquitin interaction based on our UIM1:distal ubiquitin NOEs. In the S5a (196-306):monoubiquitin complex, the relative position of UIM1 and UIM2 is not defined as the two UIMs are separated by two flexible linker regions in addition to the intervening a-helix (*241*). The relative orientation of the two UIMs is more restricted in the complexes with diubiquitin by the simultaneous binding of the two UIMs to the ubiquitin subunits (Figure 4.3A). This restriction provides an explanation for the resonance broadening and shifting observed for residues in the intervening helix (Figure 4.S1A). Diubiquitin's flexible linker region does, however, enable some freedom in the location of UIM1 relative to UIM2 (Figure 4.S5).

Table 4.1. Structural statistics for the major and minor S5a (196-306):K48-linked diubiquitin complexes.

	Major	Minor
Intermolecular NOE distance restraints (total)	46	36
UIM1:distal ubiquitin	12	N/A
UIM2:proximal ubiquitin	34	N/A
UIM1:proximal ubiquitin	N/A	12*
UIM2:distal ubiquitin	N/A	24
Ramachandran plot		
Most-favorable region (%)	79.5	79.0
Additionally allowed region (%)	20.0	20.4
Generously allowed region (%)	0.5	0.6
Disallowed region (%)	0.0	0.0
r.m.s.d of backbone atoms to average structure (Å)		
UIM1: F206-M224; ubiquitin: M1-G76	1.15 ± 0.25	1.60 ± 0.85
UIM2: P276-L295; ubiquitin: M1-G76	0.91 ± 0.28	0.76 ± 0.20
r.m.s.d of all heavy atoms to average structure (Å)		
UIM1: F206-M224; ubiquitin: M1-G76	1.47 ± 0.20	1.88 ± 0.73
UIM2: P276-L295; ubiquitin: M1-G76	1.27 ± 0.27	1.13 ± 0.22

*The distance restraints for UIM1:proximal ubiquitin used to calculate the structure of the minor S5a:K48-linked diubiquitin complex are derived from UIM1:distal ubiquitin intermolecular NOEs. See supplement for details.

The structure of S5a (196-306) complexed with K48-linked diubiquitin revealed interesting changes to the strictly conserved ^{206}FGVDPS^{211} region N-terminal to UIM1 (Figure 4.1A). Contacts between F206 and distal ubiquitin's L73, as demonstrated in

Figure 4.2B (red) and Figure 4.3B, promote additional intramolecular interactions between ^{206}FGVDPS^{211} and the LALAL motif to result in a more ordered structure. This consequence is apparent in our NMR data, as NOEs between P210 and A217 were strong in diubiquitin-bound S5a (196-306), but weak in spectra recorded on the unbound protein (data not shown).

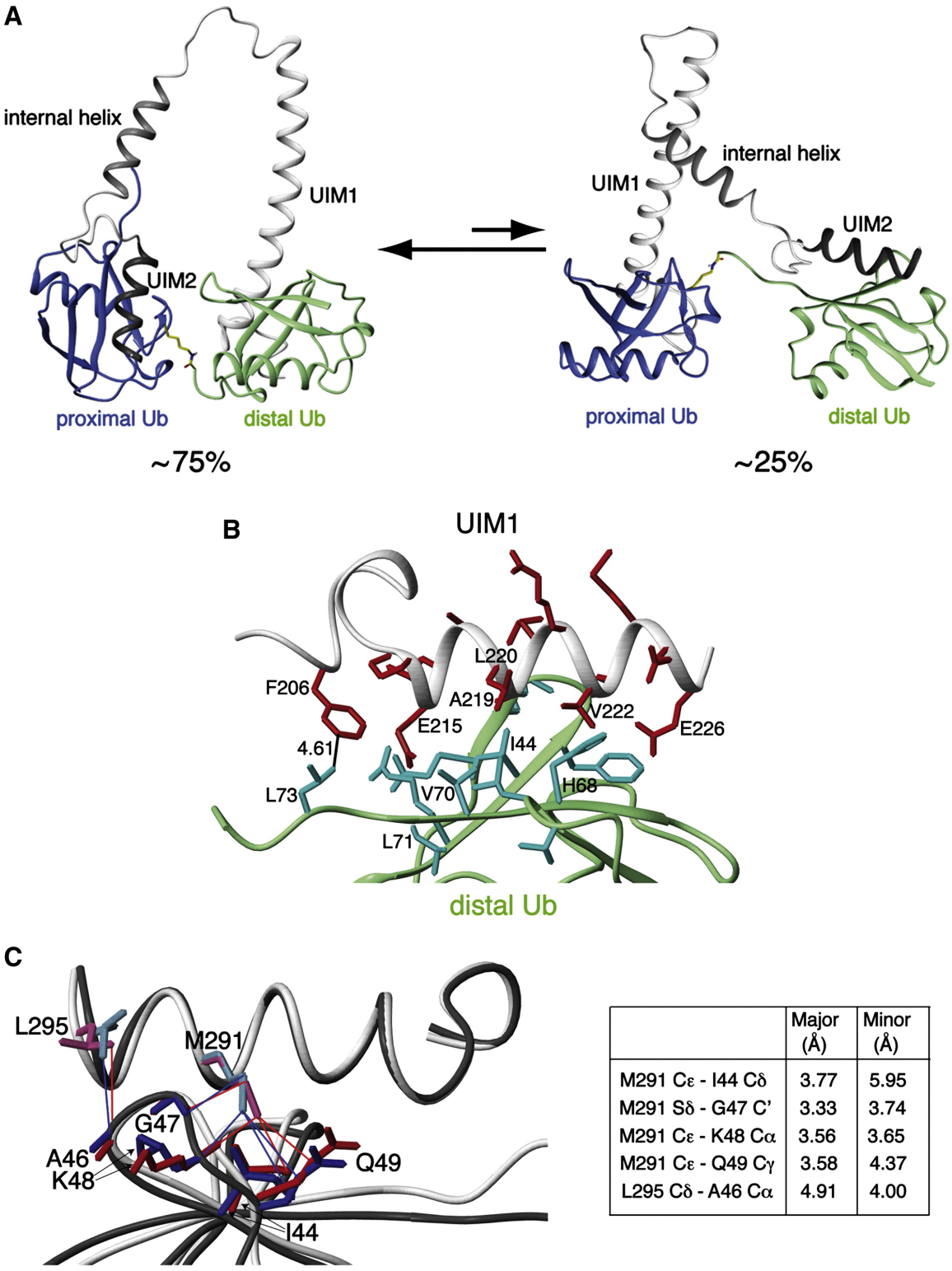

	Major (Å)	Minor (Å)
M291 Cε - I44 Cδ	3.77	5.95
M291 Sδ - G47 C'	3.33	3.74
M291 Cε - K48 Cα	3.56	3.65
M291 Cε - Q49 Cγ	3.58	4.37
L295 Cδ - A46 Cα	4.91	4.00

Figure 4.3. Structure of S5a:K48-linked diubiquitin complexes. (A) Ribbon representation of the major and minor binding modes for S5a:K48-linked diubiquitin with

S5a's UIM1 and UIM2 motifs in white and black, respectively, and diubiquitin's proximal and distal subunits in blue and green, respectively. Diubiquitin's K48-G76 linkage is highlighted in yellow. (B) Expanded view of the UIM1:distal ubiquitin complex reveals critical interactions. Residues of UIM1 and distal ubiquitin are highlighted in red and cyan, respectively, whereas their ribbon structures are grey and green respectively. (C) Multiple contacts become more compact when UIM2 binds to the proximal subunit of K48-linked diubiquitin. UIM2's M291 and L295 are displayed bound to proximal (pink and red) or distal (blue) ubiquitin. Selected distances are listed between M291 and L295 of UIM2 and proximal or distal ubiquitin atoms.

We sought to understand why the preferred diubiquitin binding mode was with UIM2 bound to the proximal subunit and UIM1 bound to the distal subunit and conversely, how the two UIMs could accommodate the minor binding species with such a small energy difference between the two. Comparison of the UIM2:distal ubiquitin and UIM2:proximal ubiquitin structures revealed M291 to form unique van der Waals interactions with I44 and more compact contacts with G47 and Q49 of the proximal compared to distal subunit (Figure 4.3C). These differences are derived from our experimental data. For example, the intermolecular NOEs between G47's Ha protons and L295's methyl group are greatly diminished in the spectrum recorded on the sample with the proximal subunit silenced by deuterium labeling (Figure 4.2C). Some distances however lengthen in the proximal subunit, the most significant of which is that between one of L295's methyl groups and A46's Cb, as supported by the corresponding intermolecular NOEs displayed in Figure 4.2C. Therefore, UIM2 favors slightly different interactions with the two subunits.

UIM1 showed the strongest interactions with the C-terminal end of distal ubiquitin (Figure 4.2B, red). This region's dynamic motions are more restricted in the distal subunit due to the presence of the isopeptide linker (*243*), which apparently

enhances its interaction with UIM1. These effects likely contribute to S5a's preferred diubiquitin binding mode. UIM1's importance in determining S5a's diubiquitin binding mode is supported by previous studies on a UIM2 fragment, which exhibited little preference for the proximal versus distal subunit (*244*).

4.3.4 S5a binds the distal subunit of K48-linked diubiquitin while Rpn13 binds the proximal subunit

Rpn13's ubiquitin binding domain binds to K48-linked diubiquitin with an affinity of 90 nM (*92*). Therefore, we tested whether it precludes S5a from binding to K48-linked diubiquitin. We added equimolar quantities of K48-linked diubiquitin and Rpn13 (1-150) to ^{13}C labeled S5a (196-306). A $^{1}H,^{13}C$ HMQC experiment revealed S5a UIM1 and UIM2 resonances that shift upon addition of K48-linked diubiquitin (Figure 4.4A, green) to appear at similar positions when Rpn13 was added with diubiquitin (Figure 4.4A, blue). Hence, Rpn13 does not preclude S5a from binding to K48-linked diubiquitin. To test whether Rpn13 and S5a bind diubiquitin simultaneously, we added equimolar quantities of unlabeled K48-linked diubiquitin and S5a to ^{15}N labeled Rpn13. Rpn13 amino acids that are close to the isopeptide bond linkage when bound to the proximal subunit shift in a different manner when bound to K48-linked polyubiquitin versus monoubiquitin (*240*). We found these Rpn13 resonances to shift to their proximal-bound state when S5a (196-306) is present (Figure 4.4B). Therefore, we hypothesized that Rpn13 binds to the proximal subunit while S5a binds to the distal subunit.

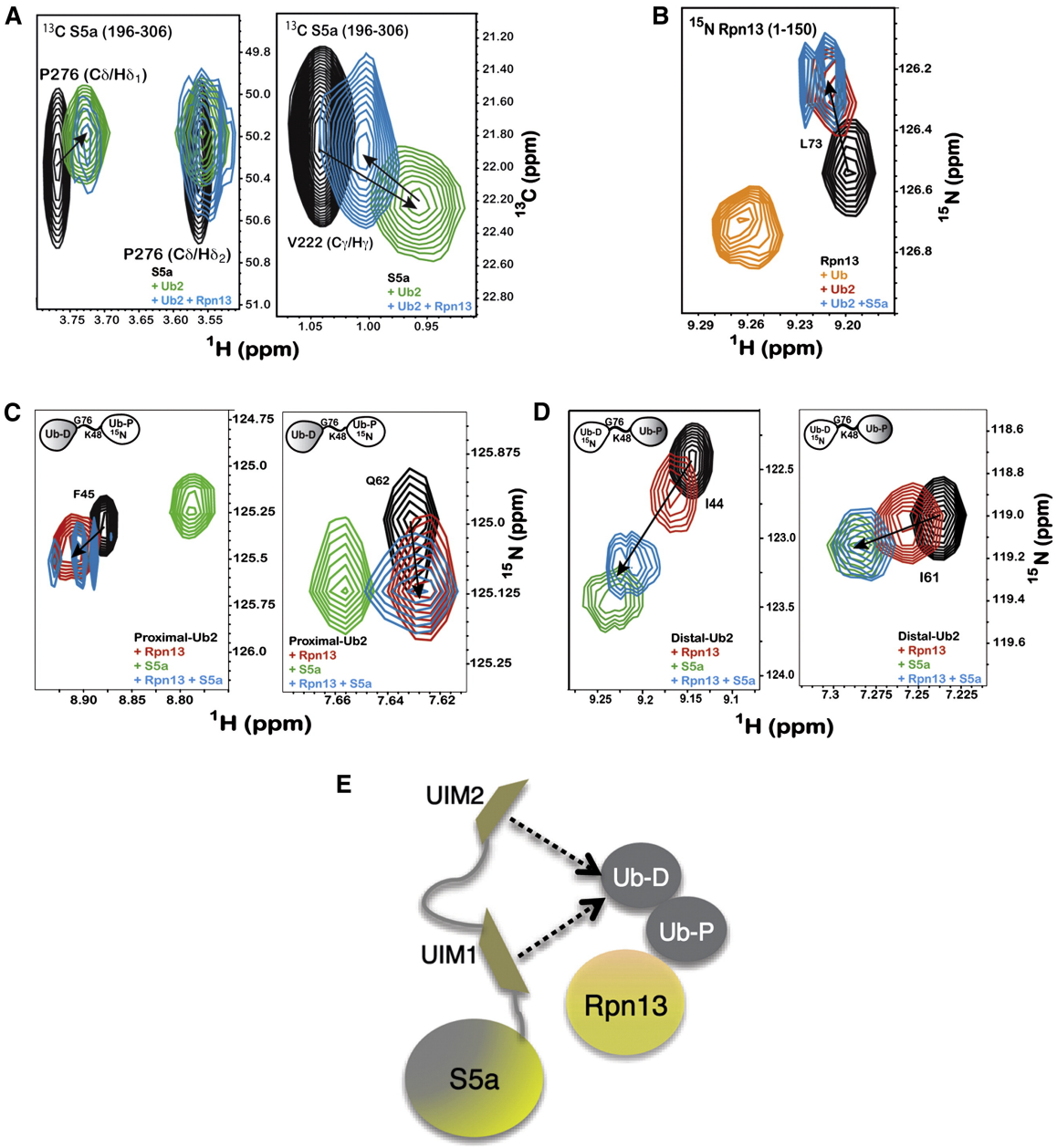

Figure 4.4. Ubiquitin receptors Rpn13 and S5a bind K48-linked diubiquitin simultaneously. (A) ^{1}H, ^{13}C HSQC experiments recorded on ^{13}C labeled S5a (196-306) alone (black) or with equimolar K48-linked diubiquitin (green) or K48-linked diubiquitin and Rpn13 (1-150) (blue) reveal P276 (left panel) and V222 (right panel) to interact with diubiquitin when Rpn13 is present. B) ^{1}H, ^{15}N HSQC experiments on ^{15}N labeled Rpn13 (1-150) alone (black) and with monoubiquitin (orange), K48-linked diubiquitin (red) or K48-linked diubiquitin and S5a (196-306) (blue) reveals L73 to shift to its diubiquitin-bound state when S5a is present. K48-linked diubiquitin with its (C) proximal or (D) distal subunit ^{15}N labeled alone (black) or with Rpn13 (1-150) (red), S5a (196-306)

(green), or both of these receptors (blue) indicates shifting that mimics Rpn13 binding to the proximal subunit, but S5a binding to the distal one, as shown for F45 and Q62 of the proximal subunit and I44 and I61 of the distal subunit. Additional data is provided in Supplementary Figure 6. (E) Model illustrating Rpn13 bound to K48-linked diubiquitin's proximal subunit and S5a's UIMs interacting dynamically with the distal one.

To test more directly which receptor binds K48-linked diubiquitin's proximal subunit, we added S5a (196-306) and Rpn13 (1-150) or just one of these proteins to equimolar quantities of K48-linked diubiquitin with its proximal subunit ^{15}N labeled. The observed chemical shift changes with both receptors present were similar to those caused by only Rpn13 addition, as demonstrated for F45 and Q62 (Figure 4.4C; see also Figure 4.S6). By contrast, the addition of equimolar quantities of S5a (196-306) and Rpn13 (1-150) to K48-linked diubiquitin with its distal subunit ^{15}N labeled revealed the larger chemical shift changes characteristic of S5a (196-306) interaction, as illustrated for I44 and I61 in Figure 4.4D. Altogether, our data indicate that S5a binds predominately to diubiquitin's distal subunit while the stronger binding Rpn13 maintains its position at the proximal subunit.

Although UIM2 has the stronger affinity for K48-linked diubiquitin, ^{13}C resonances from both UIM motifs shift upon addition of K48-linked diubiquitin when Rpn13 is present (Figure 4.4A, blue). Rpn13 however either mitigates the chemical shift perturbations, as shown in Figure 4.4A for V222, or causes attenuation, as shown in Figure 4.4A for P276. These differences suggest that UIM1 and UIM2 compete for K48-linked diubiquitin's distal subunit when Rpn13 occupies the proximal one (Figure 4.4E). Dynamic binding behavior was also evident in spectra recorded on the proximal subunit, although to a lesser extent. The observed spectral changes with both receptors present

largely mimic those caused by only Rpn13; however, additional attenuations are observed for A46 and H68 (Figure 4.S6).

We tested the model presented in Figure 4.4E directly by labeling either S5a's UIM1 or UIM2 region with the paramagnetic spin label *S*-(2,2,5,5-tetramethyl-2,5-dihydro-1H-pyrrol-3-yl)methyl methanesulfonothioate (MTSL). MTSL causes distance-dependent attenuation with effects apparent up to distances of ~20 Å. It forms a disulfide bond with cysteine residues and since S5a (196-306) contains no cysteines, it was straightforward to produce proteins samples with either UIM1 or UIM2 labeled. UIM1 and UIM2 labeling was performed by substituting Q227 and A298 with cysteine, respectively. These two residues were chosen based on our NMR structure. They do not contact diubiquitin directly and their mutation is therefore not expected to disrupt S5a:diubiquitin interaction; however, they are close enough for MTSL-induced attenuation of diubiquitin atoms (model structures are provided for the major conformation in Figure 4.5A).

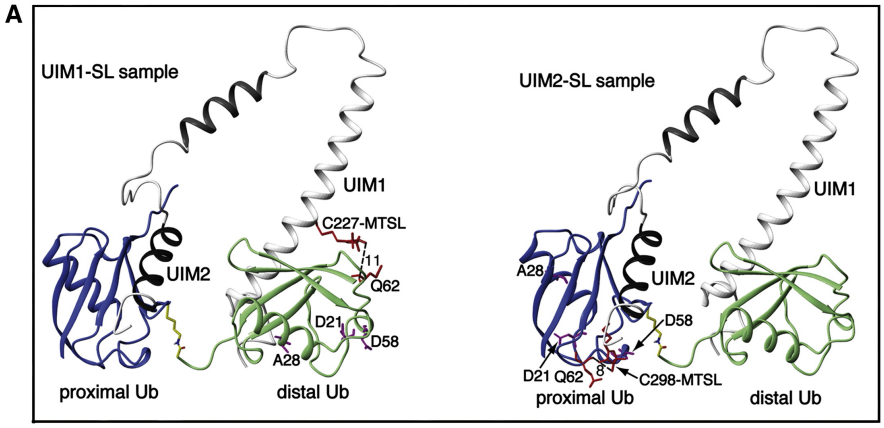
A
UIM1-SL sample
UIM1
C227-MTSL
UIM2
Q62
D21
D58
A28
proximal Ub
distal Ub
UIM2-SL sample
UIM1
A28
UIM2
D58
D21 Q62
C298-MTSL
proximal Ub
distal Ub

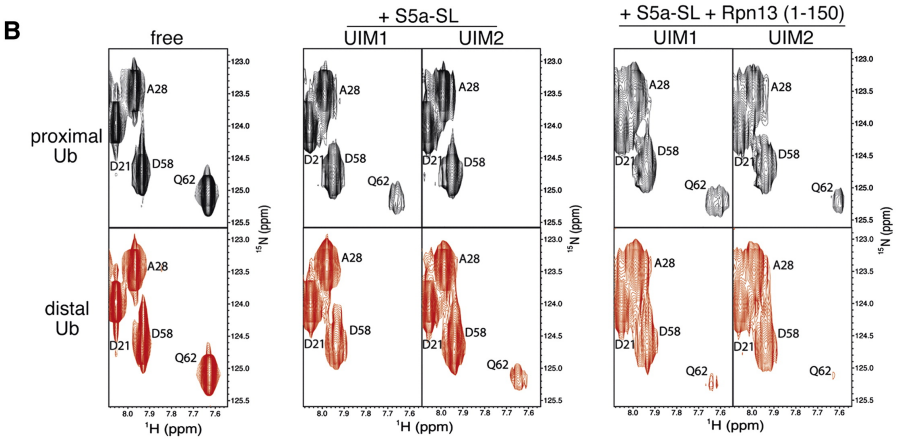
B
free
+ S5a-SL
+ S5a-SL + Rpn13 (1-150)
UIM1
UIM2
proximal Ub
distal Ub
A28
D21
D58
Q62
^{15}N (ppm)
^{1}H (ppm)

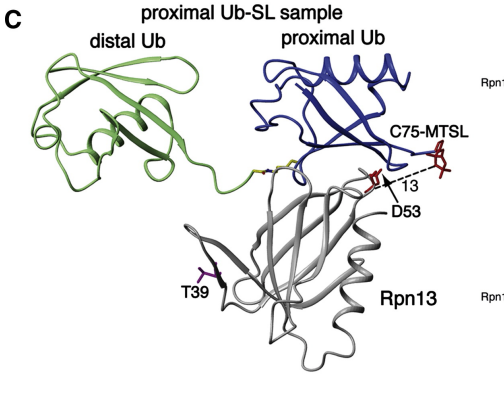
C
proximal Ub-SL sample
distal Ub
proximal Ub
C75-MTSL
13
D53
T39
Rpn13

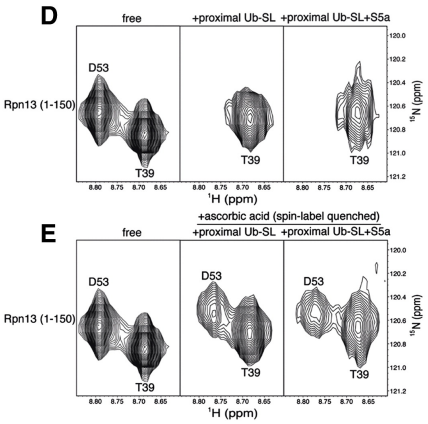
D
free
+proximal Ub-SL
+proximal Ub-SL+S5a
Rpn13 (1-150)
D53
T39
^{15}N (ppm)
^{1}H (ppm)
E
+ascorbic acid (spin-label quenched)
free
+proximal Ub-SL
+proximal Ub-SL+S5a
Rpn13 (1-150)
D53
T39
^{15}N (ppm)
^{1}H (ppm)

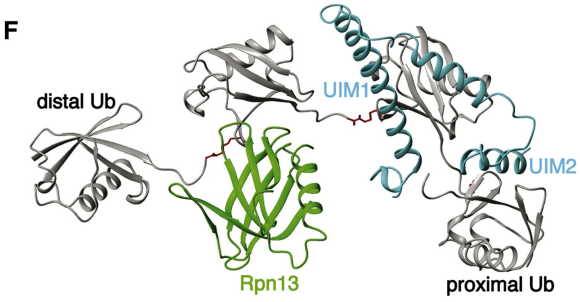
F
distal Ub
UIM1
UIM2
Rpn13
proximal Ub

Figure 4.5. MTSL-labeling demonstrates hRpn13's preference for K48-linked diubiquitin's proximal subunit as S5a's two UIMs bind the distal subunit. (A) Ribbon representation of the major S5a (196-306):K48-linked diubiquitin structure displaying MTSL covalently attached to C227 (left) or C298 (right). Each of these cysteines was introduced for UIM1 or UIM2 spin labeling by MTSL. Q62 is also displayed as well as approximate distances in Å between its backbone amide proton atom and MTSL's single-electron center (oxygen atom). It is worth noting that MTSL and the cysteine sidechain atoms are flexible such that the distances shown are only approximations. D21, A28 and D58 are also displayed and highlighted in purple, as they are used for comparison. (B) Expanded view of ^{1}H, ^{15}N HSQC spectra for the proximal (top panels) or distal (bottom panels) subunit of K48-linked diubiquitin alone (left panel) with added MTSL labeled C227 (UIM1) or C298 (UIM2) only (middle panel), or with hRpn13 (1-150) in addition (right panel), as labeled. S5a-SL refers to MTSL labeled S5a (196-306). (C) Ribbon representation of Rpn13:K48-linked diubiquitin structure displaying MTSL covalently attached to C75 of the proximal ubiquitin. D53 of hRpn13 is displayed as well as the approximate distance in Å between its backbone amide proton atom and MTSL's single-electron center (oxygen atom). T39 is displayed and highlighted in purple, as it is used for comparison. (D) Expanded view of ^{1}H, ^{15}N HSQC spectra for the hRpn13 (1-150) alone (left panel) with MTSL labeled K48-linked diubiquitin only (middle panel), or with S5a (196-306) in addition (right panel), as labeled. Proximal Ub-SL refers to K48 diubiquitin with its proximal subunit MTSL labeled. (E) Expanded view of ^{1}H, ^{15}N HSQC spectra for the hRpn13 (1-150) alone (left panel) and with either spin label quenched K48-linked diubiquitin G75C only (middle panel) or with unlabeled S5a (196-306) in addition (right panel). All spectra of protein mixtures were acquired with all components at 0.3 mM. (F) Model of one possible binding configuration for Rpn13 (1-150) (green) and S5a (196-306) (blue) simultaneously bound to K48-linked tetraubiquitin (grey with K48-G76 linker region in red). In a tetraubiquitin chain, a ubiquitin subunit is available to each ubiquitin-binding module and K48 and G76 of the interior subunits are both engaged in isopeptide bonds with neighboring units. It is worth noting that the highly dynamic nature of S5a binding to polyubiquitin ensures that other configurations are possible.

We produced samples in which either diubiquitin's proximal or distal subunit is ^{15}N labeled and mixed these at 1:1 molar ratio with S5a (196-306) samples with either Q227C or A298C MTSL labeled. The amide resonance of Q62 from diubiquitin's proximal subunit was partially attenuated by UIM1 spin labeling, but obliterated by UIM2 spin labeling (Figure 4.5B, middle panel compared to one on left). Q62 is not attenuated upon S5a (196-306) addition when S5a is not spin labeled (Figure 4.S7).

Moreover, D21 and A28, which are over 20 Å away from each of S5a's MTSL labels, are not greatly attenuated, whereas D58, which is ~15 Å away is slightly attenuated (Figure 4.5B). This finding is consistent with the presence of two S5a:diubiquitin conformations, with the predominant species having UIM2 bound to the proximal subunit and the minor species with it bound to the distal one. Consistent with this model, UIM1 spin labeling resulted in partial attenuation of Q62 from the proximal subunit, but obliterated this residue's amide resonance from the distal subunit (Figure 4.5B, middle panel compared to one on left). Similarly, D58 is slightly affected by the induced paramagnetic relaxation effects from S5a MTSL labeling whereas the more remote D21 and A28 are not affected. Altogether, these data are consistent with the NOE-derived S5a:diubiquitin structures of Figure 4.3A. Confident that our approach is effective, we next tested the effect of having hRpn13 (1-150) present.

hRpn13 (1-150) and S5a (196-306) with either its UIM1 or UIM2 spin labeled was added to diubiquitin with either its proximal or distal subunits ^{15}N labeled. All three proteins were at 0.3 mM concentration. In this case, general resonance broadening is observed due to the larger size of the ternary complex. However, Q62 of the proximal subunit is only slightly more broadened than D21, A28, and D58 when either UIM1 or UIM2 is MTSL labeled (Figure 4.5B, right panel compared to left one). By contrast, the NMR signal of this residue in the distal subunit is almost obliterated by UIM1 and UIM2 MTSL labeling. The greatly reduced attenuation of the proximal subunit's Q62 upon Rpn13 addition indicates that S5a's UIM2 is largely displaced from this subunit by Rpn13, as modeled in Figure 4.4E. That UIM2 spin labeling causes increased attenuation

of Q62 from the distal subunit indicates that it now interacts with this ubiquitin moiety. The UIM2-distal ubiquitin interaction causes partial restoration of Q62 in the sample with UIM1 labeled and hRpn13 present (Figure 4.5B, right panel compared to one on left). Hence, UIM1 and UIM2 appear to compete for diubiquitin's distal subunit when Rpn13 is present.

We tested directly whether hRpn13 binds to K48-linked diubiquitin's proximal subunit when S5a (196-306) is present by substituting G75 of the proximal subunit with cysteine and then labeling it with MTSL. Proximal G75 is not in the immediate Rpn13 binding surface and therefore its mutation is not expected to disrupt binding; however, it is close enough to some residues to cause paramagnetic attenuation when labeled with MTSL (Figure 4.5C). Addition of proximal G75C MTSL diubiquitin to ^{15}N labeled hRpn13 (1-150) obliterates NMR signals from Rpn13 residues that are close to the proximal subunit in the Rpn13 (1-150):K48-linked diubiquitin complex (*231*), as demonstrated for D53 in Figure 4.5D, middle panel. When this experiment is repeated with unlabeled S5a (196-306) present, the obliteration due to hRpn13 binding to the proximal subunit is preserved (Figure 4.5D, right panel). These experiments were performed with all three proteins at 0.3 mM. Residues with distances to the MTSL label that are too far for paramagnetic relaxation enhancement effects do not exhibit such dramatic signal attenuation, as demonstrated for T39 in Figure 4.5D. Moreover, the D53 resonance reappears in the binary and ternary complexes after spin label quenching (Figure 4.5E). The quenching reaction was done by reducing the MTSL moiety with 5-fold molar excess ascorbic acid (Figure 4.5E). Therefore, the attenuation observed in

Figure 4.5D is due to the distance-dependent paramagnetic relaxation enhancement induced by MTSL. This data indicates that Rpn13 predominately binds to the proximal subunit when S5a is present, as suggested by the chemical shift perturbation data and the results of spin labeling S5a.

Altogether, our data indicate that Rpn13 and S5a can bind to a common K48-linked polyubiquitin chain, even for diubiquitin, which has only two ubiquitin subunits. In longer chains, each ubiquitin-binding element can readily bind a ubiquitin subunit. The internal subunits of longer chains harbor the advantages of both the proximal and distal subunits of a diubiquitin chain, as K48 and G76 of these subunits are both engaged in isopeptide bonds with neighboring ubiquitin subunits. Internal ubiquitins therefore provide the additional contact of the linker region preferred by S5a's UIM2 and Rpn13 as well as the increased rigidity of the C-terminal stretch of residues (*243*), which is preferred by UIM1. A model of Rpn13 and S5a's UIMs bound to internal and proximal subunits is provided in Figure 4.5F.

4.4 Discussion

We demonstrate in this Chapter that the coordinated binding of S5a's two UIMs greatly enhances its affinity for K48-linked diubiquitin over monoubiquitin and that although the UIMs can be accommodated on either subunit, a preference exists for UIM1 on the distal subunit while UIM2 occupies the proximal one. We find that S5a and Rpn13 are able to bind a common diubiquitin chain and that as Rpn13 retains its preferred position at the proximal subunit, S5a binds the distal one. In a diubiquitin chain, the two

UIMs compete for the distal subunit when Rpn13 is present; however, in a longer chain these two ubiquitin binding elements would no doubt occupy separate subunits, as they did in Rpn13's absence (Figure 4.3). In the absence of the proteasome, our data suggest that multiple binding configurations are available for Rpn13 and S5a binding to K48-linked tetraubiquitin, one of which is shown in Figure 4.5F.

It is not yet clear whether such coordinated binding occurs in the context of the proteasome; however, it is possible that Rpn13 and S5a bind chains simultaneously to orient substrates for optimal capture and deubiquitination. The distance across the proteasome's regulatory particle is similar to that spanned by an opened tetraubiquitin structure and therefore, even if S5a and Rpn13 are not docked next to each other it is still conceivable for them to bind a common ubiquitin chain, as modeled in Figure 4.S8. The proteasome appears to require most substrates to be conjugated to a chain of four or more ubiquitins (*245*). This minimal chain length may be preferred to allow for the coordinated binding of ubiquitin receptors, which may in turn, orient the chain in a manner conducive for the effective activity of deubiquitinating enzymes. For example, S5a and Rpn13 coordinated binding may lead to the substrate end of the ubiquitin chain being proximal to Rpn11, which performs degradation-coupled deubiquitination (*206, 207, 246*) and the distal end of the chain near Uch37, which performs distal end deubiquitination (*174*). Future experiments are required to test this hypothetical model.

We focused here on K48-linked chains because of their established importance in triggering degradation by the proteasome. S5a can also bind to K63-linkages with no apparent reduction in affinity compared to K48-linked chains (*241*). Rpn13's ubiquitin

binding domain has high affinity for even monoubiquitin (*240*), suggesting that it too can bind chains of varying linkage. Although K63-linked chains mediate non-proteasomal events, they can support degradation by the proteasome (*247*). We propose that the outcome of K63-linked ubiquitination is not determined by the proteasome's ubiquitin receptors. Rather, as demonstrated here, S5a and Rpn13 are adaptive and collaborative in their binding to ubiquitin chains, which supports their primary job of enabling proteasome to capture ubiquitinated proteins.

Although contacts were revealed between the UIMs and diubiquitin that were unique to the conjugated subunits, their overall binding mode is similar to that used to bind monoubiquitin. Moreover the two UIMs share the same basic ubiquitin-binding scaffold. The key residues involved in binding to ubiquitin units are ^{216}LALAL^{220} for UIM1 and ^{287}IAYAM^{291} for UIM2 and, in both cases residues N-terminal to these helical structures participate in binding ubiquitin (Figure 4.3). UIM1 is conserved in *Saccharomyces cerevisiae*, and we propose that UIM2 evolved in higher eukaryotes by UIM1 duplication and optimization for ubiquitin binding, as UIM2 is the stronger binding partner for diubiquitin (Figure 4.1B and 4.1C) and monoubiquitin (*241*). We determined S5a (196-306)'s affinity for diubiquitin to be significantly higher than either UIM's affinity for monoubiquitin (Figure 4.1E) (*241, 242*) and showed that S5a binds diubiquitin with 1:1 stoichiometry even when diubiquitin is 8-fold in excess. Thus, UIM2 is apparently not used to recruit in multiple substrates simultaneously, but rather to enhance affinity for each substrate.

Although not essential in budding yeast (*235*), S5a is required for murine embryonic development (*236*). It is also essential in *Drosophila melanogaster*, in which its deletion results in larval-pupal polyphasic lethality, multiple mitotic defects, as well as accumulation of ubiquitinated proteins and defective 26S proteasome (*237*). Therefore, in higher eukaryotes, Rpn13 and the UBL-UBA proteins cannot substitute for S5a.

In a prior study, we demonstrated S5a-bound K48-linked tetraubiquitin can also bind to hHR23a, even though hHR23a precludes additional UBL-UBA family members from binding a common ubiquitin chain (*238*). In this ternary complex, S5a's UIM1 physically contacts the ubiquitin chain, as UIM2 binds to hHR23a's UBL domain. S5a therefore appears to be able to share ubiquitinated substrates with other ubiquitin receptors. Altogether, our data support a model in which S5a has evolved to bind polyubiquitinated substrates in a manner that takes advantage of other ubiquitin receptors.

4.5 Methods summary

4.5.1 Preparation of NMR samples and NMR spectroscopy

S5a (196-306), K48-linked diubiquitin and hRpn13 (1-150) were produced as described in the Section 4.8. Methods used for the NMR experiments and their analyses as well as for solving the S5a (196-306):K48-linked diubiquitin complexes and for modeling the S5a (196-306):Rpn13 (1-150):K48-linked tetraubiquitin complex are described in the Section 4.8.

4.5.2 Analytical ultracentrifugation

Sedimentation velocity experiments were performed as previously described (*238*). Seven samples were prepared in which the molar ratio of K48-linked diubiquitin to S5a (196-306) was varied from 1:7 to 8:1. The s_w for each mixture was calculated as previously described (*238*). Dissociation constants were obtained by global analysis using SEDPHAT (*248*).

4.5.3 Spin labeling experiments

Based on the S5a (196-306):K48-linked diubiquitin complex structure of the major species (Figure 4.3A), two S5a (196-306) mutants were designed for MTSL labelling, namely Q227C and A298C. These two residues are not directly involved in binding diubiquitin, so their mutation was not expected to disrupt binding. They were also chosen because they are close enough to K48-linked diubiquitin amide atoms to cause distance-dependent attenuations (Figure 4.5A). After being treated with the spin labeling reagent (1-oxyl-2,2,5,5-tetramethylpyrroline-3-methyl) methane thiosulfonate (MTSL), a single electron (carried by oxygen atom) containing moiety will be attached to the sulfur atom of cysteine residue in S5a mutants. The strong magnetic field of the NMR instrument causes the single electron carried by oxygen atom to accelerate the relaxation of residues within ~20 Å. Sample preparation and NMR spectra recorded for spin labeling experiments are described in Section 4.8.

4.6 Data Bank accession numbers

The atomic coordinates of S5a (196-306) in complex with K48-linked diubiquitin have been deposited in the Protein Data Bank with the accession codes of 2KDE and 2KDF.

4.7 Supplementary information

4.7.1 Material and methods

4.7.1.1 Preparation of NMR samples

S5a (196-306) and K48-linked diubiquitin were produced as described (*50, 124, 194, 249, 250*). Briefly, we used recombinant monoubiquitin in which either an aspartic acid is added to the chain (Ub-D77) or the lysine at position 48 was mutated to an arginine (Ub-K48R). Using these two monoubiquitin samples, K48-linked diubiquitin could be synthesized. Ub-D77 and Ub-K48R that were selectively labeled or unlabeled were incubated with 0.1 μM UBE1 (E1, Boston Biochem), 25 μM UBE2K (E2), 2 mM ATP, and 1/5 total volume PBDM8 buffer at 37°C for ~12 hours. The diubiquitin formed was subsequently purified by using a monoQ column, followed by monoS ion-exchange columns (GE Healthcare). A similar procedure was used to produce K48-linked diubiquitin mutant with its proximal subunit MTSL labeled. In this case, however, a ubiquitin truncated mutant (Ub-G75C) with the C-terminal G75 substituted with cysteine was used.

His-tagged S5a (196-306) and GST-tagged hRpn13 (1-150) are expressed in *Escherichia coli* and purified by using a combination of affinity chromatography and size exclusion chromatography on an FPLC system. hRpn13 (1-150) is cleaved from its GST-tag during elution from glutathione S-sepharose resin by using PreScission protease (GE healthcare). ^{15}N, ^{13}C, and ^{2}H labeled samples are produced by growth in M9 minimal media with ^{15}N labeled ammonium chloride, ^{13}C labeled glucose, and D_2O used as the nitrogen, carbon, and water sources, respectively. Amide atoms are exchanged into D_2O when desired by using lyophilisation.

4.7.1.2 NMR spectroscopy

Chemical shift perturbation analysis was done by using $^{1}H,^{15}N$ HSQC experiments which were recorded on ^{15}N labeled S5a (196-306) with increasing molar ratios of unlabeled diubiquitin. Since UIM1 and UIM2 binding to diubiquitin was in the intermediate to slow exchange regime, the affected resonances could not be readily followed from their free to their bound states as increasing amounts of the binding partner was added. Therefore, an ^{15}N-dispersed NOESY spectrum recorded on ^{15}N labeled S5a (196-306) and unlabeled diubiquitin was used to obtain chemical shift assignments for diubiquitin-bound S5a (196-306). The concentration of S5a (196-306) for the $^{1}H,^{15}N$ HSQC titration and ^{15}N dispersed NOESY experiments was 0.40 mM. The spectra were recorded at 25°C and in Buffer 1 (20 mM $NaPO_4$, 100 mM NaCl, at pH 6.5).

Since many backbone HN groups belonging to UIM1 resonances were broadened beyond detection, a 3D ^{13}C-edited NOESY spectrum (100 ms mixing time) on ^{13}C-

labeled S5a (196-306) mixed with 3-fold molar excess unlabeled diubiquitin was recorded to assign the diubiquitin-bound state of S5a. This molar ratio ensures that essentially all of S5a is diubiquitin-bound. Since sedimentation velocity analysis revealed a 1:1 binding stoichiometry for the S5a (196-306):diubiquitin complex, even with either component is at 7-fold molar excess (Figure 4.1D), we are able to use molar ratios greater than 1:1 to increase sensitivity by increasing the population of the bound state for the labeled protein. Unlike amide groups, the NMR resonances for aliphatic CH groups in proteins are less sensitive to dynamic motions and therefore those of UIM2, the internal helix, and part of UIM1 are observable in the recorded ^{13}C-edited NOESY spectrum (Figure 4.S2B).

Intermolecular NOE interactions between S5a (196-306) and K48-linked diubiquitin were obtained through four sets of NOESY experiments including ^{13}C-filtered, ^{13}C-edited NOESY spectra acquired ^{13}C-labeled S5a (196-306) mixed with 3-fold molar excess unlabeled diubiquitin, ^{13}C-labeled S5a (196-306) mixed with 3-fold molar excess diubiquitin with its proximal subunit 100% deuterated, diubiquitin with its proximal subunit ^{13}C labeled mixed with 2-fold molar excess unlabeled S5a (196-306), and diubiquitin with its distal subunit ^{13}C labeled mixed with 2-fold molar excess unlabeled S5a (196-306). In all spectra, the concentration of ^{13}C labeled protein was 0.4 - 0.5 mM and they were recorded at 25°C and on either 800 or 900 MHz spectrometers equipped with cryogenically cooled probes in Buffer 2 (20 mM $NaPO_4$, 50 mM NaCl, at pH 6.5). Whereas assignment of diubiquitin-bound S5a (196-306) resonances required the NOESY experiment described in the previous section, S5a-bound diubiquitin was

straightforward to assign. Firstly, the chemical shift dispersion of ubiquitin is greater than S5a (196-306) and secondly, the chemical shift values for each subunit differed little from monoubiquitin's S5a-bound state. With the four half-filtered experiments, we readily assigned intermolecular NOEs, as NOEs between ^{13}C-labeled S5a and unlabeled ubiquitin were matched with though of ^{13}C labeled ubiquitin and unlabeled S5a. For example, the intermolecular NOE between K48's Ca proton from proximal ubiquitin and UIM2's M291's methyl protons was observed in S5a was ^{13}C labeled (Figure 2C) as well as when the proximal subunit of ubiquitin was ^{13}C labeled (Figure 4.S3A).

Chemical shift perturbation analysis was conducted by recording ^{1}H, ^{15}N HSQC or ^{1}H, ^{13}C HMQC experiments. Samples contained ^{15}N labeled Rpn13 (1-150), ^{13}C labeled S5a (196-306) and unlabeled diubiquitin or unlabeled Rpn13 (1-150), ^{13}C labeled S5a (196-306) and diubiquitin with one of its subunits ^{15}N labeled. The NMR spectra were acquired at 0.3 mM and all mixtures were equimolar. Spectra were taken in Buffer 2 on a Varian Inova 800 MHz spectrometer with a cryogenically cooled probe.

4.7.1.3 Structure calculations

Structure calculations of the S5a (196-306):K48-linked diubiquitin complex were performed based on the NOE-derived distance and dihedral angle constraints. Intramolecular constraints for S5a (196-306) and those published for ubiquitin (PDB code 1D3Z) (*251*) were incorporated to maintain the structure of each component, as neither protein undergoes gross structural change upon binding (see Section 4.3). The structure of the major binding mode was defined by 34 UIM2:proximal ubiquitin and 12

UIM1:distal ubiquitin intermolecular NOE derived distance restraints. The UIM2:distal interaction for the minor S5a:diubiquitin complex was defined by 24 intermolecular NOE derived distance restraints, which were still observable when the proximal subunit of diubiquitin was fully deuterated (Figure 4.2C red). Intermolecular NOEs between UIM1 and proximal ubiquitin were too weak to be observed and therefore the UIM1 constraints to distal ubiquitin were used to model the UIM1:proximal interaction. For both S5a:diubiquitin complexes, simulated annealing in XPLOR version 3.851 was performed on a Linux operating system. 30 randomly coiled structures were subjected to 15,000 simulated annealing and cooling steps of 0.005 ps to generate seven converged structures. These were selected because they have no NOE violation > 0.3 Å or dihedral angle violation > 10°. For the model demonstrating expected distances between MTSL and specific amide atoms of interest, the exact MTSL orientation is not known.

4.7.1.4 Gibbs free energy calculation

The Gibbs free energy required for a 3:1 population difference was determined by using Equations 4.1 and 4.2, in which R, T, and K are the gas constant (8.3145 $JK^{-1}mol^{-1}$), temperature of the NMR experiments (298K), and equilibrium constant, respectively.

$$\Delta G = -RT(\ln K_{major} - \ln K_{minor}) = -RT\ln(\frac{K_{major}}{K_{minor}}) \qquad (1)$$

$$K_{major} = \frac{[(S5a:diUb)_{major}]}{[S5a][diUb]} \qquad K_{minor} = \frac{[(S5a:diUb)_{minor}]}{[S5a][diUb]} \qquad (2)$$

4.7.1.5 Spin labeling experiments

The expression plasmids for the S5a (196-306) mutants and hRpn13 (1-150) CtoA mutant, in which all of its cysteines are mutated to alanine, were made by using Quick Change Site Directed Mutagenesis Kit (Stratagene). S5a (196-306) Q227C and A298C mutants (His-tagged) and hRpn13 (1-150) CtoA mutant (GST-tagged) were expressed and purified from *Escherichia coli* by using a combination of affinity and size exclusion chromatography on an FPLC system, as described above for the wild-type proteins. Diubiquitin with G75 of its proximal subunit substituted with cysteine was also produced as described above. Purified diubiquitin-proximal G75C as well as S5a (196-306) Q227C and A298C proteins were spin labeled by reacting them with MTSL purchased from TRC (Toronto). Spin labeling reactions were performed in 50 mM Tris, pH 7.6, in a 10-fold excess of MTSL, and the reaction tubes were incubated in the dark at 4 °C overnight. Excess MTSL reagent was removed by extensive dialysis at 4 °C into NMR buffer (20 mM sodium phosphate, 50 mM sodium chloride, pH 6.5).

A series of $^{1}H,^{15}N$ HSQC experiments were recorded on 0.3 mM K48-linked diubiquitin with its proximal or distal subunits ^{15}N labeled without or with the addition of equimolar MTSL labeled S5a Q227C or A298C. $^{1}H,^{15}N$ HSQC experiments for protein samples of K48-linked diubiquitin with its proximal or distal subunits ^{15}N labeled in the presence of equimolar hRpn13 (1-150) CtoA and MTSL labeled S5a Q227C or A298C were also acquired under identical conditions.

We also recorded a series of $^{1}H,^{15}N$ HSQC experiments on 0.3 mM ^{15}N labeled Rpn13 (1-150) CtoA protein without or with the addition of equimolar MTSL labeled

diubiquitin G75C. These experiments were also done with equimolar S5a (196-306) present under identical conditions. For both the binary and ternary NMR samples, two HSQC experiments were acquired, one with MTSL in the oxidized state (paramagnetic state) and one with MTSL reduced to ensure effects were MTSL specific. The spin label quenching was achieved by addition of 5-fold molar excess ascorbic acid to the binary NMR sample (Rpn13 plus spin labeled diubiquitin G75C) and also the ternary NMR sample (Rpn13 plus spin labeled diubiquitin G75C and S5a (196-306)). Samples were placed in the magnet at 25 °C for 1 hour to ensure complete reduction of the spin label moiety.

4.7.2 Supplemental figures

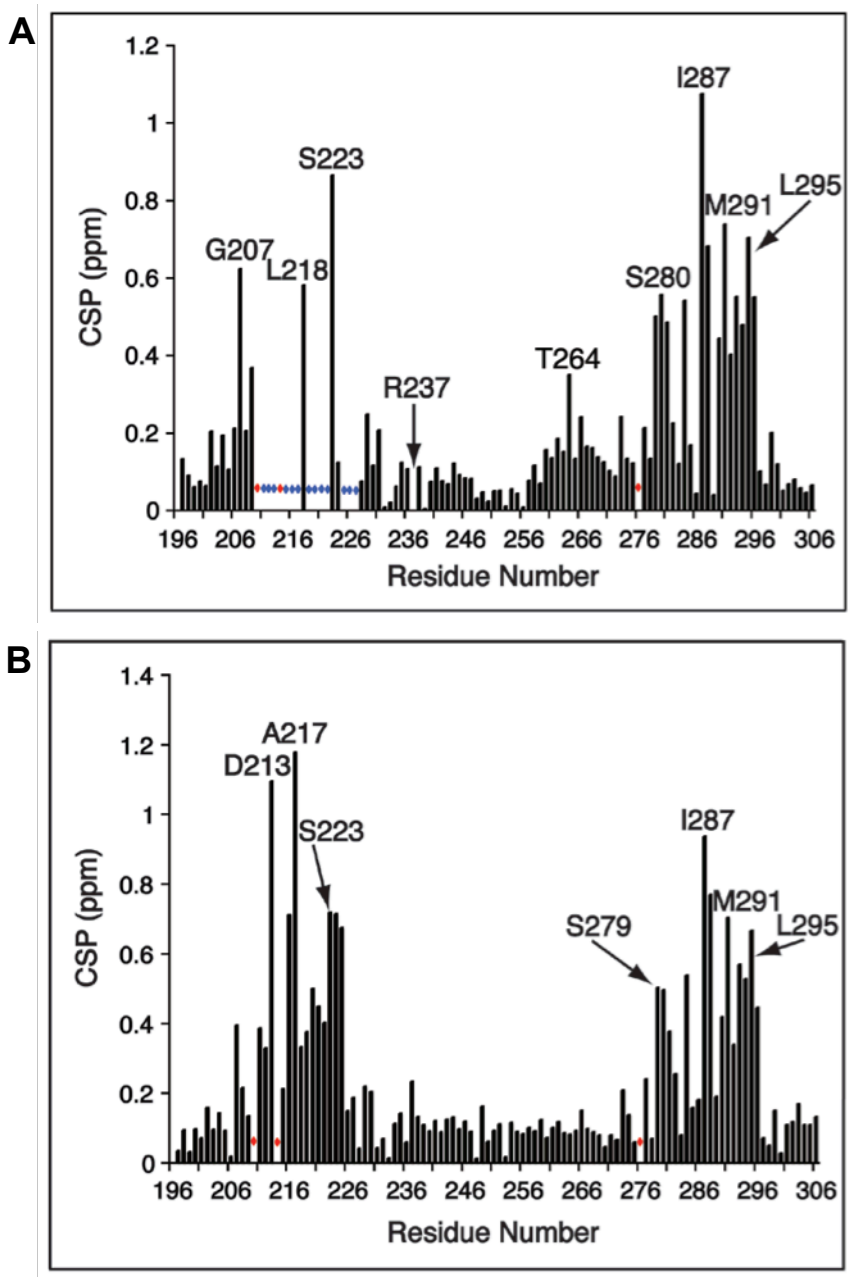

Figure 4.S1. Amide chemical shift perturbation experiments reveal new spectral changes for diubiquitin binding. (A) Amide chemical shift perturbation analysis reveals the residues of S5a involved in binding diubiquitin. Residues that disappear upon diubiquitin binding and prolines, which lack amide protons, are labeled with blue and red stars, respectively. R237 of S5a could not be followed during the titration series due to resonance overlap. (B) Amide chemical shift perturbation analysis reveals the residues of S5a involved in binding monoubiquitin. Prolines are labeled with red stars. Chemical

shift perturbation values ($\Delta\delta_{avg}$) for ^{15}N and ^{1}H nuclei were derived from $CSP = \sqrt{0.2\Delta\delta_N^2 + \Delta\delta_H^2}$, where $\Delta\delta_N$ and $\Delta\delta_H$ represent the changes in the amide nitrogen and proton chemical shifts (in parts per million), respectively.

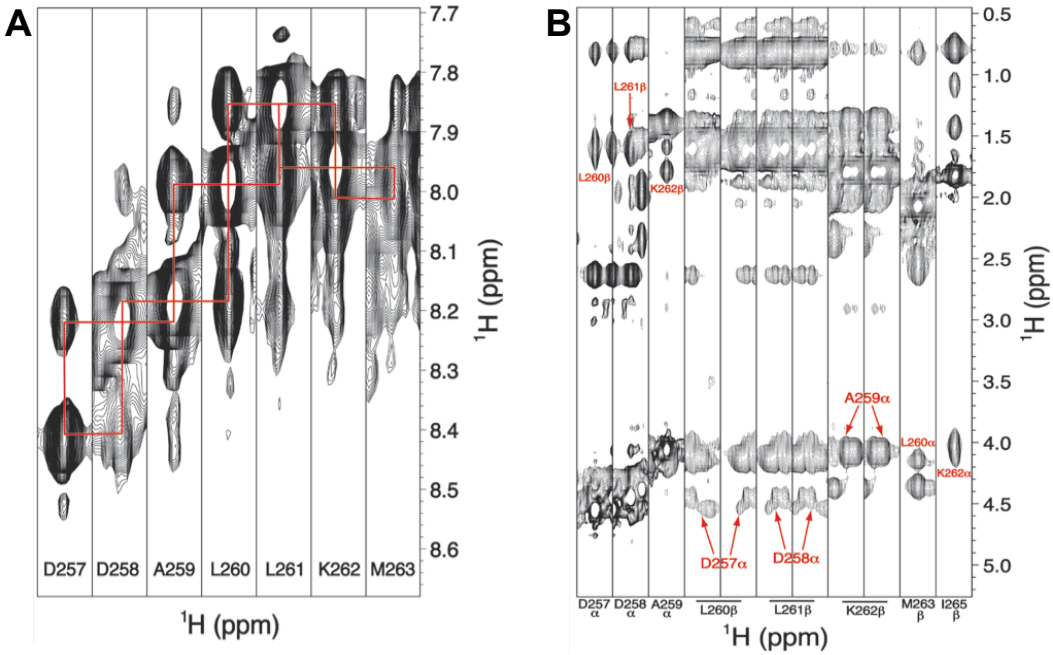

Figure 4.S2. S5a binding to diubiquitin does not disrupt the secondary structure of the helix between UIM1 and UIM2. (A) An ^{15}N-dipersed NOESY spectrum recorded on ^{15}N-labeled S5a (196-306) and 3-fold molar excess unlabeled diubiquitin reveals strong amide-to-amide NOE crosspeaks, which are a signature for helices. (B) A ^{13}C-dipersed NOESY spectrum recorded on ^{13}C-labeled S5a (196-306) and 3-fold molar excess unlabeled diubiquitin reveals NOE crosspeaks between Hα (i) and Hβ (i+3) atoms, which are a hallmark of helices.

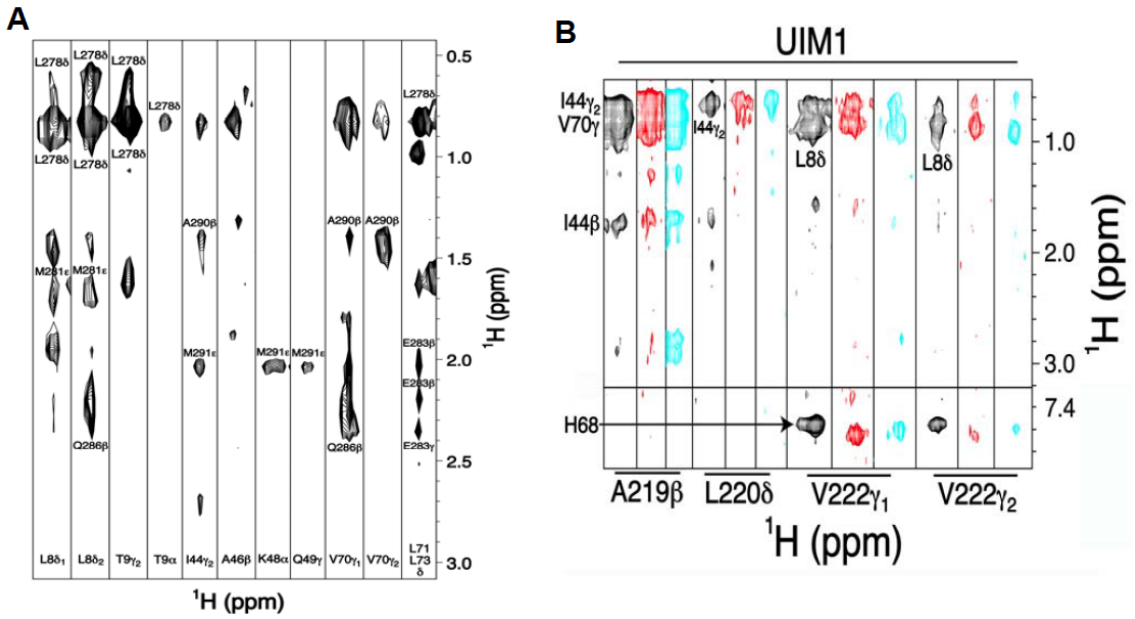

Figure 4.S3. UIM2 binds the proximal subunit while UIM1 binds the distal one. (A) Abundant intermolecular interactions appear between UIM2 and K48-linked diubiquitin's proximal subunit. The spectrum of Figure 4.2A displayed in black, which contains NOEs between S5a and the proximal subunit of diubiquitin, is expanded to illustrate abundant NOE interactions. Intermolecular NOEs between S5a and proximal K48 reveal that S5a has contacts with the atoms connecting the two ubiquitin subunits. (B) Selected regions of experiments containing intermolecular NOE interactions between UIM1 of S5a (196-306) and diubiquitin (black and red) or monoubiquitin (light blue). ^{13}C half-filtered NOESY spectra recorded on ^{13}C-labeled S5a (196-306) mixed with 3-fold molar excess unlabeled K48-linked diubiquitin (black) or K48-linked diubiquitin with its proximal subunit deuterated (red) indicates the interactions to be unaffected by deuterating the proximal subunit. The binding pattern between UIM1 and diubiquitin mimics that with monoubiquitin, which is demonstrated by analogous intermolecular NOEs (light blue).

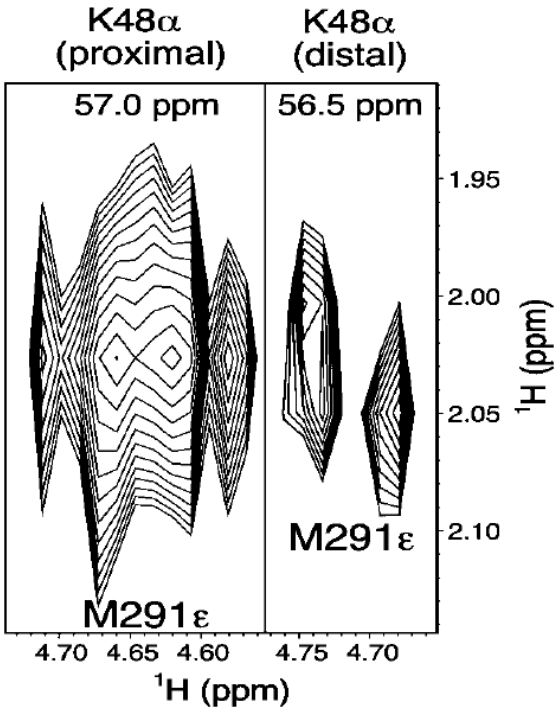

Figure 4.S4. The population of S5a's UIM2 bound to K48-linked diubiquitin's proximal subunit is in 3-fold molar excess over that bound to the distal one. ^{13}C half-filtered experiments were recorded in an identical manner on K48-linked diubiquitin with either its proximal (left) or distal (right) subunit ^{13}C labeled and mixed with unlabeled S5a (196-306). Intermolecular NOE interactions between M291's sidechain methyl group and proximal (left) or distal (right) K48's Ha proton were integrated to reveal population differences. Both experiments were performed with diubiquitin at 0.5 mM and S5a at 2-fold molar excess.

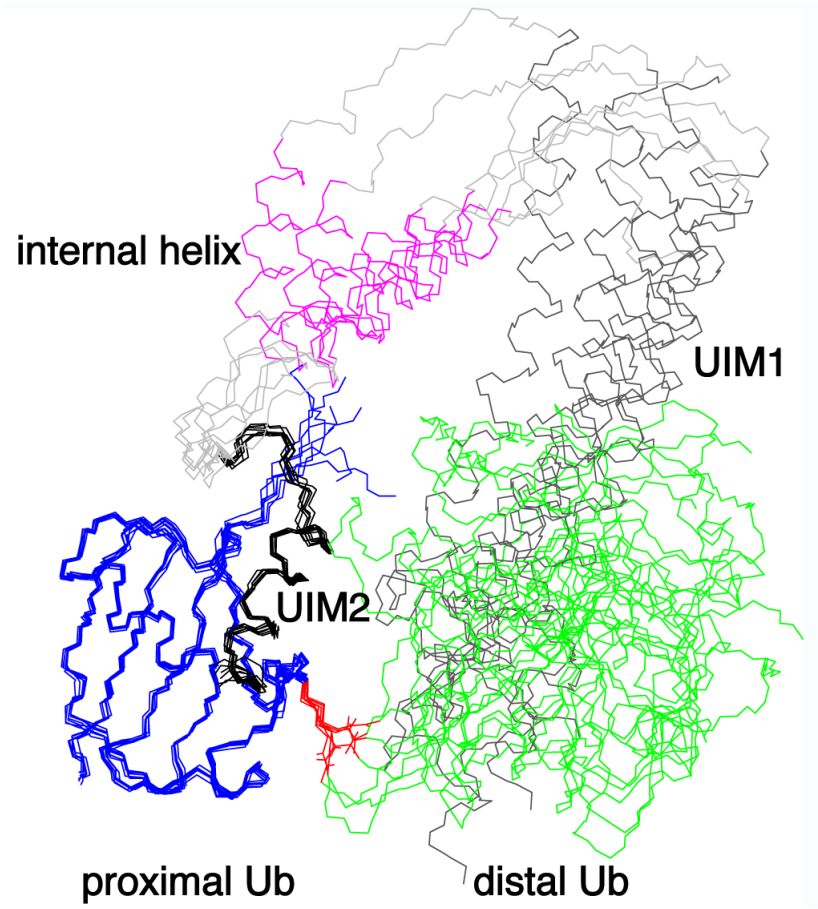

Figure 4.S5. Although significantly more restricted than when bound to monoubiquitin, S5a's UIMs retain some freedom in their relative positions due to the flexibility of the diubiquitin's linker region. The S5a (196-306):K48-linked diubiquitin structures with no NOE violation above 0.3 Å are displayed with the backbone heavy atoms of proximal ubiquitin and UIM2 superimposed. 7 structures are displayed from 30 randomly coiled starting structures. UIM1, the internal helix, and UIM2 of S5a are colored in dark grey, purple and black, respectively, whereas diubiquitin's distal and proximal subunits are highlighted in green and blue, respectively. The linker residues of diubiquitin (proximal K48 and distal G76) are highlighted in red.

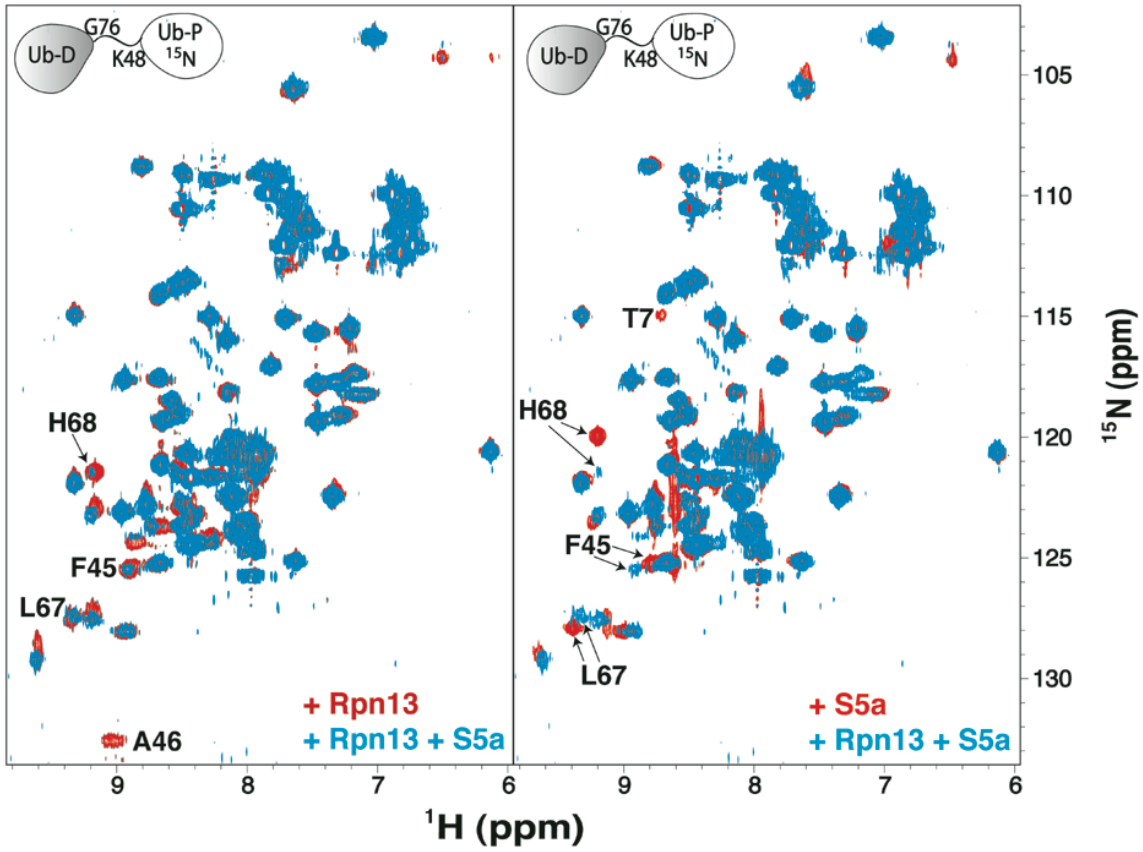

Figure 4.S6. Diubiquitin's proximal subunit binds predominately to Rpn13. $^{1}H,^{15}N$ HSQC spectra of K48-linked diubiquitin with its proximal subunit ^{15}N labeled in the presence of equimolar Rpn13 (left, red), S5a (right, red), or both of these ubiquitin receptors (blue). Selected ubiquitin resonances are labeled, including T7, F45, L67, and H68, which shift in a manner that reflects Rpn13 binding. Attenuation of A46 and H68 in the presence of Rpn13 and S5a suggests that, although a large fraction of the proximal subunit is bound to Rpn13, some minor exchange most likely occurs.

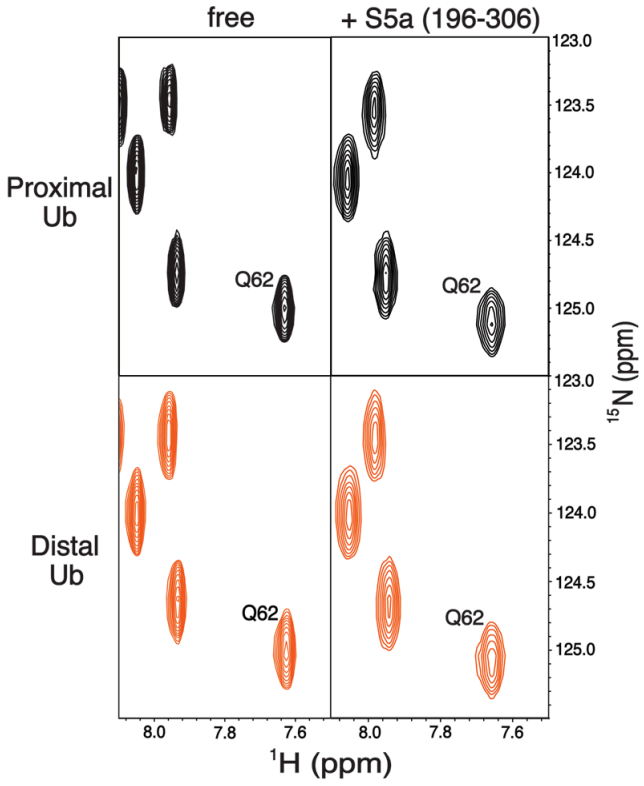

Figure 4.S7. Q62 of diubiquitin's proximal and distal subunits is not attenuated upon addition of unlabeled S5a (196-306). Expanded view of ^{1}H, ^{15}N HSQC spectra for the proximal (top panels) or distal (bottom panels) subunit of K48-linked diubiquitin alone (left panel), or with added unlabeled S5a (196-306) (right panel).

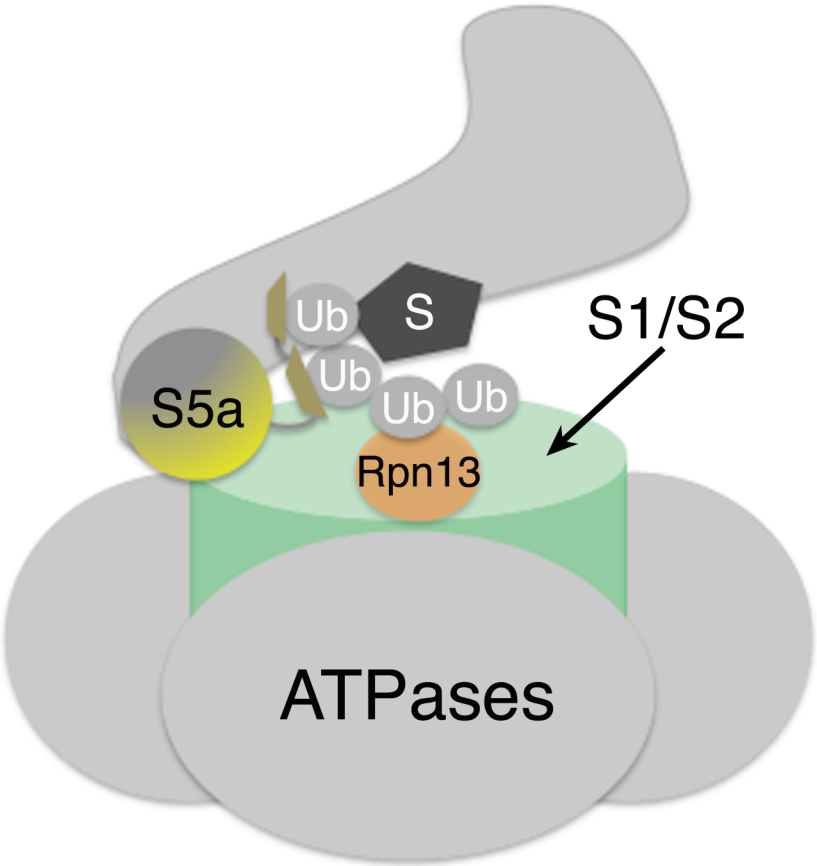

Figure 4.S8. Proposed model of Rpn13 and S5a binding simultaneously to a ubiquitinated substrate in the proteasome. Rpn13's ubiquitin-binding domain and S5a's N-terminal VWA domain are displayed bound to the S1 and S2 scaffolding proteins of the proteasome's regulatory particle as their ubiquitin-binding regions bind ubiquitin subunits of a ubiquitinated substrate. This coordinated binding may serve to properly orient the ubiquitin chain for subsequent processing by deubiquitinating enzymes in the proteasome.

Chapter 5

Ubiquitin receptor hRpn13 binds E2 enzyme hCdc34

Leah Randles *and Kylie J Walters*

Department of Biochemistry, Molecular Biology and Biophysics, University of Minnesota, Minneapolis, Minnesota, USA 55455

In preparation[a]

Leah Randles Contributions: Contributed to the development of all experiments, the analysis of the data, and the writing of the paper. Performed all experiments and produced all figures.

[a] We gratefully acknowledge Dr. Fen Liu for helpful discussions and Dr. Gary S. Shaw (University of Western Ontario) for generously providing us with the prokaryotic hCdc34 expression vector and for together with Dr. Donald E. Spratt providing us with their hCdc34 C-terminal tail amide assignments. NMR data was acquired at MNMR and all computation was performed in the MSI BSCL. This research was supported by the National Institutes of Health (CA097004 and CA136472). L.R. was funded in part by a University of Minnesota Doctoral Dissertation Fellowship.

5.1 Synopsis

Regulated protein degradation by proteasome is essential and contributes to a large spectrum of cellular events, including cell cycle progression, DNA repair, and signal transduction. Substrate ubiquitination by a 3-step E1-E2-E3 enzymatic cascade is typically used to signal for proteolysis by proteasome, which houses two ubiquitin receptors in its 19S regulatory particle, Rpn13 and S5a. Prior to proteolysis, substrates are deubiquitinated and Rpn13 recognizes ubiquitin with an N-terminal Pru (pleckstrin-like receptor for ubiquitin) domain and deubiquitinating enzyme Uch37 with a C-terminal domain. We reveal here that human Rpn13's Pru domain also binds to the human E2 ubiquitin-conjugating enzyme Cdc34, which functions in cell cycle progression. NMR titration experiments reveal that an hRpn13 surface that neighbors its ubiquitin-binding loops binds to the unique C-terminal tail of hCdc34 and that this interaction does not restrict hRpn13 binding to ubiquitin. Immunoprecipitation experiments performed with HeLa cells demonstrate that this interaction occurs in the cellular environment. Altogether, these data suggest that hRpn13 may contribute to regulated substrate ubiquitination by Cdc34 in proliferating cells.

5.2 Introduction

The ubiquitin-proteasome pathway is the major route for regulated protein degradation in eukaryotes, reviewed in (*252, 253*). Substrates are ubiquitinated by the coordinated efforts of E1, E2 and E3 enzymes and in turn, recognized by ubiquitin receptors in the proteasome's regulatory particle or that associate with it, reviewed in

(*254, 255*). E1 activating enzymes prime ubiquitin for a thioester bond with an E2's catalytic cysteine, reviewed in (*255-257*). The vast majority of E3 ligating enzymes contain RING domains that bind ubiquitin-charged E2s to serve as scaffolds, which enable the transfer of ubiquitin from the E2 to a substrate, reviewed in (*258*). HECT domain E3s and two reported RING-in-between-RING E3s (*259*) can accept activated ubiquitin from E2s at their own catalytic cysteine for subsequent transfer to a substrate. Multiple rounds through the E1-E2-E3 enzymatic cascade enables substrates to be monoubiquitinated at multiple sites or conjugated with a ubiquitin chain that is linked together through ubiquitin's seven lysines or its N-terminal methionine. Ubiquitination signals for a myriad of cellular events, the outcome of which is generally governed by multivalent interactions defined by the type of ubiquitin modification and subcellular context (*254, 260*).

Humans are predicted to have ~650 E3s with nearly half being cullin-RING ligases (CRLs) (*258*), which use a cullin scaffold (CUL1, CUL2, CUL3, CUL4A, CUL4B, CUL5, or CUL7), a catalytic RING domain (Rbx1 or Rbx2), and adaptor-substrate receptor proteins, reviewed in (*261*). CRLs are activated by the conjugation of ubiquitin-like modifier Nedd8 to a conserved lysine on the cullin subunit, which is thought to promote RING-E2 conformational heterogeneity and in turn processive substrate ubiquitination (*262-266*).

The first discovered CRLs were the SCF (Skp1-Cul1-F-box protein) complexes, which contain RING E3 Rbx1 bound to the Cul1 catalytic C-terminal domain and various F-box adaptor proteins that recruit specific substrates. The E2 UbcH5 functions with the

SCF to attach the initial ubiquitin to substrates while E2 Cdc34 adds successive ubiquitin moieties to form a chain (*267*). E1 and E3 binding surfaces overlap on E2s (*268-271*) and ubiquitin-charged Cdc34 binds Rbx1 with 50-fold greater affinity compared to unmodified Cdc34 (*272*), which would facilitate its release from Rbx1 after ubiquitin transfer. Cdc34 also contains a unique intrinsically disordered C-terminal acidic tail that binds ubiquitin (*273*) and a basic canyon of Cul1 (*274, 275*), with the latter interaction promoting processive Lys48-linked ubiquitin chain assembly on substrates (*274, 275*).

Through its interaction with the SCF complex, Cdc34 ubiquitinates numerous proteasome substrates, including p27/Kip1 (*276-278*), IκBα (*279, 280*), and the Wee1 kinase (*281*). Recently, a small molecule inhibitor of Cdc34 (CC0651) was reported and found to cause p27/Kip1 accumulation and to inhibit proliferation of human cancer cell lines (*282*). Cdc34 protein levels are elevated in pediatric T cell acute lymphoblastic leukemia (*283*) and it is a target of the tumor suppressor (*284*) *let-7* microRNA (*285*).

Proteasome ubiquitin receptors Rpn13 (*92, 93*) and S5a/Rpn10 (*132*) recognize ubiquitinated substrates through a Pru (pleckstrin-like receptor for ubiquitin) domain (*92, 93*) and UIMs (ubiquitin-interacting motifs) (*286, 287*), respectively. Prior to translocation into the proteasome's catalytic core particle, substrates are deubiquitinated by the proteasome's deubiquitinating enzymes, which include Rpn11 (*206, 207, 288*), Ubp6/Usp14 (*289*) and Uch37/UCHL5 (*174*). Ubiquitin receptor Rpn13 contributes Uch37 to the proteasome (*290-292*), which has been proposed to act as an editing isopeptidase, capable of freeing poorly ubiquitinated substrates from proteasome prior to degradation (*174*). When free of proteasome, hRpn13's C-terminal Uch37-binding

domain interacts with its Pru domain and restricts its ubiquitin-binding affinity (*293*). CryoEM studies in yeast map Rpn13 to an apical location in proteasome (*294, 295*) and immunodepletion analysis suggest that not all proteasome contains hRpn13 (*290*).

Unexpectedly, we found that human Rpn13's Pru domain binds to human Cdc34's unique C-terminal tail. NMR spectroscopy experiments demonstrated the hRpn13:hCdc34 interaction to be specific and to not interfere with Rpn13 binding to ubiquitin. Rpn13 and Cdc34 interact in HeLa cells according to immunoprecipitation experiments and this interaction is preserved with hRpn13 F76R, which cannot bind ubiquitin (*93*). Altogether these data suggest that Rpn13 may influence substrate ubiquitination by Cdc34 in proliferating cells.

5.3 Results

5.3.1 Ubiquitin receptor hRpn13 binds E2 conjugating enzyme hCdc34

We use ubiquitinated hCdc34 as a model substrate and therefore, as a negative control, tested whether unmodified hCdc34 interacts with hRpn13. Unexpectedly, we found that hCdc34 is retained on glutathione sepharose resin preincubated with GST-hRpn13 or GST-hRpn13 Pru domain; as expected, it was not retained with GST (Figure 5.1A). We next tested whether endogenous Rpn13 and Cdc34 interact in HeLa cell lysate by using anti-Cdc34 antibody (Novus Biologicals) for immunoprecipitation and anti-Rpn13 antibody (Biomol) for visualization. Rpn13 was observed to immunoprecipitate with Cdc34 (Figure 5.1B). This interaction was also detected in HeLa cells expressing FLAG-tagged hCdc34. Rpn13 was immunoprecipitated and Cdc34 visualized with anti-

FLAG antibody (Figure 5.1C); endogenous Cdc34 overlaps with light chain. We used hRpn13 F76R, which does not bind ubiquitin (*93*), to test whether this interaction is mediated by ubiquitin. Lysates from HeLa cells expressing FLAG-hRpn13 F76R were subjected to immunoprecipitation by anti-Cdc34 antibody and immunoblotting with anti-FLAG antibody. FLAG-hRpn13 F76R immunoprecipitated with hCdc34 (Figure 5.1D), indicating that the hRpn13:hCdc34 complex is not formed due to hRpn13 binding to ubiquitin.

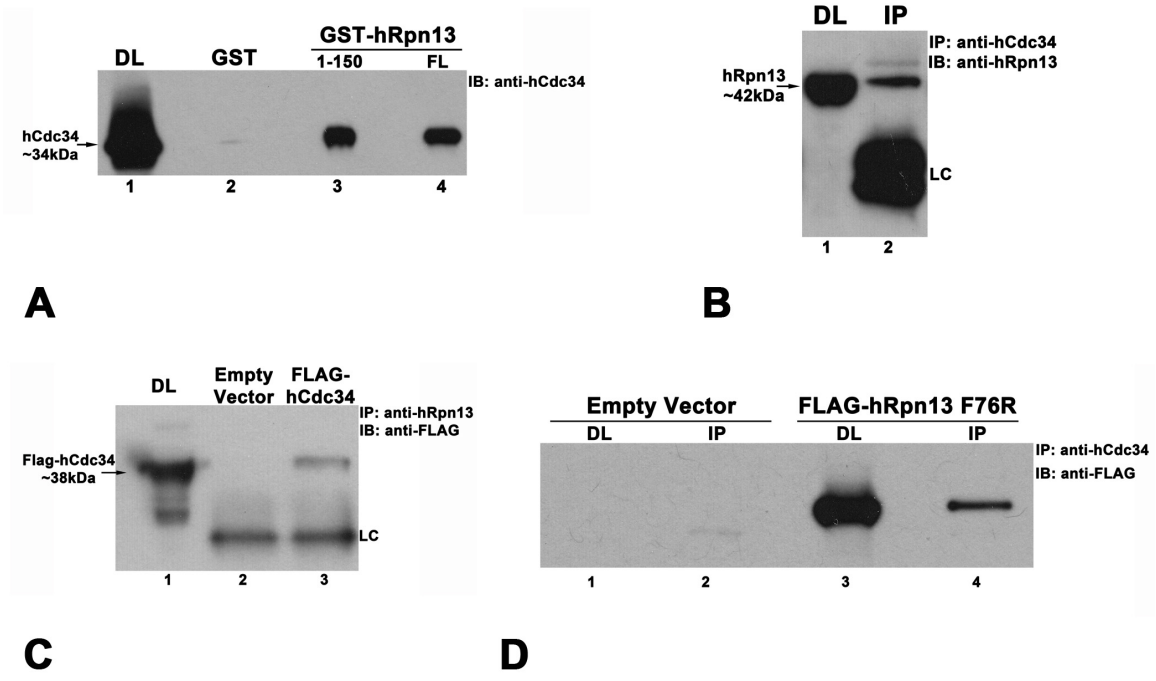

Figure 5.1. hRpn13 and hCdc34 interact *in vitro* and *in vivo*. (A) The retention of Cdc34 on glutathione sepharose resin pre-bound with GST, GST-hRpn13 Pru domain (1-150), or GST-hRpn13 full length protein (FL) is tested, as indicated by Western blot analysis. Direct load (DL) of hCdc34 is included in lane 1. (B) Endogenous levels of hCdc34 from HeLa cells is immunoprecipitated (IP) by anti-hCdc34 antibody (Novus Biologicals) and Western blot analysis used to detect the presence of endogenous hRpn13 by using anti-hRpn13 antibody (Biomol) (lane 2). Lane 1 shows a direct load of HeLa lysate used for immunoprecipitation. (C) HeLa cells transfected with FLAG-tagged hCdc34 were

subjected to an immunoprecipitation experiment with anti-hRpn13 antibody (Biomol) followed by Western blot analysis for FLAG-tagged hCdc34 with anti-FLAG antibody (Sigma) (lane 3). A control experiment with empty vector is included (lane 2), as is a direct load of the transfected HeLa cell lysate (lane 1). (D). *In vivo* immunoprecipitation of hCdc34 from HeLa cells transfected with p3xFLAG-CMV7.1 empty vector (lane 2) or Flag-hRpn13 F76R mutant (lane 4). hCdc34 was immuniprecipitated with anti-hCdc34 antibody (Novus Biologicals) and the resulting samples were probed with anti-FLAG (Sigma) antibody.

5.3.2 hRpn13 binds hCdc34 through a surface that abuts its ubiquitin-binding loops

We used NMR spectroscopy, to test whether hRpn13 and hCdc34 can directly bind each other. hRpn13 (1-150), which includes its Pru domain, and full length hCdc34 were expressed and purified as described previously (*93, 273*). Unlabeled hCdc34 was titrated into ^{15}N labeled hRpn13 Pru domain, which was monitored by ^{1}H, ^{15}N HSQC experiments. A select group of hRpn13 signals shift upon hCdc34 addition, thus confirming their interaction (Figure 5.2A). The binding occurred in the fast exchange regime on the NMR time scale such that hRpn13 signals could be readily followed from their free state to their hCdc34-bound state; an example is provided for Lys34 in Figure 5.2B.

In the absence of structural rearrangement, NMR signal shifting upon titration of a binding partner can be used to map binding surfaces (*296, 297*). We therefore quantified the extent to which each hRpn13 amide signal is affected by hCdc34 addition, as described in Materials and Methods. The most affected amino acids localize to a surface that neighbors, but does not overlap with hRpn13's ubiquitin-binding loops (Figure 5.2C and 5.2D). Electrostatic analysis of the hRpn13 surface demonstrated its hCdc34-interacting region to be basic (Figure 5.2E).

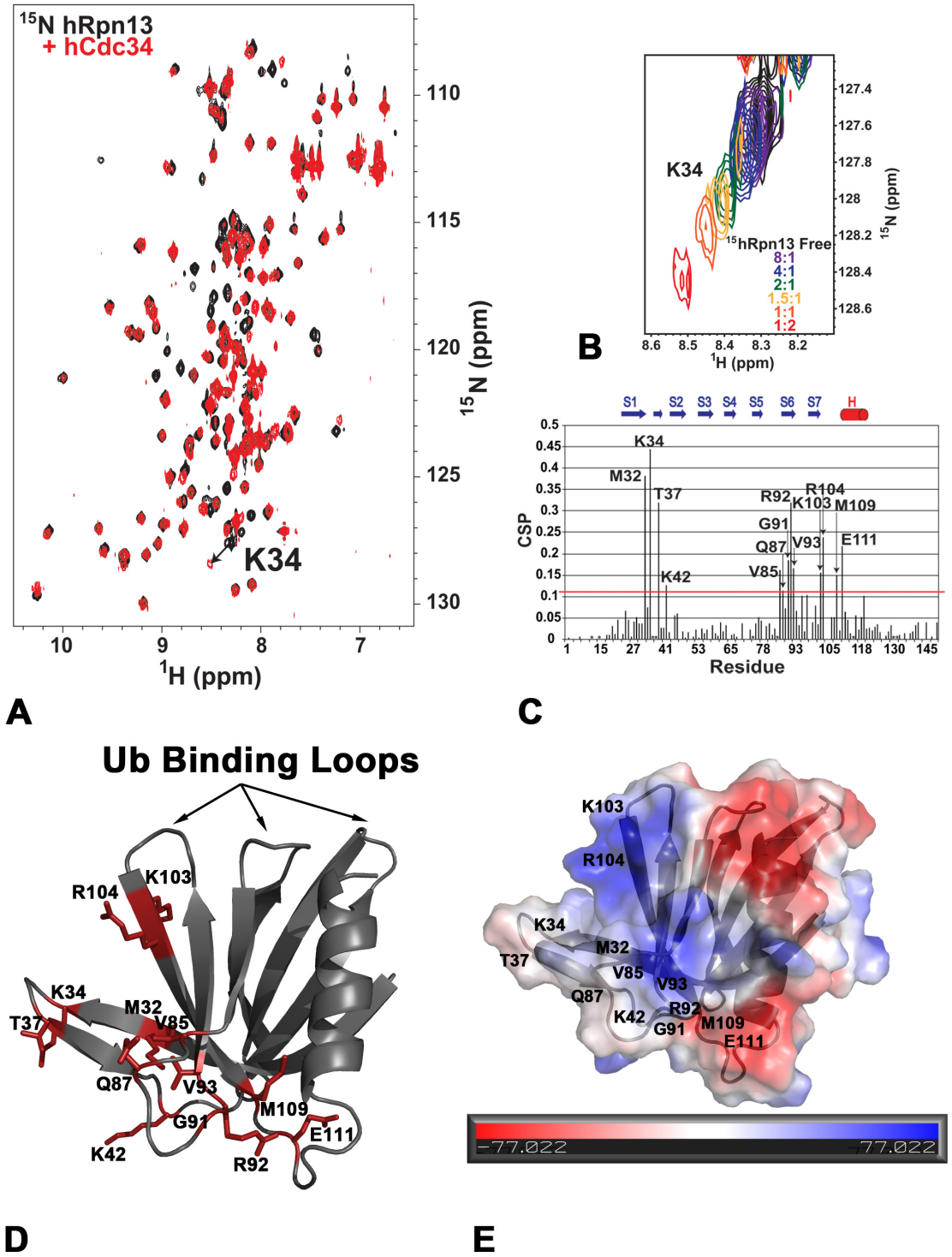
15N hRpn13
+ hCdc34
K34
1H (ppm)
15N (ppm)
A
K34
15hRpn13 Free
8:1
4:1
2:1
1.5:1
1:1
1:2
1H (ppm)
15N (ppm)
B
S1 S2 S3 S4 S5 S6 S7 H
CSP
Residue
K34
M32
T37
R92
R104
K103
M109
G91
Q87
V93
E111
V85
K42
C
Ub Binding Loops
R104
K103
K34
T37
M32
V85
Q87
V93
M109
G91
E111
K42
R92
D
-77.022
77.022
E

Figure 5.2. hCdc34 binds hRpn13 at a surface that juxtaposes its ubiquitin binding loops. (A) ^{1}H, ^{15}N HSQC spectra of ^{15}N-labeled hRpn13 alone (black) and with 2-fold excess unlabeled hCdc34 (red) (B) hRpn13 exhibits 'fast exchange' dynamics on the NMR timescale (100ms) when binding to hCdc34 as exhibited by Lys34 which is exhibited with different molar ratios of hRpn13 Pru:hCdc34 as indicated. (C) Chemical shift perturbation analysis reveals residues within hRpn13 that bind hCdc34. Residues that were significantly affected (>Avg+StDEV) are labeled and highlighted in red on the Rpn13 structure (D). (E) Electrostatic image of hRpn13 showing acidic and basic residues with residues implicated in hCdc34 binding labeled.

5.3.3 hRpn13 binds to Cdc34's C-terminal tail

To define the region of hCdc34 that binds to hRpn13, we added unlabeled hRpn13 to ^{15}N labeled hCdc34 (Figure 5.3A and Supplementary Figure 5.S1A) or its N-terminal catalytic domain, hCdc34 (7-182) (Supplementary Figure 5.S1B). Whereas chemical shift assignments are not available for hCdc34's catalytic domain, those of its C-terminal tail were generously provided by Dr. Gary S. Shaw and Dr. Donald E. Spratt. ^{1}H, ^{15}N HSQC experiments revealed significant signal shifting for amino acids in the C-terminal tail of the full-length protein and not for the unassigned signals (Figure 5.3A and Supplementary Figure 5.S1A). Similarly, hRpn13 did not affect the NMR signals of hCdc34 (7-182) (Supplementary Figure 5.S1B). Quantification of hRpn13's effect on hCdc34's C-terminal tail demonstrates signal shifting that spans Glu201 – Asp230 (Figure 5.3B). Altogether, these results demonstrate that hRpn13 binds to hCdc34's unique C-terminal tail and not its catalytic domain.

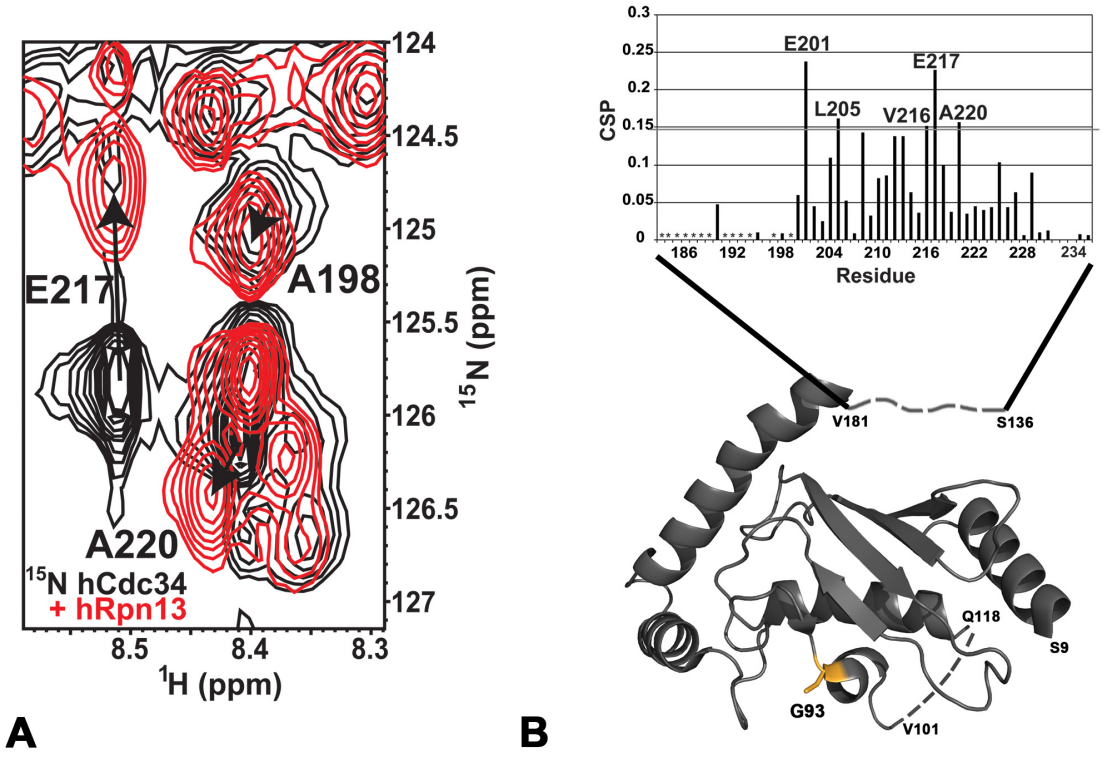

Figure 5.3. hRpn13 binds hCdc34's C-terminal tail. (A) Expanded $^{1}H,^{15}N$ HSQC spectra of ^{15}N-labeled full length hCdc34 alone (black) and with 3-fold molar excess unlabeled hRpn13 (red). (B) Chemical shift perturbation analysis upon hRpn13 addition for hCdc34's assigned C-terminal tail by using the data of (A). Amides that were shifted by a standard deviation greater than average are labeled.

5.3.4 hRpn13 and hCdc34 can form a ternary complex with ubiquitin, but not S1 (797-953)

To test whether hRpn13 can bind to ubiquitin and hCdc34 simultaneously, we added unlabeled hCdc34 and ubiquitin to ^{15}N labeled hRpn13 Pru domain, which was monitored by NMR. This experiment revealed hRpn13 interaction with both proteins simultaneously. In particular, hRpn13 signals that shift upon hCdc34 addition (Figure 5.3A, red) remain shifted in the presence of hCdc34 and ubiquitin (Figure 5.3A, cyan), as demonstrated for Lys34. Similarly, Rpn13 signals that shift in a ubiquitin-specific

manner are also shifted with both binding partners present, as demonstrated for Ile75 (Figure 5.3A, dark blue versus cyan).

In previous work (*93, 293*), we mapped the hRpn13 amino acids that are affected by binding to S1 (797-953), a fragment of Rpn13's binding partner in the proteasome's regulatory particle (*293*). The hRpn13 amino acids identified to be affected by hCdc34 overlap with those involved in binding to S1 (797-953) and this region is also implicated in binding to the S1 *S. cerevisiae* analog Rpn2, as scRpn13 Lys119, which corresponds to hRpn13 Glu118, cross-linked to Lys911 in Rpn2 (*298*). We tested directly whether hRpn13 can bind to hCdc34 and S1 (797-953) simultaneously. ^{15}N labeled hRpn13 was saturated with unlabeled S1 (797-953) and then mixed with 2-fold molar excess unlabeled hCdc34. Comparison of this 3-protein mixture with spectra derived from ^{15}N labeled hRpn13:Cdc34 and ^{15}N labeled hRpn13:S1 (797-953) demonstrates that Rpn13 binds preferentially to S1 (797-953) at the exclusion of hCdc34 (Figure 5.4B). Met109 illustrates this effect as it shifts to its S1-bound state and is unperturbed by hCdc34 (Figure 5.4B). In addition, we did not find hCdc34 to immunoprecipitate with proteasome from HeLa cells (data not shown), although the SCF complex has been found to co-purify with proteasome from *Saccharomyces cerevisiae* (*299*).

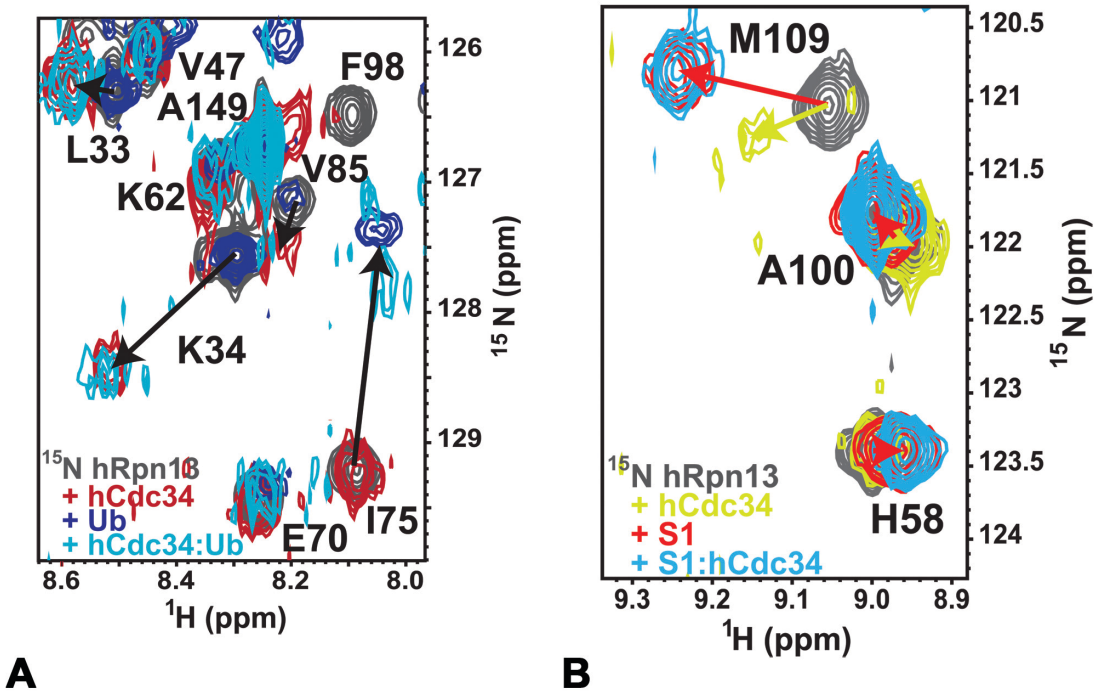

Figure 5.4. hRpn13 can interact with hCdc34 and monoubiquitin at the same time but not S1. (A) Expanded ^{1}H,^{15}N HSQC spectra are displayed of ^{15}N-labeled hRpn13 alone (grey), with 2-fold excess hCdc34 (red) or with 2-fold excess hCdc34 and monoubiquitin (cyan) (B) ^{1}H, ^{15}N HSQC spectra are displayed of ^{15}N-labeled hRpn13 alone (grey), with hCdc34 (green) or proteasome scaffolding protein S1 (797-953) (red), or with hCdc34 and the S1 fragment (cyan).

5.4 Concluding Remarks

We provide evidence that proteasome ubiquitin receptor hRpn13 binds to the E2 enzyme hCdc34. IkBa (*279, 280*) is also a Cdc34 substrate and interestingly, it and iNOS are the only other reported hRpn13 substrates (*300*). Since hRpn13's hCdc34-binding surface overlaps with its S1 (797-953)-binding surface, we do not expect hCdc34 to interact with hRpn13 when docked into proteasome. The SCF complex has been demonstrated in landmark studies to function *in vitro* with Cdc34 and without addition of Rpn13 (*274, 275, 301-304*). Therefore, Rpn13 is not required for substrate ubiquitination

by this complex. Rather, it appears to play a regulatory role. Future experiments are needed to dissect the mechanistic relationship between hRpn13 and hCdc34. Testing the effect of hRpn13 knockdown on an hCdc34 specific substrate, such as p27/Kip1, could do this. It would also be worthwhile to test whether Uch37 plays an important role in p27/Kip1 protein stability. Nonetheless, we have described here a novel interaction between hRpn13 and hCdc34 that suggests an important regulatory role for hRpn13 in proliferating cells.

5.5 Materials and Methods

5.5.1 Protein expression and cell culture

hRpn13, hRpn13 (1-150), hCdc34, hCdc34-cat, and S1 (797-953) were expressed and purified as described previously (*93, 273, 293*). Ubiquitin was purchased (R&D Systems). All NMR experiments were done in 20 mM $NaPO_4$ pH 7.3, 100 mM NaCl, 1 mM DTT, 0.1% NaN_3 and 10% D_2O. The hCdc34 plasmid for mammalian expression was generated by PCR amplification of its prokaryotic expression vector followed by cloning into empty mammalian expression vector p3xFLAG-CMV-7.1 (Sigma). FLAG-hRpn13 F76R was produced by using the QuickChange Site-Directed Mutagenesis Kit (Agilent Technologies) and a p3xFLAG-CMV-7.1 plasmid encoding wild-type hRpn13 (*92*). HeLa cells were transfected with expression vectors using Lipofectamine 2000 transfection reagent (Life Technologies) according to the manufacturer's instruction. HeLa cells were grown at 37°C in EMEM supplemented with 10% FBS in a humidified

atmosphere of 5% CO_2. To harvest cells, 0.25% Trypsin-EDTA (Gibco) was used and after washing in PBS, cell pellets were stored at -80 °C.

5.5.2 NMR experiments

Chemical shift perturbation analysis was performed as described previously (*93, 287*). Briefly, ^{1}H, ^{15}N HSQC experiments were recorded on either ^{15}N hRpn13, ^{15}N hCdc34, or ^{15}N hCdc34-Cat with increasing molar ratios of either unlabeled hCdc34 or hRpn13. All experiments were performed at 25°C on a Bruker 850 MHz spectrometer equipped with a cryogenically cooled probe. NMRPipe (*305*) was used for NMR data processing and the resulting spectra visualized with XEASY (*306*). The amide and hydrogen chemical shift perturbations (CSP) were mapped for each residue according to Equation 5.1.

$$CSP = \sqrt{0.2\Delta\delta_N^2 + \Delta\delta_H^2} \qquad (5.1)$$

5.5.3 GST pull-down

GST-fused hRpn13 and hRpn13 (1-150) were bound to GST resin (GE Healthcare) and then rocked with His-tagged hCdc34 (Boston Biochem) for 3 hours at 4°C. Unbound protein was removed by washing in 20 mM $NaPO_4$, 50 mM NaCl, 0.5% Triton X-100, pH 6.5. Proteins retained on the resin were dissolved in 8M urea-SDS loading dye, heated to 70°C for 7 minutes, resolved by SDS-PAGE, transferred to PVDF membrane (Life Technologies) and immunoblotted with anti-Cdc34 antibody (Santa Cruz Biotechnology).

5.5.4 Immunoprecipitation experiments

HeLa cells used for immunoprecipitation experiments were harvested and sonicated in Buffer 1 (20 mM Hepes, 150 mM NaCl, 5 mM $MgCl_2$, 1 mM EDTA, 0.1 mM PMSF, pH 7.5) supplemented with protease inhibitor cocktail (Roche). After removing cellular debris by centrifugation, 500-1000 μg of total protein, as measured by a Bradford assay (Sigma), was pre-cleared and rocked at 4°C overnight with primary antibodies, anti-Rpn13 (Biomol) or anti-Cdc34 (Novus Biologicals). 40 μL of washed protein G beads were added and the samples rocked for an additional 5 hours followed by washing in Buffer 1. The proteins were eluted by the addition of 8 M urea-SDS loading buffer, heated at 70°C for 7 minutes, resolved by SDS-PAGE and transferred to PVDF membranes for visualization with anti-Rpn13 (Biomol) or anti-FLAG (Sigma) antibodies and ECL Western blotting detection reagents (Amersham).

5.6 Supplemental Figures

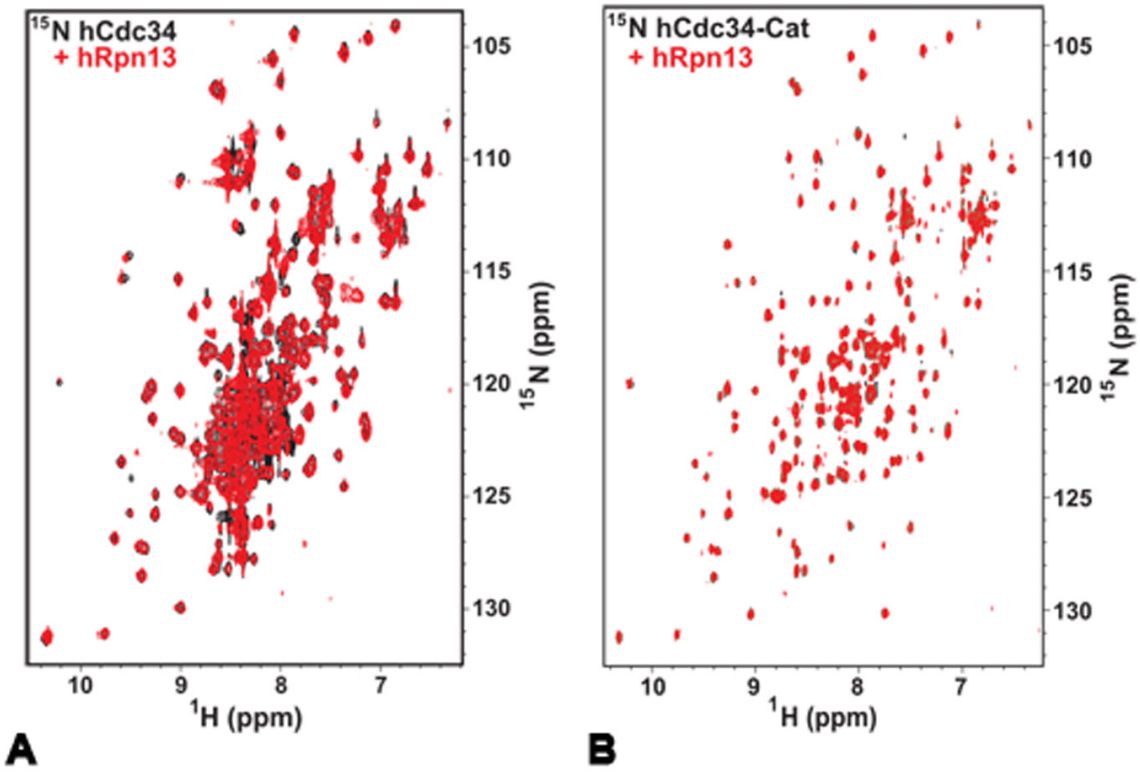

Figure 5.S1. hRpn13 binds exclusively to hCdc34's C-terminal tail. (A) ^{1}H, ^{15}N HSQC of ^{15}N labeled hCdc34 full-length alone (black) and with 3-fold molar excess unlabeled hRpn13 (red). (B) ^{1}H, ^{15}N HSQC of ^{15}N labeled hCdc34 catalytic domain (7-182) alone (black) and with 2-fold molar excess unlabeled hRpn13 (red).

Chapter 6

Summary and Future Directions

In this thesis, I have provided evidence that Rpn13 is a ubiquitin receptor in the proteasome's regulatory particle, the only other of which is S5a. I have shown that Rpn13 and S5a can bind simultaneously to ubiquitin chains, although we are not yet sure whether this happens at the proteasome. Furthermore, we know that loss of ubiquitin-binding by Rpn13 and S5a does not completely abrogate ubiquitin-mediated protein degradation. Therefore, we expect there to be other proteins in proteasome capable of binding to ubiquitin. Future experiments are needed to identify such components and to decipher whether the multiple ubiquitin receptors in proteasome act in concert or independently. It is currently not clear why proteasome requires more than one ubiquitin receptor.

I have also shown that Rpn13 binds to the E2 conjugating enzyme Cdc34. This finding is surprising and the interaction seems to occur when Rpn13 is not docked into proteasome. Future experiments are needed to dissect whether Rpn13 binding to Cdc34 serves a regulatory role. Rpn13's effect on the Cdc34 specific substrate p27/Kip1 will be assayed using RNAi specific to Rpn13. Rescue experiments using Rpn13's ubiquitin-binding domain are also planned to test whether Uch37 plays a role in p27/Kip1 protein stability. Nonetheless this work suggests that Rpn13 may play an important role in proliferating cells.

References Cited

1. Ciechanover, A., and Ben-Saadon, R. (2004) N-terminal ubiquitination: more protein substrates join in, *Trends Cell Biol 14*, 103-106.
2. Cadwell, K., and Coscoy, L. (2005) Ubiquitination on nonlysine residues by a viral E3 ubiquitin ligase, *Science 309*, 127-130.
3. Ravid, T., and Hochstrasser, M. (2007) Autoregulation of an E2 enzyme by ubiquitin-chain assembly on its catalytic residue, *Nat Cell Biol 9*, 422-427.
4. Deshaies, R. J., and Joazeiro, C. A. (2009) RING domain E3 ubiquitin ligases, *Annu Rev Biochem 78*, 399-434.
5. Haas, A. L., Warms, J. V., Hershko, A., and Rose, I. A. (1982) Ubiquitin-activating enzyme. Mechanism and role in protein-ubiquitin conjugation, *J Biol Chem 257*, 2543-2548.
6. Dye, B. T., and Schulman, B. A. (2007) Structural mechanisms underlying posttranslational modification by ubiquitin-like proteins, *Annu Rev Biophys Biomol Struct 36*, 131-150.
7. Schulman, B. A., and Harper, J. W. (2009) Ubiquitin-like protein activation by E1 enzymes: the apex for downstream signalling pathways, *Nat Rev Mol Cell Biol 10*, 319-331.
8. Rotin, D., and Kumar, S. (2009) Physiological functions of the HECT family of ubiquitin ligases, *Nat Rev Mol Cell Biol 10*, 398-409.
9. Wenzel, D. M., Lissounov, A., Brzovic, P. S., and Klevit, R. E. UBCH7 reactivity profile reveals parkin and HHARI to be RING/HECT hybrids, *Nature 474*, 105-108.
10. Peng, J., Schwartz, D., Elias, J. E., Thoreen, C. C., Cheng, D., Marsischky, G., Roelofs, J., Finley, D., and Gygi, S. P. (2003) A proteomics approach to understanding protein ubiquitination, *Nat Biotechnol 21*, 921-926.
11. Kirisako, T., Kamei, K., Murata, S., Kato, M., Fukumoto, H., Kanie, M., Sano, S., Tokunaga, F., Tanaka, K., and Iwai, K. (2006) A ubiquitin ligase complex assembles linear polyubiquitin chains, *EMBO J 25*, 4877-4887.
12. Tagwerker, C., Flick, K., Cui, M., Guerrero, C., Dou, Y., Auer, B., Baldi, P., Huang, L., and Kaiser, P. (2006) A tandem affinity tag for two-step purification under fully denaturing conditions: application in ubiquitin profiling and protein complex identification combined with in vivocross-linking, *Mol Cell Proteomics 5*, 737-748.
13. Xu, P., Duong, D. M., Seyfried, N. T., Cheng, D., Xie, Y., Robert, J., Rush, J., Hochstrasser, M., Finley, D., and Peng, J. (2009) Quantitative proteomics reveals the function of unconventional ubiquitin chains in proteasomal degradation, *Cell 137*, 133-145.
14. Dammer, E. B., Na, C. H., Xu, P., Seyfried, N. T., Duong, D. M., Cheng, D., Gearing, M., Rees, H., Lah, J. J., Levey, A. I., Rush, J., and Peng, J. Polyubiquitin linkage profiles in three models of proteolytic stress suggest the etiology of Alzheimer disease, *J Biol Chem 286*, 10457-10465.

15. Ikeda, F., and Dikic, I. (2008) Atypical ubiquitin chains: new molecular signals. 'Protein Modifications: Beyond the Usual Suspects' review series, *EMBO Rep 9*, 536-542.
16. Kim, H. T., Kim, K. P., Lledias, F., Kisselev, A. F., Scaglione, K. M., Skowyra, D., Gygi, S. P., and Goldberg, A. L. (2007) Certain pairs of ubiquitin-conjugating enzymes (E2s) and ubiquitin-protein ligases (E3s) synthesize nondegradable forked ubiquitin chains containing all possible isopeptide linkages, *J Biol Chem 282*, 17375-17386.
17. Finley, D. (2009) Recognition and processing of ubiquitin-protein conjugates by the proteasome, *Annu Rev Biochem 78*, 477-513.
18. Clague, M. J., and Urbe, S. Ubiquitin: same molecule, different degradation pathways, *Cell 143*, 682-685.
19. Haglund, K., and Dikic, I. (2005) Ubiquitylation and cell signaling, *EMBO J 24*, 3353-3359.
20. Hayden, M. S., and Ghosh, S. (2008) Shared principles in NF-kappaB signaling, *Cell 132*, 344-362.
21. Iwai, K., and Tokunaga, F. (2009) Linear polyubiquitination: a new regulator of NF-kappaB activation, *EMBO Rep 10*, 706-713.
22. Chastagner, P., Israel, A., and Brou, C. (2006) Itch/AIP4 mediates Deltex degradation through the formation of K29-linked polyubiquitin chains, *EMBO Rep 7*, 1147-1153.
23. You, J., and Pickart, C. M. (2001) A HECT domain E3 enzyme assembles novel polyubiquitin chains, *J Biol Chem 276*, 19871-19878.
24. Al-Hakim, A. K., Zagorska, A., Chapman, L., Deak, M., Peggie, M., and Alessi, D. R. (2008) Control of AMPK-related kinases by USP9X and atypical Lys(29)/Lys(33)-linked polyubiquitin chains, *Biochem J 411*, 249-260.
25. Bremm, A., and Komander, D. Emerging roles for Lys11-linked polyubiquitin in cellular regulation, *Trends Biochem Sci 36*, 355-363.
26. Nishikawa, H., Ooka, S., Sato, K., Arima, K., Okamoto, J., Klevit, R. E., Fukuda, M., and Ohta, T. (2004) Mass spectrometric and mutational analyses reveal Lys-6-linked polyubiquitin chains catalyzed by BRCA1-BARD1 ubiquitin ligase, *J Biol Chem 279*, 3916-3924.
27. Hatakeyama, S., Yada, M., Matsumoto, M., Ishida, N., and Nakayama, K. I. (2001) U box proteins as a new family of ubiquitin-protein ligases, *J Biol Chem 276*, 33111-33120.
28. Grabbe, C., and Dikic, I. (2009) Functional roles of ubiquitin-like domain (ULD) and ubiquitin-binding domain (UBD) containing proteins, *Chem Rev 109*, 1481-1494.
29. Hochstrasser, M. (2009) Origin and function of ubiquitin-like proteins, *Nature 458*, 422-429.
30. Sloper-Mould, K. E., Jemc, J. C., Pickart, C. M., and Hicke, L. (2001) Distinct functional surface regions on ubiquitin, *The Journal of biological chemistry 276*, 30483-30489.

31. Sundquist, W. I., Schubert, H. L., Kelly, B. N., Hill, G. C., Holton, J. M., and Hill, C. P. (2004) Ubiquitin recognition by the human TSG101 protein, *Mol Cell 13*, 783-789.
32. Hirano, S., Kawasaki, M., Ura, H., Kato, R., Raiborg, C., Stenmark, H., and Wakatsuki, S. (2006) Double-sided ubiquitin binding of Hrs-UIM in endosomal protein sorting, *Nat Struct Mol Biol 13*, 272-277.
33. Lange, O. F., Lakomek, N. A., Fares, C., Schroder, G. F., Walter, K. F., Becker, S., Meiler, J., Grubmuller, H., Griesinger, C., and de Groot, B. L. (2008) Recognition dynamics up to microseconds revealed from an RDC-derived ubiquitin ensemble in solution, *Science 320*, 1471-1475.
34. Wintrode, P. L., Makhatadze, G. I., and Privalov, P. L. (1994) Thermodynamics of ubiquitin unfolding, *Proteins 18*, 246-253.
35. Kumar, A., Srivastava, S., and Hosur, R. V. (2007) NMR characterization of the energy landscape of SUMO-1 in the native-state ensemble, *J Mol Biol 367*, 1480-1493.
36. Newton, K., Matsumoto, M. L., Wertz, I. E., Kirkpatrick, D. S., Lill, J. R., Tan, J., Dugger, D., Gordon, N., Sidhu, S. S., Fellouse, F. A., Komuves, L., French, D. M., Ferrando, R. E., Lam, C., Compaan, D., Yu, C., Bosanac, I., Hymowitz, S. G., Kelley, R. F., and Dixit, V. M. (2008) Ubiquitin chain editing revealed by polyubiquitin linkage-specific antibodies, *Cell 134*, 668-678.
37. Sato, Y., Yoshikawa, A., Yamagata, A., Mimura, H., Yamashita, M., Ookata, K., Nureki, O., Iwai, K., Komada, M., and Fukai, S. (2008) Structural basis for specific cleavage of Lys 63-linked polyubiquitin chains, *Nature 455*, 358-362.
38. Ryabov, Y., and Fushman, D. (2006) Interdomain mobility in di-ubiquitin revealed by NMR, *Proteins 63*, 787-796.
39. Cook, W. J., Jeffrey, L. C., Kasperek, E., and Pickart, C. M. (1994) Structure of tetraubiquitin shows how multiubiquitin chains can be formed, *J Mol Biol 236*, 601-609.
40. Eddins, M. J., Varadan, R., Fushman, D., Pickart, C. M., and Wolberger, C. (2007) Crystal structure and solution NMR studies of Lys48-linked tetraubiquitin at neutral pH, *J Mol Biol 367*, 204-211.
41. Trempe, J. F., Brown, N. R., Noble, M. E., and Endicott, J. A. A new crystal form of Lys48-linked diubiquitin, *Acta Crystallogr Sect F Struct Biol Cryst Commun 66*, 994-998.
42. Varadan, R., Assfalg, M., Raasi, S., Pickart, C., and Fushman, D. (2005) Structural determinants for selective recognition of a Lys48-linked polyubiquitin chain by a UBA domain, *Mol Cell 18*, 687-698.
43. Komander, D., Reyes-Turcu, F., Licchesi, J. D., Odenwaelder, P., Wilkinson, K. D., and Barford, D. (2009) Molecular discrimination of structurally equivalent Lys 63-linked and linear polyubiquitin chains, *EMBO Rep 10*, 466-473.
44. Bremm, A., Freund, S. M., and Komander, D. Lys11-linked ubiquitin chains adopt compact conformations and are preferentially hydrolyzed by the deubiquitinase Cezanne, *Nat Struct Mol Biol 17*, 939-947.

45. Matsumoto, M. L., Wickliffe, K. E., Dong, K. C., Yu, C., Bosanac, I., Bustos, D., Phu, L., Kirkpatrick, D. S., Hymowitz, S. G., Rape, M., Kelley, R. F., and Dixit, V. M. K11-linked polyubiquitination in cell cycle control revealed by a K11 linkage-specific antibody, *Mol Cell 39*, 477-484.
46. Fushman, D., and Walker, O. Exploring the linkage dependence of polyubiquitin conformations using molecular modeling, *J Mol Biol 395*, 803-814.
47. Sato, Y., Yoshikawa, A., Mimura, H., Yamashita, M., Yamagata, A., and Fukai, S. (2009) Structural basis for specific recognition of Lys 63-linked polyubiquitin chains by tandem UIMs of RAP80, *EMBO J 28*, 2461-2468.
48. Sims, J. J., and Cohen, R. E. (2009) Linkage-specific avidity defines the lysine 63-linked polyubiquitin-binding preference of rap80, *Mol Cell 33*, 775-783.
49. Swanson, K. A., Kang, R. S., Stamenova, S. D., Hicke, L., and Radhakrishnan, I. (2003) Solution structure of Vps27 UIM-ubiquitin complex important for endosomal sorting and receptor downregulation, *EMBO J 22*, 4597-4606.
50. Young, P., Deveraux, Q., Beal, R. E., Pickart, C. M., and Rechsteiner, M. (1998) Characterization of two polyubiquitin binding sites in the 26 S protease subunit 5a, *J Biol Chem 273*, 5461-5467.
51. Wang, Q., Young, P., and Walters, K. J. (2005) Structure of S5a bound to monoubiquitin provides a model for polyubiquitin recognition, *J Mol Biol 348*, 727-739.
52. Zhang, N., Wang, Q., Ehlinger, A., Randles, L., Lary, J. W., Kang, Y., Haririnia, A., Storaska, A. J., Cole, J. L., Fushman, D., and Walters, K. J. (2009) Structure of the s5a:k48-linked diubiquitin complex and its interactions with rpn13, *Mol Cell 35*, 280-290.
53. Mizuno, E., Kawahata, K., Kato, M., Kitamura, N., and Komada, M. (2003) STAM proteins bind ubiquitinated proteins on the early endosome via the VHS domain and ubiquitin-interacting motif, *Mol Biol Cell 14*, 3675-3689.
54. Sugiyama, S., Kishida, S., Chayama, K., Koyama, S., and Kikuchi, A. (2005) Ubiquitin-interacting motifs of Epsin are involved in the regulation of insulin-dependent endocytosis, *J Biochem 137*, 355-364.
55. Song, A. X., Zhou, C. J., Peng, Y., Gao, X. C., Zhou, Z. R., Fu, Q. S., Hong, J., Lin, D. H., and Hu, H. Y. Structural transformation of the tandem ubiquitin-interacting motifs in ataxin-3 and their cooperative interactions with ubiquitin chains, *PLoS One 5*, e13202.
56. Lee, S., Tsai, Y. C., Mattera, R., Smith, W. J., Kostelansky, M. S., Weissman, A. M., Bonifacino, J. S., and Hurley, J. H. (2006) Structural basis for ubiquitin recognition and autoubiquitination by Rabex-5, *Nat Struct Mol Biol 13*, 264-271.
57. Penengo, L., Mapelli, M., Murachelli, A. G., Confalonieri, S., Magri, L., Musacchio, A., Di Fiore, P. P., Polo, S., and Schneider, T. R. (2006) Crystal structure of the ubiquitin binding domains of rabex-5 reveals two modes of interaction with ubiquitin, *Cell 124*, 1183-1195.
58. Mattera, R., Tsai, Y. C., Weissman, A. M., and Bonifacino, J. S. (2006) The Rab5 guanine nucleotide exchange factor Rabex-5 binds ubiquitin (Ub) and functions as

a Ub ligase through an atypical Ub-interacting motif and a zinc finger domain, *J Biol Chem 281*, 6874-6883.
59. Pinato, S., Scandiuzzi, C., Arnaudo, N., Citterio, E., Gaudino, G., and Penengo, L. (2009) RNF168, a new RING finger, MIU-containing protein that modifies chromatin by ubiquitination of histones H2A and H2AX, *BMC Mol Biol 10*, 55.
60. Bomar, M. G., D'Souza, S., Bienko, M., Dikic, I., Walker, G. C., and Zhou, P. (2010) Unconventional ubiquitin recognition by the ubiquitin-binding motif within the Y family DNA polymerases iota and Rev1, *Molecular cell 37*, 408-417.
61. Burschowsky, D., Rudolf, F., Rabut, G., Herrmann, T., Peter, M., and Wider, G. (2011) Structural analysis of the conserved ubiquitin-binding motifs (UBMs) of the translesion polymerase iota in complex with ubiquitin, *The Journal of biological chemistry 286*, 1364-1373.
62. Rahighi, S., Ikeda, F., Kawasaki, M., Akutsu, M., Suzuki, N., Kato, R., Kensche, T., Uejima, T., Bloor, S., Komander, D., Randow, F., Wakatsuki, S., and Dikic, I. (2009) Specific recognition of linear ubiquitin chains by NEMO is important for NF-kappaB activation, *Cell 136*, 1098-1109.
63. Yoshikawa, A., Sato, Y., Yamashita, M., Mimura, H., Yamagata, A., and Fukai, S. (2009) Crystal structure of the NEMO ubiquitin-binding domain in complex with Lys 63-linked di-ubiquitin, *FEBS Lett 583*, 3317-3322.
64. Wagner, S., Carpentier, I., Rogov, V., Kreike, M., Ikeda, F., Lohr, F., Wu, C. J., Ashwell, J. D., Dotsch, V., Dikic, I., and Beyaert, R. (2008) Ubiquitin binding mediates the NF-kappaB inhibitory potential of ABIN proteins, *Oncogene 27*, 3739-3745.
65. Ohno, A., Jee, J., Fujiwara, K., Tenno, T., Goda, N., Tochio, H., Kobayashi, H., Hiroaki, H., and Shirakawa, M. (2005) Structure of the UBA domain of Dsk2p in complex with ubiquitin molecular determinants for ubiquitin recognition, *Structure 13*, 521-532.
66. Kang, Y., Vossler, R. A., Diaz-Martinez, L. A., Winter, N. S., Clarke, D. J., and Walters, K. J. (2006) UBL/UBA ubiquitin receptor proteins bind a common tetraubiquitin chain, *J Mol Biol 356*, 1027-1035.
67. Raasi, S., Orlov, I., Fleming, K. G., and Pickart, C. M. (2004) Binding of polyubiquitin chains to ubiquitin-associated (UBA) domains of HHR23A, *J Mol Biol 341*, 1367-1379.
68. Varadan, R., Assfalg, M., Raasi, S., Pickart, C., and Fushman, D. (2005) Structural determinants for selective recognition of a Lys48-linked polyubiquitin chain by a UBA domain, *Molecular cell 18*, 687-698.
69. Kirkin, V., Lamark, T., Sou, Y. S., Bjorkoy, G., Nunn, J. L., Bruun, J. A., Shvets, E., McEwan, D. G., Clausen, T. H., Wild, P., Bilusic, I., Theurillat, J. P., Overvatn, A., Ishii, T., Elazar, Z., Komatsu, M., Dikic, I., and Johansen, T. (2009) A role for NBR1 in autophagosomal degradation of ubiquitinated substrates, *Mol Cell 33*, 505-516.

70. Isogai, S., Morimoto, D., Arita, K., Unzai, S., Tenno, T., Hasegawa, J., Sou, Y. S., Komatsu, M., Tanaka, K., Shirakawa, M., and Tochio, H. Crystal structure of the UBA domain of p62 and its interaction with ubiquitin, *J Biol Chem*.
71. Prag, G., Misra, S., Jones, E. A., Ghirlando, R., Davies, B. A., Horazdovsky, B. F., and Hurley, J. H. (2003) Mechanism of ubiquitin recognition by the CUE domain of Vps9p, *Cell 113*, 609-620.
72. Akutsu, M., Kawasaki, M., Katoh, Y., Shiba, T., Yamaguchi, Y., Kato, R., Kato, K., Nakayama, K., and Wakatsuki, S. (2005) Structural basis for recognition of ubiquitinated cargo by Tom1-GAT domain, *FEBS Lett 579*, 5385-5391.
73. Katoh, Y., Shiba, Y., Mitsuhashi, H., Yanagida, Y., Takatsu, H., and Nakayama, K. (2004) Tollip and Tom1 form a complex and recruit ubiquitin-conjugated proteins onto early endosomes, *J Biol Chem 279*, 24435-24443.
74. Prag, G., Lee, S., Mattera, R., Arighi, C. N., Beach, B. M., Bonifacino, J. S., and Hurley, J. H. (2005) Structural mechanism for ubiquitinated-cargo recognition by the Golgi-localized, gamma-ear-containing, ADP-ribosylation-factor-binding proteins, *Proc Natl Acad Sci U S A 102*, 2334-2339.
75. Kawasaki, M., Shiba, T., Shiba, Y., Yamaguchi, Y., Matsugaki, N., Igarashi, N., Suzuki, M., Kato, R., Kato, K., Nakayama, K., and Wakatsuki, S. (2005) Molecular mechanism of ubiquitin recognition by GGA3 GAT domain, *Genes Cells 10*, 639-654.
76. Hong, Y. H., Ahn, H. C., Lim, J., Kim, H. M., Ji, H. Y., Lee, S., Kim, J. H., Park, E. Y., Song, H. K., and Lee, B. J. (2009) Identification of a novel ubiquitin binding site of STAM1 VHS domain by NMR spectroscopy, *FEBS Lett 583*, 287-292.
77. Lange, A., Hoeller, D., Wienk, H., Marcillat, O., Lancelin, J. M., and Walker, O. NMR Reveals a Different Mode of Binding of the Stam2 VHS Domain to Ubiquitin and Diubiquitin, *Biochemistry*.
78. Puertollano, R., and Bonifacino, J. S. (2004) Interactions of GGA3 with the ubiquitin sorting machinery, *Nature cell biology 6*, 244-251.
79. Pinato, S., Gatti, M., Scandiuzzi, C., Confalonieri, S., and Penengo, L. UMI, a novel RNF168 ubiquitin binding domain involved in the DNA damage signaling pathway, *Mol Cell Biol 31*, 118-126.
80. Ai, Y., Wang, J., Johnson, R. E., Haracska, L., Prakash, L., and Zhuang, Z. A novel ubiquitin binding mode in the S. cerevisiae translesion synthesis DNA polymerase eta, *Mol Biosyst 7*, 1874-1882.
81. Cui, G., Benirschke, R. C., Tuan, H. F., Juranic, N., Macura, S., Botuyan, M. V., and Mer, G. (2010) Structural basis of ubiquitin recognition by translesion synthesis DNA polymerase iota, *Biochemistry 49*, 10198-10207.
82. Iha, H., Peloponese, J. M., Verstrepen, L., Zapart, G., Ikeda, F., Smith, C. D., Starost, M. F., Yedavalli, V., Heyninck, K., Dikic, I., Beyaert, R., and Jeang, K. T. (2008) Inflammatory cardiac valvulitis in TAX1BP1-deficient mice through selective NF-kappaB activation, *EMBO J 27*, 629-641.

83. Sato, Y., Yoshikawa, A., Yamashita, M., Yamagata, A., and Fukai, S. (2009) Structural basis for specific recognition of Lys 63-linked polyubiquitin chains by NZF domains of TAB2 and TAB3, *EMBO J 28*, 3903-3909.
84. Kanayama, A., Seth, R. B., Sun, L., Ea, C. K., Hong, M., Shaito, A., Chiu, Y. H., Deng, L., and Chen, Z. J. (2004) TAB2 and TAB3 activate the NF-kappaB pathway through binding to polyubiquitin chains, *Mol Cell 15*, 535-548.
85. Kulathu, Y., Akutsu, M., Bremm, A., Hofmann, K., and Komander, D. (2009) Two-sided ubiquitin binding explains specificity of the TAB2 NZF domain, *Nat Struct Mol Biol 16*, 1328-1330.
86. Alam, S. L., Sun, J., Payne, M., Welch, B. D., Blake, B. K., Davis, D. R., Meyer, H. H., Emr, S. D., and Sundquist, W. I. (2004) Ubiquitin interactions of NZF zinc fingers, *EMBO J 23*, 1411-1421.
87. Wang, B., Alam, S. L., Meyer, H. H., Payne, M., Stemmler, T. L., Davis, D. R., and Sundquist, W. I. (2003) Structure and ubiquitin interactions of the conserved zinc finger domain of Npl4, *J Biol Chem 278*, 20225-20234.
88. Komander, D., and Barford, D. (2008) Structure of the A20 OTU domain and mechanistic insights into deubiquitination, *The Biochemical journal 409*, 77-85.
89. Reyes-Turcu, F. E., Horton, J. R., Mullally, J. E., Heroux, A., Cheng, X., and Wilkinson, K. D. (2006) The ubiquitin binding domain ZnF UBP recognizes the C-terminal diglycine motif of unanchored ubiquitin, *Cell 124*, 1197-1208.
90. Boyault, C., Gilquin, B., Zhang, Y., Rybin, V., Garman, E., Meyer-Klaucke, W., Matthias, P., Muller, C. W., and Khochbin, S. (2006) HDAC6-p97/VCP controlled polyubiquitin chain turnover, *EMBO J 25*, 3357-3366.
91. Seigneurin-Berny, D., Verdel, A., Curtet, S., Lemercier, C., Garin, J., Rousseaux, S., and Khochbin, S. (2001) Identification of components of the murine histone deacetylase 6 complex: link between acetylation and ubiquitination signaling pathways, *Mol Cell Biol 21*, 8035-8044.
92. Husnjak, K., Elsasser, S., Zhang, N., Chen, X., Randles, L., Shi, Y., Hofmann, K., Walters, K. J., Finley, D., and Dikic, I. (2008) Proteasome subunit Rpn13 is a novel ubiquitin receptor, *Nature 453*, 481-488.
93. Schreiner, P., Chen, X., Husnjak, K., Randles, L., Zhang, N., Elsasser, S., Finley, D., Dikic, I., Walters, K. J., and Groll, M. (2008) Ubiquitin docking at the proteasome through a novel pleckstrin-homology domain interaction, *Nature 453*, 548-552.
94. Alam, S. L., Langelier, C., Whitby, F. G., Koirala, S., Robinson, H., Hill, C. P., and Sundquist, W. I. (2006) Structural basis for ubiquitin recognition by the human ESCRT-II EAP45 GLUE domain, *Nat Struct Mol Biol 13*, 1029-1030.
95. Hirano, S., Suzuki, N., Slagsvold, T., Kawasaki, M., Trambaiolo, D., Kato, R., Stenmark, H., and Wakatsuki, S. (2006) Structural basis of ubiquitin recognition by mammalian Eap45 GLUE domain, *Nat Struct Mol Biol 13*, 1031-1032.
96. Slagsvold, T., Aasland, R., Hirano, S., Bache, K. G., Raiborg, C., Trambaiolo, D., Wakatsuki, S., and Stenmark, H. (2005) Eap45 in mammalian ESCRT-II binds ubiquitin via a phosphoinositide-interacting GLUE domain, *J Biol Chem 280*, 19600-19606.

97. Pornillos, O., Alam, S. L., Rich, R. L., Myszka, D. G., Davis, D. R., and Sundquist, W. I. (2002) Structure and functional interactions of the Tsg101 UEV domain, *EMBO J 21*, 2397-2406.
98. Tsui, C., Raguraj, A., and Pickart, C. M. (2005) Ubiquitin binding site of the ubiquitin E2 variant (UEV) protein Mms2 is required for DNA damage tolerance in the yeast RAD6 pathway, *The Journal of biological chemistry 280*, 19829-19835.
99. Brzovic, P. S., Lissounov, A., Christensen, D. E., Hoyt, D. W., and Klevit, R. E. (2006) A UbcH5/ubiquitin noncovalent complex is required for processive BRCA1-directed ubiquitination, *Mol Cell 21*, 873-880.
100. Stamenova, S. D., French, M. E., He, Y., Francis, S. A., Kramer, Z. B., and Hicke, L. (2007) Ubiquitin binds to and regulates a subset of SH3 domains, *Mol Cell 25*, 273-284.
101. He, Y., Hicke, L., and Radhakrishnan, I. (2007) Structural basis for ubiquitin recognition by SH3 domains, *J Mol Biol 373*, 190-196.
102. Bezsonova, I., Bruce, M. C., Wiesner, S., Lin, H., Rotin, D., and Forman-Kay, J. D. (2008) Interactions between the three CIN85 SH3 domains and ubiquitin: implications for CIN85 ubiquitination, *Biochemistry 47*, 8937-8949.
103. Pashkova, N., Gakhar, L., Winistorfer, S. C., Yu, L., Ramaswamy, S., and Piper, R. C. WD40 repeat propellers define a ubiquitin-binding domain that regulates turnover of F box proteins, *Mol Cell 40*, 433-443.
104. Fu, Q. S., Zhou, C. J., Gao, H. C., Jiang, Y. J., Zhou, Z. R., Hong, J., Yao, W. M., Song, A. X., Lin, D. H., and Hu, H. Y. (2009) Structural basis for ubiquitin recognition by a novel domain from human phospholipase A2-activating protein, *J Biol Chem 284*, 19043-19052.
105. Mullally, J. E., Chernova, T., and Wilkinson, K. D. (2006) Doa1 is a Cdc48 adapter that possesses a novel ubiquitin binding domain, *Mol Cell Biol 26*, 822-830.
106. Bellare, P., Kutach, A. K., Rines, A. K., Guthrie, C., and Sontheimer, E. J. (2006) Ubiquitin binding by a variant Jab1/MPN domain in the essential pre-mRNA splicing factor Prp8p, *RNA 12*, 292-302.
107. Okumura, F., Yoshida, K., Liang, F., and Hatakeyama, S. MDA-9/syntenin interacts with ubiquitin via a novel ubiquitin-binding motif, *Mol Cell Biochem 352*, 163-172.
108. Hofmann, K., and Falquet, L. (2001) A ubiquitin-interacting motif conserved in components of the proteasomal and lysosomal protein degradation systems, *Trends Biochem Sci 26*, 347-350.
109. Polo, S., Confalonieri, S., Salcini, A. E., and Di Fiore, P. P. (2003) EH and UIM: endocytosis and more, *Sci STKE 2003*, re17.
110. Raiborg, C., and Stenmark, H. (2002) Hrs and endocytic sorting of ubiquitinated membrane proteins, *Cell Struct Funct 27*, 403-408.
111. Raiborg, C., Rusten, T. E., and Stenmark, H. (2003) Protein sorting into multivesicular endosomes, *Curr Opin Cell Biol 15*, 446-455.

112. Raasi, S., Varadan, R., Fushman, D., and Pickart, C. M. (2005) Diverse polyubiquitin interaction properties of ubiquitin-associated domains, *Nat Struct Mol Biol 12*, 708-714.
113. Baboshina, O. V., and Haas, A. L. (1996) Novel multiubiquitin chain linkages catalyzed by the conjugating enzymes E2EPF and RAD6 are recognized by 26 S proteasome subunit 5, *J Biol Chem 271*, 2823-2831.
114. Jin, L., Williamson, A., Banerjee, S., Philipp, I., and Rape, M. (2008) Mechanism of ubiquitin-chain formation by the human anaphase-promoting complex, *Cell 133*, 653-665.
115. Hofmann, K. (2009) Ubiquitin-binding domains and their role in the DNA damage response, *DNA Repair (Amst) 8*, 544-556.
116. Lo, Y. C., Lin, S. C., Rospigliosi, C. C., Conze, D. B., Wu, C. J., Ashwell, J. D., Eliezer, D., and Wu, H. (2009) Structural basis for recognition of diubiquitins by NEMO, *Mol Cell 33*, 602-615.
117. Ea, C. K., Deng, L., Xia, Z. P., Pineda, G., and Chen, Z. J. (2006) Activation of IKK by TNFalpha requires site-specific ubiquitination of RIP1 and polyubiquitin binding by NEMO, *Mol Cell 22*, 245-257.
118. Wu, C. J., Conze, D. B., Li, T., Srinivasula, S. M., and Ashwell, J. D. (2006) Sensing of Lys 63-linked polyubiquitination by NEMO is a key event in NF-kappaB activation [corrected], *Nat Cell Biol 8*, 398-406.
119. Bienko, M., Green, C. M., Crosetto, N., Rudolf, F., Zapart, G., Coull, B., Kannouche, P., Wider, G., Peter, M., Lehmann, A. R., Hofmann, K., and Dikic, I. (2005) Ubiquitin-binding domains in Y-family polymerases regulate translesion synthesis, *Science 310*, 1821-1824.
120. Bomar, M. G., D'Souza, S., Bienko, M., Dikic, I., Walker, G. C., and Zhou, P. Unconventional ubiquitin recognition by the ubiquitin-binding motif within the Y family DNA polymerases iota and Rev1, *Mol Cell 37*, 408-417.
121. Mueller, T. D., and Feigon, J. (2002) Solution structures of UBA domains reveal a conserved hydrophobic surface for protein-protein interactions, *Journal of molecular biology 319*, 1243-1255.
122. Zhang, D., Raasi, S., and Fushman, D. (2008) Affinity makes the difference: nonselective interaction of the UBA domain of Ubiquilin-1 with monomeric ubiquitin and polyubiquitin chains, *J Mol Biol 377*, 162-180.
123. Varadan, R., Assfalg, M., Haririnia, A., Raasi, S., Pickart, C., and Fushman, D. (2004) Solution conformation of Lys63-linked di-ubiquitin chain provides clues to functional diversity of polyubiquitin signaling, *The Journal of biological chemistry 279*, 7055-7063.
124. Wang, Q., Goh, A. M., Howley, P. M., and Walters, K. J. (2003) Ubiquitin recognition by the DNA repair protein hHR23a, *Biochemistry 42*, 13529-13535.
125. Bertolaet, B. L., Clarke, D. J., Wolff, M., Watson, M. H., Henze, M., Divita, G., and Reed, S. I. (2001) UBA domains mediate protein-protein interactions between two DNA damage-inducible proteins, *J Mol Biol 313*, 955-963.

126. Shih, S. C., Prag, G., Francis, S. A., Sutanto, M. A., Hurley, J. H., and Hicke, L. (2003) A ubiquitin-binding motif required for intramolecular monoubiquitylation, the CUE domain, *EMBO J 22*, 1273-1281.
127. Donaldson, K. M., Yin, H., Gekakis, N., Supek, F., and Joazeiro, C. A. (2003) Ubiquitin signals protein trafficking via interaction with a novel ubiquitin binding domain in the membrane fusion regulator, Vps9p, *Curr Biol 13*, 258-262.
128. Ren, X., and Hurley, J. H. VHS domains of ESCRT-0 cooperate in high-avidity binding to polyubiquitinated cargo, *EMBO J 29*, 1045-1054.
129. Lemmon, M. A. (2005) Pleckstrin homology domains: two halves make a hole?, *Cell 120*, 574-576.
130. Yan, J., Wen, W., Xu, W., Long, J. F., Adams, M. E., Froehner, S. C., and Zhang, M. (2005) Structure of the split PH domain and distinct lipid-binding properties of the PH-PDZ supramodule of alpha-syntrophin, *EMBO J 24*, 3985-3995.
131. Chen, X., Lee, B. H., Finley, D., and Walters, K. J. Structure of proteasome ubiquitin receptor hRpn13 and its activation by the scaffolding protein hRpn2, *Mol Cell 38*, 404-415.
132. Deveraux, Q., Ustrell, V., Pickart, C., and Rechsteiner, M. (1994) A 26 S protease subunit that binds ubiquitin conjugates, *The Journal of biological chemistry 269*, 7059-7061.
133. Pickart, C. M. (2001) Mechanisms underlying ubiquitination, *Annu Rev Biochem 70*, 503-533.
134. Sakata, E., Satoh, T., Yamamoto, S., Yamaguchi, Y., Yagi-Utsumi, M., Kurimoto, E., Tanaka, K., Wakatsuki, S., and Kato, K. Crystal structure of UbcH5b~ubiquitin intermediate: insight into the formation of the self-assembled E2~Ub conjugates, *Structure 18*, 138-147.
135. Bosanac, I., Phu, L., Pan, B., Zilberleyb, I., Maurer, B., Dixit, V. M., Hymowitz, S. G., and Kirkpatrick, D. S. Modulation of K11-linkage formation by variable loop residues within UbcH5A, *J Mol Biol 408*, 420-431.
136. Karkkainen, S., Hiipakka, M., Wang, J. H., Kleino, I., Vaha-Jaakkola, M., Renkema, G. H., Liss, M., Wagner, R., and Saksela, K. (2006) Identification of preferred protein interactions by phage-display of the human Src homology-3 proteome, *EMBO Rep 7*, 186-191.
137. Mayer, B. J. (2001) SH3 domains: complexity in moderation, *J Cell Sci 114*, 1253-1263.
138. Gao, Y. G., Song, A. X., Shi, Y. H., Chang, Y. G., Liu, S. X., Yu, Y. Z., Cao, X. T., Lin, D. H., and Hu, H. Y. (2005) Solution structure of the ubiquitin-like domain of human DC-UbP from dendritic cells, *Protein Sci 14*, 2044-2050.
139. Russell, N. S., and Wilkinson, K. D. (2004) Identification of a novel 29-linked polyubiquitin binding protein, Ufd3, using polyubiquitin chain analogues, *Biochemistry 43*, 4844-4854.
140. Walters, K. J., Lech, P. J., Goh, A. M., Wang, Q., and Howley, P. M. (2003) DNA-repair protein hHR23a alters its protein structure upon binding proteasomal subunit S5a, *Proc Natl Acad Sci U S A 100*, 12694-12699.

141. Woelk, T., Oldrini, B., Maspero, E., Confalonieri, S., Cavallaro, E., Di Fiore, P. P., and Polo, S. (2006) Molecular mechanisms of coupled monoubiquitination, *Nat Cell Biol 8*, 1246-1254.
142. Hoeller, D., and Dikic, I. (2010) Regulation of ubiquitin receptors by coupled monoubiquitination, *Subcell Biochem 54*, 31-40.
143. Polo, S., Sigismund, S., Faretta, M., Guidi, M., Capua, M. R., Bossi, G., Chen, H., De Camilli, P., and Di Fiore, P. P. (2002) A single motif responsible for ubiquitin recognition and monoubiquitination in endocytic proteins, *Nature 416*, 451-455.
144. Hoeller, D., Crosetto, N., Blagoev, B., Raiborg, C., Tikkanen, R., Wagner, S., Kowanetz, K., Breitling, R., Mann, M., Stenmark, H., and Dikic, I. (2006) Regulation of ubiquitin-binding proteins by monoubiquitination, *Nat Cell Biol 8*, 163-169.
145. Meyer, H. H., Wang, Y., and Warren, G. (2002) Direct binding of ubiquitin conjugates by the mammalian p97 adaptor complexes, p47 and Ufd1-Npl4, *EMBO J 21*, 5645-5652.
146. Yuan, X., Simpson, P., McKeown, C., Kondo, H., Uchiyama, K., Wallis, R., Dreveny, I., Keetch, C., Zhang, X., Robinson, C., Freemont, P., and Matthews, S. (2004) Structure, dynamics and interactions of p47, a major adaptor of the AAA ATPase, p97, *EMBO J 23*, 1463-1473.
147. Hunter, T. (2007) The age of crosstalk: phosphorylation, ubiquitination, and beyond, *Molecular cell 28*, 730-738.
148. Miura, K., and Hasegawa, P. M. (2010) Sumoylation and other ubiquitin-like post-translational modifications in plants, *Trends in cell biology 20*, 223-232.
149. Desiere, F., Deutsch, E. W., Nesvizhskii, A. I., Mallick, P., King, N. L., Eng, J. K., Aderem, A., Boyle, R., Brunner, E., Donohoe, S., Fausto, N., Hafen, E., Hood, L., Katze, M. G., Kennedy, K. A., Kregenow, F., Lee, H., Lin, B., Martin, D., Ranish, J. A., Rawlings, D. J., Samelson, L. E., Shiio, Y., Watts, J. D., Wollscheid, B., Wright, M. E., Yan, W., Yang, L., Yi, E. C., Zhang, H., and Aebersold, R. (2005) Integration with the human genome of peptide sequences obtained by high-throughput mass spectrometry, *Genome Biol 6*, R9.
150. Pang, C. N., Gasteiger, E., and Wilkins, M. R. Identification of arginine- and lysine-methylation in the proteome of Saccharomyces cerevisiae and its functional implications, *BMC Genomics 11*, 92.
151. Hershko, A., Ciechanover, A., Heller, H., Haas, A. L., and Rose, I. A. (1980) Proposed role of ATP in protein breakdown: conjugation of protein with multiple chains of the polypeptide of ATP-dependent proteolysis, *Proceedings of the National Academy of Sciences of the United States of America 77*, 1783-1786.
152. Wilkinson, K. D., Urban, M. K., and Haas, A. L. (1980) Ubiquitin is the ATP-dependent proteolysis factor I of rabbit reticulocytes, *The Journal of biological chemistry 255*, 7529-7532.
153. Voges, D., Zwickl, P., and Baumeister, W. (1999) The 26S proteasome: a molecular machine designed for controlled proteolysis, *Annu Rev Biochem 68*, 1015-1068.

154. Elsasser, S., and Finley, D. (2005) Delivery of ubiquitinated substrates to protein-unfolding machines, *Nat. Cell Biol. 7*, 742-749.
155. Madura, K. (2004) Rad23 and Rpn10: perennial wallflowers join the melee, *Trends Biochem. Sci. 29*, 637-640.
156. Elsasser, S., Chandler-Militello, D., Muller, B., Hanna, J., and Finley, D. (2004) Rad23 and Rpn10 serve as alternative ubiquitin receptors for the proteasome, *J Biol Chem 279*, 26817-26822.
157. Verma, R., Oania, R., Graumann, J., and Deshaies, R. J. (2004) Multiubiquitin chain receptors define a layer of substrate selectivity in the ubiquitin-proteasome system, *Cell 118*, 99-110.
158. Kleijnen, M. F., Shih, A. H., Zhou, P., Kumar, S., Soccio, R. E., Kedersha, N. L., Gill, G., and Howley, P. M. (2000) The hPLIC proteins may provide a link between the ubiquitination machinery and the proteasome, *Molecular cell 6*, 409-419.
159. Chen, L., and Madura, K. (2002) Rad23 promotes the targeting of proteolytic substrates to the proteasome, *Mol Cell Biol 22*, 4902-4913.
160. Kaplun, L., Tzirkin, R., Bakhrat, A., Shabek, N., Ivantsiv, Y., and Raveh, D. (2005) The DNA damage-inducible UbL-UbA protein Ddi1 participates in Mec1-mediated degradation of Ho endonuclease, *Mol Cell Biol 25*, 5355-5362.
161. Bertolaet, B. L., Clarke, D. J., Wolff, M., Watson, M. H., Henze, M., Divita, G., and Reed, S. I. (2001) UBA domains of DNA damage-inducible proteins interact with ubiquitin, *Nat Struct Biol 8*, 417-422.
162. Wilkinson, C. R., Seeger, M., Hartmann-Petersen, R., Stone, M., Wallace, M., Semple, C., and Gordon, C. (2001) Proteins containing the UBA domain are able to bind to multi-ubiquitin chains, *Nat Cell Biol 3*, 939-943.
163. Yao, T., Song, L., Xu, W., DeMartino, G. N., Florens, L., Swanson, S. K., Washburn, M. P., Conaway, R. C., Conaway, J. W., and Cohen, R. E. (2006) Proteasome recruitment and activation of the Uch37 deubiquitinating enzyme by Adrm1, *Nat Cell Biol 8*, 994-1002.
164. Hiyama, H., Yokoi, M., Masutani, C., Sugasawa, K., Maekawa, T., Tanaka, K., Hoeijmakers, J. H., and Hanaoka, F. (1999) Interaction of hHR23 with S5a. The ubiquitin-like domain of hHR23 mediates interaction with S5a subunit of 26 S proteasome, *J Biol Chem 274*, 28019-28025.
165. Elsasser, S., Gali, R. R., Schwickart, M., Larsen, C. N., Leggett, D. S., Muller, B., Feng, M. T., Tubing, F., Dittmar, G. A., and Finley, D. (2002) Proteasome subunit Rpn1 binds ubiquitin-like protein domains, *Nat Cell Biol 4*, 725-730.
166. Walters, K. J., Kleijnen, M. F., Goh, A. M., Wagner, G., and Howley, P. M. (2002) Structural studies of the interaction between ubiquitin family proteins and proteasome subunit S5a, *Biochemistry 41*, 1767-1777.
167. Verma, R., Chen, S., Feldman, R., Schieltz, D., Yates, J., Dohmen, J., and Deshaies, R. J. (2000) Proteasomal proteomics: identification of nucleotide-sensitive proteasome-interacting proteins by mass spectrometric analysis of affinity-purified proteasomes, *Mol Biol Cell 11*, 3425-3439.

168. Sone, T., Saeki, Y., Toh-e, A., and Yokosawa, H. (2004) Sem1p is a novel subunit of the 26 S proteasome from Saccharomyces cerevisiae, *J Biol Chem 279*, 28807-28816.
169. Hamazaki, J., Iemura, S., Natsume, T., Yashiroda, H., Tanaka, K., and Murata, S. (2006) A novel proteasome interacting protein recruits the deubiquitinating enzyme UCH37 to 26S proteasomes, *EMBO J 25*, 4524-4536.
170. Jorgensen, J. P., Lauridsen, A. M., Kristensen, P., Dissing, K., Johnsen, A. H., Hendil, K. B., and Hartmann-Petersen, R. (2006) Adrm1, a putative cell adhesion regulating protein, is a novel proteasome-associated factor, *J Mol Biol 360*, 1043-1052.
171. Qiu, X. B., Ouyang, S. Y., Li, C. J., Miao, S., Wang, L., and Goldberg, A. L. (2006) hRpn13/ADRM1/GP110 is a novel proteasome subunit that binds the deubiquitinating enzyme, UCH37, *EMBO J 25*, 5742-5753.
172. Ito, T., Chiba, T., Ozawa, R., Yoshida, M., Hattori, M., and Sakaki, Y. (2001) A comprehensive two-hybrid analysis to explore the yeast protein interactome, *Proc. Natl. Acad. Sci. U S A 98*, 4569-4574.
173. Gandhi, T. K., Zhong, J., Mathivanan, S., Karthick, L., Chandrika, K. N., Mohan, S. S., Sharma, S., Pinkert, S., Nagaraju, S., Periaswamy, B., Mishra, G., Nandakumar, K., Shen, B., Deshpande, N., Nayak, R., Sarker, M., Boeke, J. D., Parmigiani, G., Schultz, J., Bader, J. S., and Pandey, A. (2006) Analysis of the human protein interactome and comparison with yeast, worm and fly interaction datasets, *Nat. Genet. 38*, 285-293.
174. Lam, Y. A., Xu, W., DeMartino, G. N., and Cohen, R. E. (1997) Editing of ubiquitin conjugates by an isopeptidase in the 26S proteasome, *Nature 385*, 737-740.
175. Seong, K. M., Baek, J. H., Yu, M. H., and Kim, J. (2007) Rpn13p and Rpn14p are involved in the recognition of ubiquitinated Gcn4p by the 26S proteasome, *FEBS Lett 581*, 2567-2573.
176. Glickman, M. H., Rubin, D. M., Coux, O., Wefes, I., Pfeifer, G., Cjeka, Z., Baumeister, W., Fried, V. A., and Finley, D. (1998) A subcomplex of the proteasome regulatory particle required for ubiquitin-conjugate degradation and related to the COP9-signalosome and eIF3, *Cell 94*, 615-623.
177. Johnson, E. S., Bartel, B., Seufert, W., and Varshavsky, A. (1992) Ubiquitin as a degradation signal, *The EMBO journal 11*, 497-505.
178. Schmidt, M., Hanna, J., Elsasser, S., and Finley, D. (2005) Proteasome-associated proteins: regulation of a proteolytic machine, *Biol. Chem. 386*, 725-737.
179. Saeki, Y., Saitoh, A., Toh-e, A., and Yokosawa, H. (2002) Ubiquitin-like proteins and Rpn10 play cooperative roles in ubiquitin-dependent proteolysis, *Biochem Biophys Res Commun 293*, 986-992.
180. Raasi, S., and Pickart, C. M. (2003) Rad23 ubiquitin-associated domains (UBA) inhibit 26 S proteasome-catalyzed proteolysis by sequestering lysine 48-linked polyubiquitin chains, *J Biol Chem 278*, 8951-8959.

181. Guterman, A., and Glickman, M. H. (2004) Complementary roles for Rpn11 and Ubp6 in deubiquitination and proteolysis by the proteasome, *J. Biol. Chem. 279*, 1729-1738.
182. Boutet, S. C., Disatnik, M. H., Chan, L. S., Iori, K., and Rando, T. A. (2007) Regulation of pax3 by proteasomal degradation of monoubiquitinated protein in skeletal muscle progenitors, *Cell 130*, 349-362.
183. Soubeyran, P., Kowanetz, K., Szymkiewicz, I., Langdon, W. Y., and Dikic, I. (2002) Cbl-CIN85-endophilin complex mediates ligand-induced downregulation of EGF receptors, *Nature 416*, 183-187.
184. Leggett, D. S., Hanna, J., Borodovsky, A., Crosas, B., Schmidt, M., Baker, R. T., Walz, T., Ploegh, H., and Finley, D. (2002) Multiple associated proteins regulate proteasome structure and function, *Mol. Cell 10*, 495-507.
185. Lamerant, N., and Kieda, C. (2005) Adhesion properties of adhesion-regulating molecule 1 protein on endothelial cells, *Febs J 272*, 1833-1844.
186. Goldstein, A. L., and McCusker, J. H. (1999) Three new dominant drug resistance cassettes for gene disruption in Saccharomyces cerevisiae, *Yeast 15*, 1541-1553.
187. Knop, M., Siegers, K., Pereira, G., Zachariae, W., Winsor, B., Nasmyth, K., and Schiebel, E. (1999) Epitope tagging of yeast genes using a PCR-based strategy: more tags and improved practical routines, *Yeast 15*, 963-972.
188. Goldstein, A. L., Pan, X., and McCusker, J. H. (1999) Heterologous URA3MX cassettes for gene replacement in Saccharomyces cerevisiae, *Yeast 15*, 507-511.
189. Hanna, J., Hathaway, N. A., Tone, Y., Crosas, B., Elsasser, S., Kirkpatrick, D. S., Leggett, D. S., Gygi, S. P., King, R. W., and Finley, D. (2006) Deubiquitinating enzyme Ubp6 functions noncatalytically to delay proteasomal degradation, *Cell 127*, 99-111.
190. Leggett, D. S., Glickman, M. H., and Finley, D. (2005) Purification of proteasomes, proteasome subcomplexes, and proteasome-associated proteins from budding yeast, *Methods Mol Biol 301*, 57-70.
191. Elsasser, S., Schmidt, M., and Finley, D. (2005) Characterization of the proteasome using native gel electrophoresis, *Methods Enzymol. 398*, 353-363.
192. Finley, D., Ozkaynak, E., and Varshavsky, A. (1987) The yeast polyubiquitin gene is essential for resistance to high temperatures, starvation, and other stresses, *Cell 48*, 1035-1046.
193. Kang, Y., Zhang, N., Koepp, D. M., and Walters, K. J. (2007) Ubiquitin receptor proteins hHR23a and hPLIC2 interact, *J Mol Biol 365*, 1093-1101.
194. Pickart, C. M., and Raasi, S. (2005) Controlled synthesis of polyubiquitin chains, *Methods Enzymol 399*, 21-36.
195. Cornilescu, G., Delaglio, F., and Bax, A. (1999) Protein backbone angle restraints from searching a database for chemical shift and sequence homology, *J. Biomol. NMR 13*, 289-302.
196. Delaglio, F., Grzesiek, S., Vuister, G. W., Zhu, G., Pfeifer, J., and Bax, A. (1995) NMRPipe: a multidimensional spectral processing system based on UNIX pipes, *J Biomol NMR 6*, 277-293.

197. Bartels, C., Xia, T.-H., Billeter, M., Güntert, P., and Wüthrich, K. (1995) The program XEASY for computer-supported NMR spectral analysis of biological macromolecules, *J. Biomol. NMR 6*, 1-10.
198. Kang, R. S., Daniels, C. M., Francis, S. A., Shih, S. C., Salerno, W. J., Hicke, L., and Radhakrishnan, I. (2003) Solution structure of a CUE-ubiquitin complex reveals a conserved mode of ubiquitin binding, *Cell 113*, 621-630.
199. Fu, H., Sadis, S., Rubin, D. M., Glickman, M., van Nocker, S., Finley, D., and Vierstra, R. D. (1998) Multiubiquitin chain binding and protein degradation are mediated by distinct domains within the 26 S proteasome subunit Mcb1, *J Biol Chem 273*, 1970-1981.
200. Chau, V., Tobias, J. W., Bachmair, A., Marriott, D., Ecker, D. J., Gonda, D. K., and Varshavsky, A. (1989) A multiubiquitin chain is confined to specific lysine in a targeted short-lived protein, *Science 243*, 1576-1583.
201. Finley, D., Sadis, S., Monia, B. P., Boucher, P., Ecker, D. J., Crooke, S. T., and Chau, V. (1994) Inhibition of proteolysis and cell cycle progression in a multiubiquitination-deficient yeast mutant, *Mol Cell Biol 14*, 5501-5509.
202. Lemmon, M. A. (2004) Pleckstrin homology domains: not just for phosphoinositides, *Biochem Soc Trans 32*, 707-711.
203. Fisher, R. D., Wang, B., Alam, S. L., Higginson, D. S., Robinson, H., Sundquist, W. I., and Hill, C. P. (2003) Structure and ubiquitin binding of the ubiquitin-interacting motif, *J Biol Chem 278*, 28976-28984.
204. Bomar, M. G., Pai, M. T., Tzeng, S. R., Li, S. S., and Zhou, P. (2007) Structure of the ubiquitin-binding zinc finger domain of human DNA Y-polymerase eta, *EMBO Rep 8*, 247-251.
205. Lam, Y. A., DeMartino, G. N., Pickart, C. M., and Cohen, R. E. (1997) Specificity of the ubiquitin isopeptidase in the PA700 regulatory complex of 26 S proteasomes, *J. Biol. Chem. 272*, 28438-28446.
206. Verma, R., Aravind, L., Oania, R., McDonald, W. H., Yates, J. R., 3rd, Koonin, E. V., and Deshaies, R. J. (2002) Role of Rpn11 metalloprotease in deubiquitination and degradation by the 26S proteasome, *Science 298*, 611-615.
207. Yao, T., and Cohen, R. E. (2002) A cryptic protease couples deubiquitination and degradation by the proteasome, *Nature 419*, 403-407.
208. Crosas, B., Hanna, J., Kirkpatrick, D. S., Zhang, D. P., Tone, Y., Hathaway, N. A., Buecker, C., Leggett, D. S., Schmidt, M., King, R. W., Gygi, S. P., and Finley, D. (2006) Ubiquitin chains are remodeled at the proteasome by opposing ubiquitin ligase and deubiquitinating activities, *Cell 127*, 1401-1413.
209. Budisa, N., Steipe, B., Demange, P., Eckerskorn, C., Kellermann, J., and Huber, R. (1995) High-level biosynthetic substitution of methionine in proteins by its analogs 2-aminohexanoic acid, selenomethionine, telluromethionine and ethionine in Escherichia coli, *Eur J Biochem 230*, 788-796.
210. Otwinowski, Z., and Minor, W. (1997) Processing of X-ray Diffraction Data Collected in Oscillation Mode, *Methods in Enzymology 276*, 307-326.
211. Schneider, T., and Sheldrick, G. (2002) Substructure solution with SHELXD, *Acta Crystallogr D 58*, 1772-1779.

212. CCP4. (1994) The CCP4 suite: programs for protein crystallography, *Acta Crystallogr D 50*, 760-763.
213. Potterton, E., Briggs, P., Turkenburg, M., and Dodson, E. (2003) A graphical user interface to the CCP4 program suite, *Acta Crystallogr D Biol Crystallogr 59*, 1131-1137.
214. Cowtan, K. D., and Main, P. (1996) Phase combination and cross validation in iterated density-modification calculations, *Acta Crystallogr D Biol Crystallogr 52*, 43-48.
215. Perrakis, A., Morris, R., and Lamzin, V. S. (1999) Automated protein model building combined with iterative structure refinement, *Nat Struct Biol 6*, 458-463.
216. Turk, D. (1992) Improvement of a programm for molecular graphics and manipulation of electron densities and its application for protein structure determination, In *Technische Universitaet Muenchen*.
217. Murshudov, G. N., Vagin, A. A., and Dodson, E. J. (1997) Refinement of macromolecular structures by the maximum-likelihood method, *Acta Crystallogr D Biol Crystallogr 53*, 240-255.
218. Brünger, A. T. (1992) Free R value: a novel statistical quantity for assessing the accuracy of crystal structures, *Nature 355*, 472 - 475.
219. Bartels, C., Xia, T.-H., Billeter, M., Güntert, P., and Wüthrich, K. (1995) The program XEASY for computer-supported NMR spectral analysis of biological macromolecules, *J Biomol NMR 6*, 1-10.
220. Dominguez, C., Boelens, R., and Bonvin, A. M. (2003) HADDOCK: a protein-protein docking approach based on biochemical or biophysical information, *J Am Chem Soc 125*, 1731-1737.
221. Brünger, A. T., Adams, P. D., Clore, G. M., DeLano, W. L., Gros, P., Grosse-Kunstleve, R. W., Jiang, J., Kuszewski, J., Nilges, M., Pannu, N. S., and al., e. (1998) Crystallography and NMR system: a new software system for macromolecular structure determination, *Acta Crystallog sect D 54*, 905-921.
222. Cornilescu, G., Marquardt, J. L., Ottiger, M., and Bax, A. (1998) Validation of Protein Structure from Anisotropic Carbonyl Chemical Shifts in a Dilute Liquid Crystalline Phase, *J.Am.Chem.Soc. 120*, 6836-6837.
223. Wang, J., Hu, W., Cai, S., Lee, B., Song, J., and Chen, Y. (2007) The intrinsic affinity between E2 and the Cys domain of E1 in ubiquitin-like modifications, *Mol Cell 27*, 228-237.
224. Zhang, N., Liu, L., Liu, F., Wagner, C. R., Hanna, P. E., and Walters, K. J. (2006) NMR-based model reveals the structural determinants of mammalian arylamine N-acetyltransferase substrate specificity, *J Mol Biol 363*, 188-200.
225. McDonald, I. K., and Thornton, J. M. (1994) Satisfying hydrogen bonding potential in proteins, *J Mol Biol 238*, 777-793.
226. Ciechanover, A. (1994) The ubiquitin-proteasome proteolytic pathway, *Cell 79*, 13-21.
227. Rock, K. L., and Goldberg, A. L. (1999) Degradation of cell proteins and the generation of MHC class I-presented peptides, *Annu Rev Immunol 17*, 739-779.

228. Ciechanover, A., Finley, D., and Varshavsky, A. (1984) Ubiquitin dependence of selective protein degradation demonstrated in the mammalian cell cycle mutant ts85, *Cell 37*, 57-66.
229. Finley, D., Ciechanover, A., and Varshavsky, A. (1984) Thermolability of ubiquitin-activating enzyme from the mammalian cell cycle mutant ts85, *Cell 37*, 43-55.
230. Deveraux, Q., Ustrell, V., Pickart, C., and Rechsteiner, M. (1994) A 26 S protease subunit that binds ubiquitin conjugates, *J Biol Chem 269*, 7059-7061.
231. Husnjak, K., Elsasser, S., Zhang, N., Chen, X., Randles, L., Shi, Y., Hofmann, K., Walters, K. J., Finley, D., and Dikic, I. (2008) Proteasome subunit Rpn13 is a novel ubiquitin receptor, *Nature 453*, 481-488.
232. Elsasser, S., Gali, R. R., Schwickart, M., Larsen, C. N., Leggett, D. S., Muller, B., Feng, M. T., Tubing, F., Dittmar, G. A., and Finley, D. (2002) Proteasome subunit Rpn1 binds ubiquitin-like protein domains, *Nat Cell Biol 4*, 725-730.
233. Wilkinson, C. R., Ferrell, K., Penney, M., Wallace, M., Dubiel, W., and Gordon, C. (2000) Analysis of a gene encoding Rpn10 of the fission yeast proteasome reveals that the polyubiquitin-binding site of this subunit is essential when Rpn12/Mts3 activity is compromised, *J Biol Chem 275*, 15182-15192.
234. Matiuhin, Y., Kirkpatrick, D. S., Ziv, I., Kim, W., Dakshinamurthy, A., Kleifeld, O., Gygi, S. P., Reis, N., and Glickman, M. H. (2008) Extraproteasomal Rpn10 restricts access of the polyubiquitin-binding protein Dsk2 to proteasome, *Mol Cell 32*, 415-425.
235. van Nocker, S., Sadis, S., Rubin, D. M., Glickman, M., Fu, H., Coux, O., Wefes, I., Finley, D., and Vierstra, R. D. (1996) The multiubiquitin-chain-binding protein Mcb1 is a component of the 26S proteasome in Saccharomyces cerevisiae and plays a nonessential, substrate-specific role in protein turnover, *Mol Cell Biol 16*, 6020-6028.
236. Hamazaki, J., Sasaki, K., Kawahara, H., Hisanaga, S., Tanaka, K., and Murata, S. (2007) Rpn10-mediated degradation of ubiquitinated proteins is essential for mouse development, *Mol Cell Biol 27*, 6629-6638.
237. Szlanka, T., Haracska, L., Kiss, I., Deak, P., Kurucz, E., Ando, I., Viragh, E., and Udvardy, A. (2003) Deletion of proteasomal subunit S5a/Rpn10/p54 causes lethality, multiple mitotic defects and overexpression of proteasomal genes in Drosophila melanogaster, *J Cell Sci 116*, 1023-1033.
238. Kang, Y., Chen, X., Lary, J. W., Cole, J. L., and Walters, K. J. (2007) Defining how ubiquitin receptors hHR23a and S5a bind polyubiquitin, *J Mol Biol 369*, 168-176.
239. Raasi, S., and Pickart, C. M. (2003) Rad23 UBA domains inhibit 26S proteasome-catalyzed proteolysis by sequestering lysine 48-linked polyubiquitin chains, *J Biol Chem 278*, 8951-8959.
240. Schreiner, P., Chen, X., Husnjak, K., Randles, L., Zhang, N., Elsasser, S., Finley, D., Dikic, I., Walters, K. J., and Groll, M. (2008) Ubiquitin docking at the proteasome through a novel pleckstrin-homology domain interaction, *Nature 453*, 548-552.

241. Wang, Q., Young, P., and Walters, K. J. (2005) Structure of S5a bound to monoubiquitin provides a model for polyubiquitin recognition, *J. Mol Biol. 348*, 727-739.
242. Ryu, K. S., Lee, K. J., Bae, S. H., Kim, B. K., Kim, K. A., and Choi, B. S. (2003) Binding surface mapping of intra- and interdomain interactions among hHR23B, ubiquitin, and polyubiquitin binding site 2 of S5a, *The Journal of biological chemistry 278*, 36621-36627.
243. Fushman, D., Varadan, R., Assfalg, M., and Walter, O. (2004) Determining domain orientation in macromolecules by using spin-relaxation and residual dipolar coupling measurements, *Progress NMR Spectroscopy 44*, 189-214.
244. Haririnia, A., D'Onofrio, M., and Fushman, D. (2007) Mapping the interactions between Lys48 and Lys63-linked di-ubiquitins and a ubiquitin-interacting motif of S5a, *Journal of molecular biology 368*, 753-766.
245. Thrower, J. S., Hoffman, L., Rechsteiner, M., and Pickart, C. M. (2000) Recognition of the polyubiquitin proteolytic signal, *Embo J 19*, 94-102.
246. Maytal-Kivity, V., Reis, N., Hofmann, K., and Glickman, M. H. (2002) MPN+, a putative catalytic motif found in a subset of MPN domain proteins from eukaryotes and prokaryotes, is critical for Rpn11 function, *BMC Biochem. 3*, 28.
247. Hofmann, R. M., and Pickart, C. M. (2001) In vitro assembly and recognition of Lys-63 polyubiquitin chains., *J. Biol. Chem. 276*, 27936-27943.
248. Schuck, P. (2003) On the analysis of protein self-association by sedimentation velocity analytical ultracentrifugation, *Anal Biochem 320*, 104-124.
249. Raasi, S., and Pickart, C. M. (2005) Ubiquitin chain synthesis, *Methods Mol Biol 301*, 47-55.
250. Varadan, R., Walker, O., Pickart, C., and Fushman, D. (2002) Structural properties of polyubiquitin chains in solution, *J Mol Biol 324*, 637-647.
251. Cornilescu, G., Marquardt, J. L., Ottiger, M., and Bax, A. (1998) Validation of Protein Structure from Anisotropic Carbonyl Chemical Shifts in a Dilute Liquid Crystalline Phase, *J Am Chem Soc 120*, 6836-6837.
252. Finley, D. (2009) Recognition and processing of ubiquitin-protein conjugates by the proteasome, *Annu Rev Biochem 78*, 477-513.
253. Hershko, A., and Ciechanover, A. (1998) The ubiquitin system, *Annu Rev Biochem 67*, 425-479.
254. Dikic, I., Wakatsuki, S., and Walters, K. J. (2009) Ubiquitin-binding domains - from structures to functions, *Nat Rev Mol Cell Biol 10*, 659-671.
255. Randles, L., and Walters, K. J. (2012) Ubiquitin and its binding domains, *Front Biosci 17*, 2140-2157.
256. Dye, B. T., and Schulman, B. A. (2007) Structural mechanisms underlying posttranslational modification by ubiquitin-like proteins, *Annu Rev Biophys Biomol Struct 36*, 131-150.
257. Schulman, B. A., and Harper, J. W. (2009) Ubiquitin-like protein activation by E1 enzymes: the apex for downstream signalling pathways, *Nat Rev Mol Cell Biol 10*, 319-331.

258. Deshaies, R. J., and Joazeiro, C. A. (2009) RING domain E3 ubiquitin ligases, *Annu Rev Biochem 78*, 399-434.
259. Wenzel, D. M., Lissounov, A., Brzovic, P. S., and Klevit, R. E. (2011) UBCH7 reactivity profile reveals parkin and HHARI to be RING/HECT hybrids, *Nature 474*, 105-108.
260. Liu, F., and Walters, K. J. (2010) Multitasking with ubiquitin through multivalent interactions, *Trends in biochemical sciences 35*, 352-360.
261. Zimmerman, E. S., Schulman, B. A., and Zheng, N. (2010) Structural assembly of cullin-RING ubiquitin ligase complexes, *Curr Opin Struct Biol 20*, 714-721.
262. Duda, D. M., Borg, L. A., Scott, D. C., Hunt, H. W., Hammel, M., and Schulman, B. A. (2008) Structural insights into NEDD8 activation of cullin-RING ligases: conformational control of conjugation, *Cell 134*, 995-1006.
263. Saha, A., and Deshaies, R. J. (2008) Multimodal activation of the ubiquitin ligase SCF by Nedd8 conjugation, *Mol Cell 32*, 21-31.
264. Kamura, T., Koepp, D. M., Conrad, M. N., Skowyra, D., Moreland, R. J., Iliopoulos, O., Lane, W. S., Kaelin, W. G., Jr., Elledge, S. J., Conaway, R. C., Harper, J. W., and Conaway, J. W. (1999) Rbx1, a component of the VHL tumor suppressor complex and SCF ubiquitin ligase, *Science 284*, 657-661.
265. Yamoah, K., Oashi, T., Sarikas, A., Gazdoiu, S., Osman, R., and Pan, Z. Q. (2008) Autoinhibitory regulation of SCF-mediated ubiquitination by human cullin 1's C-terminal tail, *Proceedings of the National Academy of Sciences of the United States of America 105*, 12230-12235.
266. Pan, Z. Q., Kentsis, A., Dias, D. C., Yamoah, K., and Wu, K. (2004) Nedd8 on cullin: building an expressway to protein destruction, *Oncogene 23*, 1985-1997.
267. Wu, K., Kovacev, J., and Pan, Z. Q. (2010) Priming and extending: a UbcH5/Cdc34 E2 handoff mechanism for polyubiquitination on a SCF substrate, *Mol Cell 37*, 784-796.
268. Bencsath, K. P., Podgorski, M. S., Pagala, V. R., Slaughter, C. A., and Schulman, B. A. (2002) Identification of a multifunctional binding site on Ubc9p required for Smt3p conjugation, *J Biol Chem 277*, 47938-47945.
269. Eletr, Z. M., Huang, D. T., Duda, D. M., Schulman, B. A., and Kuhlman, B. (2005) E2 conjugating enzymes must disengage from their E1 enzymes before E3-dependent ubiquitin and ubiquitin-like transfer, *Nature structural & molecular biology 12*, 933-934.
270. Huang, D. T., Paydar, A., Zhuang, M., Waddell, M. B., Holton, J. M., and Schulman, B. A. (2005) Structural basis for recruitment of Ubc12 by an E2 binding domain in NEDD8's E1, *Mol Cell 17*, 341-350.
271. Reverter, D., and Lima, C. D. (2005) Insights into E3 ligase activity revealed by a SUMO-RanGAP1-Ubc9-Nup358 complex, *Nature 435*, 687-692.
272. Spratt, D. E., Wu, K., Kovacev, J., Pan, Z. Q., and Shaw, G. S. (2012) Selective recruitment of an E2~ubiquitin complex by an E3 ubiquitin ligase, *J Biol Chem 287*, 17374-17385.

273. Spratt, D. E., and Shaw, G. S. (2011) Association of the disordered C-terminus of CDC34 with a catalytically bound ubiquitin, *Journal of molecular biology 407*, 425-438.
274. Kleiger, G., Hao, B., Mohl, D. A., and Deshaies, R. J. (2009) The acidic tail of the Cdc34 ubiquitin-conjugating enzyme functions in both binding to and catalysis with ubiquitin ligase SCFCdc4, *J Biol Chem 284*, 36012-36023.
275. Kleiger, G., Saha, A., Lewis, S., Kuhlman, B., and Deshaies, R. J. (2009) Rapid E2-E3 assembly and disassembly enable processive ubiquitylation of cullin-RING ubiquitin ligase substrates, *Cell 139*, 957-968.
276. Pagano, M., Tam, S. W., Theodoras, A. M., Beer-Romero, P., Del Sal, G., Chau, V., Yew, P. R., Draetta, G. F., and Rolfe, M. (1995) Role of the ubiquitin-proteasome pathway in regulating abundance of the cyclin-dependent kinase inhibitor p27, *Science 269*, 682-685.
277. Yew, P. R., and Kirschner, M. W. (1997) Proteolysis and DNA replication: the CDC34 requirement in the Xenopus egg cell cycle, *Science 277*, 1672-1676.
278. Tam, S. W., Theodoras, A. M., and Pagano, M. (1997) Kip1 degradation via the ubiquitin-proteasome pathway, *Leukemia 11 Suppl 3*, 363-366.
279. Gonen, H., Bercovich, B., Orian, A., Carrano, A., Takizawa, C., Yamanaka, K., Pagano, M., Iwai, K., and Ciechanover, A. (1999) Identification of the ubiquitin carrier proteins, E2s, involved in signal-induced conjugation and subsequent degradation of IkappaBalpha, *J Biol Chem 274*, 14823-14830.
280. Tan, P., Fuchs, S. Y., Chen, A., Wu, K., Gomez, C., Ronai, Z., and Pan, Z. Q. (1999) Recruitment of a ROC1-CUL1 ubiquitin ligase by Skp1 and HOS to catalyze the ubiquitination of I kappa B alpha, *Mol Cell 3*, 527-533.
281. Michael, W. M., and Newport, J. (1998) Coupling of mitosis to the completion of S phase through Cdc34-mediated degradation of Wee1, *Science 282*, 1886-1889.
282. Ceccarelli, D. F., Tang, X., Pelletier, B., Orlicky, S., Xie, W., Plantevin, V., Neculai, D., Chou, Y. C., Ogunjimi, A., Al-Hakim, A., Varelas, X., Koszela, J., Wasney, G. A., Vedadi, M., Dhe-Paganon, S., Cox, S., Xu, S., Lopez-Girona, A., Mercurio, F., Wrana, J., Durocher, D., Meloche, S., Webb, D. R., Tyers, M., and Sicheri, F. (2011) An allosteric inhibitor of the human Cdc34 ubiquitin-conjugating enzyme, *Cell 145*, 1075-1087.
283. Eliseeva, E., Pati, D., Diccinanni, M. B., Yu, A. L., Mohsin, S. K., Margolin, J. F., and Plon, S. E. (2001) Expression and localization of the CDC34 ubiquitin-conjugating enzyme in pediatric acute lymphoblastic leukemia, *Cell Growth Differ 12*, 427-433.
284. Bussing, I., Slack, F. J., and Grosshans, H. (2008) let-7 microRNAs in development, stem cells and cancer, *Trends Mol Med 14*, 400-409.
285. Legesse-Miller, A., Elemento, O., Pfau, S. J., Forman, J. J., Tavazoie, S., and Coller, H. A. (2009) let-7 Overexpression leads to an increased fraction of cells in G2/M, direct down-regulation of Cdc34, and stabilization of Wee1 kinase in primary fibroblasts, *J Biol Chem 284*, 6605-6609.

286. Wang, Q., Young, P., and Walters, K. J. (2005) Structure of S5a bound to monoubiquitin provides a model for polyubiquitin recognition, *J Mol Biol 348*, 727-739.
287. Zhang, N., Wang, Q., Ehlinger, A., Randles, L., Lary, J. W., Kang, Y., Haririnia, A., Storaska, A. J., Cole, J. L., Fushman, D., and Walters, K. J. (2009) Structure of the s5a:k48-linked diubiquitin complex and its interactions with rpn13, *Mol Cell 35*, 280-290.
288. Maytal-Kivity, V., Reis, N., Hofmann, K., and Glickman, M. H. (2002) MPN+, a putative catalytic motif found in a subset of MPN domain proteins from eukaryotes and prokaryotes, is critical for Rpn11 function, *BMC Biochem 3*, 28.
289. Leggett, D. S., Hanna, J., Borodovsky, A., Crosas, B., Schmidt, M., Baker, R. T., Walz, T., Ploegh, H., and Finley, D. (2002) Multiple associated proteins regulate proteasome structure and function, *Mol Cell 10*, 495-507.
290. Hamazaki, J., Iemura, S., Natsume, T., Yashiroda, H., Tanaka, K., and Murata, S. (2006) A novel proteasome interacting protein recruits the deubiquitinating enzyme UCH37 to 26S proteasomes, *Embo J 25*, 4524-4536.
291. Qiu, X. B., Ouyang, S. Y., Li, C. J., Miao, S., Wang, L., and Goldberg, A. L. (2006) hRpn13/ADRM1/GP110 is a novel proteasome subunit that binds the deubiquitinating enzyme, UCH37, *Embo J 25*, 5742-5753.
292. Yao, T., Song, L., Xu, W., DeMartino, G. N., Florens, L., Swanson, S. K., Washburn, M. P., Conaway, R. C., Conaway, J. W., and Cohen, R. E. (2006) Proteasome recruitment and activation of the Uch37 deubiquitinating enzyme by Adrm1, *Nat Cell Biol 8*, 994-1002.
293. Chen, X., Lee, B. H., Finley, D., and Walters, K. J. (2010) Structure of proteasome ubiquitin receptor hRpn13 and its activation by the scaffolding protein hRpn2, *Mol Cell 38*, 404-415.
294. Lander, G. C., Estrin, E., Matyskiela, M. E., Bashore, C., Nogales, E., and Martin, A. (2012) Complete subunit architecture of the proteasome regulatory particle, *Nature 482*, 186-191.
295. Sakata, E., Bohn, S., Mihalache, O., Kiss, P., Beck, F., Nagy, I., Nickell, S., Tanaka, K., Saeki, Y., Forster, F., and Baumeister, W. (2012) Localization of the proteasomal ubiquitin receptors Rpn10 and Rpn13 by electron cryomicroscopy, *Proceedings of the National Academy of Sciences of the United States of America 109*, 1479-1484.
296. Chen, X., and Walters, K. J. (2012) Identifying and studying ubiquitin receptors by NMR, *Methods Mol Biol 832*, 279-303.
297. Walters, K. J., Ferentz, A. E., Hare, B. J., Hidalgo, P., Jasanoff, A., Matsuo, H., and Wagner, G. (2001) Characterizing protein-protein complexes and oligomers by nuclear magnetic resonance spectroscopy, *Methods Enzymol 339*, 238-258.
298. Kao, A., Randall, A., Yang, Y., Patel, V. R., Kandur, W., Guan, S., Rychnovsky, S. D., Baldi, P., and Huang, L. (2012) Mapping the structural topology of the yeast 19S proteasomal regulatory particle using chemical cross-linking and probabilistic modeling, *Molecular & cellular proteomics : MCP*.

299. Verma, R., Chen, S., Feldman, R., Schieltz, D., Yates, J., Dohmen, J., and Deshaies, R. J. (2000) Proteasomal proteomics: identification of nucleotide-sensitive proteasome-interacting proteins by mass spectrometric analysis of affinity-purified proteasomes, *Mol Biol Cell 11*, 3425-3439.
300. Mazumdar, T., Gorgun, F. M., Sha, Y., Tyryshkin, A., Zeng, S., Hartmann-Petersen, R., Jorgensen, J. P., Hendil, K. B., and Eissa, N. T. (2010) Regulation of NF-kappaB activity and inducible nitric oxide synthase by regulatory particle non-ATPase subunit 13 (Rpn13), *Proceedings of the National Academy of Sciences of the United States of America 107*, 13854-13859.
301. Verma, R., Feldman, R. M., and Deshaies, R. J. (1997) SIC1 is ubiquitinated in vitro by a pathway that requires CDC4, CDC34, and cyclin/CDK activities, *Molecular biology of the cell 8*, 1427-1437.
302. Petroski, M. D., and Deshaies, R. J. (2005) Mechanism of lysine 48-linked ubiquitin-chain synthesis by the cullin-RING ubiquitin-ligase complex SCF-Cdc34, *Cell 123*, 1107-1120.
303. Petroski, M. D., Kleiger, G., and Deshaies, R. J. (2006) Evaluation of a diffusion-driven mechanism for substrate ubiquitination by the SCF-Cdc34 ubiquitin ligase complex, *Mol Cell 24*, 523-534.
304. Deffenbaugh, A. E., Scaglione, K. M., Zhang, L., Moore, J. M., Buranda, T., Sklar, L. A., and Skowyra, D. (2003) Release of ubiquitin-charged Cdc34-S - Ub from the RING domain is essential for ubiquitination of the SCF(Cdc4)-bound substrate Sic1, *Cell 114*, 611-622.
305. Delaglio, F., Grzesiek, S., Vuister, G. W., Zhu, G., Pfeifer, J., and Bax, A. (1995) NMRPipe: a multidimensional spectral processing system based on UNIX pipes, *J Biomol NMR 6*, 277-293.
306. Bartels, C., Xia, T. H., Billeter, M., Guntert, P., and Wuthrich, K. (1995) The program XEASY for computer-supported NMR spectral analysis of biological macromolecules, *Journal of biomolecular NMR 6*, 1-10.